Tuning, understanding and evaluating the mechanical properties of peptide-based low molecular weight hydrogels over different length scales

Ana María Fuentes Caparrós

Submitted in fulfilment of the requirements for the Degree of Doctor of Philosophy

School of Chemistry

College of Science and Engineering

University of Glasgow

February 2021

“Tu único límite eres tú”

Abstract

We report the ability to tune and characterise the mechanical properties of low molecular weight hydrogels over different length scales. These materials have been investigated due to their potential for use in a wide range of biomedical applications including drug delivery, tissue engineering, cell culture and wound healing. As such, it is really important to not only being able to characterise the properties of this class of materials at different length scales, but also to find new approaches that will open up new opportunities to control gel networks on demand to provide tuneable, triggerable materials.

We describe a multicomponent system of two gelators that forms a gel via a solvent-trigger approach. After gelation, thermal annealing leads to a self-sorted network which interestingly exhibits significantly different mechanical properties to the as-prepared gel. The changes in the mechanical properties affect the stiffness of the resulting gel system, which will also impact on the diffusion and transport within the gel network. Furthermore, we demonstrate that it is also possible to selectively anneal only one component within the mixture. This also leads to a change in the final gel properties, but in a different manner than when both gelators were annealed.

We also describe the use of cavitation rheology to characterise the linear elastic modulus of a range of hydrogels at a different scale that traditional shear rheology cannot access. We investigate a quantitative relationship, k_{sc}, between the gel modulus determined using both cavitation and traditional shear rheology, that will allow to interconvert between both techniques. We show that the data from the cavitation rheology correlates with the underlying microstructure within the gels, which allows a greater degree of understanding of the gel systems than can be obtained from the bulk measurements using traditional shear rheology, as well as allowing information to be gathered on a local environment, which can be used to determine gel homogeneity.

Finally, we successfully developed new rheological protocols to characterise the mechanical properties of multi-layered hydrogels prepared in situ and post 3D-printing with a high degree of control. From rheological analysis, we show that not only a high control of the measured mechanical properties of the individual layers within the multi-layered constructions can be achieved, but also the contribution of each layer on the resulting properties being measured can be assessed. We also emphasise the importance of using different measuring systems for rheological measurements, as these impact heavily on the resulting properties being measured. We present this study as a tool for assessing the mechanical properties of 3D printed gels and we hope this will open up new opportunities to characterise new biomaterials on demand.

Acknowledgements

Firstly, I would like to say a huge thank you to my supervisor Prof. Dave Adams. Thank you for believing in me and giving me the opportunity to work within your group. You have always encouraged me to do my best, and I will be forever grateful. I cannot thank you enough for the endless support, advices and guidance over the years. It has been a real pleasure working for you and I wish you all the best. ¡Muchas gracias por todo!

I would also like to thank Dr Michael Barrow who took care of me during my Erasmus in Liverpool and also guided me with rheology during my final year of PhD. Thank you for all the English lessons, Costa coffees and for the support and advises to pursue a PhD. Remember, I will always think of you when I eat saucisson!

Undoubtedly, living in Glasgow has been a unique and unforgettable experience thanks to the people I have met. A massive thank you goes to the whole Adams group, past and present members. Thank you for all your support over the years and for making working in the lab so enjoyable. Kate McAulay and Emily Cross (my corner crew), thank you for all the fun and laughter. You always had the right words at the right moment. Thank you for all the adventures, you are both amazing! Bart Dietrich, massive thank you for all your help during my PhD, for the free bananas and the salsa lessons (Voy a reír, voy a bailar, vivir mi vida, la la la la). Thank you so much, you are irreplaceable! To Lisa Thomson, thank you for being an amazing student and later lab mate. Thank you for always caring about others and making working with you super enjoyable. To Sam O'Nion, thank you for all the fun adventures and the Glaswegian lessons. Becky and Jaki, my partners in crime during the last months of my PhD, thank you for creating a fantastic atmosphere in the lab during a pandemic. Really appreciated! Thank you for the rest of occupants of the C3-08, Dan (thank you for the hikes and for getting us lost in the woods), Santanu (thank you for all your advices and chats, also for the card signatures in Bengali which I never managed to understand haha), Courtenay (I will miss our dances and hysterical laughs around the lab), Libby (thank you for bringing sanity to our lives and for more dancing nights), Valentina (grazzi tal-

klassijiet qosra tal-Malti tagħna), Maria Laura (thank you for all the chats in the rheometers back room) and the new arrivals Max, Chloe and Rebecca, all the luck. Thank you for making spending time in the lab the most enjoyable experience. A big thank you to all the past and present members of the Symes and Cooke groups for their kindness and friendship during my PhD. Thank you also to all the students with whom I have had the pleasure of working with, Lisa, Charles, Katie, Johnathan and Zaloa. Also, thanks to the Spanish mafia Curro, Laura, Alazne, Pedro, Jose y Juan for all the laughs and experiences.

Thank you "Glasgowlianos" for all the food, trips and adventures. Thanks to "mis cerditas", Aranza and Carolina, for always having the door of your kitchen open haha. Gracias por todas las gorduras deliciosas que nos hemos apretado, los domingos de Master Chef, palomitas y mantita time, los viajes por toda Europa y las macrofiestas en mi cocina en pijama y con Billy de DJ. Realmente me llevo a dos grandes amigas para siempre! Huge thank you also to my adoptive parents in Glasgow, Michele ("mi veneno") and Stefania ("mi farfallina"). Thank you for the amazing panzerotti nights, all the food comas, hiking, trip attempts (we have a few pending), but above all thanks for your friendship. You are family to me! A special thanks go to Billy, the most amazing flat mate I could have asked for. Thank you for making me feel like home, with the morning carrot smoothies, Patry Jordan morning trainings (they did not last long, haha), your super spiced curries, your mum's Sunday roasts, our chats, dances, hysterical laughs, company and support. Thank you from the deepest of my heart! I would also like to thank my friends from Turre and from University and High School (mis realfooders, mi guarri, mi niña Irene, Pilar, Andrey) for their support during my PhD, their visits to Glasgow and making my trips back to Spain always wonderful.

To Davide, "mi bichi", gracias por siempre estar ahí apoyándome y recordándome constantemente que no hay nada que se me resista. ¡No lo habría conseguido sin tu apoyo!

Gracias a toda mi familia por su apoyo incondicional a lo largo de todos estos años. Pero sobre todo a mis padres, gracias por haberme apoyado siempre en todas mis decisiones y haber luchado por darnos el mejor futuro a mi hermano y a mí. A mi

hermano Martín, gracias por tus consejos de hermano mayor que siempre me transmiten paz y seguridad.

¡Y en especial a tí Papá, porque sé que hoy te sentirías la persona más orgullosa del mundo!

List of publications arising from this thesis

Fuentes-Caparrós, A. M.; Canales-Galarza, Z.; Barrow, M.; Dietrich, B.; Läuger, J.; Nemeth, M.; Draper, E.R.; Adams, D. J., Mechanical Characterization of Multilayered Hydrogels: A Rheological Study for 3D-Printed Systems. *Biomacromolecules* 2021, *22* (4), 1625-1638.

McDowall, D. G., B.; McAulay, K.; Fuentes-Caparrós, A.M.; Thomson, L.; Khunti, N.; Cowieson,N.; Nolan, M.; Wallace, M.; Cooper, A. I.; Draper, E. R.; Cowan, A.; Adams, D.; Clowes, R.. , Controlling Activity by Self-assembly – Tuning Perylene Bisimide Photocatalysts for the Hydrogen Evolution Reaction. *Advanced Energy Materials* 2020, *10* (46), 2002469.

McAulay, K.; Wang, H.; Fuentes-Caparrós, A. M.; Thomson, L.; Khunti, N.; Cowieson, N.; Cui, H.; Seddon, A.; Adams, D. J., Isotopic Control over Self-Assembly in Supramolecular Gels. *Langmuir* 2020, *36* (29), 8626-8631.

Cross, E. R.; Coulter, S. M.; Fuentes-Caparrós, A. M.; McAulay, K.; Schweins, R.; Laverty,G.; Adams, D. J., Tuning the antimicrobial activity of low molecular weight hydrogels using dopamine autoxidation. *Chemical Communications* 2020, *56* (58), 8135-8138.

Panja, S.; Fuentes-Caparrós, A. M.; Cross, E. R.; Cavalcanti, L.; Adams, D. J., Annealing Supramolecular Gels by a Reaction Relay. *Chemistry of Materials* 2020, *32* (12), 5264-5271.

Fuentes, E.; Boháčová, K.; Fuentes-Caparrós, A. M.; Schweins, R.; Draper, E. R.; Adams, D.J.; Pujals, S.; Albertazzi, L., PAINT-ing Fluorenylmethoxycarbonyl (Fmoc)-Diphenylalanine Hydrogels. *Chemistry – A European Journal* 2020, *26* (44), 9869-9873.

McAulay, K.; Ucha, P. A.; Wang, H.; Fuentes-Caparrós, A. M.; Thomson, L.; Maklad, O.; Khunti, N.; Cowieson, N.; Wallace, M.; Cui, H.; Poole, R. J.; Seddon, A.; Adams, D. J., Con-trolling the properties of the micellar and gel phase by varying the counterion in functionalised-dipeptide systems. *Chemical Communications* 2020, *56* (29), 4094-4097.

Fuentes-Caparrós, A. M.; McAulay, K.; Rogers, S. E.; Dalgliesh, R. M.; Adams, D. J. On the Mechanical Properties of N-Functionalised Dipeptide Gels. *Molecules* 2019, *24* (21), 3855.

Fuentes-Caparrós, A. M.; Dietrich, B.; Thomson, L.; Chauveau, C.; Adams, D. J., Using cavitation rheology to understand dipeptide-based low molecular weight gels. *Soft Matter* 2019, *15* (31), 6340-6347.

Fuentes-Caparrós, A. M.; de Paula Gómez-Franco, F.; Dietrich, B.; Wilson, C.; Brasnett, C.; Seddon, A.; Adams, D. J., Annealing multicomponent supramolecular gels. *Nanoscale* 2019, *11* (7), 3275-3280.

List of abbreviations

1D	One dimensional
^{1}H NMR	Proton nuclear magnetic resonance
3D	Three dimensional
Å	Ångström
AFM	Atomic force microscopy
CLSM	Confocal laser scanning microscopy
Cmc	Critical micelle concentration
CRAB	Cavitation Rheology Analyser Box
CSR	Controlled shear rate
CSS	Controlled shear stress
D_2O	Deuterated water
DMSO	Dimethyl sulfoxide
DMSO-d_6	Deuterated dimethyl sulfoxide
E_c	Elastic cavitation modulus
ECM	Extracellular matrix
ECs	Epithelial cells
G"	Shear loss modulus
G'	Shear storage modulus
GdL	Glucono-δ-lactone
H_2O	Water
HCl	Hydrochloric acid
i.e.	Meaning
LMWG	Low molecular weight gelator
LMWGs	Low molecular weight gel
LVER	Linear viscoelastic region
M	Torque
MSCs	Mesenchymal stem cells
PA	Peptide amphiphiles
PAG	Photoacids generator
P_c	Critical pressure
PDMS	Polydimethylsiloxane
PERC	Tetrachloroethylene

PP	Parallel plate
PVA	Polyvinyl alcohol
SANS	Small angle neutron scattering
SAXS	Small angle X-ray scattering
SEM	Scanning electron microscopy
TEM	Transmission electron microscopy
UV-Vis	Ultraviolet and visible
v/v	Volume per volume
δ	Damping factor, G"/G'
γ	Shear strain
γ_c	Critical strain
δ	Phase shift
τ	Shear stress
ω	Angular frequency

Table of contents

List of tables

List of figures

Declaration of authorship

I declare that, except where explicit reference is made to the contribution of others, that this thesis is the result of my own work and has not been submitted for any other degree at the University of Glasgow or any other institution.

Ana María Fuentes Caparrós

CHAPTER 1

Introduction

1.1. Hydrogels

Hydrogels are a class of soft materials consisting of a three-dimensional network structure, which entraps water.[1] Hydrogels can retain large amounts of water, sometimes more than 99% by weight,[2] and still possess properties that are characteristic of a solid.[3, 4] In these materials, two different phases co-exist: a "solid-like" phase responsible for preventing the flow of a "liquid-like" phase. Since the pioneering research on hydrogels in the 1960s,[5] these materials have been extensively investigated due to their extraordinary potential for use in a wide range of applications including cosmetics,[6] environment,[7, 8] agriculture,[9] personal care,[10] medicine[11] and electronics.[12] Hydrogels are viscoelastic in nature; the solid network is responsible for their elasticity, whereas the viscous behaviour arises from the aqueous solution.[13] In addition, due to their high water content, hydrogels are often biocompatible and their biological applications are manifold, including drug delivery,[14] tissue engineering,[15] cell culture[16] and wound healing.[17]

Hydrogels can be made from a wide range of polymers, including synthetic[18,19] and naturally[20] occurring polymers. Hydrogels are also classified as either chemical or physical gels depending on the nature of the cross-linking that forms the gel network. Chemical hydrogels are the result of the cross-linking of polymer chains through covalent bonds, usually making these material irreversible but rendering excellent mechanical strength (Figure 1.1a-I.).[21] In contrast, physical hydrogels, also known as supramolecular gels, are formed when the polymer chains are held together by non-covalent interactions such as hydrogen bonding, hydrophobic interactions and aromatic π-π stacking, making them reversible when an external stimuli is applied (Figure 1.1b-II).[22] In recent years, low molecular weight gels (LMWGs) have emerged as an important class of physical hydrogel. Small building blocks, known as low molecular weight gelators (LMWG), self-assemble through non-covalent interactions to form fibres which entangle to form a supramolecular gel (Figure 1.1b).[4, 23]

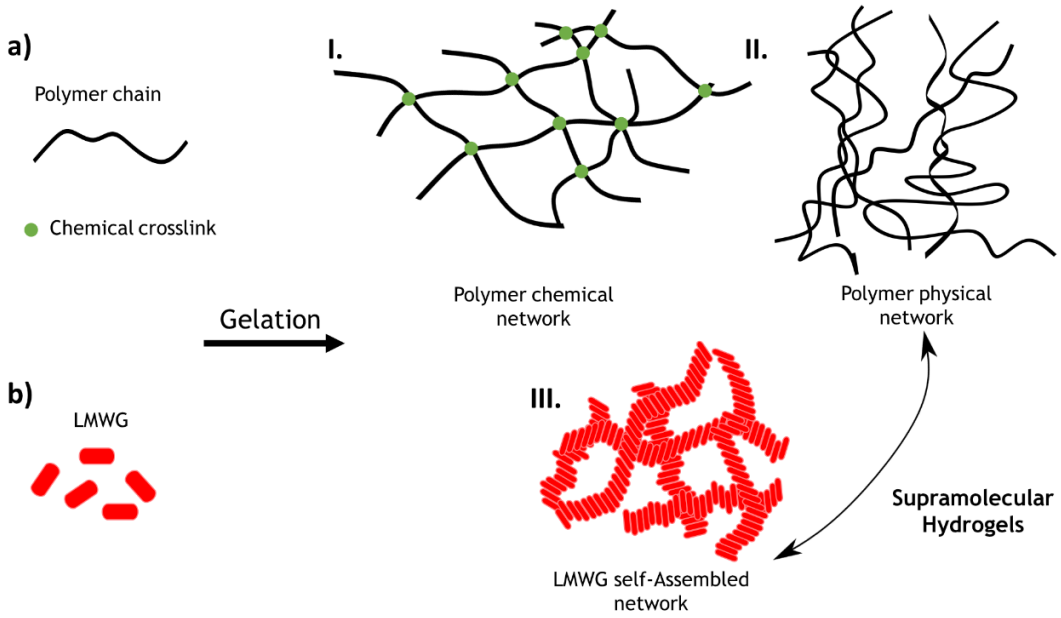

Figure 1.1 Cartoon showing the differences in gelation for (a) polymers and (b) low molecular weight gelators.

1.2. Low Molecular Weight Hydrogels

Recently, interest has emerged in the use of LMWG to form hydrogels. These are small molecules that self-assemble into long anisotropic fibrillar structures through non covalent interactions.[24] Many examples of effective LMWG have been reported over the last years, including functionalised sugars,[25,26] surfactants,[27,28] aliphatic hydrocarbons [29] and peptides,[30,31,32] among many others.[29] Molecules with the potential for directional interactions and with abundant functional groups capable of hydrogen bonding interactions are considered effective gelators. Peptides are widely studied since they are naturally occurring biological molecules that can be found in all living organisms, making them ideal candidates for biological applications.[33] The main difference between chemically cross-linked polymer and low molecular weight hydrogels is that in the latter the gelator molecules interact through non-covalent bonds during assembly, rather than irreversible covalent bonds.[34] In the same way, physically cross-linked polymer gels are formed by a network of polymer chains held together by non-covalent interactions. Comparatively, LMWGs offer advantages compared to polymer hydrogels such as their ease of synthesis, reversibility and their tuneable and stimulus responsive properties.[35]

1.2.1. Self-assembly of LMWG

Low molecular weight hydrogels arise from the self-assembly of LMWG (Figure 1.2). Initially, LMWG are dissolved or suspended in water (Figure 1.2a). Next, a trigger is applied, which lowers the solubility of these molecules, driving the self-assembly of the LMWG into long anisotropic 1D aggregates through non-covalent interactions including hydrogen bonding and π-π stacking (Figure 1.2b).[36] These 1D aggregates are typically nanofibres, nanotubes, nanotapes or helical structures.[4] Although these non-covalent interactions are individually weak, when they work in tandem, self-assembly takes place. At a sufficiently high concentration, these fibres bundle and entangle resulting in the formation of a 3D network that immobilise the water through surface tension and capillary forces (Figure 1.2c).[29,4]

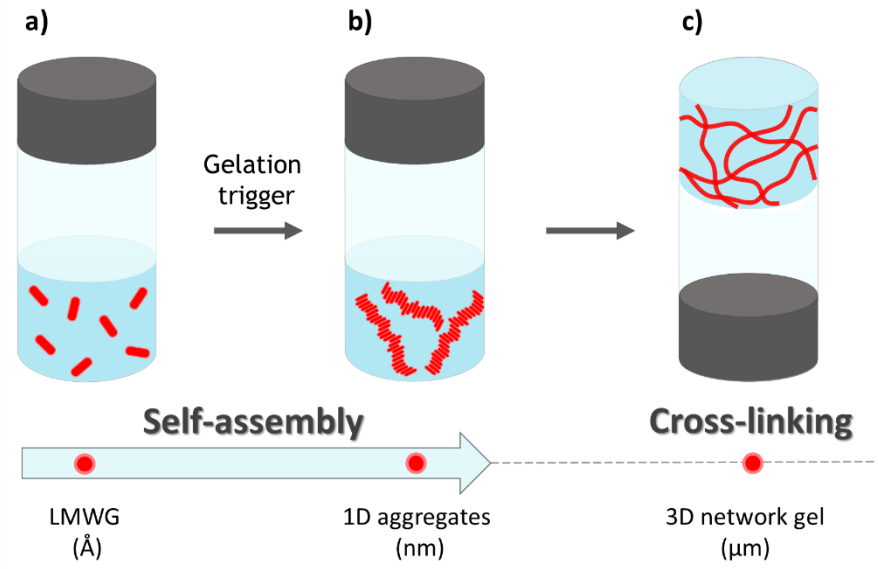

Figure 1.2 Cartoon showing the self-assembly of LMWG via non-covalent interactions. Initially, LMWG are suspended in solution (a) and when a trigger is applied, these molecules assemble leading to 1D fibres-like aggregates (b), which entangle and result in a self-supporting gel network (c). The length scale of each stage is indicated beneath the cartoon.

Due to the diversity of functional groups that can be used for the design of LMWG,[37] differences in properties such as their ability to pack, the number of hydrogen bonds, steric bulk and solubility of the molecules can affect the

intermolecular interactions which promote 1D growth.[34] In the same way, depending on the different interactions between the 1D structures, networks with different morphologies and therefore different properties can result.[34]

As a result of their weak interactions, some supramolecular gels formed from LMWG can recover their original state after being subjected to external forces. Firstly, they undergo a gel-to-sol transition upon stress, i.e., the gel's viscosity decreases with time when stress is applied. The consequent release of stress is followed by a sol-to-gel transition, where the gel recovers the original viscosity if it is left to stand.[38,39] This characteristic is called thixotropy, and make these class of materials excellent candidates as injectable hydrogels due to their ability to recover their original shape after injection.[40] Also, if LMWGs are made from naturally occurring molecules, they can usually easily degrade within the body and be removed after they have completed their function. These hydrogels can be used as scaffolds or as carriers of therapeutic agents in the treatment of diseases and cancers and the repair and regeneration of damaged tissues.[41]

1.2.2. Multicomponent LMWG Systems

In general, LMWGs are used as single component systems. However, there is an increasing interest in the self-assembly of multicomponent systems with the potential of each individual component to endow the gel with a different function.[42-46] In contrast with functional gel systems, where the different functional groups endow the gel with different properties, multicomponent gels go one step further. These systems, in which the two components form a gel by themselves, present the advantage of preparing gels with properties that cannot be accessed with either of the individual components.[47-52] By mixing two components, self-assembly can generate different situations. The molecules may segregate and self-sort, or they may co-assemble (Figure 1.3). In a self-sorting system, the molecules tend to differentiate between self and non-self, such that each fibre contains only one LMWG (Figure 1.3a), or both LMWG are present in the same fibre but have sorted themselves into a pattern (Figure

1.3b). It is also possible that the two different LMWG mix, randomly forming a fibre where different amounts of each LMWG are present (Figure 1.3c).

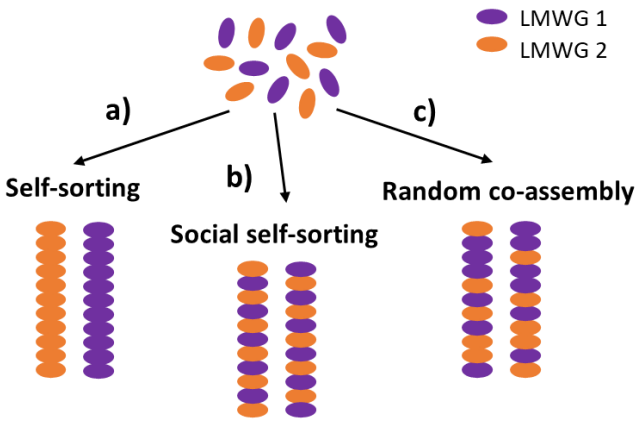

Figure 1.3 Different fibre assemblies that may occur in a two components system. (a) self-sorting; (b) social self-sorting and (c) random co-assembly.

Multicomponent systems present some intrinsic advantages over single-component hydrogels. These multicomponent systems have emerged as a versatile option to design hydrogels with molecular complexity, modulate kinetics of gelation, tune the mechanical properties and generate new materials.[49, 53-58] These properties make multicomponent hydrogels suitable for a wide range of applications including tissue engineering,[59] drug delivery[60] and optoelectronics.[61] For example, Gough and co-workers have shown the ability of a hydrogel based on co-assembly of two peptide amphiphiles molecules to support attachment, spreading and proliferation of encapsulated dermal fibroblasts for extracellular matrix secretion in tissue regeneration.[62] Self-sorting systems have emerged as an exciting strategy to generate bulk heterojuntions for optoelectronic devices. As an example, Shinkai and co-workers have shown that p-n heterojuntions can be formed when electron acceptor and electron donor gelators self-assemble into independent fibres, which then interact and entangle, allowing for charge mobility in the p-n junction.[46]

The design rules for a multicomponent system to self-assemble into a self-sorting or co-assembled system are not well understood. Generally, a system

containing LMWG with different structural motifs encourage self-sorting, whether two LMWG with very similar structures tend to co-assemble.[58] Also, gelators with very different thermal properties encourage self-sorting to occur.[63] The efficiency of driving self-assembly towards a self-sorting system using two gelators with different pK_a values has been described, where a controlled protonation drives the self-assembly sequentially.[43]

Importantly, due to the difficulty of designing new gelators that form gels with specific properties, multicomponent systems have emerged as an alternative that allows to tune several key properties and offer materials with advantageous characteristics.

1.3. Peptide-based Low Molecular Weight Gels

Peptide-based gelators represent a commonly-used class of LMWG. Peptide hydrogels are widely used to construct self-assembling biomaterials and possess a number of advantages that make them particularly effective for this purpose.[64, 65] As opposed to more complex biomolecules like proteins, peptides are feasible and easy to scale. It is possible to construct long sequences of amino acids and easily incorporate different functional groups that will render the molecule greater complexity and functionality.[64] On top of this, peptide hydrogels often degrade into natural amino acids that can be metabolised, which make them ideal for *in vivo* nanomedical applications.[64]

In the early 1990s, Zhang pioneered the use of peptide with alternating ionic hydrophilic and hydrophobic amino acids such as gelators EAK16 and RADA16-I, among others.[66] The amino acids arrangement gives each peptide a hydrophilic and hydrophobic facial character. The hydrophobic interactions between the peptides from the hydrophobic amino acid residues try to “hide away” from the aqueous media, while the complementary charged residues interact with water and form hydrogen bonds and other intermolecular interactions leading to peptide assembly. The amphiphilic character of these molecules leads to the formation of a ß-sheet peptide bilayer, where the hydrophobic side chains

remain in the middle of the bilayer, which lead to the unidimensional growth of fibres and therefore gel formation.[66] The thixotropic character of RADA16-I was proved by subjecting the peptide to mechanical stress, which showed the breakdown of the fibres into fibrous fragments. After the stress was released the fibres reformed back to their original form. Using circular dichroism, Zhang et al. showed no changes in the molecular packing occurred during the exposure to stress, which showed the potential use of these type of molecules.[66] Following the concept developed by Zhang, many other ionic-complementary peptides have been studied.[67] Although the ß-sheet is the most common structure studied in peptide assembly, α-helical peptides that formed nanofibril network hydrogels have also being examined.[68,69]

Schneider and Pochan have successfully developed a series of short amphiphilic alternating hydrophobic and hydrophilic residues with a tetrapeptide ß-turn (V^DPPT) in the middle that change the structural conformation according to external stimuli.[70-74] MAX1 was the first peptide synthesised composed of 20 amino acids consisting of two strands altering valine (V) and lysine (K) residues connected to a V^DPPT (**10.** in Figure 1.4,).[70] In aqueous solution, MAX1 exists as a random coil due to the repulsion between the positively charged lysine residues in the peptide side chain. Under basic aqueous solution conditions, MAX1 coils folds into a β-hairpin due to the less favourable interactions between the positively charged lysine residues. The β-hairpins pack along their hydrophobic faces, forming bilayers that further aggregate and form crosslinked fibrils that result in gel formation. The Schneider and Pochan groups have developed a series of MAX peptides that have shown to be responsive to numerous stimuli including light,[71] pH,[72] temperature[73] and ionic strength,[74] and all of them result in different rheological properties.

Similarly, there are numerous short peptides that can also form hydrogels. One class is that of peptide amphiphiles (PA), which consist of a peptide sequence conjugated to an alkyl tail that gives hydrophobic and hydrophilic regions (Figure 1.4, **9.**). These molecules combine the structural features from the amphiphiles with the functionality of bioactive peptides. In 1995, Tirrell's group

pioneered the research of such class of molecules.[75] His group synthesised a series of amphiphiles containing different peptides derived from extracellular matrix collagen.[75] Since then, Stupp's group has widely investigated PA peptides.[76-78] They demonstrated that the selection of amino acids and alkyl tail will directly yield the formation of different morphologies, surface chemistry and bioactivity in the molecules. This shows the adaptability and functionality of this type of molecules to form hydrogels with tuneable properties.

Over the last decades, shorter amphiphiles peptides have been widely studied. An amino acid or dipeptide conjugated gelators are a class of short amphiphiles molecules consisting of one and two amino acids, typically N-protected with an aromatic group (Figure 1.4, **1-8**). Examples of protecting groups are naphthalene (Nap),[79] fluorenylmethoxycarbonyl (Fmoc),[80,81] cinnamoyl,[82] pyrene,[83] indole,[84] among others.[85] The aromatic groups contribute to the hydrophobicity of the peptide gelators, promoting hydrogen bonding, π- π stacking and Van der Waals forces that are needed for self-assembly to occur. Depending on the nature of the protecting group, redox-responsive, fluorescent and drug delivering hydrogels can be developed.[85] The modification of the N-terminal protecting group facilitate the tuning of peptides self-assembly and, therefore, the resulting hydrogel properties. Dipeptide conjugated hydrogels are the focus of this Thesis.

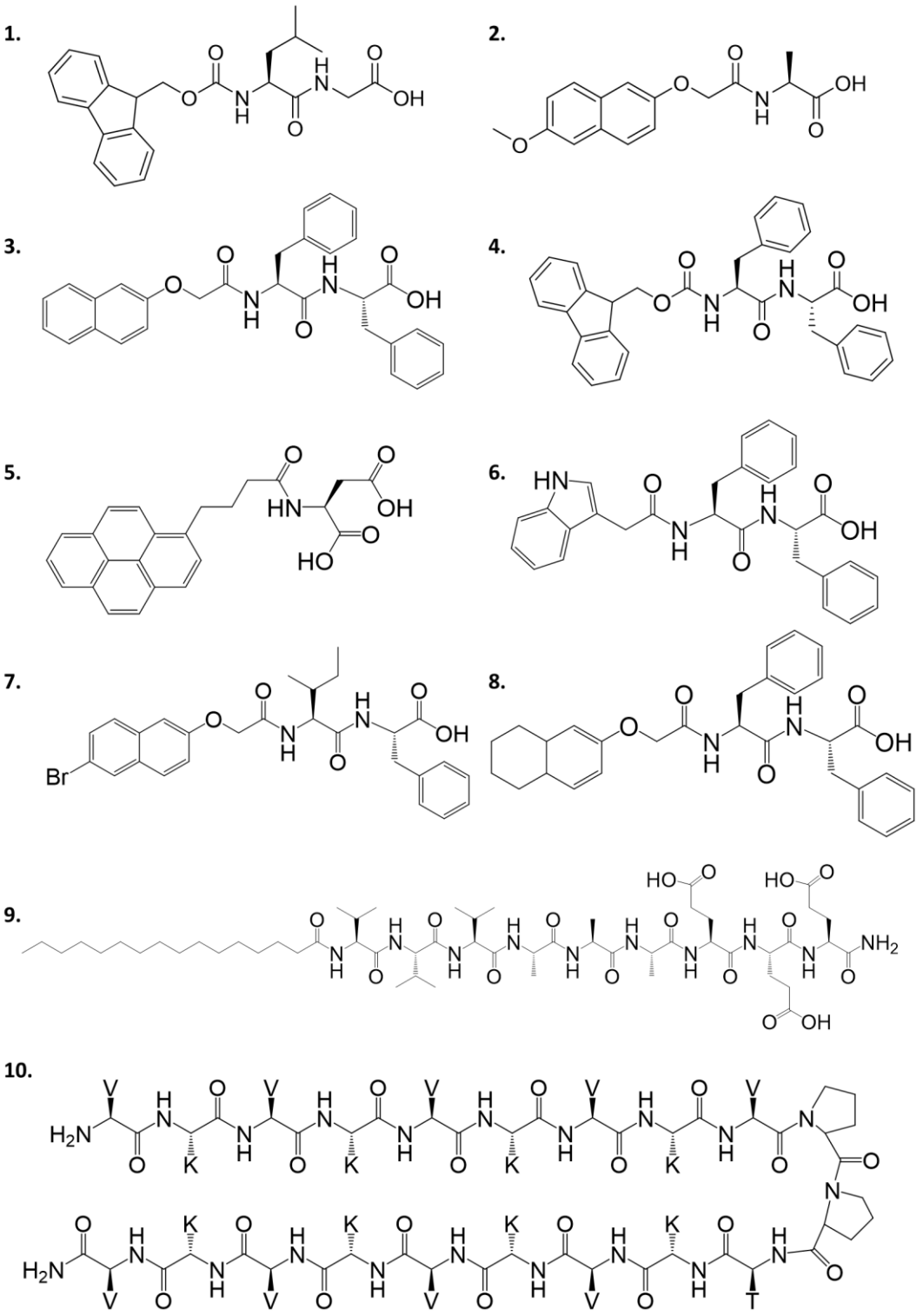

Figure 1.4 Some examples of peptide LMWG.

Fluorenylmethyloxycarbonyl-diphenylalanine (FmocFF) is probably the most studied dipeptide gelator (**4**. In Figure 1.4). Hydrogel made of **4** was first reported by Gazit's[86] and Ulijn's[87] groups and since then numerous researchers have recognised the potential use of this peptide molecule. Gelator **4** forms hydrogels at physiological pH, making this class of materials ideal candidates to be used cell culture or drug delivery. Furthermore, Gazit and co-workers also showed that diphenylalanine (FF) forms well-ordered tubular assemblies with similar structural properties with those of β-amyloid fibrils associated with Alzheimer's disease.[88]

1.4. Gelation Triggers

There are numerous potential triggers reported in the literature to form hydrogels such as changes in temperature[89] or pH,[80] a solvent switch,[74] addition of a salt[85] or enzymes.[94] Notwithstanding the differences between different triggers, all of these operate on the same basis; a stimulus is applied which will encourage the system to dissolve and a subsequent trigger decreases the solubility of the molecules to induce the self-assembly. As will be explained later, the properties of the resulting gels depend on how the gels are formed. As such, gels with different properties can be prepared from a single gelator if different gelation triggers are used.[34] It is even possible that the use of the same trigger causes differences in the gel properties since different methods can be employed.[90] Therefore, it is really important to control the trigger used if the gel needs to meet specific properties for a given application.

1.4.1. Temperature Trigger

A heating and cooling cycle is often used to trigger gelation. Generally, due to their hydrophobic nature, LMWG are insoluble in water at room temperature. If the gelator solution is heated, the gelator solubility increases. On cooling, the solubility is reduced once again, driving the self-assembly of the gelator molecules.[89] Although this is one of the simplest methods to form a gel, the resulting gel properties can sometimes lack reproducibility.[91] This is likely to

be a consequence of the differences in cooling rates through the hydrogel sample. In the same way, the rate at which the temperature is reduced will affect the kinetic of aggregation and, therefore, the resulting properties of the gel.[92] Instead, a heating and cooling approach is often reported as a way to tune the mechanical properties post-gelation.[93,94,95,96]

1.4.2. Solvent Trigger

The use of a solvent trigger is very common to activate gelation.[86, 90, 97] Due to the hydrophobic nature of the LMWG, these are insoluble in water. As such, the gelator molecules are firstly dissolved in a suitable water-miscible organic solvent. This solution is then diluted by the addition of water, which lowers the solubility of the gelator molecules and forces the self-assembly into 1D fibril aggregates.[86] Occasionally, upon addition of water, a turbid solution is formed that clarifies over time as the gel forms. Chen *et al*. interpreted this process as a phase separation occurring initially before the gel is formed.[94] Firstly, there is a transition to a non-equilibrium state where nucleation centres are formed (Figure 1.5a). Consequently, nucleation takes places and the fibres arise from the surface of the spheres (Figure 1.5b), expanding into the solution and thus forming a spherulitic multi-domain fibre network (Figure 1.5c).[98]

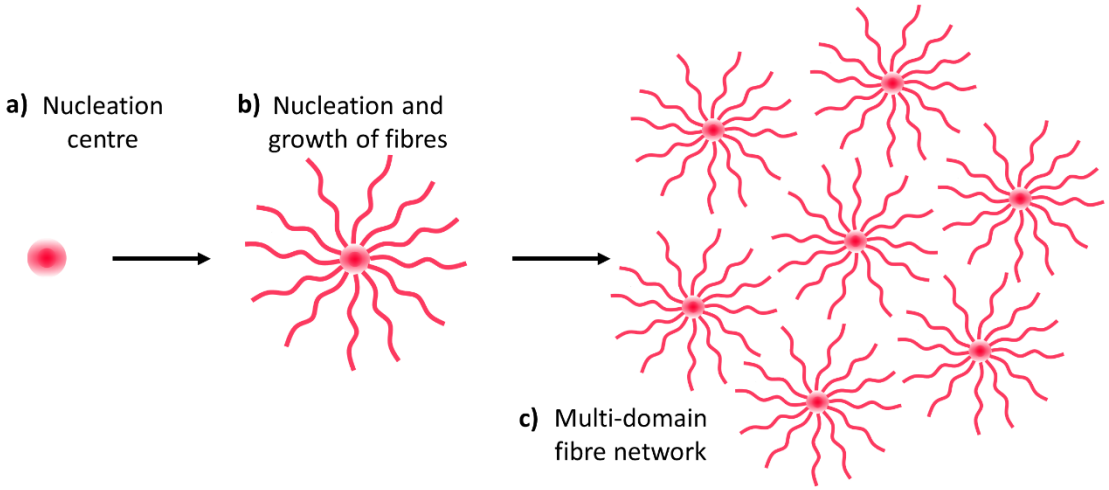

Figure 1.5 Schematic representation of a multi-domain fibre network formation through the nucleation and growth of fibres when a solvent trigger is used.

The final gel properties depend upon the water:solvent ratio, the gelator concentration and the nature of the organic solvent used.[86, 90] It may happen that only a specific solvent or a range of different solvents will be suitable for gel formation. This will depend on the interactions between the solvent and the gelator molecules.

The use of this method is widespread due to the ease of preparation and the quick gelation times. Sometimes only few seconds are needed for a gel to form using a solvent-triggered approach, as it is the case for peptides **7** or **8** (Figure 1.4),[99] compared to the slow gelation when using a pH trigger, that can take few hours to complete gelation.[100]

1.4.3. pH Trigger

A pH trigger is a widely used method to prepare hydrogels from LMWG. The cooperation of charged interactions during the self-assembly process, makes many LMWGs intrinsically pH responsive. Therefore, the solubility of the gelator molecules is also pH dependent. For dipeptides, the *C*-terminus (carboxylic acid) is deprotonated at a pH above the apparent pK_a, so the gelator molecules can be solubilised in water under these conditions (Figure 1.6a). If the pH is then lowered below the apparent pK_a, the *C*-terminus is re-protonated reducing the solubility of the LMWG, thus activating the self-assembly of the gelator molecules into fibres that form a hydrogel (Figure 1.6,b-c). Some LMWG can form surfactant-like aggregates at high pH. As a result, a high viscosity solution is formed, but typically no gelation occurs unless the pH is lowered.[101] This is, gelation will only take place when the pH of the solution is below the pK_a and thus, the molecules will start to protonate, driving the assembly of the molecules into the long fibres.

Lowering the pH to trigger gelation can be achieved by different methods. The addition of hydrochloric acid (HCl) to lower the pH has been extensively used to form hydrogels.[102,103,80] Xu's group reported the use of HCl to lower the pH and trigger gelation for a series of naphthyl-protected dipeptide based

hydrogels.[79] The dipeptides were suspended in solution at high pH to deprotonate the *C*-terminus. A small volume of HCl 1M was added until gels were formed.[79] Ulijn's group demonstrated in 2006 that a number of Fmoc-dipeptides also formed gels by lowering the pH using HCl, including **4**.[87] Hydrogel made of **4** has the highest pK_a value of any dipeptide conjugate gelator reported so far in the literature, with a pK_a of around 9.9.[104] Because of this high pK_a, hydrogels can form at physiological pH, which make them of interest in many biological applications.[86, 87, 105-107] Later, Adams et *al*. showed that the use of hydrochloric acid to trigger gelation of a Fmoc dipeptide gel resulted in inhomogeneous turbid gel network. This behaviour was associated to the differences in kinetics of mixing HCl being slower than the initial kinetics of gelation.[100] As an alternative, Adams et *al*. reported the use of glucono-δ-lactone (GdL) to control the pH in dipeptide gels.[100] GdL slowly hydrolyses in water to gluconic acid. The dissolution of GdL is quicker than the hydrolysis to gluconic acid, which result in a slow decrease in pH, this allowing to form a visibly more homogeneous hydrogel. Since then, this method has been extensively used. [108-114]

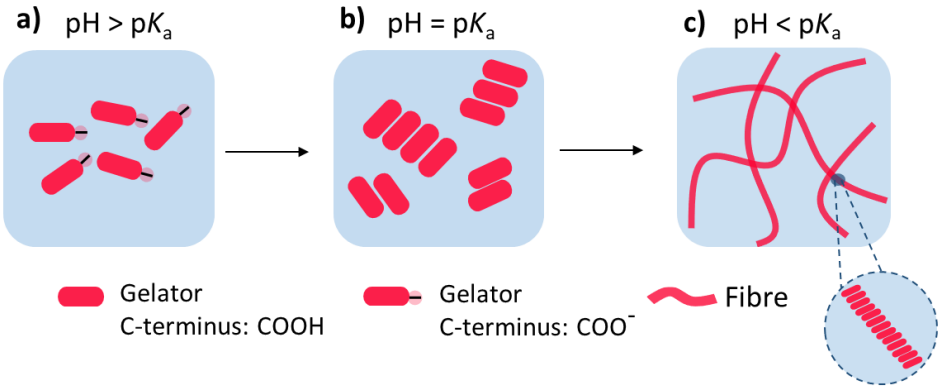

Figure 1.6 Schematic representation of self-assembly when pH is lowered; (a) At high pH the C-terminus is deprotonated and the gelator can be solubilised in water under these conditions. It is important to note that numerous gelator molecules can be dispersed as a surfactant-like aggregate above the pK_a. (b) When the pH reaches the pK_a value, the gelator molecules start to self-assemble. In the case of surfactant aggregates, these are disrupted and self-assembly also starts to occur. (c) Further decrease in pH leads to the formation of fibres that entrap the solvent and form the gel.

Alternatively, the use of photoacid generator (PAG) can also be used to lower the pH of a solution. Upon UV light exposure, PAG molecules dissociate into acidic species, which will allow to drop the pH and therefore form a gel.[112, 115] This method allows gel patterning since UV light can be applied in specific areas rather than applying the trigger to the bulk sample, as happens when using GdL or HCl. As such, this method has potential for use in cell differentiation.[116]

1.4.4. Salt Trigger

The use of metal ions have been extensively used as a way to trigger gelation in a wide range of peptide based LMWG.[94, 117-120] Numerous peptides including some naphthalene dipeptide gelators,[108] a carbazole protected dipeptide[121] and a Fmoc protected dipeptide (**4** in Figure 1.4)[115] at a high pH, and when the molecules concentration is above the critical micelle concentration (cmc), it leads to the aggregation of the gelator into worm-like micelles. Chen et al. have shown the aggregation of a range of naphthalene functionalised dipeptides into worm-like micelles at high pH (for example **3** in Figure 1.4).[94] The model proposed suggests that the naphthalene protecting group and the hydrophobic amino acids are driven away from water, thus forming the core of the micelles, with the carboxylates stabilising the micelles in solution (Figure 1.7a). When divalent cations Ca^{2+} are added, carboxylates are attracted by the positively charged Ca^{2+}, this bringing together the worm like micelles and crosslinking to them through the negatively charged carboxylates (Figure 1.7b). The crosslinking results in the gel formation.

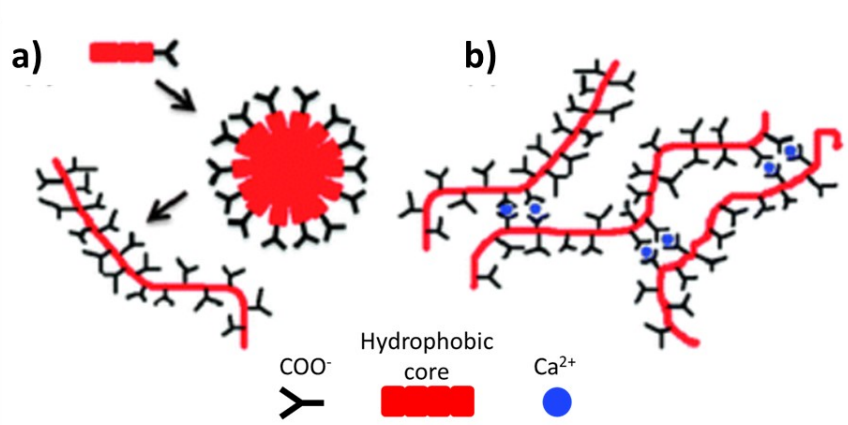

Figure 1.7 Schematic representation of a) the assembly into worm-like micelles and b) the cross-linking of the micelles through the metal ion to form a network. Adapted from ref. [94].

1.4.5. Enzyme Trigger

In nature, self-assembly is often under the control of enzymatic reactions.[122] As such, enzymes can be used as a catalytic tool to convert a non-gelling precursor molecule to a self-assembling gelator. Generally, there are two possible modes of enzymatic hydrogelation, this is by either breaking or forming bonds.[123] In the former, the attachment of a hydrophilic group to the gelator molecule forms an ideal soluble precursor. Then, if the hydrophilic group is removed by the action of an enzyme-catalysed bond cleavage, the precursor is converted back to an efficient gelator capable of self-assembly (Figure 1.8a). The groups of Xu and Ulijn have extensively used this method of self-assembly.[80, 122-125] They use a phosphorylated tyrosine as the cleavable side and by addition of alkaline enzyme, dephosphorylation takes place, which makes the molecule insoluble, driving the self-assembly and hydrogel formation. The other method consists of an enzyme-catalysed reaction, where the two soluble precursors are linked together and form an efficient gelator (Figure 1.8b).[126] The advantage of using enzymatic triggers is that they are highly specific and can exhibit selective response to different environments.[127]

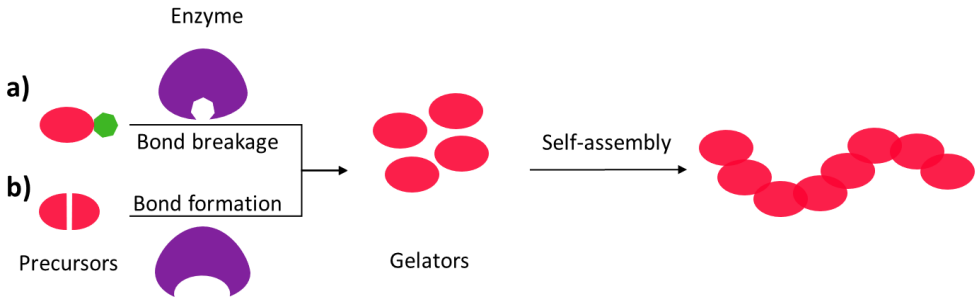

Figure 1.8 Schematic representation of enzymatic self-assembly via (a) bond cleavage and (b) bond formation.

Naturally, the final properties of the gel will not only be affected by the choice of the LMWG, but also by the process by which gelation is triggered.[34] Even using the same trigger of gelation, different methodologies are required and gels with different properties can result.[42]

1.5. Mechanical Properties of LMWGs

Low molecular weight hydrogels have emerged as a promising class of soft materials due to their extraordinary properties. By virtue of their inherent reversibility, dynamism and vast range of mechanical properties, LMWGs are suitable for a wide range of applications.[8, 128-131] In general, for any material, the understanding of mechanical properties is key in determining whether these materials are potentially suitable for specific applications.

The mechanical properties of gels prepared from LMWG are controlled by the kinetics, the nature of the gelator molecules and the assembly environment (pH, solvent, temperature, etc.). Hence, it is possible to prepare gels with a wide range of mechanical properties if we can control these parameters. The diversity in mechanical properties can be exploited to access different materials on demand. This is one of the main reasons why hydrogels are appealing in biomedical applications, as a result of their ease to mimic human tissue.[132] For example, if the hydrogel is going to be used for controlled release, it is important that we can control the pore size, as it plays an important role to control if small molecular or macromolecular drugs can be trapped as well

as the rate of release.[133] In the same way, the rigidity of the hydrogel plays an important role if it is to be used as a scaffold for cell growth where stiffness is essential for cell adhesion and survival.[128] Recently, Cross *et al*. have also shown the importance of the hydrogel stiffness to control the antimicrobial activity of a LMWG.[134]

The understanding and tuneability of LMWGs mechanical properties are of growing interest. It is therefore important to understand the mechanical properties of hydrogels at different length scales as well as their tuneability to access mechanical properties on demand.

1.5.1. Mechanical Properties Across Multiple Length Scales

For gelation to occur, self-assembly of LMWG involves inter- and intra-molecular interactions across multiple length scales.[54,154] Firstly, molecular interactions drive the self-assembly of the gelator molecules into 1D aggregates through non-covalent forces such as hydrogen bonds, hydrophobic forces and π-π stacking. The 1D nanostructures formed can be vesicles, micelles but are most commonly fibrillar structures (fibres and nanotubes). At the next level, the resulting fibres crosslinks to form the microstructure through entanglement or branching of the fibres. These crosslinks are non-covalent in nature, which allow the reversibility of the system. Therefore, the mechanical properties of supramolecular hydrogels are controlled by multiple parameters across multiple length scales.[154]

The mechanical properties of the bulk gel arise from the properties of the single fibres and their thickness, the degree of entanglement, number and types of crosslink, how the fibres are arranged across the whole network, the interaction with the media and the homogeneity or lack thereof of the network.[135] The self-assembly process governs all these parameters. Firstly, the nature of the gelator molecule will control the intermolecular interactions that drive the assembly into 1D aggregates, which partly control the properties of the resulting gel.[135] Numerous researchers have shown how subtle changes in the

gelator molecule can dramatically affect the resulting gel properties.[99, 136, 137] The mechanical properties of 1D fibres can be assessed using atomic force microscopy (AFM). Many researchers have studied the mechanical properties and morphology of fibres at the nano-scale using AFM technique.[138,139,140] However, the mechanical properties do not just depend on the molecular structure and the intermolecular interactions, but also on the degree of crosslinking, i.e., how the fibres interact. The microstructure of the gel can be described by the distribution of fibres and the way they crosslink.

Typically, the crosslinking of the fibres can be either entanglement or branching,[141] but it is also possible to find different branching and entanglement of fibres in the same gel network.[141] One class of microstructure is the one where a dense network of fibres is present.[142] Other type of fibre networks can give rise to spherulitic patterns.[142] In the latter, there is an initial nucleation of the gelator molecule, followed by growth of fibres. As such, the system results in multi-domain fibre networks.[108] In Chapter 3, we show a comprehensive study of the effect that different microstructures has on the resulting mechanical properties at different length scales using different characterisation methods. We have also shown previously the importance of characterising the differences in the microstructure, as it governs their ability to be used in 3D printing, for example.[143]

1.5.2. Importance of the Kinetics During Self-Assembly

The self-assembly is considered a non-equilibrium process[144] in which the system moves from a "highly soluble state" toward a "less soluble state", this implying a high kinetic dependence. Self-assembly is based on the synergistic effect of various non-covalent interactions, which will determine the thermodynamic stability and the state of minimum energy of the resulting structure. These non-covalent forces are relatively weak in nature, and as such they can be easily modulated with different kinetic parameters including temperature, pH, concentrations, solvents, etc. Therefore, the resulting self-assembled structures may not reach the thermodynamic equilibrium but rather

they will be trapped in a kinetic state (Figure 1.9, states #1 and #2).[145] This can lead to kinetically favoured outcomes which are permanently or temporarily stabilised at a local minimum of the free energy landscape. The permanently stabilised state is known as the kinetically trapped state (Figure 1.9, state #2), while the temporarily stabilised state corresponds to a metastable state (Figure 1.9, state #1). The latter can convert into a thermodynamic state over time without the intervention of kinetic parameters. Although the kinetic trapped state possesses higher energies, the energy barriers between the thermodynamic minimum and the kinetic trapped state are relatively low. Thus, by input of external stimuli it is possible to move between different energy states, this allowing the fabrication of responsive and adaptive materials. Intrinsically, a kinetically trapped product will differ from the thermodynamic counterpart in their structure and properties, but will still possess the same compositions.[135, 145, 146]

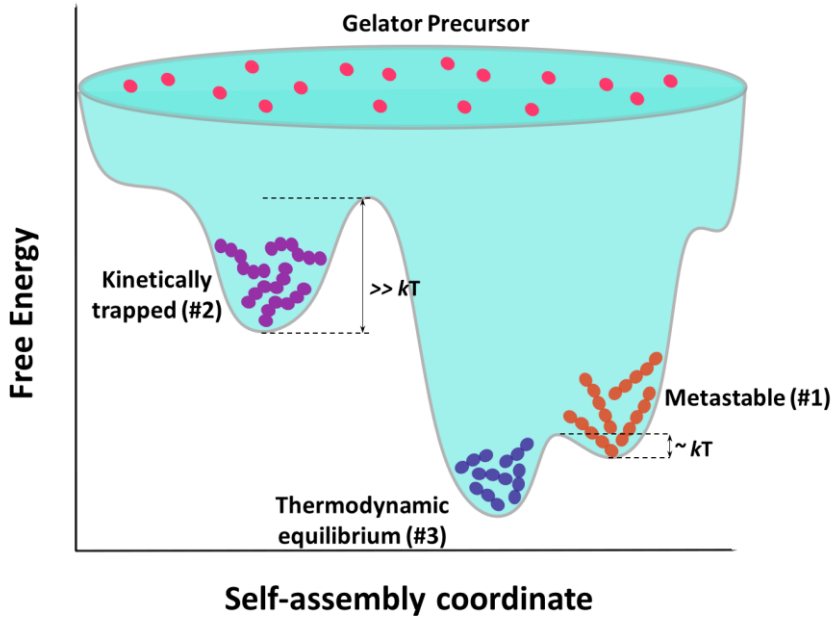

Figure 1.9 Schematic of a free energy landscape showing the different thermodynamic states that a precursor can reach during self-assembly.

In this context, the competition between thermodynamic and kinetic states of assembly provides the opportunity to transform from thermodynamic control to kinetic control, allowing the system to stay in a kinetically trapped state. As

such, materials with different properties can be prepared from the same precursor depending on the assembly pathway kinetics.[34] Kinetically trapped states provide opportunities to prepare materials with different properties from the same gelator depending on the method used to access the different states.

1.5.3. Tuneability of Mechanical Properties

Although a large number of effective gelators are known, to date it is still difficult to predict which gelator molecule will form a gel and which will not.[60] Furthermore, predicting what the properties of the resulting gel will be is still uncertain. Therefore, an efficient approach is to find robust LMWG and by use of kinetic parameters, tune their properties into the desired characteristics. The kinetic factors will influence the thermodynamic interactions between the gelator molecules and with their environment. This is very useful, as depending on the final application, gels with different mechanical properties are needed. As such, careful selection of gelator molecule and concentration, self-assembly method, solvent choice, gelation temperature, as well as other parameters, can be crucial to control the final hydrogel properties.

1.5.3.I. Influence of precursor concentration

Prior to self-assembly, some LMWG form colloidal aggregates at high pH. In this case, hydrophobic and electrostatic forces may dominate and lead the gelator to form micellar aggregates. These aggregates can be spherical structures or worm-like micelles. [101, 147] For example, for a specific naphthalene dipeptide, Adams and co-workers have shown the formation of different structures when the concentration of the gelator was increased for a specific dipeptide.[148] Initially, at a critical micelle concentration (cmc) at low concentration, spherical domains were formed. Then, when the concentration of the gelator is increased, there is a second cmc where worm-like micelles are formed. If the concentration is increased further, the worm-like micelles turn to liquid crystals. The different structures are likely to influence the resulting mechanical properties of the gels formed from these solutions.

1.5.3.II. Influence of the gelation trigger choice

In recent years, the effect that changing the trigger of assembly has on the resulting gel mechanical properties have been reported.[34] Different triggers can be used such as heat-cool cycle, changes in solvents or pH, application of light and addition of an enzyme, among others. All of these result in different kinetics of assembly and, as such, gels with different properties can be made from the same LMWG.[149] Colquhoun et al. have shown that using three different triggers to form gels from **5** (Figure 1.4), resulted in differences in the structures formed and, therefore, differences in the mechanical properties.[34] This is a clear example of how changing the self-assembly process have an effect on the different pathways the system can undergoes, thus affecting the kinetics of assembly and resulting in hydrogels with different mechanical properties.

Likewise, even when using the same trigger, different methods are possible. A pH trigger can be performed following different methods as mentioned earlier in this Chapter.[100, 42, 115, 150] There have been examples were acids such as HCl have been used to lower the pH.[79,80] However, inhomogeneous gels were obtained due to the kinetics of mixing HCl being different to the kinetics of gelation.[100] Alternatively, the hydrolysis of GdL to gluconic acid have been extensively used as it slowly decreases the pH, resulting in reproducible hydrogels.[100] Additionally, the use of different anhydrides that hydrolyse to give acids, has also been shown to result in differences in the final gels properties.[151] In the same way, for gels made using the addition of a salt, the nature of the salt added can affect the mechanical properties. For example, for gels formed from **5 (**Figure 1.4), when monovalent cations are used, less stiff gels result than if divalent cations are utilised. These changes are attributed to differences in the charge affecting the ability of the micelles to bind together.[152]

1.5.3.III. Influence of solvent choice

Similarly, the choice of the organic solvent in which the gelator is initially dissolved when using a solvent trigger affects the outcome properties.[90,86] This can be explained by the fact that different solvents, each of which have specific solubilities, will trigger different rates of mixing between the solvent and the water. In the same way, varying the ratio of solvent:water will result in different rates of assembly. As such, different kinetics will drive the assembly process, resulting in gels with different properties.[90,86] Mayans et *al*. have shown how depending on the solvent:co-solvent conditions, molecules of a series of peptide gelators organise themselves in different ways, resulting in materials with different microstructures.[153] Similarly, He and co-workers have demonstrated a structural transition of self-assembled diphenylalanine peptide from microtubes to nanofibres by progressively introducing an organic solvent to the water phase.[154] Raeburn et *al*. demonstrated the tuneability of the rheological properties of Fmoc-diphenylalanine by varying the solvent conditions.[90] They used four different solvents, in which the resulting primary fibres were very similar in all cases when water was added, but the fibres arrangement was controlled by the solvent choice. This allowed control of the mechanical properties of the resulting hydrogels.

1.5.3.IV. Influence of Temperature

There is also a great potential to use molecules sensitive to temperature to control the mechanical properties of hydrogels.[155, 156] Pochan and co-workers have shown that the degree of folding and ß-sheet formation of MAX1 is dependent on temperature.[156] Below 25°C, MAX1 is in a random coil state, however when the temperature is above 25°C, a ß-sheet structure results. Rheological data show the differences in stiffness of the resulting gels at 20 and 37°C. Chen et al. have also shown the temperature dependence of the apparent p*K*a for a particular naphthalene dipeptide.[108] They have shown a linear relationship between p*K*a and temperature, where the apparent p*K*a decreased as the temperature of the solution was increased. This implies that there is a

the reduction in the interactions between the dipeptide conjugates as the temperature is increased.[108] Recently, Ulijn and co-workers have demonstrated that a range of architectures with different rheological properties can be formed from the same peptide molecule by simple controlling the pre-assembly temperature.[157] Given that the different non-covalent interactions involved during assembly possess different temperature dependencies, they tuned the different assembly pathways by varying the thermal history.[157]

Alternatively, using a heating-cooling cycle, also known as annealing, to a gel has been widely used as means of changing the physical properties of gels after gelation has occured.[94, 96] LMWGs are often kinetically trapped (see above), and as such annealing can be used as means of driving towards the, or at least, thermodynamic minimum. By controlling the rate of heating and cooling, the final gel properties can be tuned.[158] Numerous researchers have shown the tuneability of gel properties by using an annealing approach in single component systems. [95, 96, 158] However, annealing multicomponent systems should allow to prepare gel with properties that cannot be achieved with either individual components. In Chapter 2, we report for the first time the use of an annealing approach on a multicomponent system of LMWG.

1.5.3.V. Influence of pH

The self-assembly process itself comprehend charge interactions, making LMWGs responsive to pH. Therefore, the solubility of the gelator molecules will be pH dependent. Becker and co-workers reported the influence of initial pH on hydrogel formation for a peptide-functionalised oxime gelator.[159] They prepared a series of buffers at different pH values and observed that the stiffnesses of the resulting gels were different. They found gels were nearly 50 times stronger at an initial pH of 4.5 compared to pH 7.4. The differences in the mechanical properties are related to the density of the cross-link in the gel, which is determined by the nature of the different functional groups of the gelator molecules at different pH values.[159] In the Adams group, hydrogels formed from dipeptide **5** (Figure 1.4) have been extensively investigated.[34, 148,

[160] Different methods have been successfully used to trigger gelation in this particular gelator.[34, 148] Particularly, when a salt-trigger is used to form the gels, differences in the resulting rheological properties have been observed.[34,148] These differences in the mechanical properties have been attributed to differences in the initial pH of the solution before the salt was added. The initial pH was adjusted to 12.6[34] and 10.5[148] before gelation and $Ca(NO_3)_2$ was added under the same conditions in both cases, however gels with different stiffness were formed. Recently, Cross et al. presented a method to trigger gelation of a dipeptide-based LMWG by lowering the pH via the oxidation of dopamine.[161] They were able to control the stiffness of the gel by modulating the initial pH of the gelator in solution. Interestingly, a linear relationship was found between the gel stiffness and the pH of the starting solution.[161]

1.5.4. Getting a Real Insight into the Gel Properties: The Influence of Using Multiple Techniques to Characterise Gel Properties

In the sections above, we have discussed the tuneability of hydrogel properties by varying different parameters prior and post gelation, which highlights the importance of controlling the gelation conditions to get gels with reproducible properties. When it comes to characterisation, gels are subjected to different characterisation techniques in order to give a full understanding of their properties. Some of the most common techniques used to fully characterise gels include rheology, nuclear magnetic resonance (NMR), ultraviolet-visible spectroscopy (UV-Vis), microscopy techniques such as transmission electron microscopy (TEM), scanning electron microscopy (SEM), atomic force microscopy (AFM), confocal laser scanning microscopy (CLSM), as well as small angle neutron (SANS) and X-ray (SAXS) scattering. All these different techniques demand specific working conditions.[54, 162]

NMR and SANS, for example, most often involve the use of deuterated solvents. For hydrogels, self-assembly is driven primarily by hydrophobic interactions and hydrogen bonding.[29] Therefore, swapping between D_2O and H_2O may have a

direct effect on hydrogen bond strength[163] and hydrophobic interactions.[164] Hamley *et al*. observed the consequences of H/D isotopic substitution on the size of the primary structures and mechanical properties of the resulting network.[165] Grant et al. showed the enhancement in the modulus of agar gels when replacing H_2O with D_2O using AFM nanoindentation.[166] Similarly, Sabadini and co-workers also reported the increase in modulus when gels of k-carrageenan were prepared in D_2O compared with H_2O.[167] Most recently, McAulay *et al*. have also reported the effect of isotopic changes on the properties of a series of LMWGs.[168]

Furthermore, some microscopy techniques involve drying of the material prior to analysis. Recently, Mears *et al.*[169] showed the effect of drying gels using small-angle neutron scattering. They found significant differences in the scattering pattern before and after drying a number of different LMWGs.

Similarly, for all the techniques named above, each one typically uses specific container sizes and shapes in which the samples are prepared. Despite the many discussions on characterisation techniques for hydrogels,[54, 170-173] the fact that gels are made in different sizes/shapes has not received attention. We consider this could also control the hydrogel network growth and, therefore, affect the final properties.

All of the above suggests that care needs to be taken when characterising hydrogels using multiple techniques. Ideally, we should prepare the gels under the same conditions and be able to fully characterise them. However, this can be very difficult and tedious as depending on the instrument different container sizes, amounts of gels and different solvents are needed.

1.6. Characterisation of The Mechanical Properties Across Multiple Length Scales

To characterise soft materials such as hydrogels, a variety of techniques have been developed and used from bulk scale to the micro/nano scale. Shear

rheometry, or bulk rheometry, is probably the most widely used technique. This technique allows one to characterise the mechanical properties of bulk materials, thus avoiding inhomogeneities issues. However, this technique requires millilitre sample volumes and with specific shapes, which can be difficult when only small volumes of gel are available, as is the case in biological sciences. Microrheology is another technique that can be used to characterise the mechanical properties of hydrogels. This is also known as the rheology in the micrometre length scale. This approach could overcome some of the limitations of oscillatory shear rheology. This technique measures the mechanical properties on very small volumes (on the order of micro-litres) via the measurement of the trajectory of particle probes.[174] The use of a local probe allows for characterisation in a local point. This is advantageous as it could be used in heterogeneous systems, where oscillatory shear rheology just gives an average distribution of the bulk material.[175] However, one of the drawbacks of this technique is that the use of probe particles may cause changes in the local microstructure being measured, and as such only very soft materials could be measured in order to get reliable data.[176] Nanoindentation is another powerful technique that allows mechanical analysis down to the micro/nano scale.[177] This is advantageous, as it allows for region-specific mapping of hydrogels inhomogeneity. Another advantage is that there is any restriction regarding the size or shape of the material to be analysed, which avoids special preparation of gels samples. However, this technique only allows to probe the surface mechanical properties.[177] Cavitation rheology has emerged as a powerful alternative to these techniques.[178] This new technique allows for mechanical properties characterisation at the micrometre scale, in gels of any shape and size. Although numerous techniques have been presented in this section, we will just focus on few of them given their relevance in this thesis.

1.6.1. Oscillatory Rheology

Rheometry is the most extended method used for researchers to explore the bulk viscoelastic properties of hydrogels. The mechanical properties can be assessed by quantifying the response of our bulk material when a deformation

is applied.[179] Normally, the two-plates model is used to describe the parameters involved in the deformation of a viscoelastic material (Figure 1.10). During measurements, the upper plate is moving, while the lower plate is kept stationary and the sample is sandwiched between the two plates. For a controlled strain measurement, for example, a shear strain (γ) is applied in a sinusoidal oscillation and the resulting shear stress (τ) is a phase shifted sine wave (δ) under angular frequency (ω) (Figure 1.10). For an elastic material $\delta = 0$, while in a viscous deformation $\delta = 90°$. For hydrogels, the viscoelastic deformation will take place in a phase shift in between these values.[179,180]

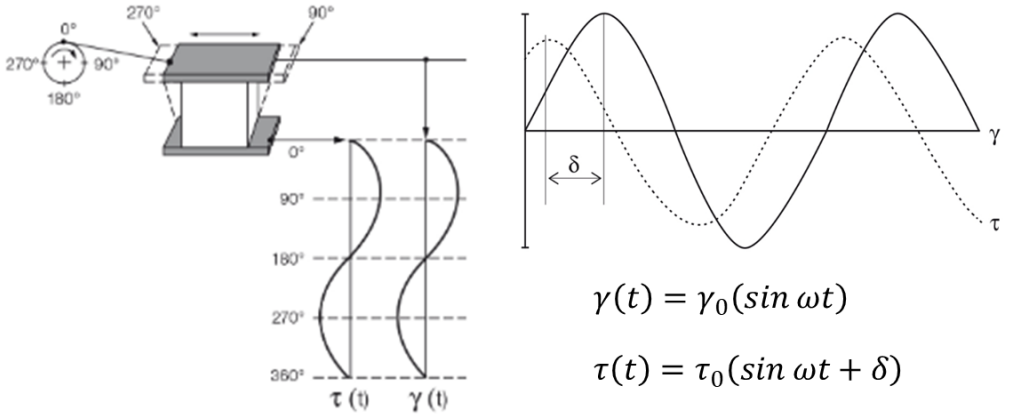

Figure 1.10 Viscoelastic model behaviour where the sine curves for shear strain γ and shear stress τ show a phase shift δ. Figure adapted from Ref. [181].

During oscillatory shear measurements, the shear storage (G') and loss (G") moduli can be monitored over strain, frequency, time or temperature. The G' is a measure of the deformation energy stored, i.e. the stiffness or how solid-like the material is, while G" is a measure of the deformation energy, i.e., how liquid-like the material is.[179] A true gel is considered when G' is an order of magnitude greater than G", or, phrased differently, when the ratio of loss energy to stored energy (tan δ = G"/G') is less than 0.1.[23]

Different tests can be carried out to fully characterise the rheological properties of hydrogels. For example, we can measure the evolution of G' and G" over time and, as such, monitor the gelation kinetics (Figure 1.11c). If

instead we monitor both moduli against strain keeping frequency constant, we can characterise the linear viscoelastic region (LVER), where the hydrogel properties are independent of the magnitude of strain applied. We can also determine the strength of our gel; this is the G' corresponding to the strain at which G' and G" start to deviate from linearity, also known as critical strain (γ_c), (Figure 1.11a). In a different experiment, both moduli are measured over frequency (Figure 1.11b).

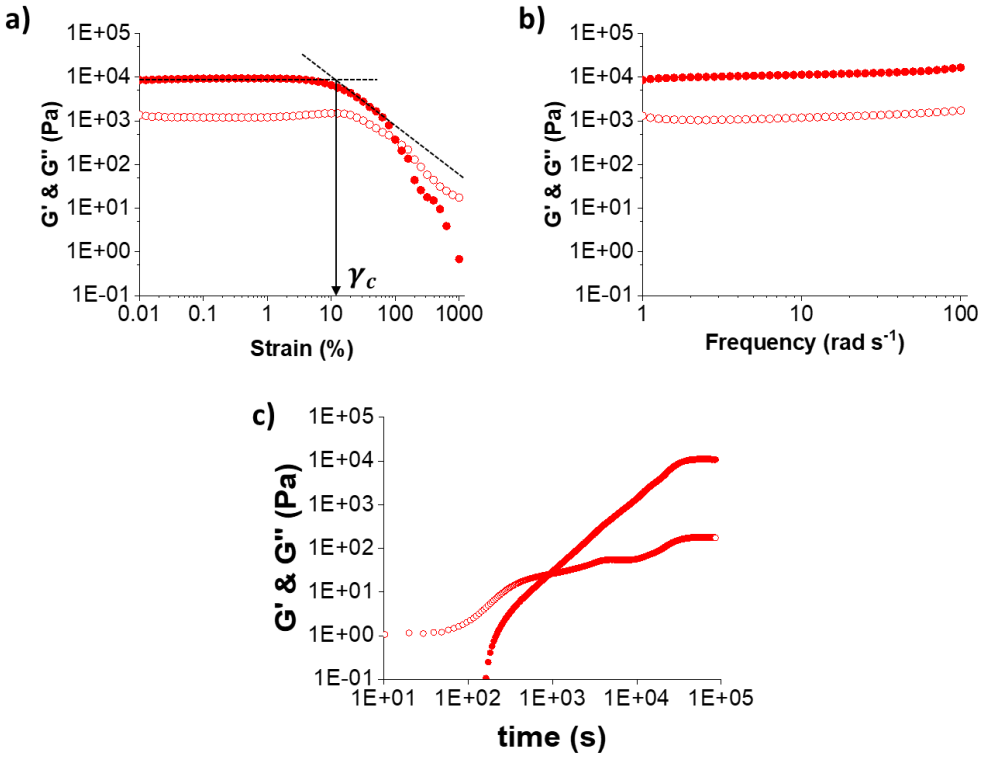

Figure 1.11 Examples of different tests that can be carried out using oscillatory shear rheology. (a) Strain sweep showing the critical strain at which the material breaks; (b) frequency sweep showing the frequency independence of such class of materials and (c) time sweep showing the kinetics of gel formation. In all cases, closed symbols represent G' and open symbols represent G".

Different geometries can be used for rheological measurements, this includes vane (Figure 1.12a) and parallel plate, PP, (Figure 1.12b) among many others. The vane geometry has blades and a flat surface that sticks out into the sample and that pushes the material as the blades move. The vane geometry is

advantageous for measuring heterogeneous samples that may slip using the parallel plate. However, the shear stress applied using this system may be undefined as the distance between the vane blades and the wall container (R_c – R_v) in which the gel is being measured, increases (Figure 1.12aI).[182] During measurements, the vane delineates a path along which the stress applied is inversely proportional to the square of the radius (Figure 1.12c).[182] Inside the limits defined by the vane blades radius (R_v), the material moves guided by the blades. However, the stress decays gradually outside these limits (Figure 1.12aII). Differences in the radius between R_v and the wall container (R_c) will therefore have an effect on the calculated rheological parameters (Figure 1.12c). Similarly, the position of the vane during measurements can affect the rheological properties being measured. Differences in the vane position will determine the height/thickness of gel touching the vane blades and, therefore, the rheological parameters measured. The vane geometry is a relative system and therefore the calculated rheological properties are "apparent". By changing the vane position, we change the amount of sample being measured and this will result in different G' values independent of the sample properties.

The PP geometry is widely used to characterise hydrogels. In this system, the sample is placed between the two plates and the measuring gap (h) can be controlled (Figure 1.12bI, top). This is advantageous as gels with different thicknesses can be measured. During measurements, the shear rate is not constant along the geometry, being higher in the outer part of the PP (Figure 1.12bI, bottom).[183] The shear stress applied also depends upon the size of PP used (Figure 1.12bIII) and the thickness of the sample, i.e. the measuring gap (Figure 1.12bII).[184] To ensure homogeneous laminar flow of the material, the sample needs to range between 0.5 mm and 2 mm in thickness.[185] Laminar flow is not guaranteed if the sample height is outside of these limits. Likewise, the shear stress is also influenced by the size of the PP used, being higher for smaller sizes of PP geometries (Figure 1.12bIII),[185] and are commercially available, which allows for a wider range of shear rates to be measured.[186]

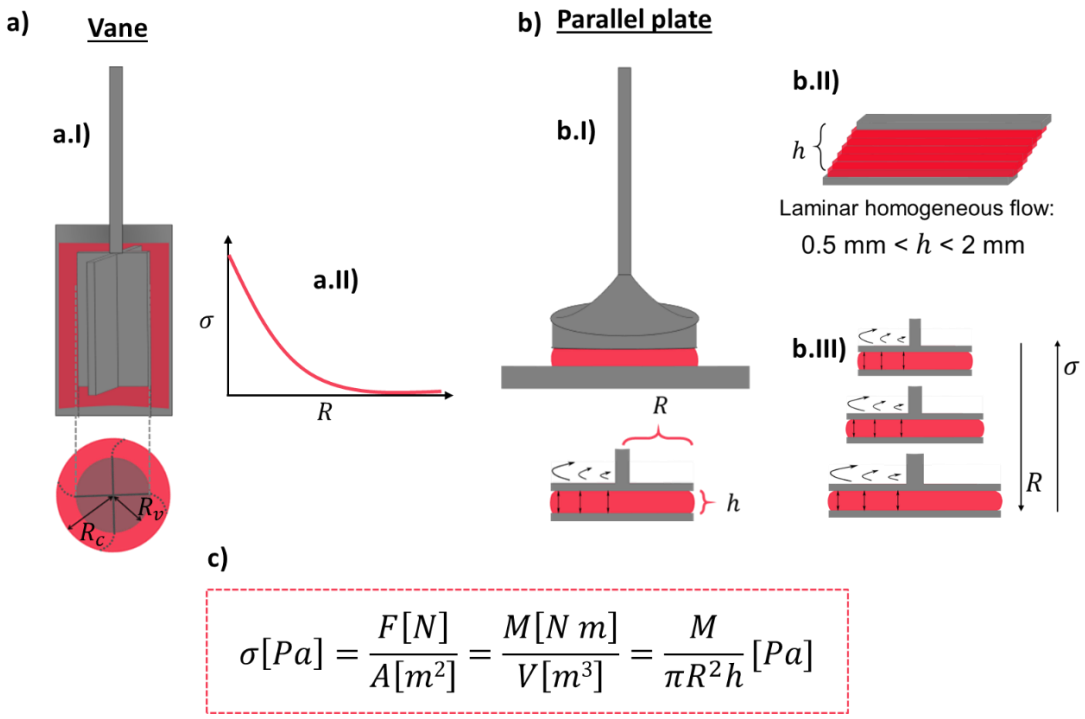

Figure 1.12 (a.I) (top) Cartoon of a four bladed vane geometry inserted into a hydrogel (red) for measurement and (bottom) cartoon of the shearing profile the material experiences during measurements. Inside the limits defined by the vane blade radius (R_v), the material moves guided by the blades. However, the stress decays gradually outside these limits, i.e., for the material trapped between the vane blades and the wall container. The distance between the centre of the vane and the wall of the container is defined as R_c. (a.II) Profile showing the gradual decay of the shear stress as the radius increases. (b.I) Cartoon showing the setup of a typical experiment using a PP geometry, where the sample is placed between the geometry and the base plate. Schematic representing (b.II) the laminar flow of a material using PP and (b.III) the shear stress dependency on the size of the geometry used. (c) Equation that defines the shear stress (σ, in Pa), where F is the force acting in shear direction (N), A is the surface (m^2), M is the torque (N m), R (or R_v) is the radius of the geometry (m) and h is the thickness (m) of the material being examined.

Oscillatory shear rheology allows to characterise the bulk mechanical properties of hydrogels in a mm scale. The use of this technique is broadly extended for hydrogels characterisation, but some considerations need to be

taken into account. Sometimes loading the sample into the rheometer can be tricky since the measuring system geometries need to be in full contact with the sample in order to get reliable data. This can be a problem when only small amounts of material is available, as could be the case of biological samples,[175] or when gels have a specific shape that do not fit in the rheometer measuring system. Also, depending on the geometry used to perform the experiment, the sample is subjected to different gradients of deformation. When a parallel plate is used, the deformation of the sample is directed to the surface of the gel, being the edges of the material suffering the stress at higher rates.[186] However, when using a vane this is immersed into the sample, where the same stress is applied along the bulk material.[182] It is common to simply assume that rheological values are comparable when using different geometries. However, in Chapter 4 we discuss this in detail and show the effect of swapping between different geometries under different circumstances.

1.6.2. Cavitation Rheology

Cavitation rheology is an emerging technique that was introduced by Zimberlin et al. in 2007.[178] In a cavitation experiment, a needle is inserted within the sample at an arbitrary position. A cavity is grown within the material via the pressurisation of either a gas or a liquid through the tip of a needle (Figure 1.13a). During pressurisation, the system pressure increases with time until the maximum pressure is reached, known as the critical pressure, P_c. The sample then undergoes mechanics deformation resulting in either elastic deformation or fracture of the sample (Figure 1.13c).[178, 187-198] This new technique presents several advantages compared to the other techniques discussed above. It allows measurement of the mechanical properties *in situ* at a micrometre scale, thus avoiding isolation problems, and it is also possible to use in materials of any shape and size.

The maximum pressure the cavity can withstand corresponds to the elastic instability limit of the material, which can be related to the elastic modulus.[178] Zimberlin *et al.*[178] related the critical pressure, P_c, to the elastic cavitation

modulus, E_c, by modelling the gel as a neo-Hookean (Figure 1.13b).[189] Cavitation modulus derived from this model will depend on the mechanics of the material.[178] Both the surface tension of the material and the needle radius will determine the critical pressure and, therefore, the cavitation modulus.

The use of cavitation rheology has grown over the last few years.[178, 187-198] Cui et al. have used cavitation rheology to measure the mechanical properties of bovine eye lenses in the nucleus and cortex.[190] They proved that differences in the elastic properties exist in the two different regions of the bovine lens. This is important as some eye diseases are related to change in elasticity in certain areas of the eyes.[199] Crosby and co-workers demonstrated the differences in mechanical properties of a bovine vitreous humour in the eye and in vitro. The modulus decreased when the vitreous humour was removed from the eye and even further decrease in modulus was observed when the vitreous cortex was disrupted.[187] This technique have also been used to characterise numerous gel systems.[196, 200-202] However, the poor understanding of the relationship with oscillatory shear rheology restricts its use in gels laboratories, particularly when comparing the gel modulus.[202]

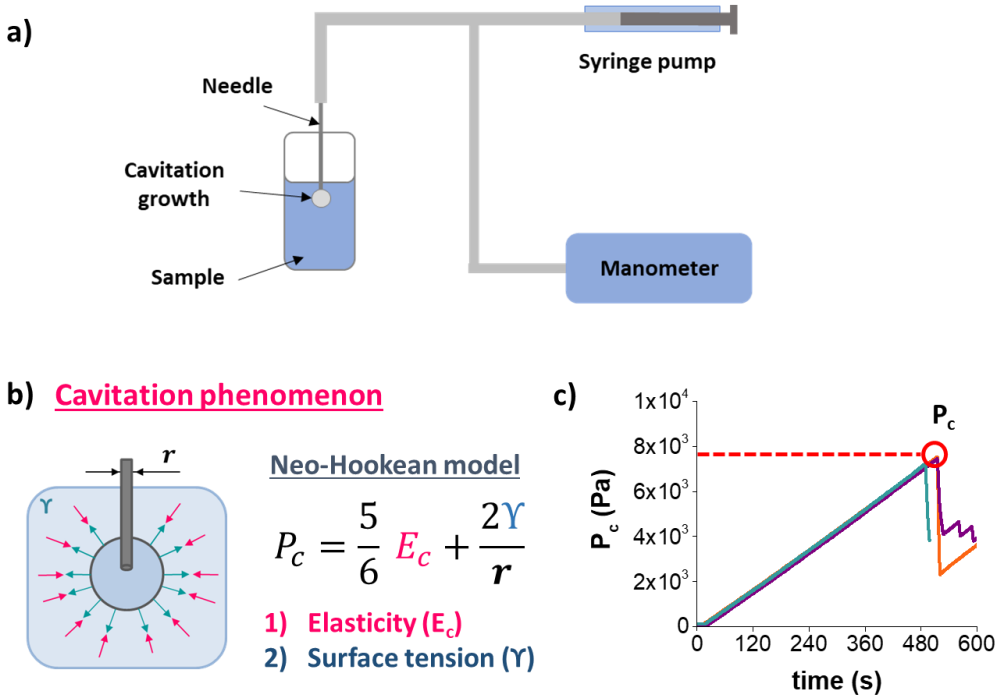

Figure 1.13 (a) Diagram showing the principles of cavitation rheology where a needle is inserted in the gel and an air bubble is grown via air pumping. (b) Cavitation phenomenon and the Neo-Hookean model relating the critical pressure P_c with the cavitation modulus E_c. (c) Experimental data for a cavitation example, where the maximum pressure recorded over time gives the critical pressure, P_c.

Pavlovsky and co-workers used a correction factor to compare both shear and cavitation moduli, although they examined solutions and not gels.[203] Other researchers have looked at the correlation between modulus obtained from shear and cavitation rheology in a number of organogels.[193, 194] Their results show cavitation moduli were always an order of magnitude greater than shear moduli. Bentz *et al*. reported recently a quantitative relationship, k_{sc}, between the gel modulus determined using shear and cavitation rheology for a series of model polymer gels.[202] This quantitative constant can be used to interconvert between shear storage (G') and cavitation (E_c) modulus (Figure 1.14). In Chapter 3, we examine the quantitative relationship between the shear storage modulus (G') and cavitation modulus (E_c) for gels formed from two different dipeptide low molecular weight gelators. The k_{sc} values obtained are statistically

different, and correlate with differences in the microstructures that lead to the gel.

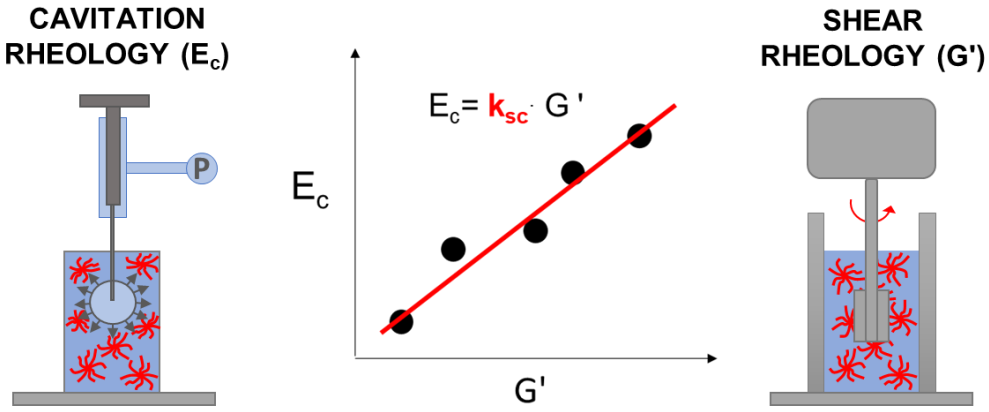

Figure 1.14 Schematic showing the differences between a shear and cavitation rheometer. The relationship between both techniques is given by a proportionality constant, k_{sc}, determined by the ratio of the moduli obtained from the two techniques.

1.7. The Importance of Mechanical Properties and their Tuneability for Biological Applications

LMWGs are a hugely important class of materials that have been extensively studied over the last years. Their popularity is in part due to the extensive list of applications in which they are suitable candidates.[8, 128-131] Although the absolute design rules are not yet recognised, their ability to be tuned makes them promising candidates capable of developing new materials on demand. Specifically, due to their biocompatibility and the wide range of mechanical properties, LMWGs have been broadly studied for biomedical applications such as tissue engineering and cell culture. Hydrogels can mimic the three-dimensional extracellular matrix (ECM) of different tissues in the body to provide a suitable environment for cells. Ulijn and co-workers successfully reported the formation of an aromatic-peptide hydrogel capable to promote adhesion, spreading and proliferation of dermal fibroblasts.[87, 204] Hydrogel stiffness plays a significant role in cell adhesion, proliferation, differentiation and functionality.[205] Emerman et al. were the first to observe the effect of the

ECM stiffness on cell differentiation.[206] They found that mammary epithelial cells (ECs) undergo stronger differentiation on soft collagen gels than on stiff tissue culture plastics.[206] Engler et al. found that mesenchymal stem cells (MSCs), for example, differentiate into neuron-like cells, myoblast and osteoblasts depending on the stiffness of the gels.[207] On the softer gel (0.1-1 kPa), cells mimicked nerve tissue properties, on the moderately stiff gel (8-17 kPa), cell mimicked muscle tissue and on the stiffer gels (25-40 kPa), cell mimicked bone tissue (Figure 1.15, a-b).[207]

For controlled release in drug delivery and tissue engineering, a key property of hydrogel is that they can hold different types of molecules, including proteins, growth factors or bioactive agents.[208, 209] Normally, hydrogels are used as homogeneous materials with homogeneous bulk properties. However, hierarchical hydrogels containing multiple layers with different mechanical properties play an important role as they can mimic complex structures of different body tissues.[209,210] Therefore, multi-layered hydrogels in which multiple cell types or drugs can be loaded, could control the release behaviour or cell interactions.[189] Recently, researchers have focused their efforts on developing new techniques capable of generate multi-layered hydrogels, thus including layer-by-layer self-assembly, step-wise technique, photo-polymerization and 3D printing, among others.[189]

3D printing allows for the deposition of a material layer-by-layer. In a typical experiment, the gel is made in a syringe and the gel is extruded through the needle. During extrusion, the gel is subjected to shear stress and as such, it converts into sol. If the gel is thixotropic, it will recover its shape after extrusion (Figure 1.15c). 3D printers are widely used to print polymer gels for the fabrication of biomaterials. However, due to the poor mechanical properties that LMWGs possess and the relatively small number of gelators with appropriate thixotropic characteristics, make their use underestimate for extrusion-based 3D printing. Nevertheless, interest in the use of 3D printing LMWGs is growing.[143, 211, 212] Nolan et al. recently reported a series of parameters to be optimised to get high quality 3D printing of dipeptide

hydrogels (Figure 1.15e-j). They found that hydrogels made from spherulitic domains exhibited better printability that hydrogels with a more uniform distribution of fibres.

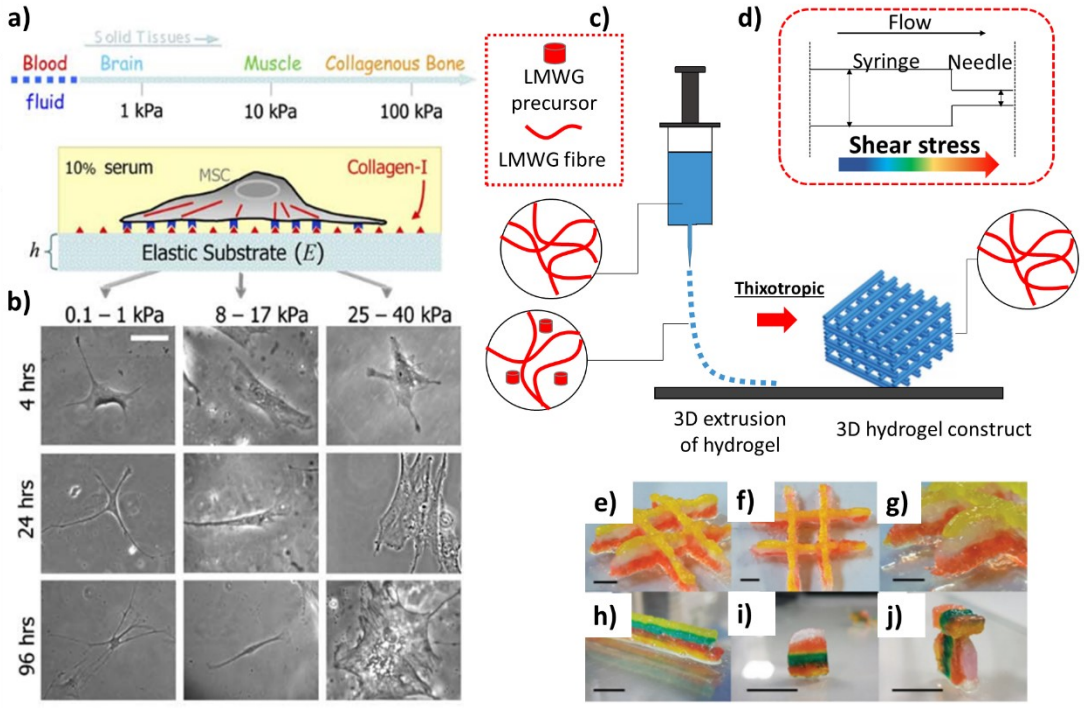

Figure 1.15 (a) Range of stiffnesses of the different tissues in the body, expressed as the elastic modulus, E. (b) Images of MSCs differentiation, where they are initially small and round (0.1-1 kPa), then they develop branches in spindle (8-17 kPa) or polygonal shapes (25-40 kPa) depending on the stiffness of the matrix. Scale bar represent 20mm. Adapted from ref [207]. (c) Schematic representing the 3D printing of a thixotropic gel, where the gel during extrusion is sheared and turns into a solution and then recovers its shape and reconverts into a gel again. (d) Schematic indicating the increase in shear stress that is applied to the gel during extrusion through the needle. (e-j) Images of multi-layered 3D printed gels where the different colours correspond to different dyes loaded before extrusion and represent different layers. The scale bars represent 1cm in all cases. Images adapted from ref [143].

The ability of LMWGs to recover their shape after extrusion is key in using them for 3D printing. Numerous examples in the literature show that numerous systems can be printed, however little importance is given to the effect of

extrusion on the resulting mechanical properties. In Chapter 4, we address this matter and show the effect of 3D printing on the properties of the extruded multi-layered hydrogels.

1.8. Aim of the Present Study

The aim of this Thesis is to understand the tuneability and characterisation of the mechanical properties of LMWGs across multiple length scales. Furthermore, we have developed a series of rheological methods to characterise multi-layered hydrogels which allow to investigate the effect that 3D printing has on the mechanical properties of such systems.

Chapter 2 discuss the tuneability of a multicomponent LMWGs system by means of using an annealing approach to move from a kinetic trapped state to the, or at least, a thermodynamic minimum. We will show that annealing in a two-component gel leads to a self-sorted network, which has significantly different mechanical properties to the as-prepared gels. Whilst the fibres are self-sorted, we show that the annealing of this system leads to significant changes in the network level of assembly, and it is this that leads to the increase in storage modulus. We also show that it is possible to selectively anneal only a single component in the mixture.

Chapter 3 demonstrates the efficiency of using a cavitation rheometer to characterise the mechanical properties of LMWGs at the μm scale. We will show that the underlying microstructure of our gels correlates with the data obtained from cavitation rheology and how it links with traditional oscillatory rheology. This will allow for a greater degree of understanding of the gels than can be obtained from the bulk measurements.

Finally, in Chapter 4 we investigate the effect that 3D printing has on the mechanical properties of LMWGs. The reversibility and recovery character of some LMWGs after being exposed to stress, make them ideal candidates for 3D printing in cell culture or tissue engineering applications. We will present a

broad rheological study on the mechanical characterisation of multi-layered gel systems. We will show not only a high degree of control of the mechanical properties' characterisation of the individual layers within multi-layered systems, but also the contribution of each layer to the resulting combined properties. Finally, the effect of 3D printing on the mechanical properties and morphology of the resulting materials is discussed.

1.9. References

1. A. S. Hoffman, *Adv. Drug Deliv. Rev.*, 2002, **54**, 3-12.

2. P. K. Ottenbrite R.M., Okano T., Peppas N.A., *in Biomedical Applications of Hydrogels Handbook*, ed. R. M. Ottenbrite, K. Park and T. Okano, Springer, New York, NY, USA, 1st edn., 2010.

3. M. de Loos, B. L. Feringa and J. H. van Esch, *Eur. J. Org. Chem.*, 2005, **2005**, 3615-3631.

4. P. Terech and R. G. Weiss, *Chem. Rev.*, 1997, **97**, 3133-3160.

5. O. Wichterle and D. Lím, *Nature*, 1960, **185**, 117-118.

6. S. G. Lee, S. R. Kim, H. I. Cho, M. H. Kang, D. W. Yeom, S. H. Lee, S. Lee and Y. W. Choi, *Biol. Pharm. Bull.*, 2014, **37**, 1674-1682.

7. A. Jayakumar, V. K. Jose and J. -M. Lee, *Small Methods*, 2020, **4**, 1900735.

8. B. O. Okesola and D. K. Smith, *Chem. Soc. Rev.*, 2016, **45**, 4226-4251.

9. T. M. Neethu, P. K. Dubey and A. R. Kaswala, *Int. J. Curr. Microbiol. App. Sci.*, 2018, **7**, 3155-3162.

10. A. Bashari, A. Rouhani Shirvan and M. Shakeri, *Polym. Adv. Technol.*, 2018, **29**, 2853-2867.

11. B. V. Slaughter, S. S. Khurshid, O. Z. Fisher, A. Khademhosseini and N. A. Peppas, *Adv. Mater.*, 2009, **21**, 3307-3329.

12. Q. Peng, J. Chen, T. Wang, X. Peng, J. Liu, X. Wang, J. Wang and H. Zeng, *J. Mater. Chem. A*, 2020, **8**, 24718-24733

13. A. Tirella, G. Mattei and A. Ahluwalia, *J. Biomed. Mater. Res.*, 2014, **102**, 3352-3360.

14. V. Pertici, C. Pin-Barre, C. Rivera, C. Pellegrino, J. Laurin, D. Gigmes and T. Trimaille, *Biomacromolecules*, 2019, **20**, 149-163.

15. C. D. Spicer, *Polym. Chem.*, 2020, **11**, 184-219.

16. N. Zanna, S. Focaroli, A. Merlettini, L. Gentilucci, G. Teti, M. Falconi and C. Tomasini, *ACS omega*, 2017, **2**, 2374-2381.

17. J. Xiang, L. Shen and Y. Hong, *Eur. Polym. J.*, 2020, **130**, 109609.

18. M. Aslam, M. A. Kalyar and Z. A. Raza, *Polym. Eng. Sci.*, 2018, **58**, 2119-2132.

19. J. Gao, C. Tang, M. A. Elsawy, A. M. Smith, A. F. Miller and A. Saiani, *Biomacromolecules*, 2017, **18**, 826-834.

20. M. C. Catoira, L. Fusaro, D. Di Francesco, M. Ramella and F. Boccafoschi, *J. Mater. Sci. Mater. Med.*, 2019, **30**, 115.

21. E. M. Ahmed, *J. Adv. Res.*, 2015, **6**, 105-121.

22. G. Fichman and E. Gazit, *Acta Biomater.*, 2014, **10**, 1671-1682.

23. R. G. Weiss, *J. Am. Chem. Soc.*, 2014, **136**, 7519-7530.

24. R. G. Weiss, *Gels*, 2018, **4**, 1-27.

25. A. M. Vibhute, V. Muvvala and K. M. Sureshan, *Angew. Chem. Int. Ed.*, 2016, **55**, 7782-7785.

26. J. H. Jung, G. John, M. Masuda, K. Yoshida, S. Shinkai and T. Shimizu, *Langmuir*, 2001, **17**, 7229-7232.

27. F. M. Menger, H. Zhang, K. L. Caran, V. A. Seredyuk and R. P. Apkarian, *J. Am. Chem. Soc.*, 2002, **124**, 1140-1141.

28. F. M. Menger, V. A. Seredyuk, R. P. Apkarian and E. R. Wright, *J. Am. Chem. Soc.*, 2002, **124**, 12408-12409.

29. L. A. Estroff and A. D. Hamilton, *Chem. Rev.*, 2004, **104**, 1201-1218.

30. E. K. Johnson, D. J. Adams and P. J. Cameron, *J. Mater. Chem*, 2011, **21**, 2024-2027.

31. C. Tomasini and N. Castellucci, *Chem. Soc. Rev.*, 2013, **42**, 156-172.

32. R. V. Ulijn and A. M. Smith, *Chem. Soc. Rev.*, 2008, **37**, 664-675.

33. N. Stephanopoulos, J. H. Ortony and S. I. Stupp, *Acta Mater.*, 2013, **61**, 912-930.

34. C. Colquhoun, E. R. Draper, R. Schweins, M. Marcello, D. Vadukul, L. C. Serpell and D. J. Adams, *Soft Matter*, 2017, **13**, 1914-1919.

35. S. Manchineella and T. Govindaraju, *Chem. Plus. Chem.*, 2017, **82**, 88-106.

36. X. Du, J. Zhou, J. Shi and B. Xu, *Chem. Rev.*, 2015, **115**, 13165-13307.

37. P. Dastidar, *Chem. Soc. Rev.*, 2008, **37**, 2699-2715.

38. X. Huang, S. R. Raghavan, P. Terech and R. G. Weiss, *J. Am. Chem. Soc.*, 2006, **128**, 15341-15352.

39. C. Yan, A. Altunbas, T. Yucel, R. P. Nagarkar, J. P. Schneider and D. J. Pochan, *Soft Matter*, 2010, **6**, 5143-5156.

40. N. Zanna and C. Tomasini, *Gels*, 2017, **3**, 39.

41. J. Gopinathan and I. Noh, *Biomater. Res.*, 2018, **22**, 11.

42. E. R. Draper, E. G. B. Eden, T. O. McDonald and D. J. Adams, *Nat. Chem.*, 2015, **7**, 848-852.

43. K. L. Morris, L. Chen, J. Raeburn, O. R. Sellick, P. Cotanda, A. Paul, P. C. Griffiths, S. M. King, R. K. O'Reilly, L. C. Serpell and D. J. Adams, *Nat. Commun.*, 2013, **4**, 1480.

44. D. J. Cornwell, O. J. Daubney and D. K. Smith, *J. Am. Chem. Soc.*, 2015, **137**, 15486-15492.

45. A. Das and S. Ghosh, *Chem. Commun.*, 2011, **47**, 8922-8924.

46. K. Sugiyasu, S. I. Kawano, N. Fujita and S. Shinkai, *Chem. Mater.*, 2008, **20**, 2863-2865.

47. L. E. Buerkle and S. J. Rowan, *Chem. Soc. Rev.*, 2012, **41**, 6089-6102.

48. A. R. Hirst and D. K. Smith, *Chem. Eur. J.*, 2005, **11**, 5496-5508.

49. E. R. Draper, E. G. Eden, T. O. McDonald and D. J. Adams, *Nat. Chem.*, 2015, **7**, 848-852.

50. J. Buendía, E. Matesanz, D. K. Smith and L. Sánchez, *Cryst. Eng. Commun.*, 2015, **17**, 8146-8152.

51. H. Shigemitsu, T. Fujisaku, W. Tanaka, R. Kubota, S. Minami, K. Urayama and I. Hamachi, *Nat. Nanotechnol.*, 2018, **13**, 165-172.

52. D. A. Tómasson, D. Ghosh, Z. Kržišnik, L. H. Fasolin, A. A. Vicente, A. D. Martin, P. Thordarson and K. K. Damodaran, *Langmuir*, 2018, **34**, 12957-12967.

53. B. O. Okesola and A. Mata , *Chem. Soc. Rev.*, 2018, **47** , 3721-3736

54. E. R. Draper and D. J. Adams, *Chem. Soc. Rev.*, 2018, **47**, 3395-3405.

55. W. Edwards and D. K. Smith, *J. Am. Chem. Soc.*, 2014, **136**, 1116-1124.

56. E. R. Cross, S. Sproules, R. Schweins, E. R. Draper and D. J. Adams, *J. Am. Chem. Soc.*, 2018, **140**, 8667-8670.

57. C. Colquhoun, E. R. Draper, E. G. Eden, B. N. Cattoz, K. L. Morris, L. Chen, T. O. McDonald, A. E. Terry, P. C. Griffiths, L. C. Serpell and D. J. Adams, *Nanoscale*, 2014, **6**, 13719-13725.

58. J. Raeburn and D. J. Adams, *Chem. Commun.*, 2015, **51**, 5170-5180.

59. X. Jia and K. L. Kiick, *Macromol. Biosci.*, 2009, **9**, 140-156.

60. P. Lin, N.-X. Zhang, J.-J. Li, J. Zhang, J.-H. Liu, B. Zhang and J. Song, *Chin. Chem. Lett.*, 2017, **28**, 771-776.

61. A. M. Castilla, E. R. Draper, M. C. Nolan, C. Brasnett, A. Seddon, L. L. E. Mears, N. Cowieson and D. J. Adams, *Sci. Rep.*, 2017, **7**, 8380.

62. M. Zhou, R. V. Ulijn and J. E. Gough, *J. Tissue Eng.*, 2014, **5**, 2041731414531593.

63. J. R. Moffat and D. K. Smith, *Chem. Commun.*, 2009, 316-318.

64. D. Tesauro, A. Accardo, C. Diaferia, V. Milano, J. Guillon, L. Ronga and F. Rossi, *Molecules*, 2019, **24**, 351.

65. A. Sunna, A. Care, P. L. Bergquist and SpringerLink, *Peptides and Peptide-based Biomaterials and their Biomedical Applications*, Springer

International Publishing, ed. A. Sunna, A. Care and P. Bergquist, Springer, New York, NY, USA, 1st edn., 2017.

66. S. Zhang, T. Holmes, C. Lockshin and A. Rich, *Proc. Natl. Acad. Sci.*, 1993, **90**, 3334.

67. A. Saiani, A. Mohammed, H. Frielinghaus, R. Collins, N. Hodson, C. M. Kielty, M. J. Sherratt and A. F. Miller, *Soft Matter*, 2009, **5**, 193-202.

68. H. Dong, S. E. Paramonov and J. D. Hartgerink, *J. Am. Chem. Soc.*, 2008, **130**, 13691-13695.

69. D. N. Woolfson, *J. Pept. Sci.*, 2010, **94**, 118-127.

70. R. V. Rughani, D. A. Salick, M. S. Lamm, T. Yucel, D. J. Pochan and J. P. Schneider, *Biomacromolecules*, 2009, **10**, 1295-1304.

71. L. A. Haines, K. Rajagopal, B. Ozbas, D. A. Salick, D. J. Pochan and J. P. Schneider, *J. Am. Chem. Soc.*, 2005, **127**, 17025-17029.

72. K. Rajagopal, M. S. Lamm, L. A. Haines-Butterick, D. J. Pochan and J. P. Schneider, *Biomacromolecules*, 2009, **10**, 2619-2625.

73. D. J. Pochan, J. P. Schneider, J. Kretsinger, B. Ozbas, K. Rajagopal and L. Haines, *J. Am. Chem. Soc.*, 2003, **125**, 11802-11803.

74. B. Ozbas, K. Rajagopal, L. Haines-Butterick, J. P. Schneider and D. J. Pochan, *J. Phys. Chem. B.*, 2007, **111**, 13901-13908.

75. P. Berndt, G. B. Fields and M. Tirrell, *J. Am. Chem. Soc.*, 1995, **117**, 9515-9522.

76. J. D. Hartgerink, E. Beniash and S. I. Stupp, *Proc. Natl. Acad. Sci.*, 2002, **99**, 5133.

77. H. Cui, M. J. Webber and S. I. Stupp, *J. Pept. Sci.*, 2010, **94**, 1-18.

78. M. J. Webber, J. A. Kessler and S. I. Stupp, *J. Intern. Med.*, 2010, **267**, 71-88.

79. Z. Yang, G. Liang, M. Ma, Y. Gao and B. Xu, *J. Mater. Chem.*, 2007, **17**, 850-854.

80. S. Toledano, R. J. Williams, V. Jayawarna and R. V. Ulijn, *J. Am. Chem. Soc.*, 2006, **128**, 1070-1071.

81. Y. Zhang, H. Gu, Z. Yang and B. Xu, *J. Am. Chem. Soc.*, 2003, **125**, 13680-13681.

82. J. Shi, Y. Gao, Z. Yang and B. Xu, *Beilstein J. Org. Chem.*, 2011, **7**, 167-172.

83. Y. Zhang, Z. Yang, F. Yuan, H. Gu, P. Gao and B. Xu, *J. Am. Chem. Soc.*, 2004, **126**, 15028-15029.

84. A. D. Martin, A. B. Robinson, A. F. Mason, J. P. Wojciechowski and P. Thordarson, *Chem. Commun.*, 2014, **50**, 15541-15544.

85. A. D. Martin and P. Thordarson, *J. Mater. Chem. B.*, 2020, **8**, 863-877.

86. A. Mahler, M. Reches, M. Rechter, S. Cohen and E. Gazit, *Adv. Mater.*, 2006, **18**, 1365-1370.

87. V. Jayawarna, M. Ali, T. A. Jowitt, A. F. Miller, A. Saiani, J. E. Gough and R. V. Ulijn, *Adv. Mater.*, 2006, **18**, 611-614.

88. M. Reches and E. Gazit, *Science*, 2003, **300**, 625.

89. J. Cui, A. Liu, Y. Guan, J. Zheng, Z. Shen and X. Wan, *Langmuir*, 2010, **26**, 3615-3622.

90. J. Raeburn, C. Mendoza-Cuenca, B. N. Cattoz, M. A. Little, A. E. Terry, A. Zamith Cardoso, P. C. Griffiths and D. J. Adams, *Soft Matter*, 2015, **11**, 927-935.

91. C. C. Piras, P. Slavik and D. K. Smith, *Angew. Chem. Int. Ed.*, 2020, **59**, 853-859.

92. I. Furman and R. G. Weiss, *Langmuir*, 1993, **9**, 2084-2088.

93. A. M. Fuentes-Caparrós, F. de Paula Gómez-Franco, B. Dietrich, C. Wilson, C. Brasnett, A. Seddon and D. J. Adams, *Nanoscale*, 2019, **11**, 3275-3280.

94. L. Chen, J. Raeburn, S. Sutton, D. G. Spiller, J. Williams, J. S. Sharp, P. C. Griffiths, R. K. Heenan, S. M. King, A. Paul, S. Furzeland, D. Atkins and D. J. Adams, *Soft Matter*, 2011, **7**, 9721-9727.

95. C. M. Rubert Pérez, L. A. Rank and J. Chmielewski, *Chem. Commun.*, 2014, **50**, 8174-8176.

96. E. C. Barker, A. D. Martin, C. J. Garvey, C. Y. Goh, F. Jones, M. Mocerino, B. W. Skelton, M. I. Ogden and T. Becker, *Soft Matter*, 2017, **13**, 1006-1011.

97. N. Amdursky, R. Orbach, E. Gazit and D. Huppert, *J. Phys. Chem. C.*, 2009, **113**, 19500-19505.

98. N. A. Dudukovic and C. F. Zukoski, *Soft Matter*, 2014, **10**, 7849-7856.

99. A. M. Fuentes-Caparrós, McAulay, K., Rogers, S.E., Dalgliesh, R.M. and Adams, D.J, *Molecules*, 2019, **24**, 3855.

100. D. J. Adams, M. F. Butler, W. J. Frith, M. Kirkland, L. Mullen and P. Sanderson, *Soft Matter*, 2009, **5**, 1856-1862.

101. L. Chen, T. O. McDonald and D. J. Adams, *RSC Adv.*, 2013, **3**, 8714-8720.

102. C. Tang, A. M. Smith, R. F. Collins, R. V. Ulijn and A. Saiani, *Langmuir*, 2009, **25**, 9447-9453.

103. A. M. Smith, R. J. Williams, C. Tang, P. Coppo, R. F. Collins, M. L. Turner, A. Saiani and R. V. Ulijn, *Adv. Mater.*, 2008, **20**, 37-41.

104. C. Tang, A. M. Smith, R. F. Collins, R. V. Ulijn and A. Saiani, *Langmuir*, 2009, **25**, 9447-9453.

105. A. P. McCloskey, E. R. Draper, B. F. Gilmore and G. Laverty, *J. Pept. Sci.*, 2017, **23**, 131-140.

106. T. Liebmann, S. Rydholm, V. Akpe and H. Brismar, *BMC Biotechnol.*, 2007, **7**, 88.

107. V. Jayawarna, S. M. Richardson, A. R. Hirst, N. W. Hodson, A. Saiani, J. E. Gough and R. V. Ulijn, *Acta Biomater.*, 2009, **5**, 934-943.

108. L. Chen, S. Revel, K. Morris, L. C. Serpell and D. J. Adams, *Langmuir*, 2010, **26**, 13466-13471.

109. D. J. Adams, L. M. Mullen, M. Berta, L. Chen and W. J. Frith, *Soft Matter*, 2010, **6**, 1971-1980.

110. E. Krieg, M. M. C. Bastings, P. Besenius and B. Rybtchinski, *Chem. Rev.*, 2016, **116**, 2414-2477.

111. D. J. Cornwell and D. K. Smith, *Chem. Commun.*, 2020, **56**, 7029-7032.

112. L. Thomson, R. Schweins, E. R. Draper and D. J. Adams, *Macromol. Rapid Commun.*, 2020, **41**, 2000093.

113. D. J. Cornwell, B. O. Okesola and D. K. Smith, *Angew. Chem. Int. Ed.*, 2014, **53**, 12461-12465.

114. A. Bernet, R. Q. Albuquerque, M. Behr, S. T. Hoffmann and H.-W. Schmidt, *Soft Matter*, 2012, **8**, 66-69.

115. J. Raeburn, G. Pont, L. Chen, Y. Cesbron, R. Lévy and D. J. Adams, *Soft Matter*, 2012, **8**, 1168-1174.

116. S. K. Davey, A. Aung, G. Agrawal, H. L. Lim, M. Kar and S. Varghese, *Tissue Eng. Part C Methods*, 2015, **21**, 1188-1196.

117. S. N. Dublin and V. P. Conticello, *J. Am. Chem. Soc.*, 2008, **130**, 49-51.

118. M. M. Pires, D. E. Przybyla and J. Chmielewski, *Angew. Chem. Int. Ed.*, 2009, **48**, 7813-7817.

119. M. M. Pires and J. Chmielewski, *J. Am. Chem. Soc.*, 2009, **131**, 2706-2712.

120. H. Yang, M. Pritzker, S. Y. Fung, Y. Sheng, W. Wang and P. Chen, *Langmuir*, 2006, **22**, 8553-8562.

121. A. D. Martin, J. P. Wojciechowski, A. B. Robinson, C. Heu, C. J. Garvey, J. Ratcliffe, L. J. Waddington, J. Gardiner and P. Thordarson, *Sci. Rep.*, 2017, **7**, 43947-43947.

122. J. Zhou, X. Du, J. Wang, N. Yamagata and B. Xu, *Front. Chem. Sci. Eng.*, 2017, **11**, 509-515.

123. Z. Yang, G. Liang and B. Xu, *Soft Matter*, 2007, **3**, 515-520.

124. Y. Gao, J. Shi, D. Yuan and B. Xu, *Nat. Commun.*, 2012, **3**, 1033.

125. M. Hughes, S. Debnath, C. W. Knapp and R. V. Ulijn, *Biomater. Sci.*, 2013, **1**, 1138-1142.

126. R. J. Williams, A. M. Smith, R. Collins, N. Hodson, A. K. Das and R. V. Ulijn, *Nat. Nanotechnol.*, 2009, **4**, 19-24.

127. Y. Gao, Z. Yang, Y. Kuang, M.-L. Ma, J. Li, F. Zhao and B. Xu, *Pept. Sci.*, 2010, **94**, 19-31.

128. Enateri V. Alakpa, V. Jayawarna, A. Lampel, Karl V. Burgess, Christopher C. West, Sanne C. J. Bakker, S. Roy, N. Javid, S. Fleming, Dimitris A. Lamprou, J. Yang, A. Miller, Andrew J. Urquhart, Pim W. J. M. Frederix, Neil T. Hunt, B. Péault, Rein V. Ulijn and Matthew J. Dalby, *Chem*, 2016, **1**, 298-319.

129. A. R. Hirst, B. Escuder, J. F. Miravet and D. K. Smith, *Angew. Chem. Int. Ed.*, 2008, **47**, 8002-8018.

130. S. S. Babu, V. K. Praveen and A. Ajayaghosh, *Chem. Rev.*, 2014, **114**, 1973-2129.

131. K. J. Skilling, F. Citossi, T. D. Bradshaw, M. Ashford, B. Kellam and M. Marlow, *Soft Matter*, 2014, **10**, 237-256.

132. S. Mantha, S. Pillai, P. Khayambashi, A. Upadhyay, Y. Zhang, O. Tao, H. M. Pham and S. D. Tran, *Materials (Basel)*, 2019, **12**, 3323.

133. J. S. Varghese, N. Chellappa and N. N. Fathima, *Colloids Surf. B.*, 2014, **113**, 346-351.

134. E. R. Cross, S. M. Coulter, A. M. Fuentes-Caparrós, K. McAulay, R. Schweins, G. Laverty and D. J. Adams, *Chem. Commun.*, 2020, **56**, 8135-8138.

135. J. Raeburn, A. Zamith Cardoso and D. J. Adams, *Chem. Soc. Rev.*, 2013, **42**, 5143-5156.

136. D. Ghosh, M. T. Mulvee and K. K. Damodaran, *Molecules*, 2019, **24**, 3472.

137. A. R. Meyer, C. R. Bender, D. M. dos Santos, F. I. Ziembowicz, C. P. Frizzo, M. A. Villetti, J. M. Reichert, N. Zanatta, H. G. Bonacorso and M. A. P. Martins, *Soft Matter*, 2018, **14**, 6716-6727.

138. W. Helen, P. de Leonardis, R. V. Ulijn, J. Gough and N. Tirelli, *Soft Matter*, 2011, **7**, 1732-1740.

139. M. G. F. Angelerou, A. Sabri, R. Creasey, P. Angelerou, M. Marlow and M. Zelzer, *Chem. Commun.*, 2016, **52**, 4298-4300.

140. K. R. Hixon, A. J. Dunn, R. Flores, B. A. Minden-Birkenmaier, E. A. Growney Kalaf, L. P. Shornick and S. A. Sell, *Electrospinning*, 2017, **2**, 31-45.

141. J.-L. Li and X.-Y. Liu, *Adv. Funct. Mater.*, 2010, **20**, 3196-3216.

142. A. M. Fuentes-Caparrós, B. Dietrich, L. Thomson, C. Chauveau and D. J. Adams, *Soft Matter*, 2019, **15**, 6340-6347.

143. M. C. Nolan, A. M. Fuentes Caparrós, B. Dietrich, M. Barrow, E. R. Cross, M. Bleuel, S. M. King and D. J. Adams, *Soft Matter*, 2017, **13**, 8426-8432.

144. A. Arango-Restrepo, J. M. Rubi and D. Barragán, *J. Phys. Chem. B.*, 2018, **122**, 4937-4945.

145. Y. Yan, J. Huang and B. Z. Tang, *Chem. Commun.*, 2016, **52**, 11870-11884.

146. F. Tantakitti, J. Boekhoven, X. Wang, R. V. Kazantsev, T. Yu, J. Li, E. Zhuang, R. Zandi, J. H. Ortony, C. J. Newcomb, L. C. Palmer, G. S. Shekhawat, M. O. de la Cruz, G. C. Schatz and S. I. Stupp, *Nat. Mater.*, 2016, **15**, 469-476.

147. A. Ghosh, M. Haverick, K. Stump, X. Yang, M. F. Tweedle and J. E. Goldberger, *J. Am. Chem. Soc.*, 2012, **134**, 3647-3650.

148. A. Z. Cardoso, L. L. E. Mears, B. N. Cattoz, P. C. Griffiths, R. Schweins and D. J. Adams, *Soft Matter*, 2016, **12**, 3612-3621.

149. J. Boekhoven, J. M. Poolman, C. Maity, F. Li, L. van der Mee, C. B. Minkenberg, E. Mendes, J. H. van Esch and R. Eelkema, *Nat. Chem.*, 2013, **5**, 433-437.

150. B. Ding, Y. Li, M. Qin, Y. Ding, Y. Cao and W. Wang, *Soft Matter*, 2013, **9**, 4672-4680.

151. E. R. Draper, L. L. E. Mears, A. M. Castilla, S. M. King, T. O. McDonald, R. Akhtar and D. J. Adams, *RSC Adv.*, 2015, **5**, 95369-95378.

152. L. Chen, G. Pont, K. Morris, G. Lotze, A. Squires, L. C. Serpell and D. J. Adams, *Chem. Commun.*, 2011, **47**, 12071-12073.

153. E. Mayans, G. Ballano, J. Casanovas, L. J. del Valle, M. M. Pérez-Madrigal, F. Estrany, A. I. Jiménez, J. Puiggalí, C. Cativiela and C. Alemán, *Soft Matter*, 2016, **12**, 5475-5488.

154. R. Huang, W. Qi, R. Su, J. Zhao and Z. He, *Soft Matter*, 2011, **7**, 6418-6421.

155. J. H. Collier, B. H. Hu, J. W. Ruberti, J. Zhang, P. Shum, D. H. Thompson and P. B. Messersmith, *J. Am. Chem. Soc.*, 2001, **123**, 9463-9464.

156. B. Ozbas, J. Kretsinger, K. Rajagopal, J. P. Schneider and D. J. Pochan, *Macromolecules*, 2004, **37**, 7331-7337.

157. S. Debnath, S. Roy, Y. M. Abul-Haija, P. W. J. M. Frederix, S. M. Ramalhete, A. R. Hirst, N. Javid, N. T. Hunt, S. M. Kelly, J. Angulo, Y. Z. Khimyak and R. V. Ulijn, *Chem. Eur. J.*, 2019, **25**, 7881-7887.

158. F. Tantakitti, J. Boekhoven, X. Wang, R. V. Kazantsev, T. Yu, J. Li, E. Zhuang, R. Zandi, J. H. Ortony, C. J. Newcomb, L. C. Palmer, G. S. Shekhawat, M. O. de la Cruz, G. C. Schatz and S. I. Stupp, *Nat. Mater.*, 2016, **15**, 469-476.

159. F. Lin, J. Yu, W. Tang, J. Zheng, A. Defante, K. Guo, C. Wesdemiotis and M. L. Becker, *Biomacromolecules*, 2013, **14**, 3749-3758.

160. E. R. Draper and D. J. Adams, *Chem.*, 2017, **3**, 390-410.

161. E. R. Cross, S. M. Coulter, A. M. Fuentes-Caparrós, K. McAulay, R. Schweins, G. Laverty and D. J. Adams, *Chem. Commun.*, 2020, **56**, 8135-8138.

162. V. S. Raghuwanshi and G. Garnier, *Adv. Colloid Interface Sci.*, 2019, **274**, 102044.

163. G. Némethy and H. A. Scheraga, *J. Chem. Phys.*, 1964, **41**, 680-689.

164. L. Dougan, A. S. R. Koti, G. Genchev, H. Lu and J. M. Fernandez, *Chem. Phys.Chem.*, 2008, **9**, 2836-2847.

165. I. W. Hamley, S. Burholt, J. Hutchinson, V. Castelletto, E. R. da Silva, W. Alves, P. Gutfreund, L. Porcar, R. Dattani, D. Hermida-Merino, G. Newby, M. Reza, J. Ruokolainen and J. Stasiak, *Biomacromolecules*, 2017, **18**, 141-149.

166. C. A. Grant, P. C. Twigg, M. D. Savage, W. H. Woon and D. Greig, *Macromol. Mater. Eng.*, 2012, **297**, 214-218.

167. M. V. C. Cardoso and E. Sabadini, *Carbohydr. Res.*, 2010, **345**, 2368-2373.

168. K. McAulay, H. Wang, A. M. Fuentes-Caparrós, L. Thomson, N. Khunti, N. Cowieson, H. Cui, A. Seddon and D. J. Adams, *Langmuir,* 2020**, 29** , 8626-8631.

169. L. L. E. Mears, E. R. Draper, A. M. Castilla, H. Su, Zhuola, B. Dietrich, M. C. Nolan, G. N. Smith, J. Doutch, S. Rogers, R. Akhtar, H. Cui and D. J. Adams, *Biomacromolecules*, 2017, **18**, 3531-3540.

170. A. Onaciu, R. A. Munteanu, A. I. Moldovan, C. S. Moldovan and I. Berindan-Neagoe, *Pharmaceutics*, 2019, **11**, 432.

171. G. Yu, X. Yan, C. Han and F. Huang, *Chem. Soc. Rev.*, 2013, **42**, 6697-6722.

172. V. J. Nebot and D. K. Smith, in *Functional Molecular Gels*, ed. B. Escuder and J. F. Miravet, The Royal Society of Chemistry, Cambridge (UK), 1st edn., 2013, ch. 2, pp. 30-66.

173. V. S. Raghuwanshi and G. Garnier, *Adv. Colloid Interface Sci.*, 2019, **274**, 102044.

174. P. Cicuta and A. M. Donald, *Soft Matter*, 2007, **3**, 1449-1455.

175. V. Breedveld and D. J. Pine, *J. Mater. Sci.*, 2003, **38**, 4461-4470.

176. N. Yang, R. Lv, J. Jia, K. Nishinari and Y. Fang, *Annu. Rev. Food Sci. Technol.*, 2017, **8**, 493-521.

177. D. Ebenstein and L. Pruitt, *Nano Today*, 2006, **1**, 26-33.

178. J. A. Zimberlin, N. Sanabria-DeLong, G. N. Tew and A. J. Crosby, *Soft Matter*, 2007, **3**, 763-767.

179. T. G. Mezger, *The rheology handbook : for users of rotational and oscillatory rheometers*, Hannover, Germany, 2nd edn., 2006.

180. C. W. Macosko, *Rheology: principles, measurements and applications*, Wiley-VCH, New York, NY, 1994.

181. A. Paar, Basics of Rheology, https://wiki.anton-paar.com/en/basics-of-rheology, (accessed June 2020).

182. C. E. Owens, A. J. Hart and G. H. McKinley, *J. Rheol.*, 2020, **64**, 643-662.

183. H. A. Barnes, *A handbook of elementary rheology*, University of Wales Institute of Non-Newtonian Fluid Mechanics, Wales (UK), 1st edn., 2000.

184. A. Perazzo, J. K. Nunes, S. Guido and H. A. Stone, *Proc. Natl. Acad. Sci.*, 2017, **114**, E8557-E8564.

185. C. W. Macosko, *Rheology: principles, measurements and applications*, Wiley-VCH, New York, NY, 1994.

186. P. De Souza Mendes, A. Alicke and R. Thompson, *Appl. Rheol.*, 2014, **24**, 52721.

187. J. A. Zimberlin, J. J. McManus and A. J. Crosby, *Soft Matter*, 2010, **6**, 3632-3635.

188. J. A. Zimberlin and A. J. Crosby, *J. Polym. Sci., Part B: Polym. Phys.*, 2010, **48**, 1423-1427.

189. S. Kundu and A. J. Crosby, *Soft Matter*, 2009, **5**, 3963-3968.

190. J. Cui, C. H. Lee, A. Delbos, J. J. McManus and A. J. Crosby, *Soft Matter*, 2011, **7**, 7827-7831.

191. J. Meid, F. Dierkes, J. Cui, R. Messing, A. J. Crosby, A. Schmidt and W. Richtering, *Soft Matter*, 2012, **8**, 4254-4263.

192. M. S. Chin, B. B. Freniere, S. Fakhouri, J. E. Harris, J. F. Lalikos and A. J. Crosby, *Plast. Reconstr. Surg.*, 2013, **131**, 303e-305e.

193. P. Fei, S. J. Wood, Y. Chen and K. A. Cavicchi, *Langmuir*, 2015, **31**, 492-498.

194. S. M. Hashemnejad and S. Kundu, *Soft Matter*, 2015, **11**, 4315-4325.

195. L. E. Jansen, N. P. Birch, J. D. Schiffman, A. J. Crosby and S. R. Peyton, *J. Mech. Behav. Biomed. Mater.*, 2015, **50**, 299-307.

196. K. C. Bentz, S. E. Walley and D. A. Savin, *Soft Matter*, 2016, **12**, 4991-5001.

197. S. B. Hutchens, S. Fakhouri and A. J. Crosby, *Soft Matter*, 2016, **12**, 2557-2566.

198. J. Kang, C. Wang and S. Cai, *Soft Matter*, 2017, **13**, 6372-6376.

199. D. A. Atchison, *Ophthal. Physl. Opt.*, 1995, **15**, 255-272.

200. S. M. Hashemnejad, M. M. Huda, N. Rai and S. Kundu, *ACS Omega*, 2017, **2**, 1864-1874.

201. S. Kundu, S. M. Hashemnejad, M. Zabet and S. Mishra, in *Gels and Other Soft Amorphous Solids*, American Chemical Society, 2018, vol. 1296, ch. 9, pp. 157-197.

202. K. C. Bentz, N. Sultan and D. A. Savin, *Soft Matter*, 2018, **14**, 8395-8400.

203. L. Pavlovsky, M. Ganesan, J. G. Younger and M. J. Solomon, *Appl. Phys. Lett.*, 2014, **105**, 114105-114105.

204. M. Zhou, A. M. Smith, A. K. Das, N. W. Hodson, R. F. Collins, R. V. Ulijn and J. E. Gough, *Biomaterials*, 2009, **30**, 2523-2530.

205. S. R. Caliari and J. A. Burdick, *Nat. Methods*, 2016, **13**, 405-414.

206. J. T. Emerman, S. J. Burwen and D. R. Pitelka, *Tissue Cell*, 1979, **11**, 109-119.

207. A. J. Engler, S. Sen, H. L. Sweeney and D. E. Discher, *Cell*, 2006, **126**, 677-689.

208. G. Liu, Z. Ding, Q. Yuan, H. Xie and Z. Gu, *Front. Chem.*, 2018, **6**, 439-439.

209. M. Martínez-Sanz, D. Mikkelsen, B. Flanagan, M. J. Gidley and E. P. Gilbert, *Carbohydr. Polym*, 2016, **147**, 542-555.

210. L. E. R. O'Leary, J. A. Fallas, E. L. Bakota, M. K. Kang and J. D. Hartgerink, *Nat. Chem.*, 2011, **3**, 821-828.

211. Q. Qin, F. Yang, X. Zhang, T. Shi, Y. Shao, H. Sun, C. Chen, J. Hao and Z. Guo, *Int. J. Refract. Met. H.*, 2019, **84**, 105014.

212. H. Yang, S. Zhang, K. Liu and Y. Fang, *RSC Adv.*, 2016, **6**, 109969-109977.

CHAPTER 2

Annealing Supramolecular Multicomponent Gels

This Chapter is adapted in part from the following publication:

"Annealing multicomponent supramolecular gels"
Nanoscale, **2019**, 11, 3275-3280.
A. M. Fuentes-Caparrós, F. P. Gómez-Franco, B. Dietrich, C. Wilson, C. Brasnett, A. Seddon and D. J. Adams.

F.P. Gómez-Franco and A. M. Fuentes-Caparrós collected rheological data. B. Dietrich and D. J. Adams synthesised the molecules. B. Dietrich and A. M. Fuentes-Caparrós carried out the temperature ^{1}H NMR experiments. A. M. Fuentes-Caparrós completed the microscopy and UV-Vis studies and analysed the ^{1}H NMR spectra. C. Brasnett carried out the SAXS experiments. A. Seddon and D. J. Adams fitted the SAXS data. C. Wilson performed the X-ray crystallography and analysed the crystal structure.

2.1. Introduction

Low molecular weight gels (LMWGs) are widely used materials due to their applications in areas as diverse as biomaterials and optoelectronics.[1-13] These gels arise from the self-assembly of small molecule sub-units into long fibrous networks. There is growing evidence that these LMWGs are often not at equilibrium, but rather the gels represent kinetically-trapped states. The approach by which the gels are prepared often govern the final properties of the gels and as a consequence it is possible to make different gels under the same final conditions by varying how the gel is formed. [14-16] This implies that it can be challenging to prepare reproducible gels if the conditions used are not sufficiently well controlled, however this also opens up opportunities. For example, instead of preparing many molecules to find one that gives gels with the required properties, we can alternatively simply vary the process of gelation for a single molecule.[4, 16]

One of the leading challenges with using LMWGs is the difficulty of predicting which molecules will form gels and which will not.[12] Furthermore, predicting what the properties of a gel formed from a particular LMWGs remains an empirical science nowadays. Hence, a more pragmatic approach is to find robust low molecular weight gelators (LMWG) and develop methods for controlling, modulating and modifying the properties of the gels that can be formed from robust LMWG.

Numerous materials are prepared in such a way that a kinetically-trapped state is formed.[3, 14, 15, 17-22] Kinetically-trapped states allow for the development of interesting and useful materials from a single set of components, as long as the energy well is not too deep.[23, 24] From the same starting material, different properties can be achieved by varying how the different states are accessed. It can be possible to move between states, hence allowing adaptive, tuneable, and triggerable materials to be accessed on demand (Figure 2.1).

Considering that LMWGs are often kinetically-trapped, and the significant interest in these materials,[25-28] there has been surprisingly little work carried out on annealing them.[29-33] Mostly, gels are prepared and used directly, or sometimes melted as a characterization method. LMWGs are a result of non-covalent interactions and so there is the potential to change between states if the energy barriers are suitably low. Adaptive and triggerable gels are being increasingly discussed,[34] and annealing has great potential here.

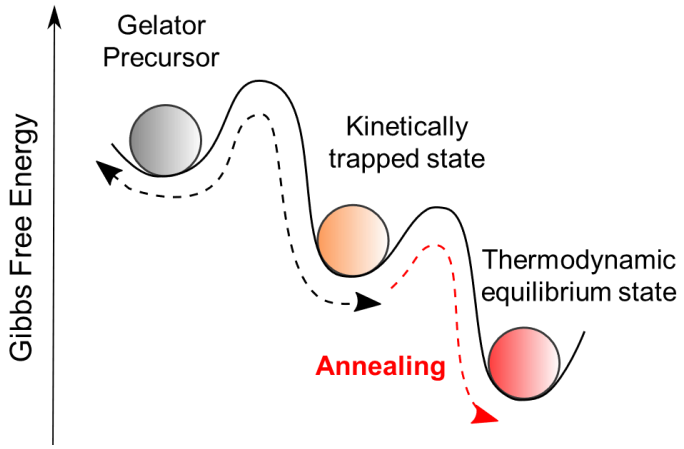

Figure 2.1 Schematic representation of the free energy landscape in the assembly process. The arrows demonstrate that transition between the kinetic traps and the thermodynamic equilibrium state is possible under external stimuli. In this case an annealing approach allows for the transition between these two states.

Most examples of LMWGs are single components.[6] These are extremely useful for many applications such as cell culturing and controlled release, but there is increasing interest in multicomponent systems.[25, 26, 35, 36] There are a small number of examples where two components are needed to form a gel, and either alone does not. Xu and co-workers,[37] for example, have shown that combination of two Fmoc-protected amino acids, hydrogels could be formed. However, neither component formed a hydrogel independently due to their limited water solubility. Here, we focus on examples where both components can form a gel by themselves. On mixing therefore, multiple scenarios are possible for self-assembly and gel formation (see Chapter 1, section 1.2.2).[25, 26]

The gelators could mix intimately to give fibres that contain both of the molecules. Alternatively, the molecules could prefer to self-sort such that each individual self-assembled structure contains only one of the molecules. At longer length-scales, the fibres could also self-sort, preferring to entangle and interact with themselves only, or simply entangle with fibres of either structure. Mixing gelators conceptually opens up greater opportunities for controlling the gel properties and accessing new states. This can lead to materials with interesting new properties; as a single example, it has recently been shown that a mixed system can be used to prepare gels in which there are very different diffusion rates depending on how the gels are formed.[38]

In this Chapter, we show how annealing multicomponent LMWGs systems can be used to prepare gels with different rheological properties depending on the history of the samples. We will show the potential of applying an annealing approach to preparing adaptive materials from multicomponent gels. The resulting gels are characterised across multiple length scales. NMR is used to investigate the aggregation of the gelator molecules; SAXS analyses the primary structures forming the gels; UV-vis evaluates the kinetics of gel formation as a means of turbidity measurements; confocal microscopy probes the microstructure and rheology interpretates the bulk properties of the gels. As such as we cover multiple length scales with these techniques.

2.2. Results and Discussion

2.2.1. Presentation of the Multicomponent System

Many functionalized amino acids and dipeptides are known to be able to form gels. This can be by a pH trigger, or a salt-trigger, to name some (see Chapter 1, section 1.4).[6] Here, we focus on a solvent-triggered approach whereby the dipeptide is initially dissolved in a water-miscible solvent such as DMSO, followed by the addition of water.[4, 39-44] This usually drives a phase separation that results in spherulitic domains of fibres that entangle sufficiently to form a self-supporting gel.[41, 45, 46] The properties of the gels can be varied by changing

the concentration of the dipeptide, and also the ratio of the solvent to water. The gels formed by this method are kinetically trapped.

Here, we discuss a multicomponent system of two gelators, based around a dipeptide or an amino acid functionalized at the *N*-terminus (**1** and **2**, Figure 1.4 and Figure 2.2).

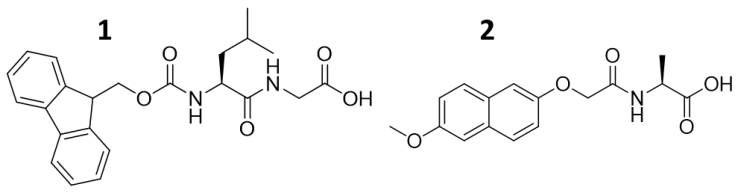

Figure 2.2 Chemical structures of **1** and **2**.

The Adams group have previously discussed the gelation of **1** in detail.[41] They have shown that heating and cooling the gels formed by **1** results in the gel melting, and then re-forming.[41] The heated and cooled gel had different properties compared to the initial gel; further heat-cool cycles result in no further changes in the final mechanical properties.[41] The Adams group and others have found that using multicomponent systems where both components can independently form gels can be an effective strategy for preparing gels with properties that cannot be achieved with either individual component.[38, 47, 48] Applying this approach, here we used gelation conditions which were optimized for mixing experiments; the concentrations of the gelators were chosen such that both **1** and **2** formed gels at the same final ratio of DMSO:water (a ratio of 3:7 was used throughout) and that the gel melting temperatures were in a suitable range for analysis (see below). We stress that we have optimized the system here to demonstrate the principle such that the concentrations and ratios of gelators as well as the solvent composition have been chosen to allow distinct melting points to be observed and compared.

2.2.2. Annealing of Single Component Gel System 1

2.2.2.I. Rheological and morphological Analysis of Gel 1

1 forms transparent gels at a ratio of DMSO:water of 3:7 and a concentration of 4 mg mL^{-1} (Figure 2.3a). The rheological properties of the gel are reproducible (Figure 2.3) and are typical of a gel formed using this method. The gel is stable until a strain of approximately 4 % before G' starts to deviate from linearity (Figure 2.3b). Both the storage modulus (G') and loss modulus (G") are relatively independent of frequency (Figure 2.3c).

When this gel is heated, G' and G" slowly decrease before reaching a plateau at around 65 °C (Figure 2.3g). On re-cooling, G' and G" only start to increase again at around 37 °C, with a gel of similar transparency formed to the original (Figure 2.3d). At 15°C, the values of both moduli are slightly higher than for the original gel (Figure 2.3g). After annealing, the gels again have reproducible rheological data, with the frequency sweep again being essentially independent of frequency (Figure 2.3f). The gels break at a very similar strain as those before annealing, although the absolute values of the moduli are higher (Figure 2.3e). The increase in moduli after annealing can be explained by a change in the gel microstructure (Figure 2.3h), from spherulitic structures to a more uniform distribution of fibres. This thermal behaviour was backed up by the dropping ball method, which showed a broadly similar melting and re-gelation temperature (Figure 2.4), although we highlight that the absolute melting temperature is difficult to pinpoint exactly using the dropping ball method as it depends on the time at which the sample is allowed to sit at each temperature.

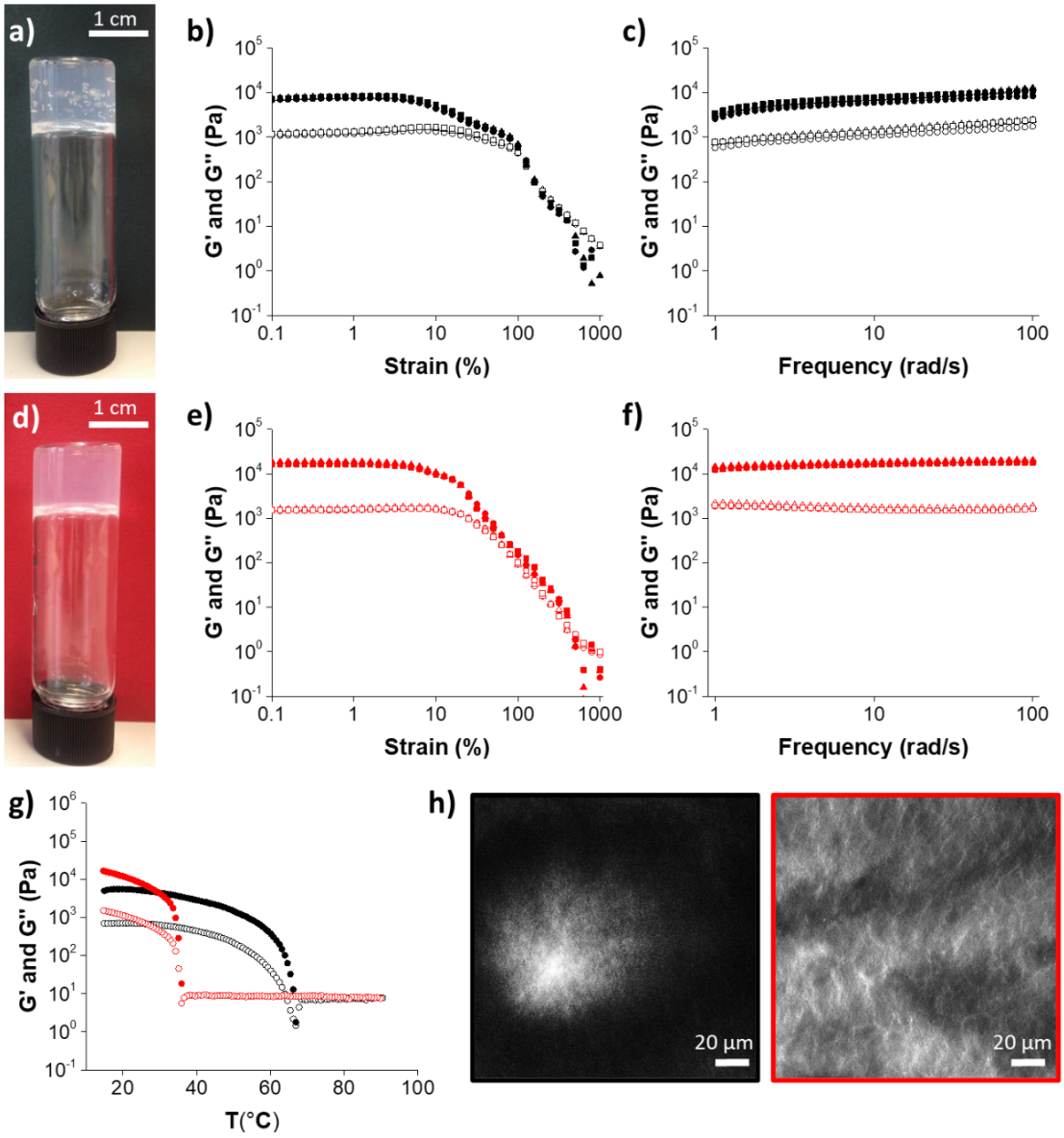

Figure 2.3 Rheological and morphological characterisation of gel **1**. (a) Photograph of a gel of **1** before annealing. (b)-(c) Overlay of three repeat strain and frequency sweeps for a gel of **1** before annealing respectively. (d) Photograph of a gel of **1** after annealing. (e)-(f) Overlay of three repeat strain and frequency sweeps for a gel of **1** after annealing respectively. (g) Rheological data for a gel of **1** on heating and cooling at a rate of 1°C min^{-1}. Black data represent the heating cycle, and the red data represent the cooling cycle. (h) Confocal images of gels of **1** before (left) and after (right) annealing. For rheological data, closed symbols represent G' and open symbols represent G".

2.2.2.II. Dropping Ball Method of Gel 1

The apparent hysteresis between the melting and re-gelling temperature can be explained by the need to form a network such that a gel is formed. On melting, the gel simply gets weaker as **1** dissolves. On cooling, **1** will start to re-assemble, but a gel will only be formed when a network is formed that spans the entire sample. We note that other low molecular weight gels do not show such a hysteresis.[29, 30] To substantiate this, variable temperature ^{1}H NMR spectroscopy experiments were performed to monitor the solubility of **1** upon heating and cooling to correlate with our rheological observations (Figure 2.5).

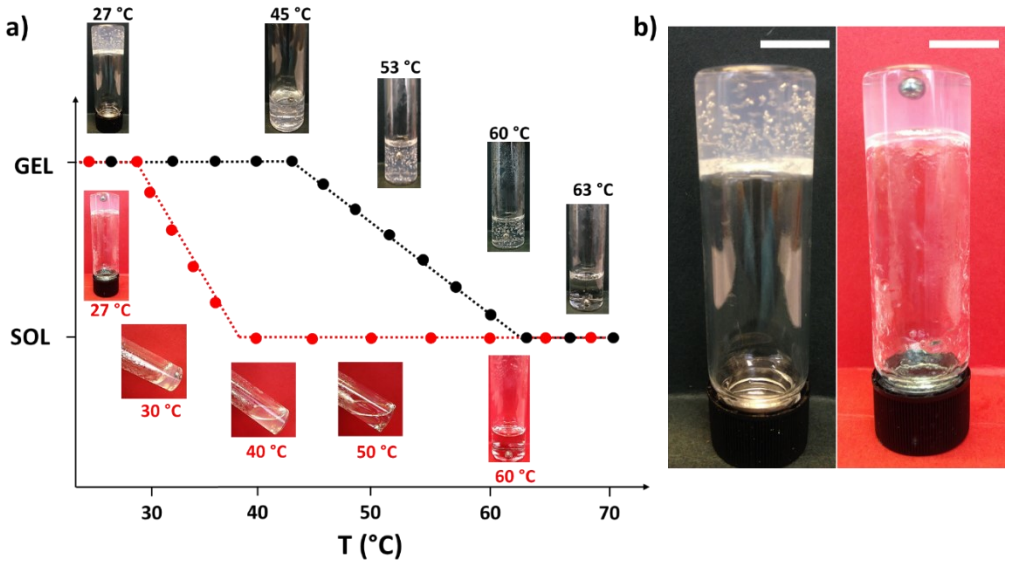

Figure 2.4 (a) Visual determination of the melting temperature and gel re-formation temperature for a gel of **1**. The black data are for heating and the red data for cooling. A ball bearing has been included at the top of the gel, that slowly falls to the bottom. On re-gelling, this ball bearing is trapped in the network. (b) Photograph of a gel of **1** before (left) and after (right) annealing. Scale bar represents 1 cm in all cases.

2.2.2.III. Nuclear Magnetic Resonance (NMR) Analysis of Gel 1

When using NMR spectroscopy for gelling systems, the reduction of the peak intensities and the chemical shift changes can provide information of the degree of gelation.[49] As the free molecules assemble into the rigid components of the gel, these molecules become invisible to solution-state NMR experiments.[50] The solubility of the molecule can be monitored from the ^{1}H NMR spectra at a range of different temperatures. At high temperatures, i.e., in the sol state, the hydrogen protons are visible as the molecule is soluble and freely tumbling in solution. However, as the temperature decreases and self-assembly takes place, the signal of hydrogen protons will decrease in intensity and eventually disappear. As such, a reference is needed to be able to integrate the peaks within the range of temperatures to analyse. Thus, a mixture of 10% DMSO-d_6, 1% poly(dimethylsiloxane), PDMS, and 89% of tetrachloroethylene was used as the internal reference. The chemical shift of proton in PDMS methyl groups is around 0.05 ppm, distant from the signals coming from the gelator molecules and as such is our reference peak for analysis. We optimised the amount of PDMS by trial and error such as the size of the peak was similar to those of the compound. The mixture was added inside a glass capillary and sealed by melting the glass with heat. The capillary containing the mixture was placed inside the NMR tube, which we had previously filled with the sample to analyse. As such, the internal standard mixture does not come into contact with the gelling system, which might result in a change in the properties of the system.

The analysis of the ^{1}H NMR spectra was focused on the CH_3 residual signal (Figure 2.5a). Initially, at room temperature, the gel state shows the presence of only a small signal in the region of the spectrum where this is expected to appear. Gradually, as the sample is heated the peak becomes sharper and the signal more intense until a maximum is reached at 85°C, when the gel is completely melted (Figure 2.5b). On cooling, the signal again gradually becomes broader and less intense, corresponding with the molecules self-assembling to reform a gel (Figure 2.5b). The symmetrical changes in intensity

of peaks during heating and cooling indicate the also symmetrical solubility of **1** (Figure 2.5c).

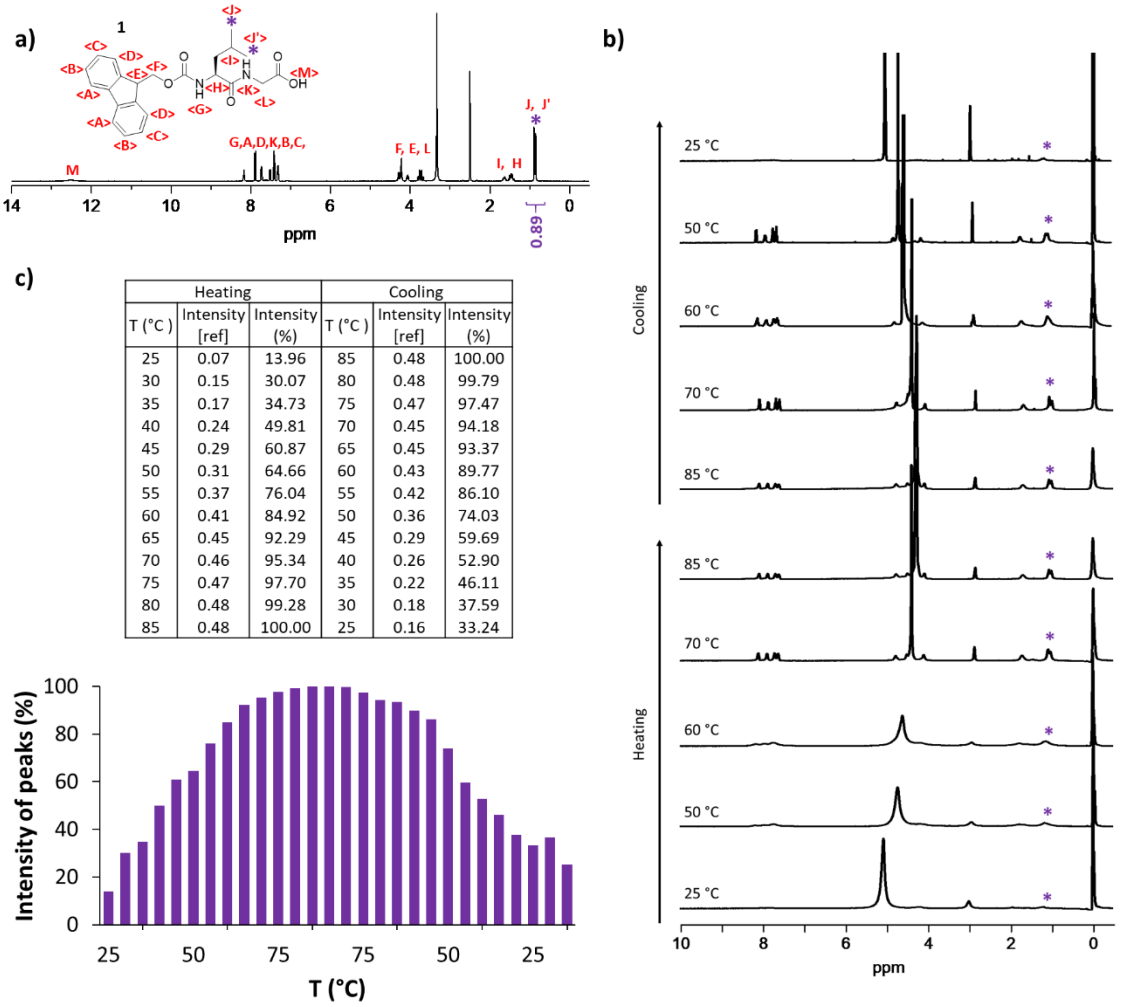

Heating			Cooling		
T (°C)	Intensity [ref]	Intensity (%)	T (°C)	Intensity [ref]	Intensity (%)
25	0.07	13.96	85	0.48	100.00
30	0.15	30.07	80	0.48	99.79
35	0.17	34.73	75	0.47	97.47
40	0.24	49.81	70	0.45	94.18
45	0.29	60.87	65	0.45	93.37
50	0.31	64.66	60	0.43	89.77
55	0.37	76.04	55	0.42	86.10
60	0.41	84.92	50	0.36	74.03
65	0.45	92.29	45	0.29	59.69
70	0.46	95.34	40	0.26	52.90
75	0.47	97.70	35	0.22	46.11
80	0.48	99.28	30	0.18	37.59
85	0.48	100.00	25	0.16	33.24

Figure 2.5 (a) ^{1}H NMR spectrum of **1** in DMSO-d_6. The purple asterisk indicates the signal correspondent to the CH_3 group. (b) Temperature ramp ^{1}H NMR spectra on heating and cooling in a range of 25°C - 85°C - 25°C. A mixture of 10% DMSO-d_6, 1% PDMS and 89% tetrachloroethylene (PERC) was used as the internal standard. (c) Integrals for 1 against the standard as determined by ^{1}H NMR spectroscopy for **1** in a mixture of DMSO-d_6 and D_2O (3/7) on heating and cooling. The sample temperature was changed by steps of 5°C, and an NMR spectrum recorded after 1 minute, before being heated or cooled to the required next temperature.

2.2.3. Annealing of Single Component Gel System 2

2.2.3.I. Rheological and morphological Analysis of Gel 2

Gels can also be formed at this ratio of DMSO:water using gelator **2** (Figure 2.1). Again, we emphasize that we optimized the conditions to allow us to prepare gels in this solvent mixture, and also such that the gels melted at a different temperature to that of **1**. Hence, gels were formed from **2** at a concentration of 8 mg mL^{-1}. In a single component system, **2** formed a turbid gel (Figure 2.6a).

From a rheological perspective, the data for gels of **2** were again reproducible. G' and G" were essentially frequency independent (Figure 2.6c), with the gels having a similar breakdown to **1** under increasing strain (Figure 2.6b). On heating, the gels become weaker as they are heated although there is not such a defined melting profile (Figure 2.6g). At 75°C, G' and G" increase before decreasing again at 83°C. It is not possible to increase the temperature further due to evaporation issues. We attribute this increase in moduli at the higher temperatures to a phase separation process such as a lower critical solution temperature (LCST) as opposed to a true melting. On cooling, there is a short plateau before G' and G" increase once again, with higher moduli than for the original gel (Figure 2.6g). As for gels from **1**, after annealing the gels of **2** are reproducible, with a similar breakdown under increasing strain (Figure 2.6e), and the gels being frequency independent (Figure 2.6f). After the annealing, the gel is perhaps a little more transparent than the original (Figure 2.6d) and there is evidence of small crystals in the gel matrix (Figure 2.7a).

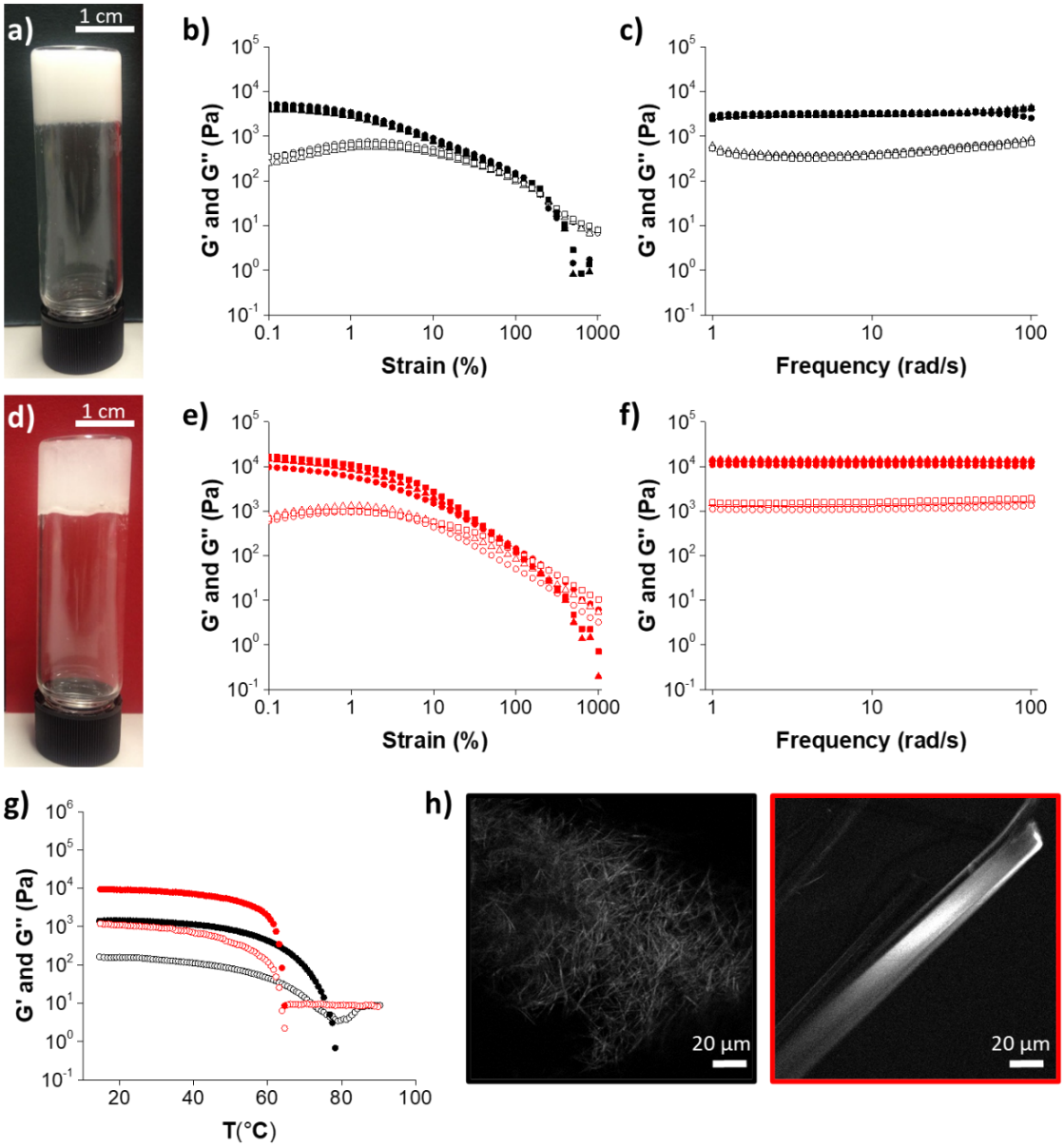

Figure 2.6 Rheological and morphological characterisation of gel **2**. (a) Photograph of a gel of **2** before annealing. (b)-(c) Overlay of three repeat strain and frequency sweeps for a gel of **2** before annealing respectively. (d) Photograph of a gel of **2** after annealing. (e)-(f) Overlay of three repeat strain and frequency sweeps for a gel of **2** after annealing respectively. (g) Rheological data for a gel of **2** on heating and cooling at a rate of 1 °C min^{-1}. Black data represent the heating cycle and the red data represent the cooling cycle. (h) Confocal images of gels of **2** before (left) and after (right) annealing. For rheological data, closed symbols represent G' and open symbols represent G".

2.2.3.II. X-ray Diffraction of Gel 2

Using a very slow cooling rate, it is possible to grow crystals from the gel phase which are suitable for crystal X-ray diffraction study (Figure 2.7). Claire Wilson (University of Glasgow) performed the X-ray crystallography and analysed the crystal structure.

The structure of the crystal molecule with formula $C_{16}H_{17}NO_5$ is given in Figure 2.7a. The unit cell corresponds to an orthorhombic system with axes a = 4.9683 (3), b = 13.7813 (7), c = 21.8629 (13) Å. The total volume of the unit cell is 1496.94 (15) $Å^3$ and the occupancy is of 4 molecules (Z=4). The space group of the unit cell is $P2_12_12_1$. A total of 8891 reflections were measured, from which only 2719 were used for the calculations. The error of the refinement was 0.130, wR(F2). Furthermore, the hydrogen bonding chains were also analysed (Figure 2.7b). Molecules of **2** are held together through hydrogen bonding between O2—H2 and O11′. The bond length is 2.604(3) Å and the angle is 175º.

A number of researchers have attempted to link gelation to crystal structures.[51, 52] Despite the assumption that there is a relationship between the interactions that contributes to crystallisation or gelation, the Adams group[31] and others[31, 53] have shown that molecules packing is different in the gel phase compared to crystals grown. The crystal structure of gel **2** has been included for completeness as there are very few crystals that can be grown directly from the gel phase.

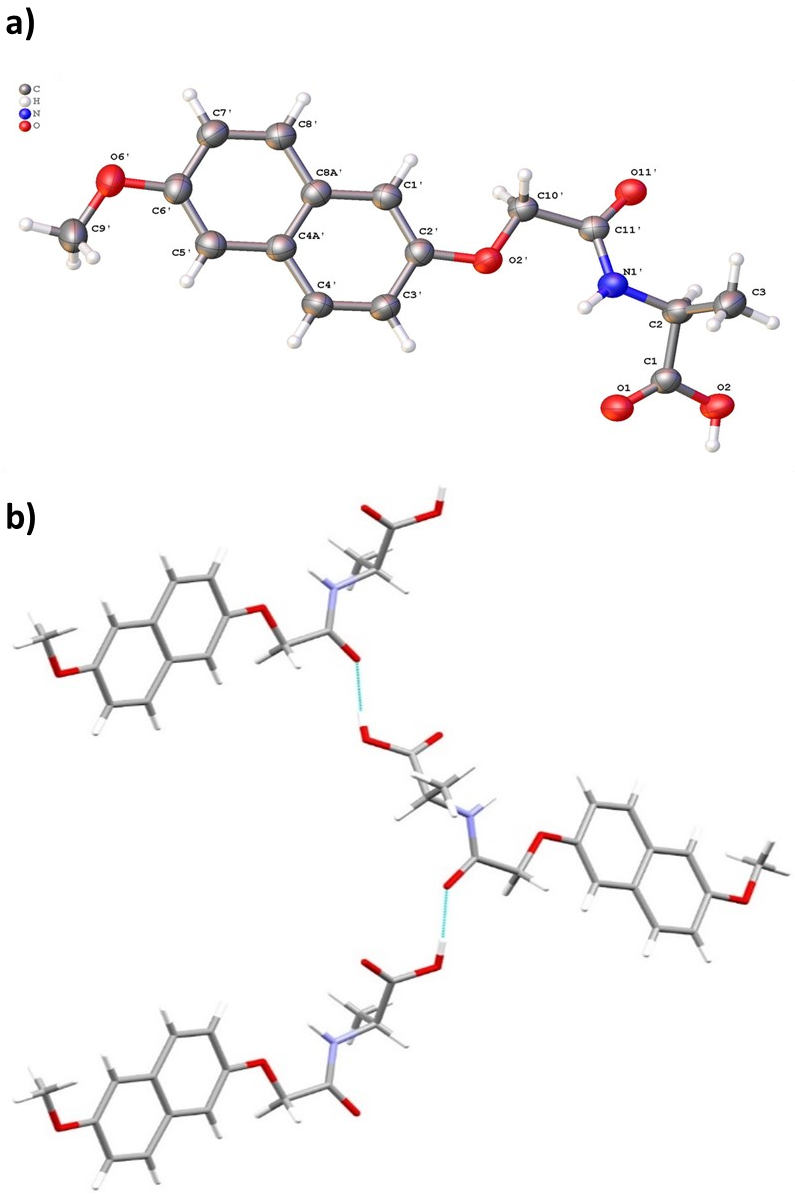

Figure 2.7 (a) Structure of **2**; crystals grown by a slow cool of a gel of **2**. Atomic displacement ellipsoids drawn at 50% probability level. Crystal data. $C_{16}H_{17}NO_5$, M = 303.30, orthorhombic, a = 4.9683 (3), b = 13.7813 (7), c = 21.8629 (13) Å, V = 1496.94 (15) Å^3, T = 150 K, I = 1.54178 Å, space group $P2_12_12_1$ (no.19), Z = 4, 8891 reflections measured, 2719 unique (Rint = 0.082), which were used in all calculations. The final wR(F2) was 0.130 (all data). Flack x, -0.05 (17), determined using 841 quotients [(I+)-(I-)]/[(I+)+(I-)].[54](b) View of structure of **2** showing the hydrogen bonding chain viewed along the c-axis; O2—H2···O11′I where (i) -x+3, y-1/2, -z+3/2. O2…O11′I = 2.604(3) Å and angle O2— H2···O11′i =175°.

2.2.4. Annealing of Multi Component Gel System 1+2

We then explored the multicomponent system. Gels were prepared from **1** and **2**, denoted (**1**+**2**). We used the same ratio of DMSO:water of 3:7 as above, with the amount of each gelator as in the single component. Hence, (**1**+**2**) contains 4 mg mL^{-1} of **1** and 8 mg mL^{-1} of **2**.

2.2.4.I. Ultraviolet-visible spectroscopy (UV-Vis)

Compared to the individual components, the rate of assembly is different for the multi-component system (**1**+**2**). This can be probed by turbidity measurements (Figure 2.8b).

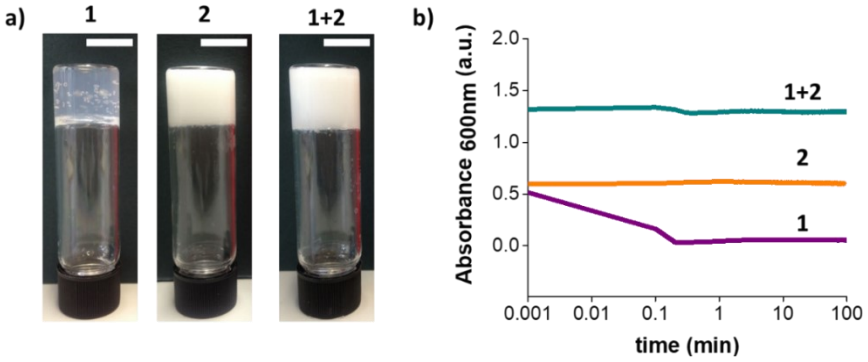

Figure 2.8 (a) Pictures of gels **1**, **2** and **1+2**. (b) Changes in absorbance at 600 nm with time after adding water to a solution of either **1**, **2** or **1+2** in DMSO. The scale bars represent 1 cm.

1 alone forms a gel via a nucleation and growth process, where highly scattering structures are initially formed, before a transparent gel phase is developed. This behaviour has been shown previously,[41, 43] and the turbidity data here is consistent with this. **2** alone forms a highly scattering gel almost immediately. In the mixture (**1**+**2**), there is an initial process which is reminiscent of the assembly of **1**, followed by an increase in turbidity associated with the gelation of **2**. Such changes in the rate of assembly have been shown in multicomponent systems as compared to the single components previously.[40]

2.2.4.II. Rheological Analysis

A typical gel formed from (**1**+**2**) is shown in Figure 2.9a.The properties of the mixed gels as prepared are again typical of a low molecular weight gel. Rheologically, the gels are frequency independent, with the value of G' being higher than that of either **1** or **2** alone, which might be expected on the basis of the higher overall gelator concentration (Figure 2.9b, black data). However, the strain sweep shows a profile which is much more similar to that of the gels of **2** alone as opposed to that of **1** (Figure 2.9c, black data). We then annealed the multicomponent gel (Figure 2.9d, top). On heating, the gel gradually becomes weaker, following the profile of **1** alone. However, at 65 °C, G' and G" increase before decreasing again. This occurs at a lower temperature than the gel of **2** alone but is a similar profile.

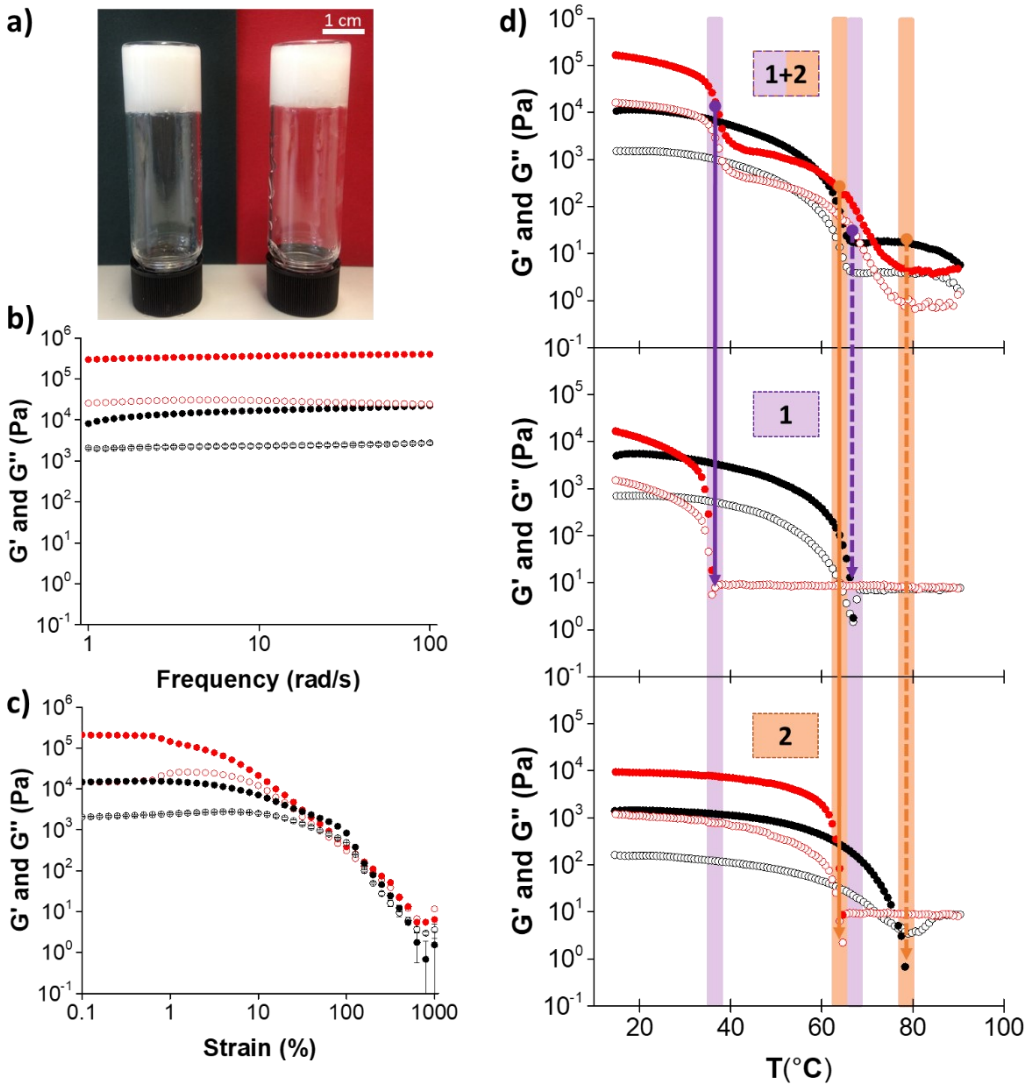

Figure 2.9 Rheological characterisation of the multicomponent system (**1**+**2**). (a) Photograph of multicomponent gel as formed (left) and after annealing (right), with the scale bar representing 1 cm. (b) Frequency sweeps for gels of (**1**+**2**); black data are before annealing and red data are after annealing. (c) Strain sweeps for gels of (**1**+**2**); black data are before annealing and red data are after annealing. (d) Rheological data comparison of gels **1**, **2** and (**1**+**2**) on heating and cooling at a rate of 1°C min^{-1}. For (b) – (d), the closed symbols represent G' and open symbols represent G". The black data are for the heating cycle, and the red data for the cooling cycle. For (d), purple and orange lines refer to **1** and **2** respectively. The dashed lines refer to the melting temperature on heating, and the soft lines to the temperature at which the gels start reforming on cooling.

Sequential melting points in a self-sorted system have been previously described,[55] but not linked to the rheological data. On cooling, there is a short plateau before G' and G" increase, stabilising around 50°C, before a second increase in G' and G". The temperatures at which both increases in G' and G" occur, closely match that for the gels formed from the individual components.

This strongly implies self-sorting is occurring. After annealing, the gels are two orders of magnitude stiffer than prior to heating and cooling and are independent of frequency (Figure 2.9b, red data). There is a significantly different breakdown under strain as compared to before heating, and there appear to be two points in the strain sweep where the moduli decrease, possibly indicating two types of network (Figure 2.9c, red data). Hence, the annealing affects both the absolute stiffness and also the breakage strain.

2.2.4.III. Small Angle X-ray Scattering (SAXS) and Morphological Analysis

To explain these differences in the gels before and after annealing, we examined small angle X-ray scattering (SAXS) and confocal microscopy. The SAXS data were collected by Chris Brasnett (University of Bristol) and fitted by Annela Seddon (University of Bristol) and Dave Adams (University of Glasgow). SAXS probes the primary structures forming the gels, whilst confocal microscopy probes the microstructure and as such as we cover the important length scales with these two techniques. Critically, both techniques allow us to probe the gel without the need for drying. Drying is known to lead to artefacts in such systems,[56] and on top of this the binary nature of the solvent mixture means that there are issues with non-homogeneous removal of the solvent.

The scattering data for the gels formed from **1** alone are very similar before and after annealing, showing that the primary structures leading to gelation are essentially the same (Figure 2.11a; fitting parameters shown in Table 2.1 and further data are shown in Figure 2.10a and b). The data in both cases are typical of this class of LMWG[41] and can be fitted to a flexible cylinder model. The

cylinders have a radius of 3.7 ± 0.04 nm before annealing, and 3.9 ± 0.06 nm afterwards, with similarly small changes in the Kuhn length. These radii and lengths are typical of such LMWG.[41] The confocal microscopy (Figure 2.11b) shows a significant difference in the microstructure. From these two sets of data, we can interpret that the primary structures leading to gelation are essentially the same, but their distribution in space is different. This is what leads to the different gel properties.

Table 2.1 Fits to the SAXS data for the different gels; [a] fits to a flexible cylinder (0.00704<Q<0.217); [b] fits to power law (0.00704<Q<0.217); [c] fits to power law and cylinder (fit to a power law does not fit well at low Q, and this fit results in a chi squared value of >50).

	1 (before annealing)[a]	**1** (after annealing)[a]	**2** (before annealing)[b]	**2** (after annealing) [c]	**(1+2)** (before annealing)[b]	**(1+2)** (after annealing)[a]
Background (1/cm)	0.0672 ± 0.021	0.0681 ± 0.000	0.075 ± 0.0005	0.002 ± 0.0003	0.0612 ± 0.0004	0.0644 ± 0.0003
Power Law			4.30 ± 0.02	4.04 ± 0.00	3.45 ± 0.01	
Scale			$1.55 \times 10^{-8} \pm 1.45 \times 10^{-9}$	$2.00 \times 10^{-7} \pm 3.21 \times 10^{-9}$	$3.66 \times 10^{-6} \pm 1.23 \times 10^{-7}$	
Length / nm	>1000	>1000		>400		>1000
Kuhn Length / nm	6.77 ± 0.21	6.00 ± 0.61				7.64 ± 0.48
Radius / nm	3.7 ± 0.04	3.9 ± 0.06		3.6 ± 0.02		4.3 ± 0.07
Scale	0.0011 ± 0.0000	0.0008 ± 0.0000		0.0003 ± 0.0000		0.0008 ± 0.0000
x^2	1.214	1.2173	2.0139	5.7811	2.2483	1.3035

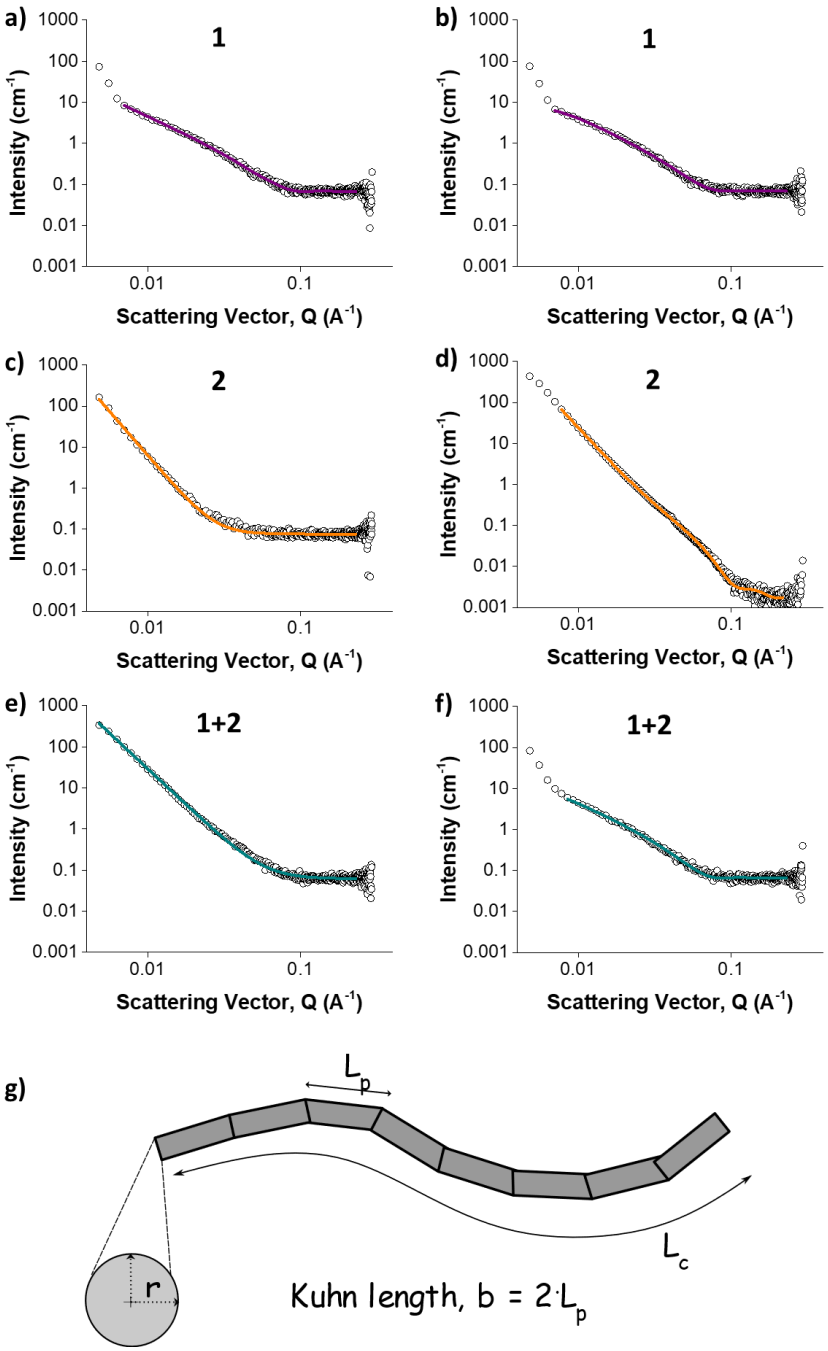

Figure 2.10 SAXS data and fits for gels of (a) **1** before annealing; (b) **1** after annealing; (c) **2** before annealing; (d) **2** after annealing; (e) (**1+2**) before annealing; (f) (**1+2**) after annealing. In all cases the data are in open circles and the fits (as described in Table 2.1) are shown as solid lines (purple for gel **1**, orange for gel **2** and cyan for gel (**1+2**)). (g) Schematic of the flexible cylinder model; L_p, persistence length, L_c, contour length, r, cylinder radius.

For gels formed from **2** alone, the SAXS data are different before and after heating (Figure 2.11c; fitting parameters shown in Table 2.1 and further data are shown in Figure 2.10c,d), which would agree with the observations above that the annealing leads to some crystallization. In these cases, the scattering is dominated by a power law, which would be consistent with the structures that are scattering being outside the accessible Q-range over which the data were collected as shown by the confocal microscopy (Figure 2.11d). In this case, the annealing has led to the structures becoming significantly larger, with a propensity to crystallize.

For the multicomponent system (**1**+**2**), the SAXS data are significantly different before and after annealing (Figure 2.11e; fitting parameters shown in Table 2.1 and further data are shown in Figure 2.10e,f). Before heating, the data are more reminiscent of that of **2** alone. However, after annealing, the data are very similar to that of **1** alone, and again the data fits well to a flexible cylinder model with a slightly increased radius of 4.3 $\pm$ 0.07 nm and a similar Kuhn length. This implies that the annealing has led to a significant change in structure. Confocal microscopy images however show structures after annealing that are most similar to those of **2** (Figure 2.11f). This apparent contradiction can be explained by the fact that, on cooling, **2** forms structures first (Figure 2.9d, top graph) so presumably entraps the dye added as stain (Nile blue). When **1** assembles, there is little dye still available and hence the structures formed by **1** are not detected by confocal microscopy (Figure 2.11f, right image).

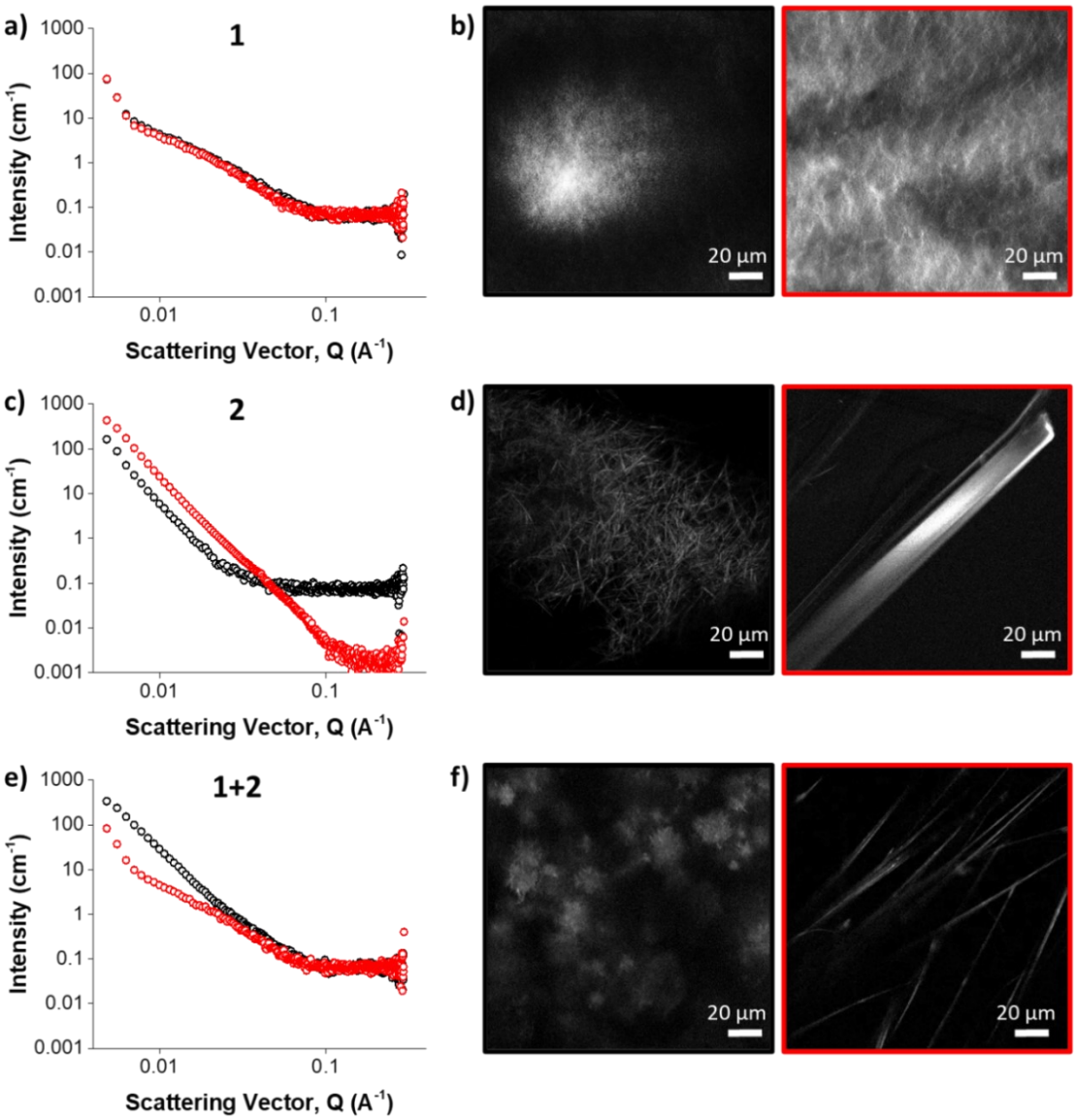

Figure 2.11 SAXS data for (a) gel **1**, (c) gel **2** and (e) multicomponent system (**1+2**). The baseline for **2** drops after annealing as there is crystallisation and a small amount of precipitation, meaning that there is less sample in the beam after annealing. Confocal images for (b) gel **1**, (d) gel **2** and (f) multicomponent gel (**1+2**). Black and red data represent gels before and after annealing respectively. Scale bars represent 20 µm.

2.2.4.IV. Nuclear Magnetic Resonance (NMR)

Under polarised light, there are limited indications of crystallinity (Figure 2.12d, bottom image), implying that the structures formed by **2** have been modified by being formed in the presence of **1**. This is backed up by ^{1}H NMR data; whilst the signal intensity for **1** in the mixture is essentially the same as for the single component (Figure 2.12b), the solubility of **2** is affected by the presence of **1** (Figure 2.12c).

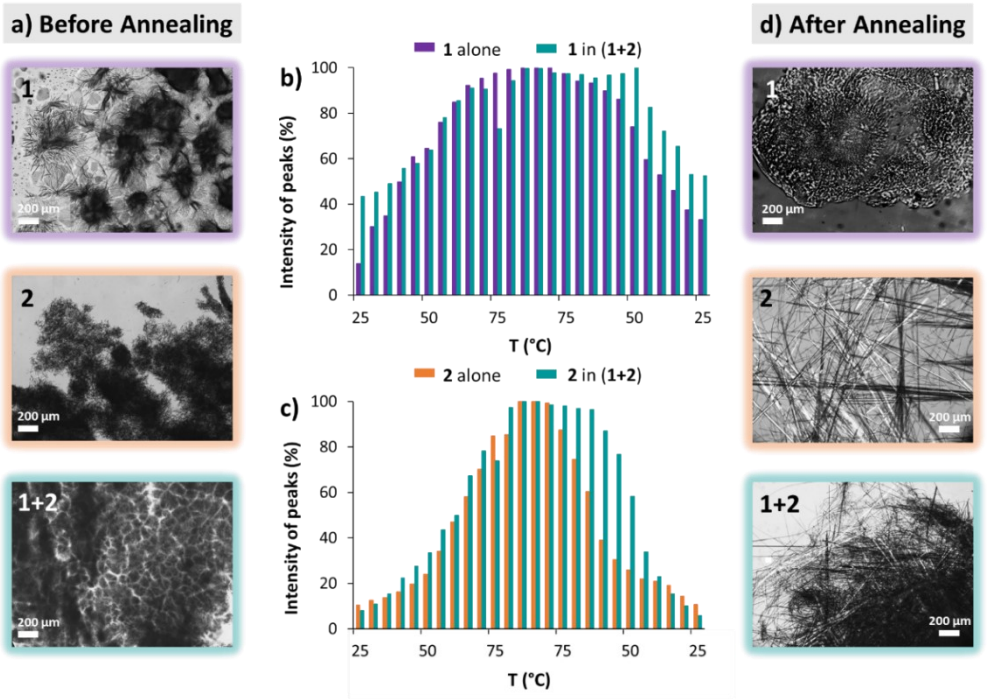

Figure 2.12 Images of gels **1**, **2** and (**1+2**) before (a) and after (d) annealing (25°C - 90°C) under polarised light. Plot of (b) integrals for **1** against a standard as determined by ^{1}H NMR for **1** alone (purple data) in a mixture of DMSO and D_2O (3/7) on heating and cooling as compared to the integral of **1** in the mixed (blue cyan data) (**1+2**) gel; (c) integrals for **2** against a standard as determined by ^{1}H NMR for **2** alone (orange data) in a mixture of DMSO and D_2O (3/7) on heating and cooling as compared to the integral of **2** in the mixed (cyan data) (**1+2**) gel. The scale bars represent 200 µm.

As mentioned previously, the solubility of a molecule can be monitored through the integration of ^{1}H NMR spectra at a range of different temperatures. We proved that the solubility of **1** alone is symmetrical during heating and cooling

as the intensity of the hydrogen atoms from the CH_3 residual peak signal (0.89 ppm) was also symmetrical. For **2** alone we also monitored the intensity of the hydrogen atoms from the CH_3 residual peak signal (1.36 ppm), which also confirmed the symmetrical solubility during heating and cooling (Figure 2.13).

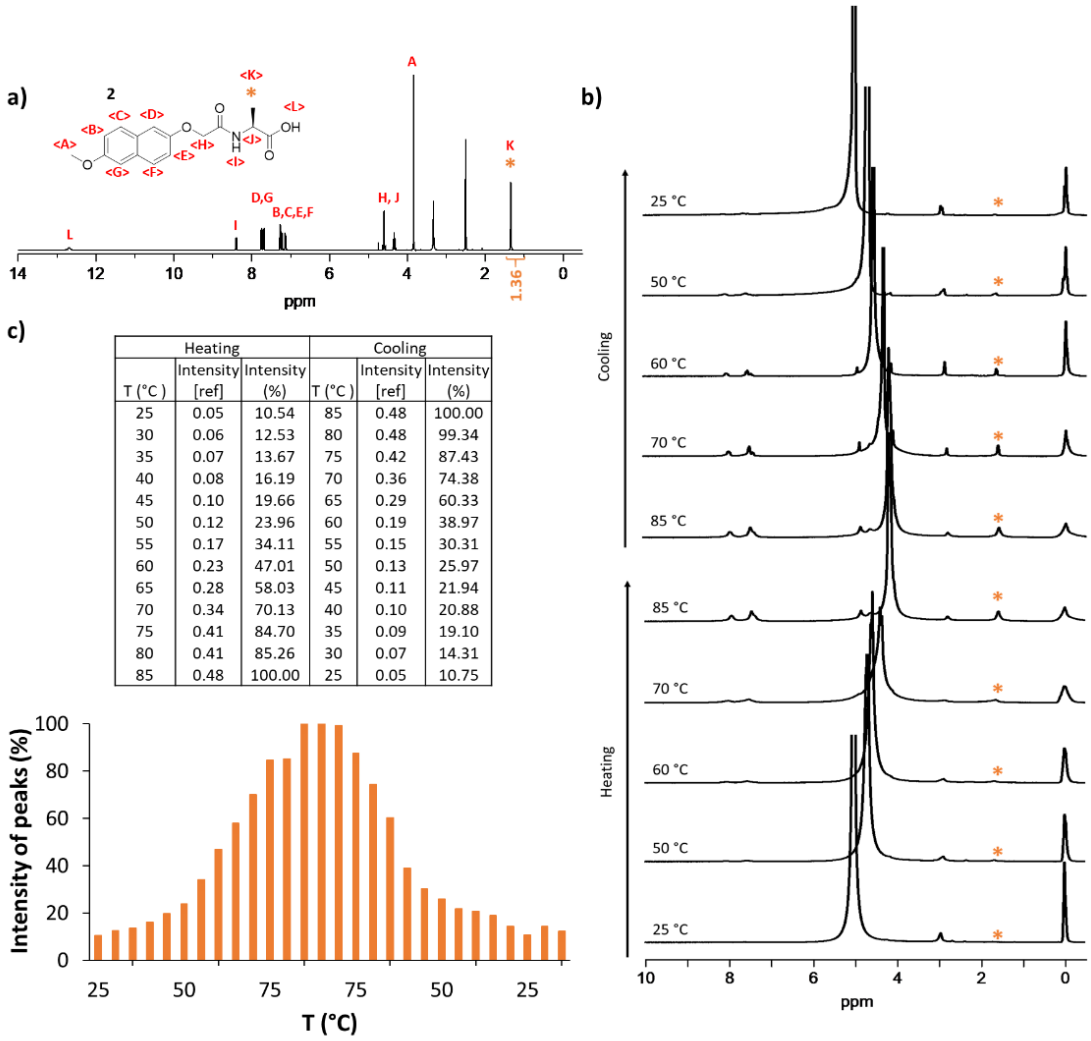

Heating			Cooling		
T (°C)	Intensity [ref]	Intensity (%)	T (°C)	Intensity [ref]	Intensity (%)
25	0.05	10.54	85	0.48	100.00
30	0.06	12.53	80	0.48	99.34
35	0.07	13.67	75	0.42	87.43
40	0.08	16.19	70	0.36	74.38
45	0.10	19.66	65	0.29	60.33
50	0.12	23.96	60	0.19	38.97
55	0.17	34.11	55	0.15	30.31
60	0.23	47.01	50	0.13	25.97
65	0.28	58.03	45	0.11	21.94
70	0.34	70.13	40	0.10	20.88
75	0.41	84.70	35	0.09	19.10
80	0.41	85.26	30	0.07	14.31
85	0.48	100.00	25	0.05	10.75

Figure 2.13 (a) ^{1}H NMR spectrum of **2** in DMSO-d_6. The orange asterisk indicates the signal correspondent to the CH_3 group. (b) Temperature ramp ^{1}H NMR spectra on heating and cooling in a range of 25°C - 85°C - 25°C. A mixture of 10% DMSO-d_6, 1% PDMS and 89% PCE was used as the internal standard. (c) Integrals for **2** against the standard as determined by ^{1}H NMR for **2** in a mixture of DMSO-d_6 and D_2O (3/7) on heating and cooling. The sample temperature was changed by steps of 5°C, and an NMR spectrum recorded after 1 minute, before being heated or cooled to the required next temperature.

For the multicomponent system (**1+2**), the solubility of **1** and **2** in the mixture was evaluated. As the chemical shift of the hydrogen atoms from CH_3 residual for **1** and **2** are different, 0.89 ppm and 1.36 ppm for **1** and **2** respectively, the solubility of each individual molecule in the mixture was easily assessed (Figure 2.14). On heating, the intensity of the peaks for **1** and **2** alone increase in line with the intensity of the peaks for **1** and **2** in the system (**1+2**) (Figure 2.14d). On cooling, although the intensity of the peaks for **1** in the system (**1+2**) evolves in parallel with those correspondents to **1** alone, the signal of the peaks for **2** in the system (**1+2**) is influenced by the presence of **1** (Figure 2.14d).

To gain further insight into the changes on the gel structures, one can also use the power law gradient of the SAXS data to rationalise the effect of the annealing approach.[57, 58] **1** has a gradient of −2, which would be expected from a mass fractal network such as the kind of gel described here. **2** has a gradient of −4, which, as with the fit of the data to a power law suggests objects too large to be resolved by the SAXS. Prior to annealing, (**1+2**) has a gradient of −3, which suggests a mass fractal with a tight, interconnected structure. However, after annealing, the gradient changes to −2, showing that the structure has returned to a network resembling gel **1**.

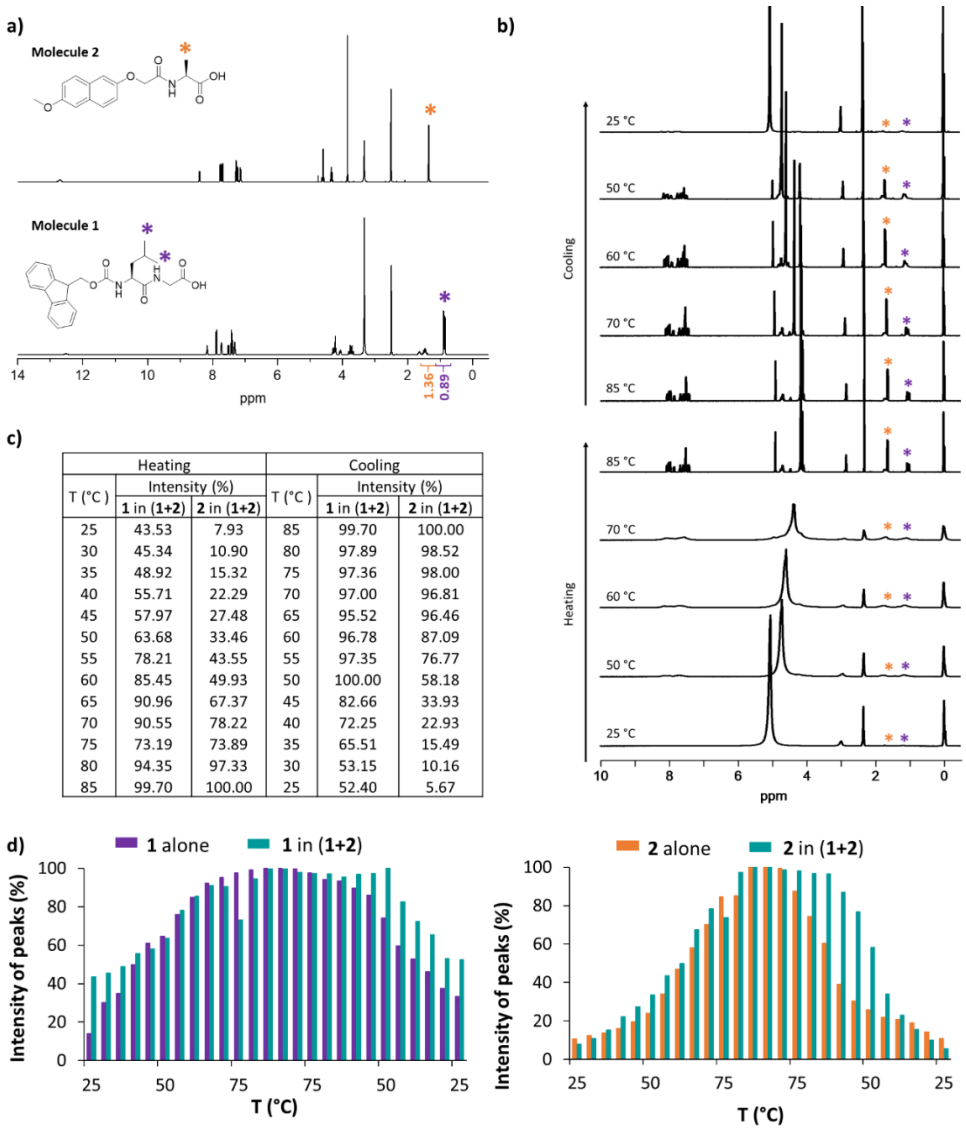

Heating			Cooling		
T (°C)	Intensity (%)		T (°C)	Intensity (%)	
	1 in (**1+2**)	**2** in (**1+2**)		**1** in (**1+2**)	**2** in (**1+2**)
25	43.53	7.93	85	99.70	100.00
30	45.34	10.90	80	97.89	98.52
35	48.92	15.32	75	97.36	98.00
40	55.71	22.29	70	97.00	96.81
45	57.97	27.48	65	95.52	96.46
50	63.68	33.46	60	96.78	87.09
55	78.21	43.55	55	97.35	76.77
60	85.45	49.93	50	100.00	58.18
65	90.96	67.37	45	82.66	33.93
70	90.55	78.22	40	72.25	22.93
75	73.19	73.89	35	65.51	15.49
80	94.35	97.33	30	53.15	10.16
85	99.70	100.00	25	52.40	5.67

Figure 2.14 (a) ^{1}H NMR spectrum of **1** and **2** in DMSO-d_6. The purple and orange asterisks indicate the signal of the hydrogen from CH_3 residual from **1** and **2** respectively. (b) Temperature ramp ^{1}H NMR spectra on heating and cooling in a range of 25°C - 85°C - 25°C for the multicomponent system (**1+2**). A mixture of 10% DMSO-d6, 1% PDMS and 89% PCE was used as the internal standard. (c)-(d) Integrals for **1** and **2** in the system (**1+2**) against the standard as determined by ^{1}H NMR in a mixture of DMSO-d_6 and D_2O (3/7) on heating and cooling. The sample temperature was changed by steps of 5°C, and an NMR spectrum recorded after 1 minute, before being heated or cooled to the required next temperature. In (d) the purple and cyan data represent the integrals for **1** alone and **1** in the system (**1+2**) respectively (left); the orange and cyan data represent the integrals for **2** alone and **2** in the system (**1+2**) respectively (right).

Hence, we clearly have a self-sorted network after annealing, and the distinct melting temperatures imply that the networks are independent on initial formation. The process for the single components and the mixture is shown schematically in Figure 2.15.

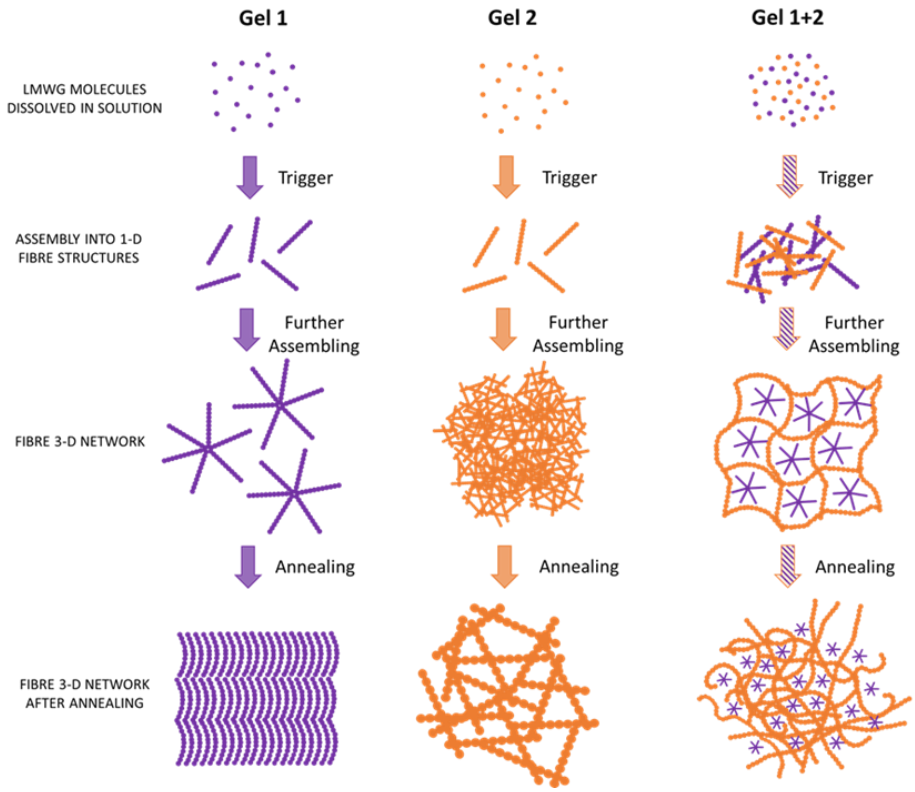

Figure 2.15 Cartoon showing the assembly networks before and after annealing for gels **1**, **2** and the multicomponent system (**1**+**2**).

2.2.4.V. Selective Annealing

The SAXS data show that the primary structures of **1** are the same in the gel of **1** alone and after annealing the gel of (**1**+**2**); the implication is that the changes we are observing are entirely due to changes in the networks. If this is the case, it should be possible to selectively melt and anneal only one of the networks. This is indeed possible. Heating the (**1**+**2**) gel to 65°C leads to a decrease in the moduli in line with the melting of the gel of **1** only in the system (**1**+**2**). Subsequent cooling leads to the expected increase in moduli consistent with our data (Figure 2.16a). Moreover, the resulting network after annealing is also different (Figure 2.16b). The absence of crystals (Figure 2.16b, bottom image)

supports the fact that gel of **2** in the system **(1+2)** has not been affected due to the selective annealing.

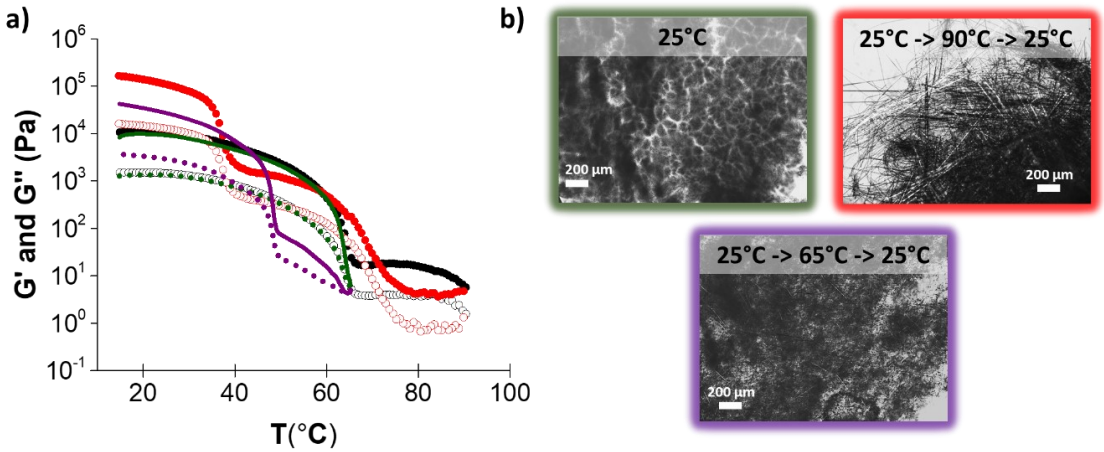

Figure 2.16 (a) Rheological data for (**1+2**) on heating and cooling at a rate of 1°C min^{-1} over a range of 15-90 °C and 15-65 °C. Closed symbols represent G' and open symbols represent G". The black and red data correspond to the heating and cooling cycle respectively in the range of 15-90°C, and the green and purple data correspond to the heating and cooling cycle respectively in the range of 15-65°C. (b) Optical images for gel (**1+2**) before annealing (green border), after heating and cooling over a range of 25-90°C (red border) and after heating and cooling over a range of 25-65°C (purple border).

2.2.4.VI. Ageing of Gels

Finally, we stress that the effects observed are due to annealing and not due to time. When the gels are allowed to stand for 5 days at room temperature, there are almost no differences in the rheological properties. Annealing gels formed overnight or after being allowed to stand for 5 days results in very similar characteristics (Figure 2.17).

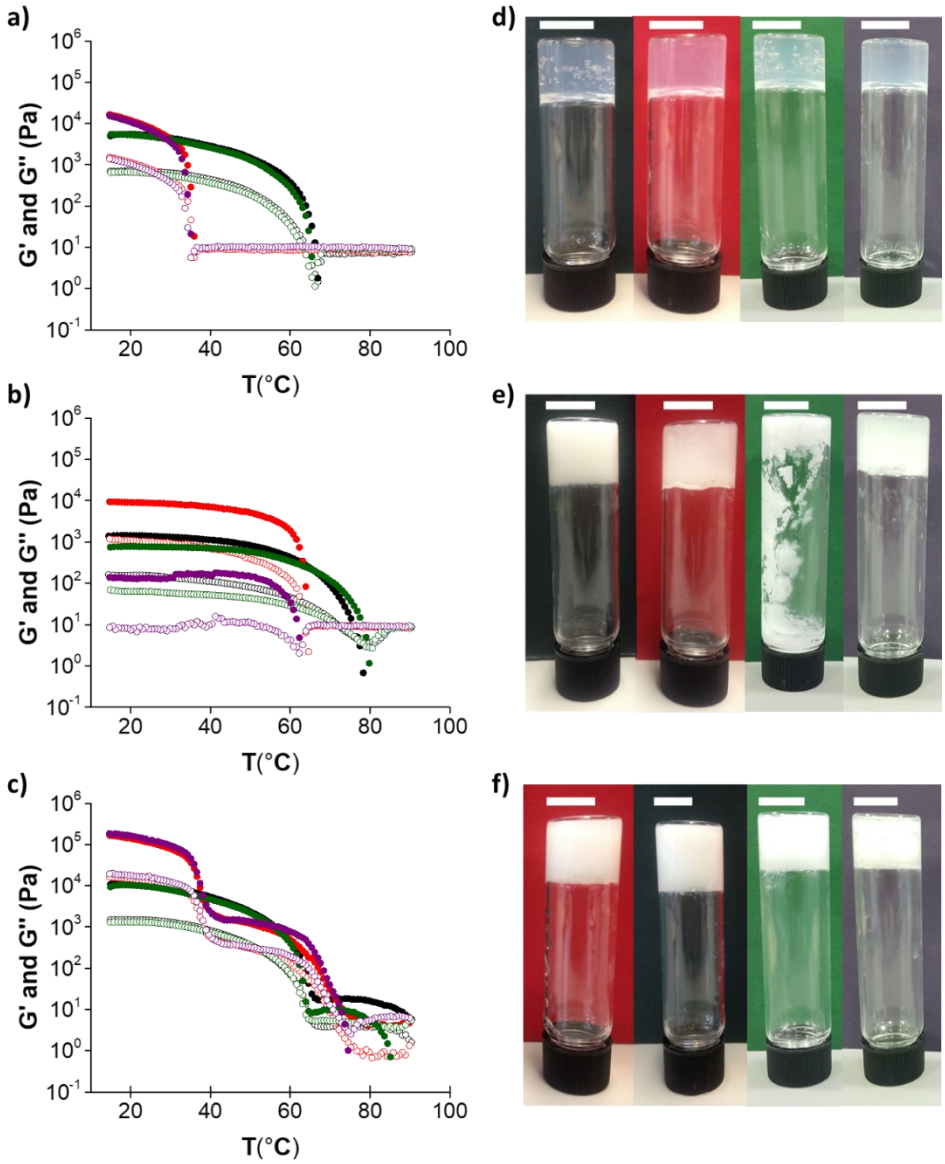

Figure 2.17 Rheological heating and cooling data for (a) **1**; (b) **2**; (c) (**1**+**2**) at a rate of 1°C min^{-1} over a range of 15-90°C. Closed symbols represent G' and open symbols represent G". The black and red data corresponds to the heating and cooling cycle respectively for Day 1, and the green and purple data corresponds to the heating and cooling cycle respectively for Day 5 after gel formation. Photographs of gels (d) **1**; (e) **2**; (f) (**1**+**2**) for Day 1 and Day 5 before and after annealing. The black and red backgrounds correspond to the gel before and after annealing respectively for Day 1, and the green and purple backgrounds refers to the gel before and after annealing respectively for Day 5. Scale bars represent 1 cm in all cases.

2.3. Conclusions

Generally, gels reported in the literature are described as static systems where a gel is formed and used as it is. With reference to tuneable materials, there are many examples of simple gel-to-sol transitions in single component systems, for example triggered by light or by heating. There has also been significant recent work on the formation of transient assemblies[59,60, 61, 62] however their use is limited to the few applications that require the networks to only exist temporally. Instead, we believe that there is more utility in being able to prepare tuneable and responsive networks, where specific input from the user results in a significant and useful change in properties.

Annealing can be applied to many different materials as a means of driving from kinetically trapped structures to those at the (or at least a local) thermodynamic minimum. While it is common to prepare gels using heat-cool cycles, it is not common to use an annealing approach in supramolecular gels. We have shown how annealing can be used to change the underlying microstructure in both single and multicomponent gels. Annealing in a two-component gel leads to a self-sorted network, with significantly different mechanical properties to the as-prepared gels. The display and demonstration of self-sorting at the fibre level does not necessarily substantiate how the network is being affected. We suggest that annealing of this system leads to significant change in the network level of assembly, resulting in the increase in storage modulus.

The apparent changes in mechanical properties are likely to not only affect the stiffness, but also diffusion and transport within the gel. This could be implemented in controlled release systems for example. There is also the possibility to selectively anneal only a single component in the mixture. Although only a specific example is reported here, we believe that this approach will be widely applicable and so opens up new opportunities to control gel networks on demand to provide tuneable, triggerable materials. We demonstrated that annealing a multicomponent system results in gels with

properties that are not simply an addition of the properties of what might be expected from the single components.

2.4. Experimental

2.4.1. Synthetic Procedures

1 and **2** were prepared as described previously.[63] **1** was synthesised by Dave Adams and **2** by Bart Dietrich (both University of Glasgow). All other chemicals used were purchased from commercial suppliers and used as received.

1 was prepared as described in detail below.

Tert-butyl 2-[(2S)-2-({[(9H-fluoren-9-yl)methoxy]carbonyl}amino)-4-methyl-pentanamido]acetate (**DG-004**)

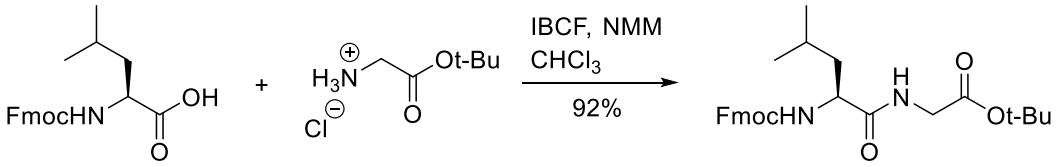

DG-004

To a solution of *N*-Fmoc-*L*-leucine (6.47 g, 18.3 mmol) in chloroform (75 mL) was added *iso*butyl chloroformate (1 eq, 2.37 mL) and *N*-methylmorpholine (1 eq, 2.01 mL) and the mixture was stirred for 30 minutes. Glycine *tert*-butyl ester hydrochloride (1 eq, 3.07 g) and another portion of *N*-methylmorpholine (1 eq, 2.01 mL) were added and the reaction mixture was stirred overnight. After this time, it was diluted with chloroform and washed in turn with 1M hydrochloric acid, water, and brine, dried ($MgSO_4$), and evaporated under reduced pressure. Crude **DG-004** was thus obtained as a cream solid (7.90 g, 92%) and used as such for the next step. A small amount was purified *via* column chromatography (1:9 ethyl acetate/dichloromethane) to afford an analytical sample. Proton NMR indicates the presence of restricted rotation (approx. 9:1 ratio of rotamers, referred to below as Rot-1 and Rot-2). The rotamer signals coalesce when the NMR is run at higher temperature.

δ_H (400 MHz, DMSO-d_6, 23 °C) 8.23 (1H, t, *J* 5.90, $CH_2N\underline{H}$), 7.89 (2H, d, *J* 7.52, $\underline{H}_{Ar}$), 7.73 (1.8H, dd, *J* 7.36, 2.80, Rot-1 $\underline{H}_{Ar}$), 7.62 (0.2H, dd, *J* 17.34, 8.02, Rot-2 $\underline{H}_{Ar}$), 7.52 (0.9H, d, *J* 8.48, Rot-1 $CH^*N\underline{H}$), 7.42 (2H, t, *J* 7.26, $\underline{H}_{Ar}$), 7.32 (2H, ddt, 3.72, 0.72, 7.40, $\underline{H}_{Ar}$), 7.08 (0.1H, d, *J* 6.52, Rot-2 $CH^*N\underline{H}$), 4.32-4.19 (3H, m, $OC\underline{H}_2C\underline{H}$), 4.09-4.02 (1H, m, $C\underline{H}^*$), 3.75 (1H, dd, *J* 17.54, 6.30, $NHC\underline{H}_aH_b$), 3.64 (1H, dd, *J* 17.28, 5.72, $NHCH_a\underline{H}_b$), 1.69-1.59 (1H, m, $C\underline{H}(CH_3)_2$), 1.54-1.39 (2H, m, $CH^*C\underline{H}_2$), 1.39 (9H, s, $CH(C\underline{H}_3)_3$), 0.90 (3H, d, *J* 6.56, $CHC_a\underline{H}_3$), 0.85 (3H, d, *J* 6.52, $CHC_b\underline{H}_3$). δ_H (400 MHz, DMSO-d_6, 80 °C) 7.86 (2H, d, *J* 7.60, $\underline{H}_{Ar}$), 7.83 (1H, br s, $CH_2N\underline{H}$), 7.69 (2H, dd, *J* 7.30, 3.35, $\underline{H}_{Ar}$), 7.41 (2H, t, *J* 7.45, $\underline{H}_{Ar}$), 7.32 (2H, ddt, *J* 2.63, 1.08, 11.17, $\underline{H}_{Ar}$), 7.06 (1H, br s, $CH^*N\underline{H}$), 4.34 (1H, dd, *J* 10.48, 7.23, $OC\underline{H}_aH_b$), 4.29 (1H, dd, *J* 10.45, 6.70, $OCH_a\underline{H}_b$), 4.22 (1H, pseudo-t, *J* 6.92, $OCH_2C\underline{H}$), 4.07 (1H, dd, *J* 15.50, 7.65, $C\underline{H}^*$), 3.76 (1H, dd, *J* 17.16, 5.95, $NHC\underline{H}_aH_b$), 3.68 (1H, dd, *J* 17.18, 5.73, $NHCH_a\underline{H}_b$), 1.67 (1H, pseudo-septet, *J* 6.70, $C\underline{H}(CH_3)_2$), 1.52 (1H, d, *J* 7.30, $CH^*C\underline{H}_aH_b$), 1.51 (1H, d, *J* 7.00, $CH^*CH_a\underline{H}_b$), 1.41 (9H, s, $C(C\underline{H}_3)_3$), 0.91 (3H, d, *J* 6.66, $CHC_a\underline{H}_3$), 0.88 (3H, d, *J* 6.58, $CHC_b\underline{H}_3$). δ_C (100 MHz, DMSO-d_6, 25 °C) 172.74, 168.80, and 155.89 ($\underline{C}$=O), 143.90, 143.72, 140.68, 127.58, 127.00, 125.30, and 120.06 ($\underline{C}_{Ar}$), 80.49 ($\underline{C}(CH_3)_3$), 65.54 ($O\underline{C}H_2$), 52.83 ($\underline{C}H^*$), 46.68 ($OCH_2\underline{C}H$), 41.38 ($NH\underline{C}H_2$), 40.76 ($CH^*\underline{C}H_2$), 27.66 ($C(\underline{C}H_3)_3$), 24.12 ($\underline{C}H(CH_3)_2$), 23.03 ($CH\underline{C}_aH_3$), 21.22 ($CH\underline{C}_bH_3$). HRMS (ESI) m/z: $[M+Na]^+$ calcd for $C_{27}H_{34}N_2NaO_5$ 489.2360; found 489.2356.

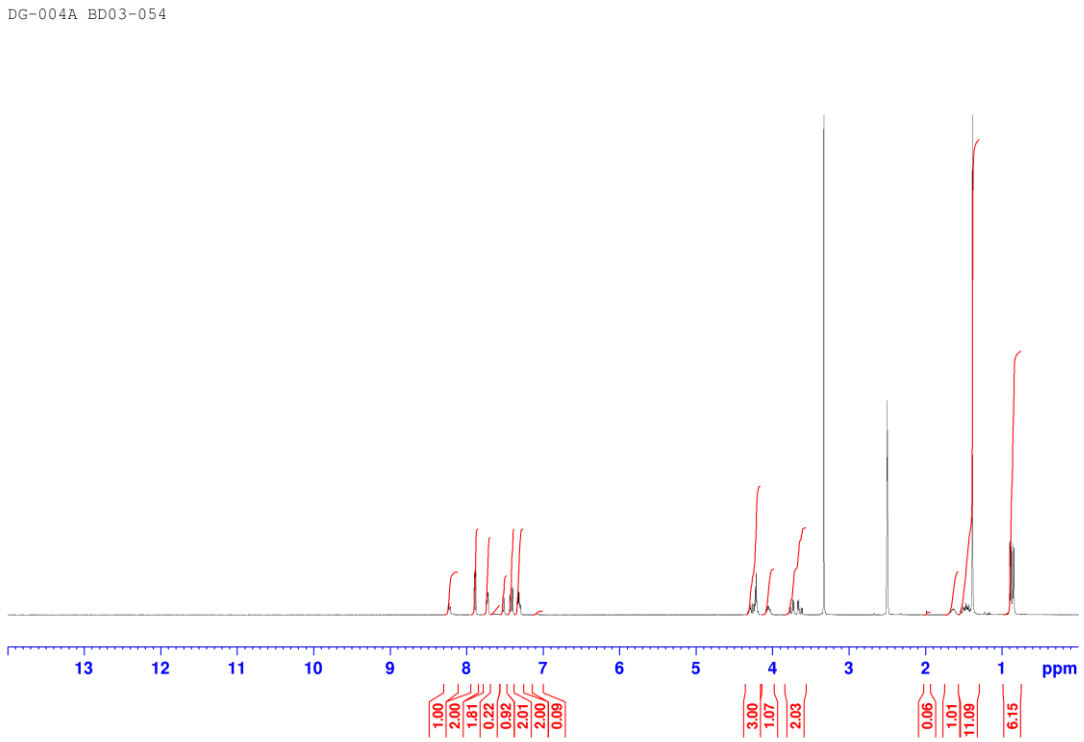

Figure 2.18 Proton NMR of **DG-004**.

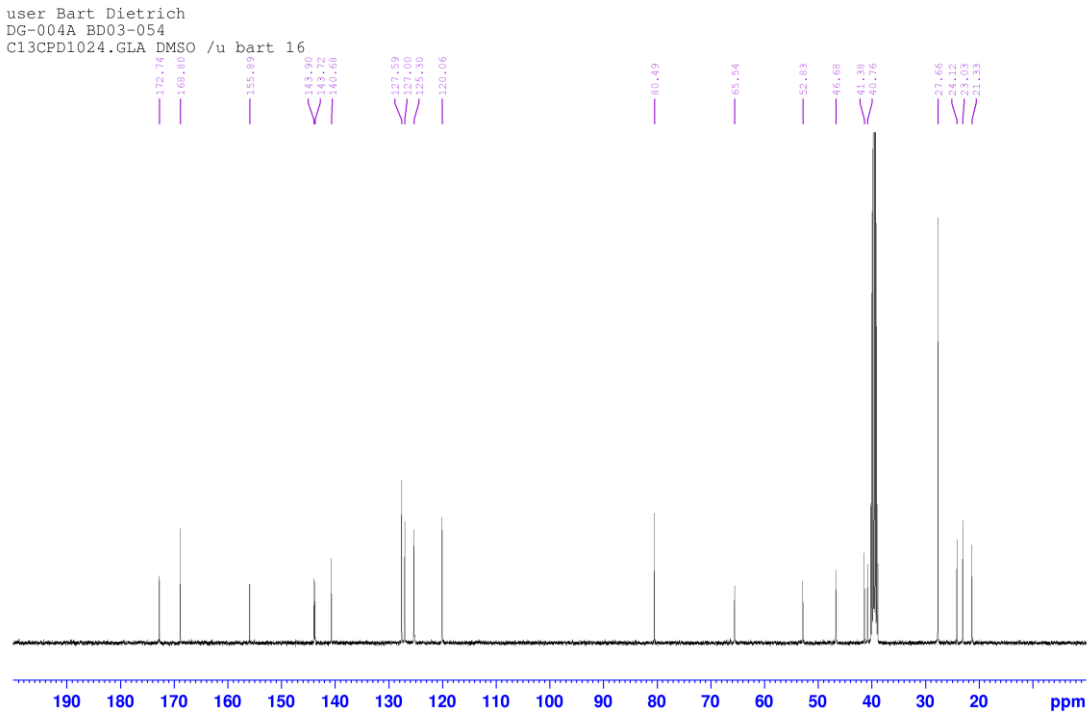

Figure 2.19 Carbon NMR of **DG-004**.

2-[(2S)-2-({[(9H-Fluoren-9-yl)methoxy]carbonyl}amino)-4-methylpentan-amido]acetic acid (**DH-001**)

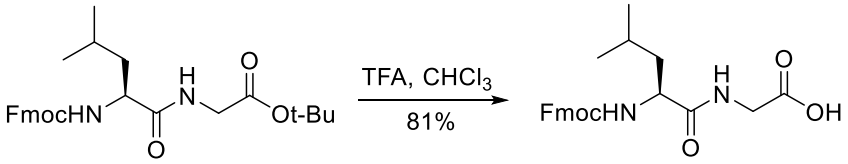

DG-004 **DH-001**

To a solution of **DG-004** (7.81 g, 16.7 mmol) in chloroform (20 mL) was added trifluoroacetic acid (10 mL, *ca.* 8 eq) and the mixture was stirred overnight. After this time, it was poured into diethyl ether (*ca.* 400 mL) and stirred for 1 hour. The white precipitate was filtered off, washed with diethyl ether in the filter and dried under vacuum. Only about 1 g of the title compound was obtained this way. The mother liquor was evaporated under reduced pressure, leaving a viscous, trifluoroacetic acid-containing oil. To this was added diethyl ether and the mixture was stirred overnight. The thick precipitate was filtered off, washed with diethyl ether in the filter and dried under reduced pressure. Including the first crop, a total of 3.80 g of **DH-001** was obtained as a white solid. A further crop of 1.74 g was obtained by another cycle of evaporation, addition of diethyl ether, and filtration. Total yield: 5.54 g (81 %). NMR of the compound suggests a *ca.* 9:1 mixture of rotamers. NMR purity (excluding any moisture) is *ca.* 99.3% (balance 0.7% **DG-004** as judged by the *tert*-butyl peak at 1.39 ppm).

δ_H (400 MHz, DMSO-d_6) 12.52 (1H, br s, COO<u>H</u>), 8.17 (1H, t, *J* 5.84, N<u>H</u>CH_2), 7.89 (2H, d, *J* 7.56, <u>H</u>$_{Ar}$), 7.75-7.72 (1.8H, m, <u>H</u>$_{Ar}$), 7.68-7.64 (0.1H, m, <u>H</u>$_{Ar}$), 7.63-7.59 (0.1H, m, <u>H</u>$_{Ar}$), 7.52 (0.9H, d, *J* 8.56, N<u>H</u>CH*), 7.43-7.40 (2H, m, <u>H</u>$_{Ar}$), 7.35-7.30 (2H, m, <u>H</u>$_{Ar}$), 7.10 (0.1H, d, *J* 7.48, N<u>H</u>CH*), 4.33-4.19 (3H, m, C<u>H</u>C<u>H</u>$_2$-O), 4.10-4.04 (1H, m, NHC<u>H</u>*), 3.74 (2H, qd, *J* 17.74, 5.83, NHC<u>H</u>$_2$), 1.67-1.59 (1H, m, C<u>H</u>$(CH_3)_2$), 1.54-1.39 (2H, m, NHCH*C<u>H</u>$_2$), 0.89 (3H, d, *J* 6.60, CH(C<u>H</u>$_3)_2$), 0.85 (3H, d, *J* 6.52, CH(C<u>H</u>$_3)_2$). δ_C (100 MHz, DMSO-d_6) 172.78, 171.18, and 155.97 (<u>C</u>=O), 143.98, 143.76, 140.74, 127.65, 127.08, 125.37, and 120.12 (<u>C</u>$_{Ar}$), 65.59 (<u>C</u>H_2O), 52.91 (<u>C</u>H*), 46.74 (<u>C</u>HCH_2O), 40.78 and 40.65 (NH<u>C</u>H_2 and NHCH*<u>C</u>H_2),

24.17 ($\underline{C}H(CH_3)_2$), 23.13 and 21.39 ($CH(\underline{C}H_3)_2$). HRMS (ESI) m/z: $[M+Na]^+$ calcd for $C_{23}H_{26}N_2NaO_5$ 433.1734; found 433.1731.

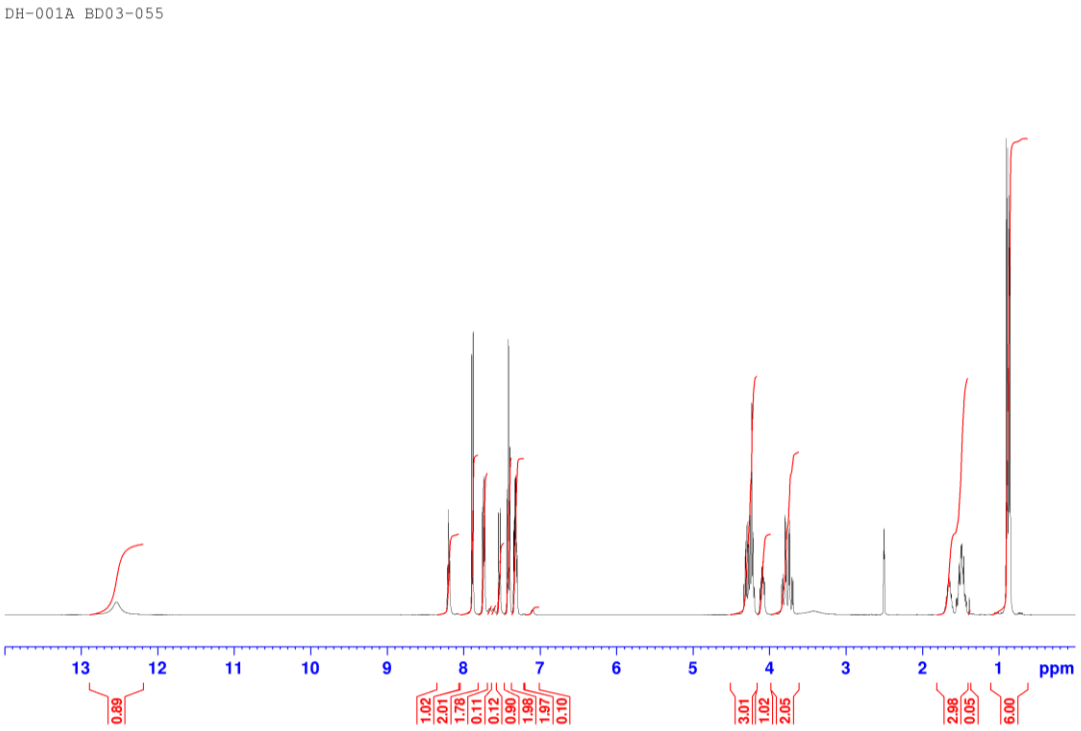

Figure 2.20 Proton NMR of **DH-001**.

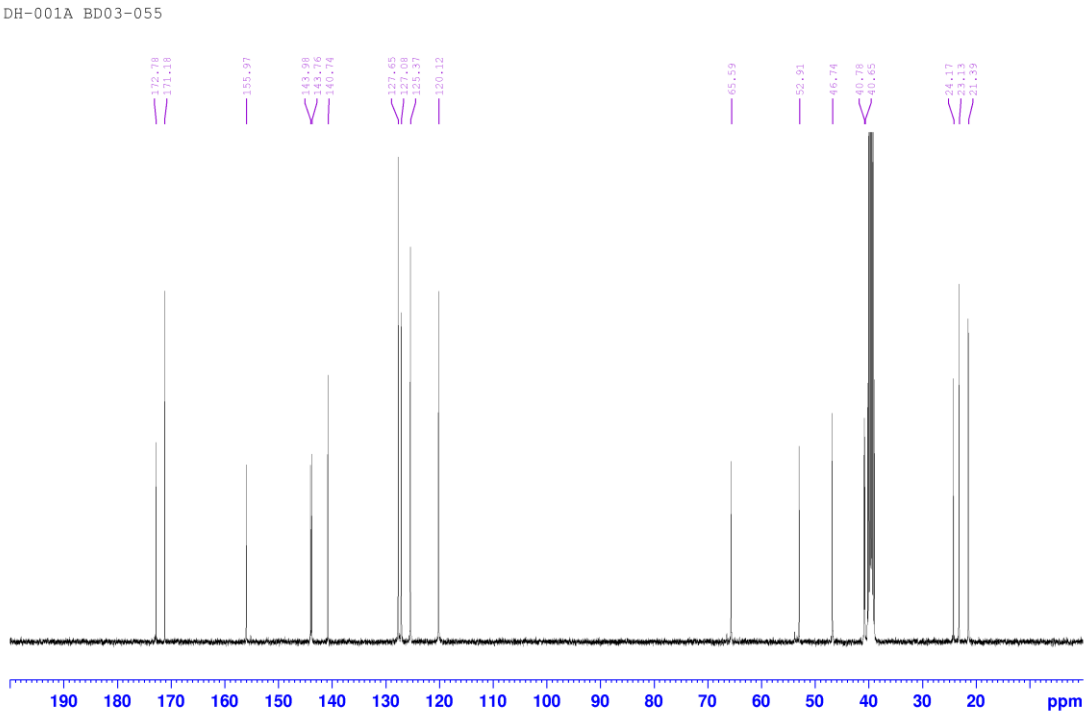

Figure 2.21 Carbon of **DH-001**.

2 was prepared as described in detail below.

Tert-butyl 2-[(6-methoxynaphthalen-2-yl)oxy]acetate (**DL-002**)

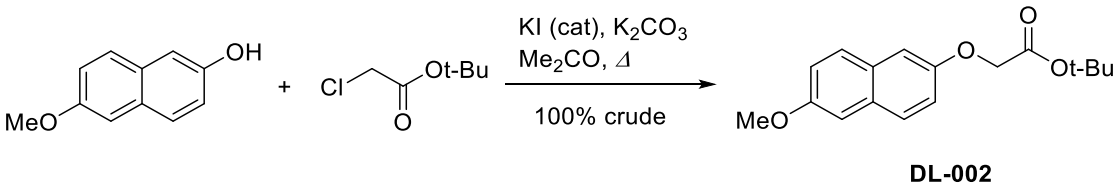

DL-002

To a solution of 6-methoxy-2-naphthol (9.47 g, 54.4 mmol) in acetone (250 mL) was added potassium carbonate (1 eq, 7.51 g) and the mixture was stirred at ambient temperature for two hours. Another portion of potassium carbonate (1 eq, 7.51 g), potassium iodide (1 mol%, 90 mg) and *tert*-butyl chloroacetate (1 eq, 7.79 mL) were added and the reaction mixture was heated at reflux (70 °C oil bath temperature) for two days. After this time, TLC (5:95 ethyl acetate/*n*-hexane) indicated the absence of starting naphthol. The reaction mixture was evaporated to dryness and the residue partitioned between dichloromethane and water and stirred until all solids had dissolved. The layers were separated and the aqueous phase was back-extracted with dichloromethane. The combined organics were washed with water, brine, dried ($MgSO_4$), and filtered through a pad of Celite. Evaporation of the solvent afforded the title compound as a brown oil, which solidified on standing (15.9 g, 100 % crude). This was used as is for the next step. A small amount was purified *via* flash chromatography (eluting with dichloromethane) to afford a sample for characterisation.

δ_H (400 MHz, DMSO-d_6) 7.74 (1H, d, *J* 8.88, H_{Ar}), 7.69 (1H, d, *J* 8.96, H_{Ar}), 7.27 (1H, d, *J* 2.52, H_{Ar}), 7.19 (1H, d, *J* 2.52, H_{Ar}), 7.16 (1H, dd, *J* 8.82, 2.62, H_{Ar}), 7.12 (1H, dd, *J* 8.96, 2.60, H_{Ar}), 4.72 (2H, s, OCH_2), 3.84 (3H, s, OCH_3), 1.43 (9H, s, $C(CH_3)_3$). δ_C (100 MHz, DMSO-d_6) 167.81 (C=O), 155.84, 153.93, 129.66, 129.12, 128.13, 128.11, 118.81, 118.50, 107.49, and 106.07 (C_{Ar}), 81.30 ($C(CH_3)_3$), 65.15 (OCH_2), 55.04 (OCH_3), 27.65 ($C(CH_3)_3$). HRMS (ESI) m/z: $[M+Na]^+$ calcd for $C_{17}H_{20}NaO_4$ 311.1254; found 311.1242.

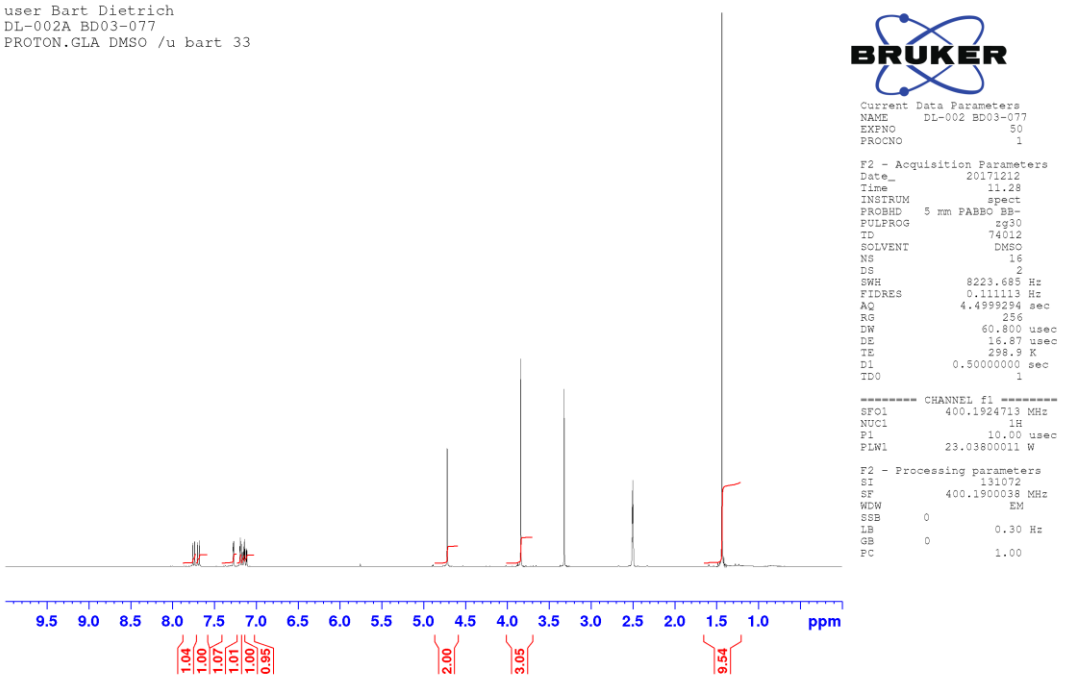

Figure 2.22 Proton NMR of **DL-002** in d_6-DMSO.

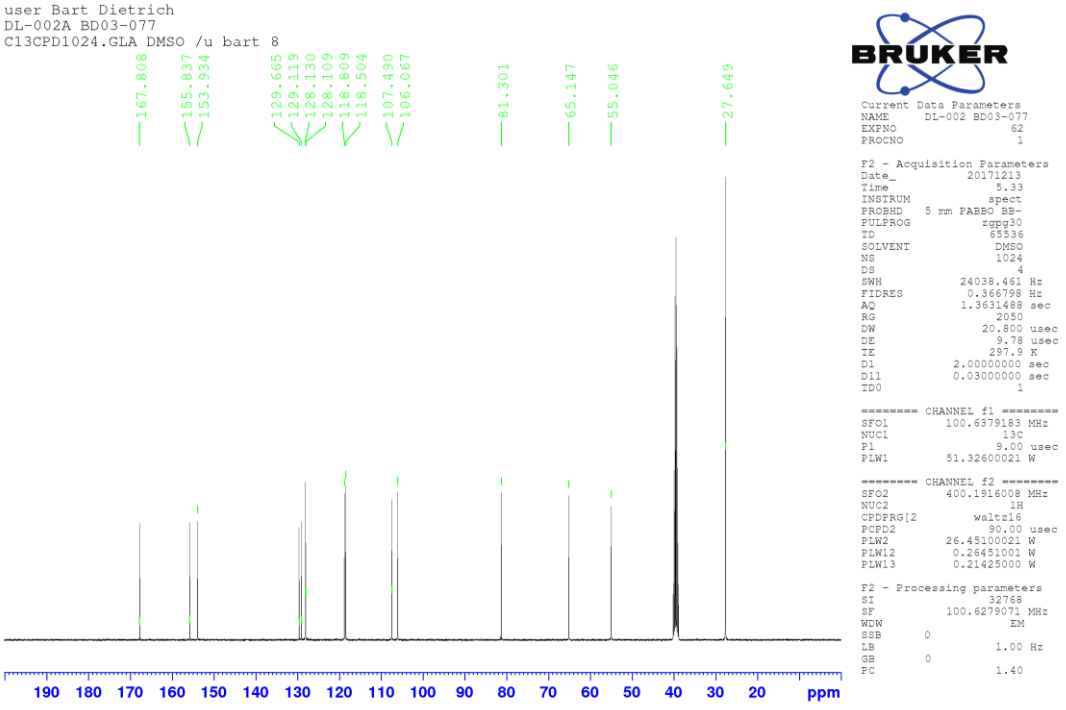

Figure 2.23 Carbon NMR of **DL-002** in d_6-DMSO.

*2-[(6-Methoxynaphthalen-2-yl)oxy]acetic acid (**DL-003**)*

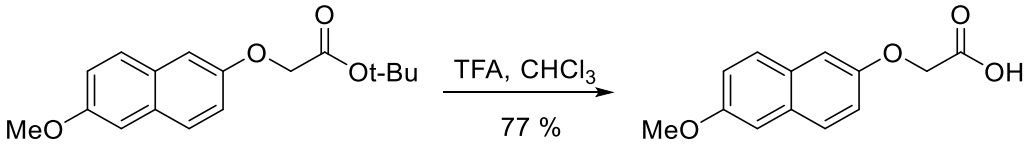

DL-002 **DL-003**

To a solution of **DL-002** (15.6 g, 54.2 mmol) in chloroform (60 mL) was added trifluoroacetic acid (30 mL, *ca.* 7 eq.) and the mixture was stirred overnight. A precipitate was found in the flask after this time. The entire reaction mixture was poured into diethyl ether (500 mL), stirred for three hours, then filtered and the solid in the filter washed with diethyl ether. After drying under reduced pressure, the title compound was obtained as a white solid (9.69 g, 77 %). One carbon NMR signal is not resolved.

δ_H (400 MHz, DMSO-d_6) 13.02 (1H, br s, COOH), 7.74 (1H, d, *J* 9.00, H_{Ar}), 7.70 (1H, d, *J* 9.00, H_{Ar}), 7.27 (1H, d, *J* 2.48, H_{Ar}), 7.21 (1H, d, *J* 2.56, H_{Ar}), 7.16 (1H, dd, *J* 8.90, 2.62, H_{Ar}), 7.12 (1H, dd, *J* 8.90, 2.58, H_{Ar}), 4.75 (2H, s, CH_2), 3.84 (3H, s, OCH_3). δ_C (100 MHz, DMSO-d_6) 170.27 (C=O), 155.86, 154.10, 129.70, 129.22, 128.22, 118.87, 118.68, 107.33, and 106.11 (C_{Ar}), 64.61 (CH_2), 55.11 (OCH_3). HRMS (ESI) m/z: $[M+Na]^+$ calcd for $C_{13}H_{12}NaO_4$ 255.0628; found 255.0623.

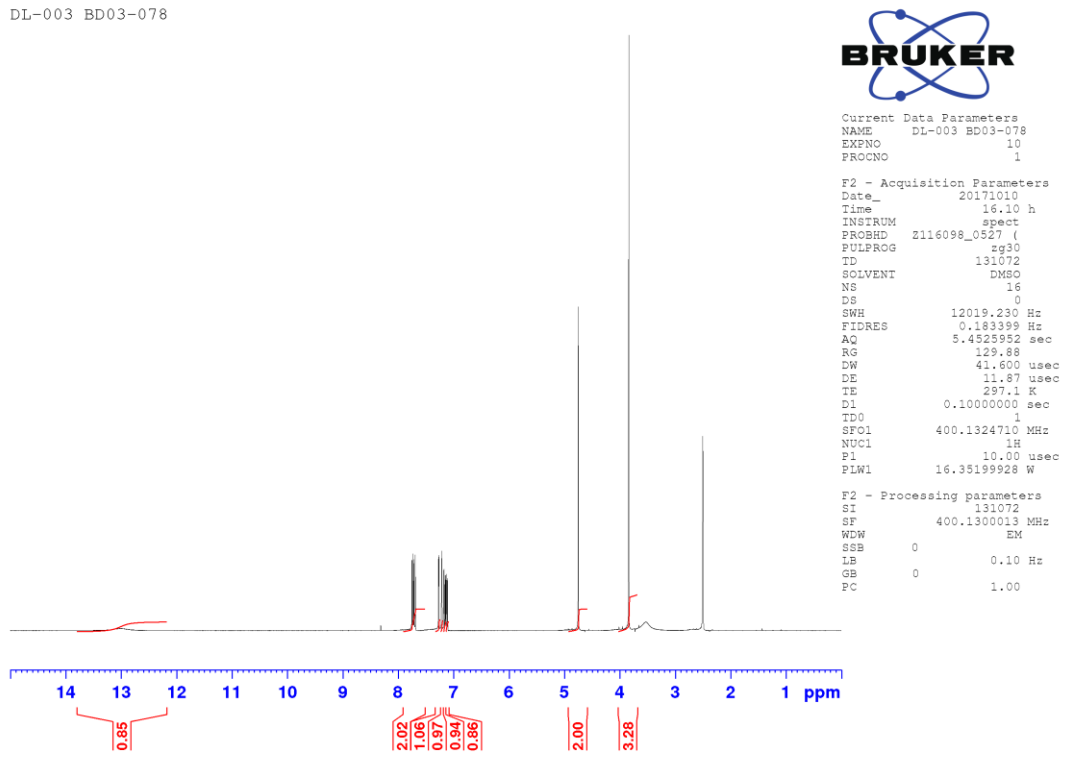

Figure 2.24 Proton NMR of **DL-003** in d_6-DMSO.

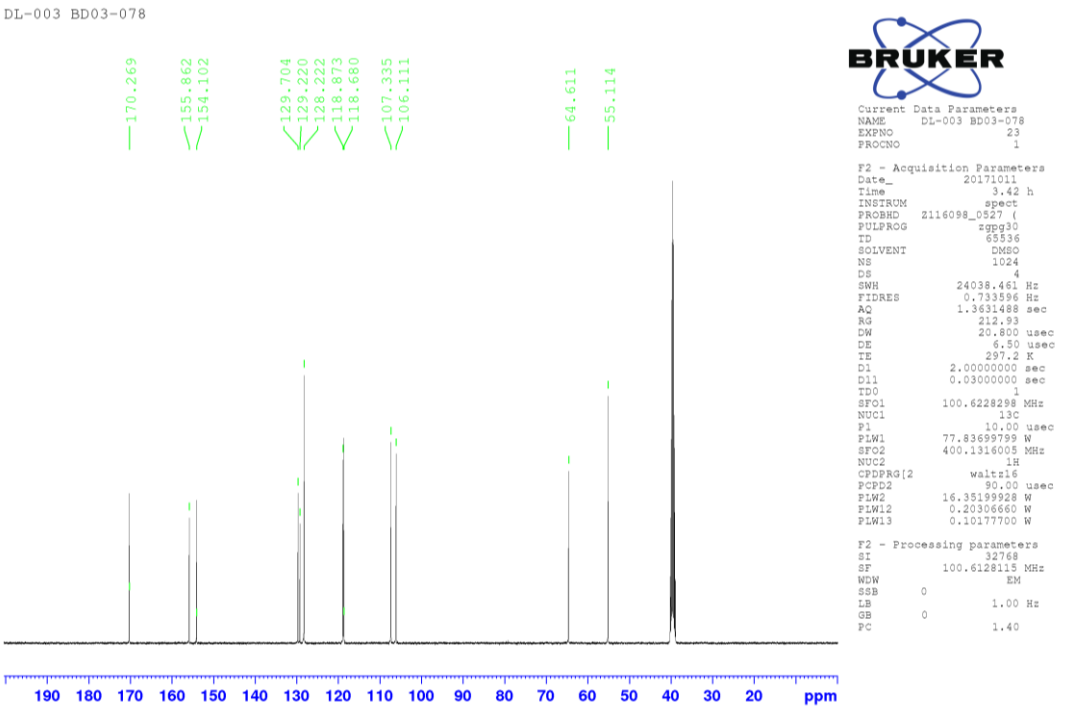

Figure 2.25 Carbon NMR of **DL-003** in d_6-DMSO.

*Methyl (2S)-2-{2-[(6-methoxynaphthalen-2-yl)oxy]acetamido}propanoate (**DL-004**)*

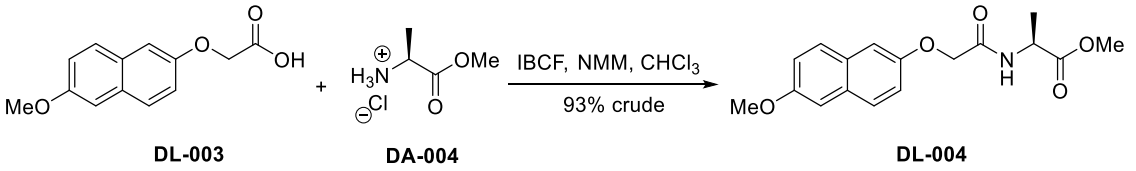

DL-003 **DA-004** **DL-004**

To a suspension of **DL-003** (4.34 g, 18.7 mmol) in chloroform (100 mL) was added *N*-methylmorpholine (1 eq., 2.06 mL) followed by *iso*butyl chloroformate (1 eq., 2.42 mL) and the mixture was stirred for two hours. Another portion of *N*-methylmorpholine (1 eq., 2.06 mL) and **DA-004** (*L*-alanine methyl ester hydrochloride, prepared from *L*-alanine, methanol and acetyl chloride) was added and the mixture stirred overnight. After this time, it was diluted with chloroform, washed with 1M hydrochloric acid, water, brine, dried ($MgSO_4$), and evaporated under reduced pressure. The title compound was thus obtained as a grey solid (5.53 g, 93% crude) and used as is for the next step. A small amount was purified *via* flash chromatography (1:9 ethyl acetate/dichloromethane) to yield a sample for characterisation.

δ_H (400 MHz, DMSO-d_6) 8.56 (1H, d, *J* 7.40, NH), 7.76 (1H, d, *J* 8.88, H_{Ar}), 7.70 (1H, d, *J* 9.00, H_{Ar}), 7.28 (1H, d, *J* 2.52, H_{Ar}), 7.25-7.21 (2H, m, H_{Ar}), 7.14 (1H, dd, *J* 8.92, 2.60, H_{Ar}), 4.62 (1H, d, *J* 14.73, CH_aH_b), 4.58 (1H, d, *J* 14.73, CH_aH_b), 4.41 (1H, pseudo-quintet, *J* 7.29, CH^*), 3.84 (3H, s, $C_{Ar}OCH_3$), 3.62 (3H, s, CO_2CH_3), 1.34 (3H, d, *J* 7.28, CH^*CH_3). δ_C (100 MHz, DMSO-d_6) 172.74 and 167.66 (C=O), 155.87, 154.03, 129.74, 129.14, 128.15, 128.08, 118.82, 118.79, 107.76, and 106.12 (C_{Ar}), 66.84 (OCH_2), 55.08 ($C_{Ar}OCH_3$), 51.92 (CO_2CH_3), 47.30 (CH^*), 16.85 (CH^*CH_3). HRMS (ESI) m/z: $[M+Na]^+$ calcd for $C_{17}H_{19}NNaO_5$ 340.1155; found 340.1149.

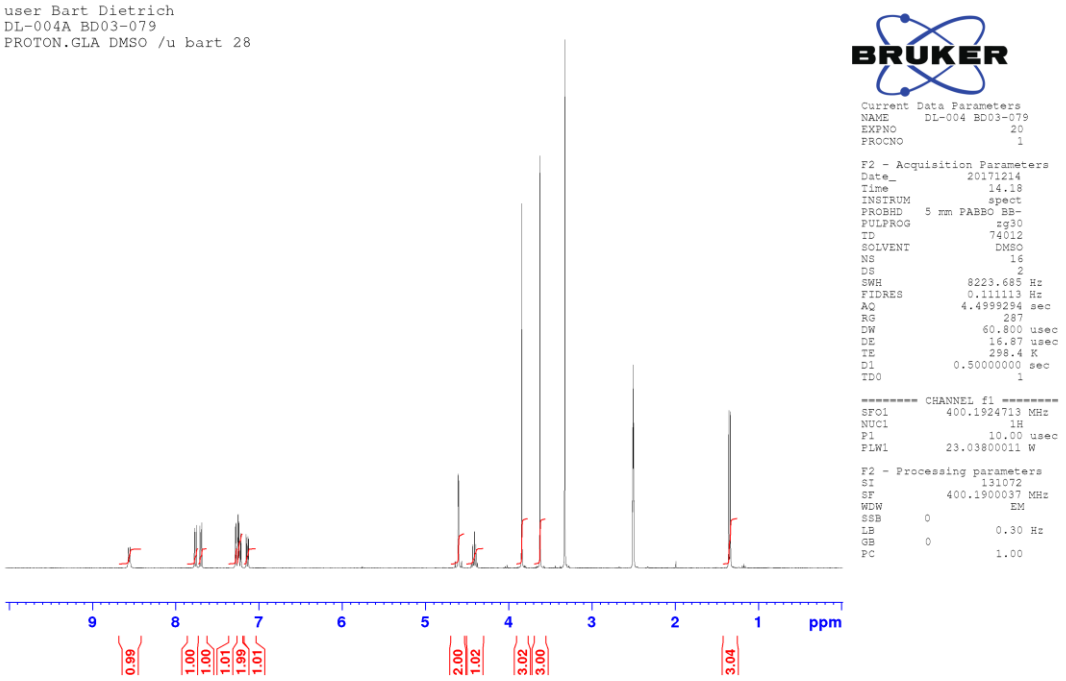

Figure 2.26 Proton NMR of **DL-004** in d_6-DMSO.

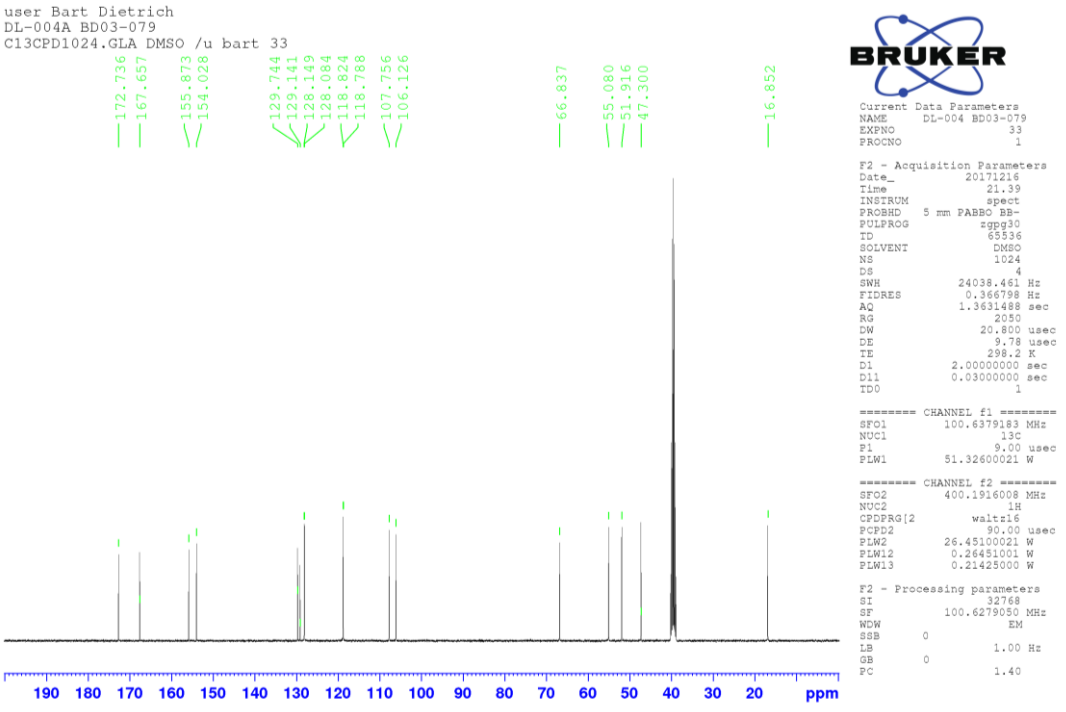

Figure 2.27 Carbon NMR of **DL-004** in d_6-DMSO.

*(2S)-2-{2-[(6-Methoxynaphthalen-2-yl)oxy]acetamido}propanoic acid (**DL-005**, **Molecule 2**)*

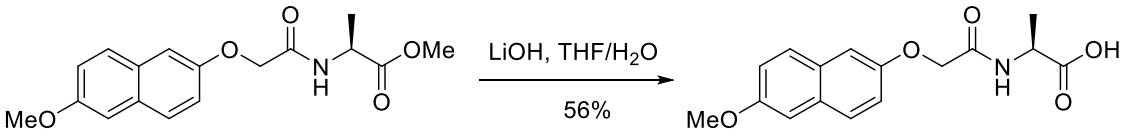

DL-004 **DL-005**

To a solution of **DL-004** (5.29 g, 16.7 mmol) in tetrahydrofuran (80 mL) was added a solution of lithium hydroxide (4 eq., 1.60 g) in water (80 mL) and the mixture was stirred overnight. After this time, it was poured into 1M hydrochloric acid (*ca.* 500 mL), stirred for one hour, and filtered. The solid in the filter was washed with water, then recrystallized from boiling methanol, affording the title compound as a white wool-like solid (2.29 g). A second crop of title compound (536 mg) was obtained by filtration of the mother liquor, which had developed a precipitate upon standing. Total yield 2.83 g (56 %). Evaporation of the mother liquor and repeated recrystallization did not yield any more **DL-005** of acceptable purity. One carbon NMR signal is not resolved. No impurity peaks of note are observed in the proton NMR and the NMR purity of **DL-005** (excluding any moisture) is taken to approach 100%.

δ_H (400 MHz, DMSO-d_6) 12.68 (1H, br s, COOH), 8.40 (1H, d, *J* 7.56, NH), 7.76 (1H, d, *J* 8.96, H_{Ar}), 7.69 (1H, d, *J* 9.00, H_{Ar}), 7.27 (2H, dd, *J* 4.56, 2.64, H_{Ar}), 7.22 (1H, dd, *J* 8.86, 2.58, H_{Ar}), 7.13 (1H, dd, *J* 8.90, 2.54, H_{Ar}), 4.62 (1H, d, *J* 14.65, OCH_aH_b), 4.57 (1H, d, *J* 14.65, OCH_aH_b), 4.33 (1H, dq, *J* 7.32, 7.38, CH^*), 3.84 (3H, s, OCH_3), 1.34 (3H, d, *J* 7.32, CH^*CH_3). δ_C (100 MHz, DMSO-d_6) 173.88 and 167.52 (C=O), 155.91, 154.08, 129.76, 129.20, 128.21, 128.12, 118.83, 107.81, and 106.14 (C_{Ar}), 66.92 (OCH_2), 55.11 (OCH_3), 47.29 (CH^*), 17.14 (CH^*CH_3). HRMS (ESI) m/z: $[M+Na]^+$ calcd for $C_{16}H_{17}NNaO_5$ 326.0999; found 326.0988.

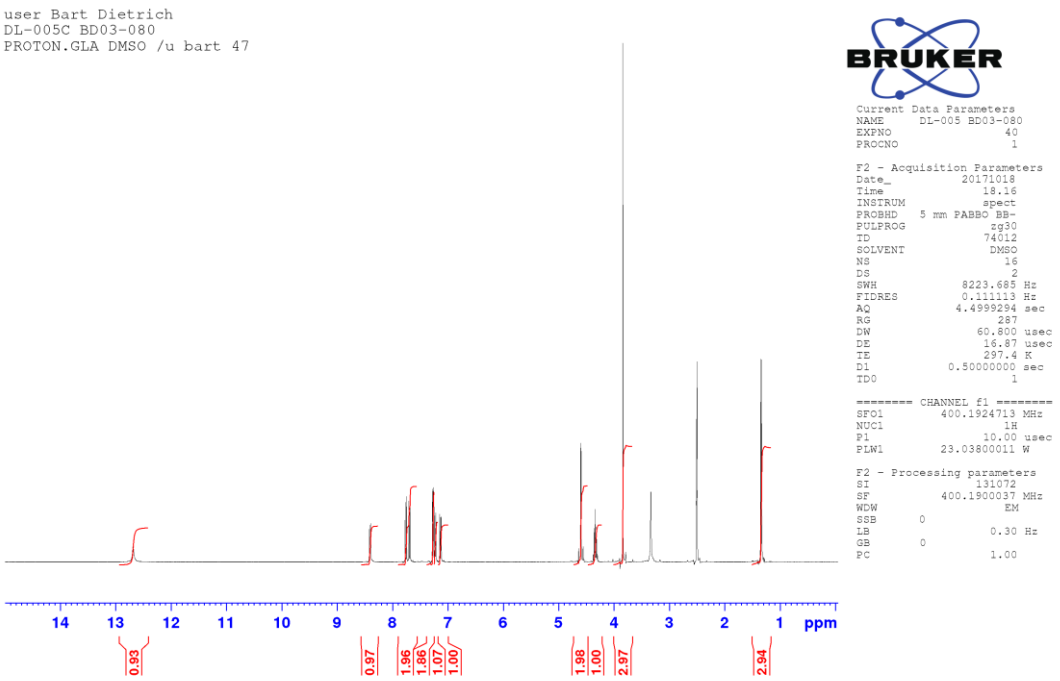

Figure 2.28 Proton NMR of **DL-005 (Molecule 2)** in d_6-DMSO.

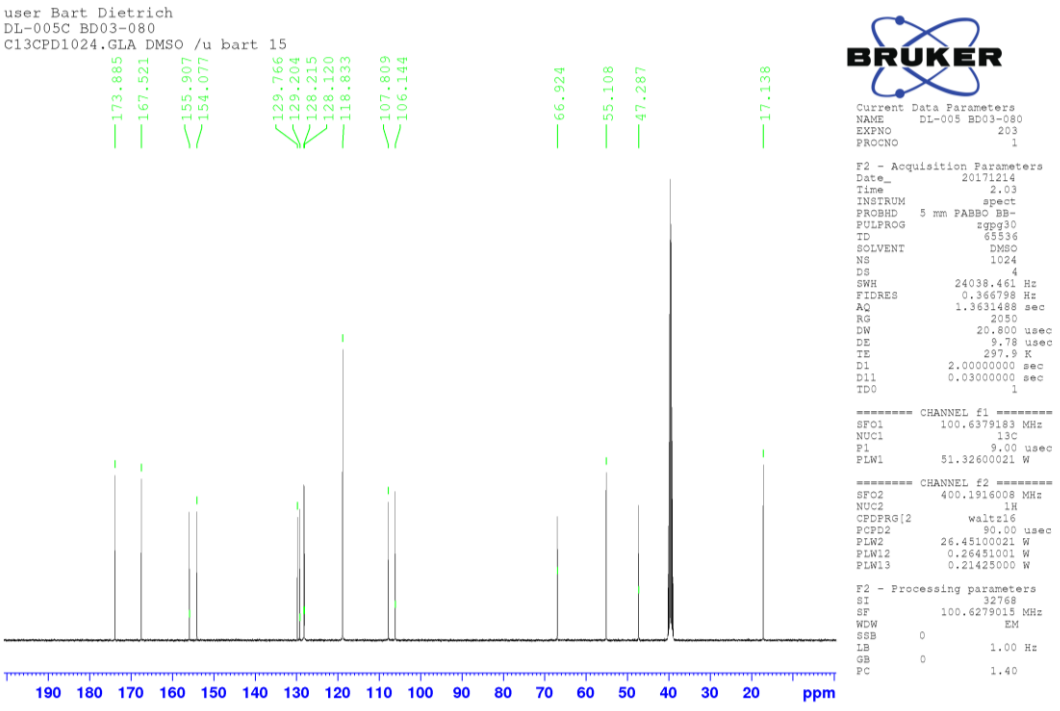

Figure 2.29 Carbon NMR of **DL-005 (Molecule 2)** in d_6-DMSO.

2.4.2. Instrument and Procedures

Gel Formation. For the single component gels, a pre-weighed amount of either **1** or **2** was dissolved in dimethyl sulfoxide (DMSO). Deionised water was added in one aliquot to either solution such that the final ratio of DMSO:water was 3:7 (final volume of 2 mL). The final concentration for **1** and **2** was 4 mg mL^{-1} and 8 mg mL^{-1} respectively. Typically, these gels are at pH 3.9 - 4.3 and are stable. For the multicomponent system (**1+2**), the amount of each gelator used was the same as in the single component (4 mg mL^{-1} of **1** and 8 mg mL^{-1} of **2**). Both **1** and **2** was dissolved again in DMSO to a final ratio of DMSO:water of 3:7, and water was added to this in one aliquot. All samples were prepared in 2 mL volume either in 7 mL Sterilin vials or in metal rheology cups and left overnight to gel prior analysis. Annealing was carried out by heating and cooling the gels typically at 1 ºC·min^{-1} in the rheometer. For photographs of gels after annealing, gels were prepared as described and annealed using an oil bath.

Rheological measurements. Dynamic rheological measurements were carried out using Anton Paar Physica MCR 101 and MCR 301 rheometers. A cup and vane system was used to perform the strain, frequency and temperature sweeps. 2 mL gels were prepared in 7 mL Sterilin vials for strain and frequency measurements and in metal rheology cups for the temperature sweeps. All samples were left overnight (~ 18 hours) at room temperature to gel before measurements. Strain and frequency sweeps were performed at 25°C for samples before annealing and at 15 °C for those after annealing. The strain sweeps were carried out over a range of 0.1 % to 1000 % strain at a frequency of 10 rad s^{-1}. The viscoelastic region was determined as the region where G′ and G″ remain constant up to a strain amplitude at which the gel breaks (γ_c) and G′ deviates from linearity. Frequency sweeps were carried out from an angular frequency of 1-100 rad s^{-1} at a constant strain of 0.5 %, value below the critical strain γ_c. Temperature sweep measurements were performed at a strain of 0.5 % and frequency of 10 rad s^{-1} over a heating-cooling cycle between 15 °C and 90°C at a rate of 1 °C min^{-1}.

pH Measurement. A calibrated FC2020 pH probe from Hanna instruments was used for pH measurements. The stated accuracy of the pH measurements is quoted as ±0.1.

Confocal Microscopy. A Zeiss LSM 710 confocal microscope was used to collect confocal images. The objective used was a LD EC Epiplan NEUFLUAR 50x (0,55 DIC). The samples were stained with 2 μL mL^{-1} of a 0.1 w% Nile Blue solution and excited at 634 nm using a He-Ne laser. All the samples were prepared in-situ using the same methodology as described above where **1** or **2** or (**1+2**) was dissolved in DMSO and then water was added such the final ratio of DMSO:water was 3:7 (final volume 2 mL) and then left overnight to gel. For all of them, 2 μL mL^{-1} of a 0.1 w% Nile Blue solution was added within the water. Thin sections of gel were cut from the central bulk region of each gel using a scalpel to avoid any surface effect. Each cut section was placed in a concave glass slide from Pearl with a cover slip from Menzel-Gläser on the top, and then sealed with nail polish to avoid evaporation. To acquire data after annealing, the samples were first heated in an oven to 90 °C and then gently left to cool down by switching off the oven to ensure a slow cooling rate. Multiple parts of the gel were imaged to ensure a representative structure.

Nuclear Magnetic Resonance (NMR) Spectroscopy. ^1H NMR spectroscopy was used to investigate the gel-sol transition when heating and cooling the samples. The ^1H NMR spectra were recorded on a Bruker Avance III 400 MHz spectrometer. Gels were prepared as above in an NMR tube, replacing DMSO and H_2O with DMSO-d_6 and D_2O (500 μL of sample). A mixture of 10 % DMSO-d_6, 1 % poly(dimethylsiloxane) and 89% of tetrachloroethylene was added in a capillary as the internal reference.

SAXS. All X-ray scattering was performed on a SAXSLAB Ganesha 300XL instrument in a Q range of 0.007-0.25 $Å^{-1}$, with an exposure time of 7200 seconds per sample. Six samples were performed in total, three before annealing and the other three after annealing. The samples before and after annealing were prepared as explained before. A thin section was cut using a

scalpel and then transferred directly to a flat mica cell for measurements. Background corrections were made using both an empty cell and one filled with water. Sample thickness corrections were made using a cell half filled with water and comparing the beam intensities. The data were fitted in the SasView software package.[64]

UV-Vis Spectroscopy. Absorbance spectra were collected on an Agilent Cary 60 spectrophotometer. Samples were prepared in 1 mm pathlength quartz cuvettes purchased from Starna. Firstly, water was added into the cuvette and then DMSO solution containing the gelator was added, such as the final ratio of DMSO:water was 3:7. After the addition of DMSO, the mixture was mixed quickly with the help of a needle. The final volume of gel measured was 300 µL and absorbance was measured at 25 °C over a period of 120 min at a wavelength of 600 nm.

Single Crystal X-Ray Diffraction. Single Crystal X-Ray diffraction data were collected at 150K using a Bruker D8 VENTURE diffractometer equipped with a Photon II CMOS detector, with an Oxford Cryosystems N-Helix device mounted on an IµS 3.0 (dual Cu and Mo) microfocus sealed tube generator at the University of Glasgow.

2.5. References

1. M. de Loos, B. L. Feringa and J. H. van Esch, *Eur. J. Org. Chem.*, 2005, **2005**, 3615-3631.

2. L. A. Estroff and A. D. Hamilton, *Chem. Rev.*, 2004, **104**, 1201-1218.

3. D. B. Amabilino, D. K. Smith and J. W. Steed, *Chem. Soc. Rev.*, 2017, **46**, 2404-2420.

4. C. Colquhoun, E. R. Draper, R. Schweins, M. Marcello, D. Vadukul, L. C. Serpell and D. J. Adams, *Soft Matter*, 2017, **13**, 1914-1919.

5. E. R. Draper and D. J. Adams, *Chem. Soc. Rev.*, 2018, **47**, 3395-3405.

6. X. Du, J. Zhou, J. Shi and B. Xu, *Chem. Rev.*, 2015, **115**, 13165-13307.

7. A. R. Hirst, B. Escuder, J. F. Miravet and D. K. Smith, *Angew. Chem. Int. Ed.*, 2008, **47**, 8002-8018.

8. K. Hong, Y. K. Kwon, J. Ryu, J. Y. Lee, S. H. Kim and K. H. Lee, *Sci. Rep.*, 2016, **6**, 29805.

9. D. K. Kumar and J. W. Steed, *Chem. Soc. Rev.*, 2014, **43**, 2080-2088.

10. J. B. Matson and S. I. Stupp, *Chem. Commun.*, 2012, **48**, 26-33.

11. P. Terech and R. G. Weiss, *Chem. Rev.*, 1997, **97**, 3133-3160.

12. R. G. Weiss, *J. Am. Chem. Soc.*, 2014, **136**, 7519-7530.

13. M. Zhou, A. M. Smith, A. K. Das, N. W. Hodson, R. F. Collins, R. V. Ulijn and J. E. Gough, *Biomaterials*, 2009, **30**, 2523-2530.

14. J. Raeburn, A. Zamith Cardoso and D. J. Adams, *Chem. Soc. Rev.*, 2013, **42**, 5143-5156.

15. F. Tantakitti, J. Boekhoven, X. Wang, R. V. Kazantsev, T. Yu, J. Li, E. Zhuang, R. Zandi, J. H. Ortony, C. J. Newcomb, L. C. Palmer, G. S. Shekhawat, M. O. de la Cruz, G. C. Schatz and S. I. Stupp, *Nat. Mater.*, 2016, **15**, 469-476.

16. J. Boekhoven, J. M. Poolman, C. Maity, F. Li, L. van der Mee, C. B. Minkenberg, E. Mendes, J. H. van Esch and R. Eelkema, *Nat. Chem.*, 2013, **5**, 433.

17. U. Mazur and K. W. Hipps, *Chem. Commun.*, 2015, **51**, 4737-4749.

18. S. Ogi, T. Fukui, M. L. Jue, M. Takeuchi and K. Sugiyasu, *Angew. Chem. Int. Ed.*, 2014, **53**, 14363-14367.

19. S. Ogi, K. Sugiyasu, S. Manna, S. Samitsu and M. Takeuchi, *Nat. Chem.*, 2014, **6**, 188-195.

20. S.-H. Shin, S. Chung, B. Sanii, L. R. Comolli, C. R. Bertozzi and J. J. De Yoreo, *Proc. Natl. Acad. Sci.*, 2012, **109**, 12968.

21. H. Weissman and B. Rybtchinski, *Curr. Opin. Colloid Interface Sci.*, 2012, **17**, 330-342.

22. Y. Yan, J. Huang and B. Z. Tang, *Chem. Commun.*, 2016, **52**, 11870-11884.

23. Y. Yan, J. Huang and B. Z. Tang, *Chem. Commun.*, 2016, **52**, 11870-11884.

24. R. Alberstein, Y. Suzuki, F. Paesani and F. A. Tezcan, *Nat. Chem.*, 2018, **10**, 732-739.

25. L. E. Buerkle and S. J. Rowan, *Chem. Soc. Rev.*, 2012, **41**, 6089-6102.

26. J. Raeburn and D. J. Adams, *Chem. Commun.*, 2015, **51**, 5170-5180.

27. E. R. Draper and D. J. Adams, *Chem. Soc. Rev.*, 2018, DOI: 10.1039/C7CS00804J.

28. B. O. Okesola and A. Mata, *Chem. Soc. Rev.*, 2018, **47**, 3721-3736.

29. L. Wang, X. Shi, Y. Wu, J. Zhang, Y. Zhu and J. Wang, *Soft Matter*, 2018, **14**, 566-573.

30. C. M. Rubert Perez, L. A. Rank and J. Chmielewski, *Chem. Commun.*, 2014, **50**, 8174-8176.

31. E. C. Barker, A. D. Martin, C. J. Garvey, C. Y. Goh, F. Jones, M. Mocerino, B. W. Skelton, M. I. Ogden and T. Becker, *Soft Matter*, 2017, **13**, 1006-1011.

32. F. Tantakitti, J. Boekhoven, X. Wang, R. V. Kazantsev, T. Yu, J. Li, E. Zhuang, R. Zandi, J. H. Ortony, C. J. Newcomb, L. C. Palmer, G. S. Shekhawat, M. O. de la Cruz, G. C. Schatz and S. I. Stupp, *Nat. Mater.*, 2016, **15**, 469.

33. H. Kumari, S. E. Armitage, S. R. Kline, K. K. Damodaran, S. R. Kennedy, J. L. Atwood and J. W. Steed, *Soft Matter*, 2015, **11**, 8471-8478.

34. S. Panettieri and R. V. Ulijn, *Curr. Opin. Struct. Biol.*, 2018, **51**, 9-18.

35. D. M. Raymond and B. L. Nilsson, *Chem. Soc. Rev.*, 2018, **47**, 3659-3720.

36. N. Singh, C. Maity, K. Zhang, C. A. Angulo-Pachón, J. H. van Esch, R. Eelkema and B. Escuder, *Chem. Eur. J.*, 2017, **23**, 2018-2021.

37. Z. Yang, H. Gu, Y. Zhang, L. Wang and B. Xu, *Chem. Commun.*, 2004, 208-209.

38. H. Shigemitsu, T. Fujisaku, W. Tanaka, R. Kubota, S. Minami, K. Urayama and I. Hamachi, *Nat. Nanotechnol.* 2018, **13**, 165-172.

39. A. Mahler, M. Reches, M. Rechter, S. Cohen and E. Gazit, *Adv. Mater.*, 2006, **18**, 1365-1370.

40. R. Orbach, L. Adler-Abramovich, S. Zigerson, I. Mironi-Harpaz, D. Seliktar and E. Gazit, *Biomacromolecules*, 2009, **10**, 2646-2651.

41. L. Chen, J. Raeburn, S. Sutton, D. G. Spiller, J. Williams, J. S. Sharp, P. C. Griffiths, R. K. Heenan, S. M. King, A. Paul, S. Furzeland, D. Atkins and D. J. Adams, *Soft Matter*, 2011, **7**, 9721-9727.

42. N. A. Dudukovic, B. C. Hudson, A. K. Paravastu and C. F. Zukoski, *Nanoscale*, 2018, **10**, 1508-1516.

43. R. Orbach, I. Mironi-Harpaz, L. Adler-Abramovich, E. Mossou, E. P. Mitchell, V. T. Forsyth, E. Gazit and D. Seliktar, *Langmuir*, 2012, **28**, 2015-2022.

44. W. Liyanage and B. L. Nilsson, *Langmuir*, 2016, **32**, 787-799.

45. N. A. Dudukovic and C. F. Zukoski, *Soft Matter*, 2014, **10**, 7849-7856.

46. J. Raeburn, G. Pont, L. Chen, Y. Cesbron, R. Lévy and D. J. Adams, *Soft Matter*, 2012, **8**, 1168-1174.

47. E. R. Draper, E. G. B. Eden, T. O. McDonald and D. J. Adams, *Nat. Chem.*, 2015, **7**, 848.

48. J. Buendia, E. Matesanz, D. K. Smith and L. Sanchez, *CrystEngComm.*, 2015, **17**, 8146-8152.

49. M. Wallace, J. A. Iggo and D. J. Adams, *Soft Matter*, 2015, **11**, 7739-7747.

50. B. Escuder, M. Llusar and J. F. Miravet, *J. Org. Chem*, 2006, **71**, 7747-7752.

51. G. K. Veits, K. K. Carter, S. J. Cox and A. J. McNeil, *J. Am. Chem. Soc.*, 2016, **138**, 12228-12233.

52. A. D. Martin, J. P. Wojciechowski, M. M. Bhadbhade and P. Thordarson, *Langmuir*, 2016, **32**, 2245-2250.

53. K. A. Houton, K. L. Morris, L. Chen, M. Schmidtmann, J. T. A. Jones, L. C. Serpell, G. O. Lloyd and D. J. Adams, *Langmuir*, 2012, **28**, 9797-9806.

54. S. Parsons, H. D. Flack and T. Wagner, *Acta Cryst.*, 2013, **69**, 249-259.

55. M. M. Smith and D. K. Smith, *Soft Matter*, 2011, **7**, 4856-4860.

56. L. L. E. Mears, E. R. Draper, A. M. Castilla, H. Su, Zhuola, B. Dietrich, M. C. Nolan, G. N. Smith, J. Doutch, S. Rogers, R. Akhtar, H. Cui and D. J. Adams, *Biomacromolecules*, 2017, **18**, 3531-3540.

57. H. D. Bale and P. W. Schmidt, *Phys. Rev. Lett.*, 1984, **53**, 596-599.

58. J. Teixeira, *J. Appl. Crystallogr.*, 1988, **21**, 781-785.

59. S. A. P. van Rossum, M. Tena-Solsona, J. H. van Esch, R. Eelkema and J. Boekhoven, *Chem. Soc. Rev.*, 2017, **46**, 5519-5535.

60. S. Panja, C. Patterson and D. J. Adams, *Macromol. Rapid Commun.*, 2019, **40**, 1900251.

61. J. H. van Esch, R. Klajn and S. Otto, *Chem. Soc. Rev.*, 2017, **46**, 5474-5475.

62. A. Jain, S. Dhiman, A. Dhayani, P. K. Vemula and S. J. George, *Nat. Commun.*, 2019, **10**, 450.

63. A. M. Fuentes-Caparrós, F. de Paula Gómez-Franco, B. Dietrich, C. Wilson, C. Brasnett, A. Seddon and D. J. Adams, *Nanoscale*, 2019, **11**, 3275-3280.

64. SasView. Available onlie: www.sasview.org (accessed on 8th June 2018).

CHAPTER 3

Using Cavitation Rheology to Study Dipeptide-Based Low Molecular Weight Gels

This Chapter is adapted in part from the following publication:

"Using cavitation rheology to understand dipeptide-based low molecular weight gels"
Soft Matter, **2019**,15, 6340-6347.
A. M. Fuentes-Caparrós, B. Dietrich, Lisa Thomson, Charles Chauveau and Dave J. Adams.

B. Dietrich built the cavitation rheometer. L. Thomson and C. Chauveau collected preliminary cavitation rheology data. B. Dietrich and D. J. Adams synthesised the molecules. A. M. Fuentes-Caparrós carried out the rheology experiments (cavitation and oscillatory) and the confocal microscopy. D. J. Adams and A.M. Fuentes-Caparrós wrote the initial draft of the paper, to which all authors contributed for the final manuscript.

3.1. Introduction

Supramolecular gels result from the self-assembly of discrete molecules into fibres by non-covalent interactions.[1-4] Such non-covalent interactions are individually weak, although when they work in conjunction, robust self-assembly can occur. As a consequence, these class of materials are reversible. Hence, application of an external stimulus can result in the reverse gel-to-sol transition. Consequently, LMWGs are an attractive class of materials that are receiving significant attention and have been examined for a wide range of different potential applications including regenerative medicine,[5] electronic devices,[5] cell culture,[6] and pollutant removal from environment.[7]

Due to their diverse applications, LMWGs should meet different specific properties. The final gel properties will be governed by both the self-assembly of the molecules into the primary structures and the subsequent entanglement, cross-linking and interaction of fibres to form the 3D network.[8-12] As such, it is necessary to characterise the mechanical properties across multiple length scales in order to fully characterise and understand this type of soft materials. Different properties can be assessed for example by controlling the volume fraction of the solvent and the temperature cycle used,[13] or even by modifying the gels post-gelation through a thermal annealing as shown in Chapter 2.

In terms of mechanical properties, the linear elastic modulus is normally measured using traditional shear rheometry. This technique requires millilitre sample volumes,[14] which can be difficult when only small amounts of gel are available,[15] and can present difficulties when loading the sample into the machine. Microrheology can overcome some of the limitations of the bulk rheology, however the use of probe particles can interfere in the local microstructure being measured.[16]

Here, we describe the use of cavitation rheology, an easy and efficient technique developed by Zimberlin *et al.*[17], to characterise the linear elastic modulus of a range of hydrogels. Unlike traditional shear rheometry, this

technique can be used to look at a local point within the gel system in their native environment, and small sample volumes are required. The basic principle of cavitation rheology consists of growing an air bubble within the material and monitoring the maximum pressure, the critical pressure, P_c, that the material can support before the bubble burst.[17-35] The P_c value can then be used to establish the elastic modulus of the material, Figure 3.1 (see Chapter 1 Section 1.6.2. for more detailed information).[17]

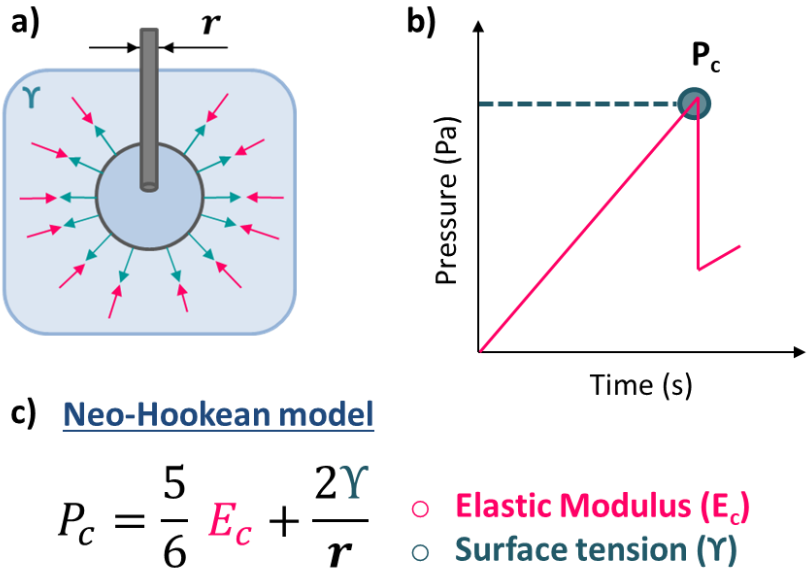

Figure 3.1 (a) Diagram showing the cavitation phenomenon where γ is the surface tension of the solvent and r represents the radius of the needle used to grow the air bubble within the gel. (b) Cartoon showing an example of cavitation rheology output. The blue circle represents the pressure at which the air bubble fails, P_c. (c) The Neo-Hookean equation that relates the critical pressure, P_c, from cavitation rheology, with the elastic modulus, E_c. P_c is the critical pressure in Pa, E_c is the elastic cavitation modulus in Pa, γ is the surface tension in N m^{-1} and r represents the radius of the needle in m.

This method allows to characterise gels of any shape in their native environment in a micrometre scale, whilst shear rheology requires precise isolated samples prepared in specific shapes and containers to be placed onto or into the rheometer.[36]

Pavlovsky and co-workers used a correction factor to compare both shear and cavitation moduli, although they examined solutions and not gels.[37] Other researchers have looked at the correlation between modulus obtained from shear and cavitation rheology in a number of organogels.[24, 25] Their results show cavitation moduli were always an order of magnitude greater than shear moduli. Bentz *et al.* reported recently a quantitative relationship, k_{sc}, between the gel modulus determined using shear and cavitation rheology for a series of model polymer gels.[38] This quantitative constant can be used to interconvert between shear storage (G') and cavitation (E_c) modulus (Figure 3.2).

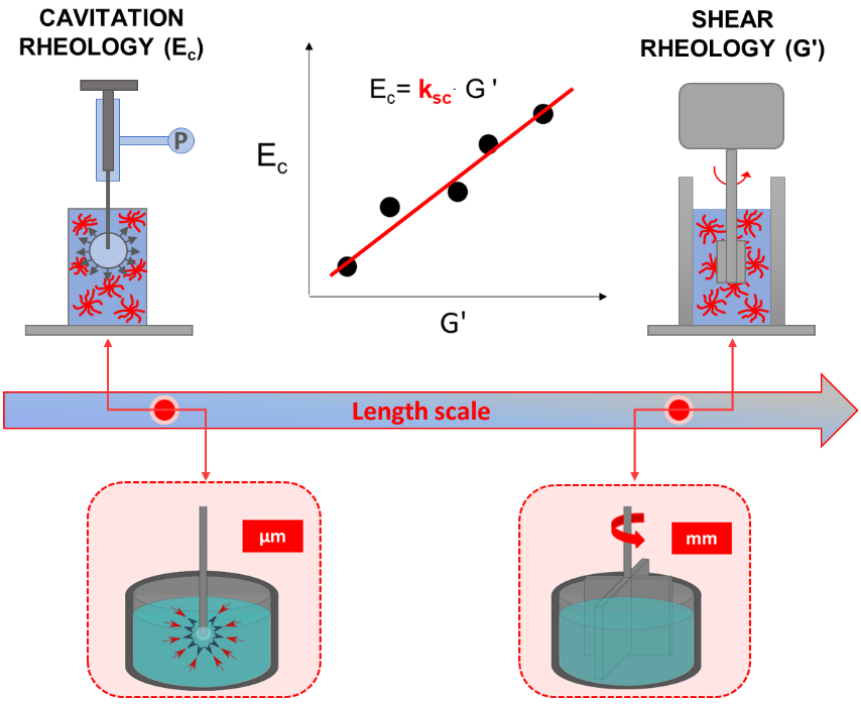

Figure 3.2 Schematic representation of a cavitation rheometer (top left) and a shear oscillatory rheometer (top right). The relationship between both techniques is given by a proportionality constant, k_{sc}, determined by the ratio of the moduli obtained from the two techniques (top middle). Closer diagram showing how both techniques work at different length scales (bottom).

In this Chapter, we examine the quantitative relationship between the shear storage modulus (G') and cavitation modulus (E_c) for gels formed from two different dipeptide low molecular weight gelators. We know that gels formed from the same gelator using different triggers results in different underlying microstructure.[39] We hypothesised that these differences in the microstructure could culminate in differences on the measured k_{sc} constant. As such, we are able to characterise the mechanical properties of gels at two different length scales.

3.2. Results and Discussion

3.2.1. Cavitation Rheometer Setup

The cavitation rheology instrument used was built and assembled by Bart Dietrich (University of Glasgow) following the description of Zimberlin et al.[17] (Figure 3.3). It includes a 10 mL Hamilton™ 1000 series Gastight syringe for air pumping mounted in a syringe pump (World Precision Instruments AL-1000). A high precision manometer (the Cavitation Rheology Analyser Box, or CRAB) with data logging capability was custom-built to control and record the pressure. A digital manometer was connected into the system via Y-junction and used to calibrate and double confirm pressure readings from the CRAB (Figure 3.3a). The setup of the cavitation rheometer is fully described in the Supporting Information (Section II) of our recent publication.[40]

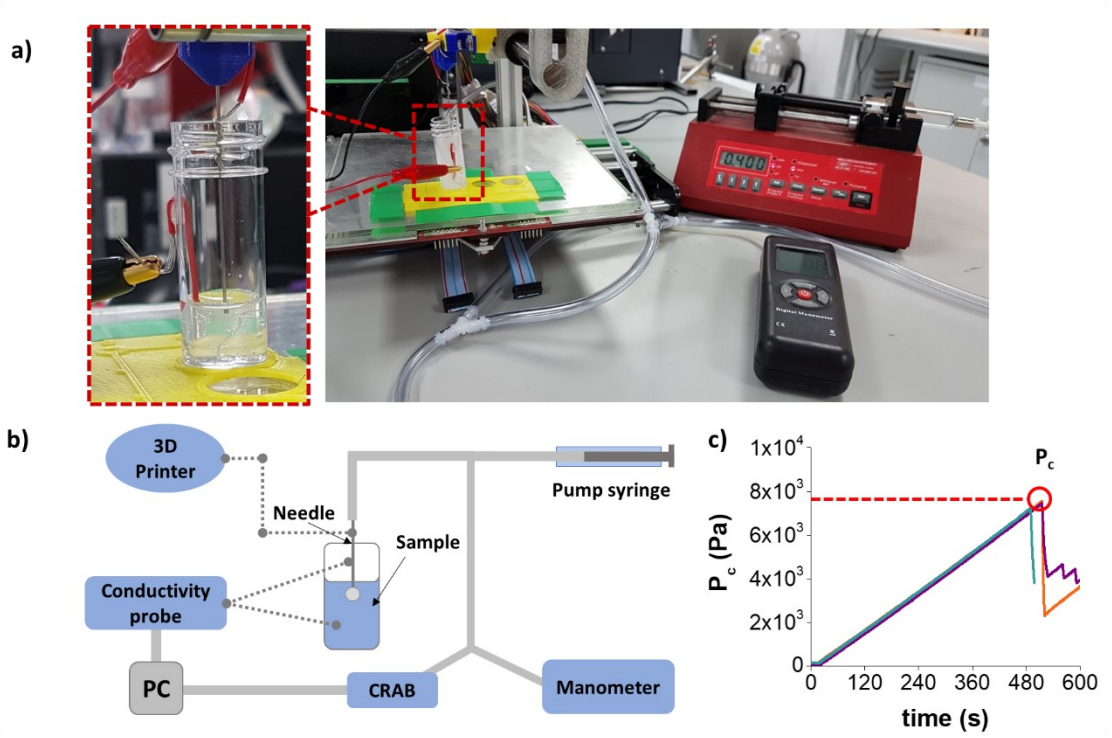

Figure 3.3 (a) Experimental setup of our cavitation rheometer including all components: syringe pump (top right), a digital manometer (bottom right) and the sample (left); the left inset shows the needle inserted into the sample. (b) Diagram of experimental setup. (c) Experimental data for a cavitation example, where the maximum pressure recorded over time gives the critical pressure, P_c.

3.2.2. Cavitation Rheology Procedure

In a typical experiment, a needle is inserted into the sample, the syringe pump is turned on and a bubble starts to grow within the material. The increase of pressure is then recorded by the CRAB, which digitises the signal from the system and translates it into pressure values. The maximum pressure recorded during the experiment is known as critical pressure, P_c (see experimental example in Figure 3.3c). The experiment is finished after a drop in the pressure is recorded.

Prior to the start of the experiment, we must consider the position of the needle. The depth at which the needle is inserted in the sample is critical for

modulus measurement. There is an increase of the critical pressure as a function of the depth at which the needle is inserted within the material (Figure 3.4a). In experiments with water and glycerol mixtures, we found that the increase in depth of the needle immersion leads to a proportional increase in maximum bubble pressure as expected from increasing hydrostatic pressure with increasing depth (Figure 3.4b). The proportionality constant relating the measured pressure using the cavitation rheometer to the calculated hydrostatic pressure for the liquid mixture under examination at a given depth was found to be ρg (ρ being the density, g the gravitational acceleration), in excellent agreement with the hydrostatic pressure equation (p = ρgh). The data in Figure 3.4b was collected by Bart Dietrich (University of Glasgow).

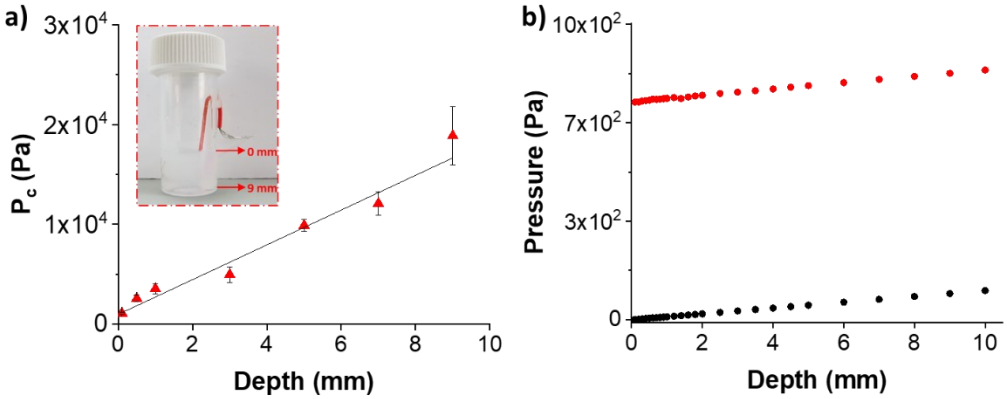

Figure 3.4 (a) Critical pressure, Pc, as a function of depth within the material for gel **1** using a solvent switch to trigger gelation. Error bars represent three measurements at each depth to ensure reproducibility. (b) Experimental pressure obtained from cavitation rheometer (red data) and calculated hydrostatic pressure (black data) as a function of needle depth immersion. The sample studied is a liquid mixture water/glycerol.

Since control of the needle position is of paramount importance in order to obtain reliable experimental data, a conductivity probe was designed in order to detect the contact of the needle tip with the sample surface and control axis movement of an Ormerod model 1 3D printer, which allows the precise positioning of the needle below the sample surface, (see Figure 3.3).[40] One of the probe electrodes wires is wrapped around the needle, while the other is

connected to a piece of wire inserted in the sample vial prior to filling the vial with gel. When the needle touches the gel surface, a small current flows and sends a signal to the 3D printer, which stops the movement and set the z coordinate to zero. This height reference allows for a precise positioning of the needle below the gel surface. A depth immersion of 1 mm is used throughout. The CRAB has a limited pressure operation and, as the pressure increases with depth immersion, using a small depth allows us to examine the greatest range of concentrations for each material. Three different samples are measured in all cases to ensure reproducibility and the needle is positioned in the middle of each sample to ensure any artefact is blocking or restricting the bubble growth.

3.2.3. Validation of Cavitation Rheometer

3.2.3.I. Gelatine Gels

First, gelatine gels were analysed in order to endorse our cavitation technique. Gelatine is a polypeptide obtained from the denaturation of collagen, which is mainly formed of three amino acids (glycine (33 %), proline and hydroxyproline (22 %)) in a triplex helix composed by three alpha chains. Each alpha chain is composed for 1014 amino acids. Here, we chose gelatine gels due to the similarity with the LMWG systems that we want to study using the cavitation rheometer.

Critical pressure, P_c, using the cavitation rheometer (Figure 3.5), and shear storage modulus, G', using shear rheology (Figure 3.6), were collected at different concentrations for gelatine gels.

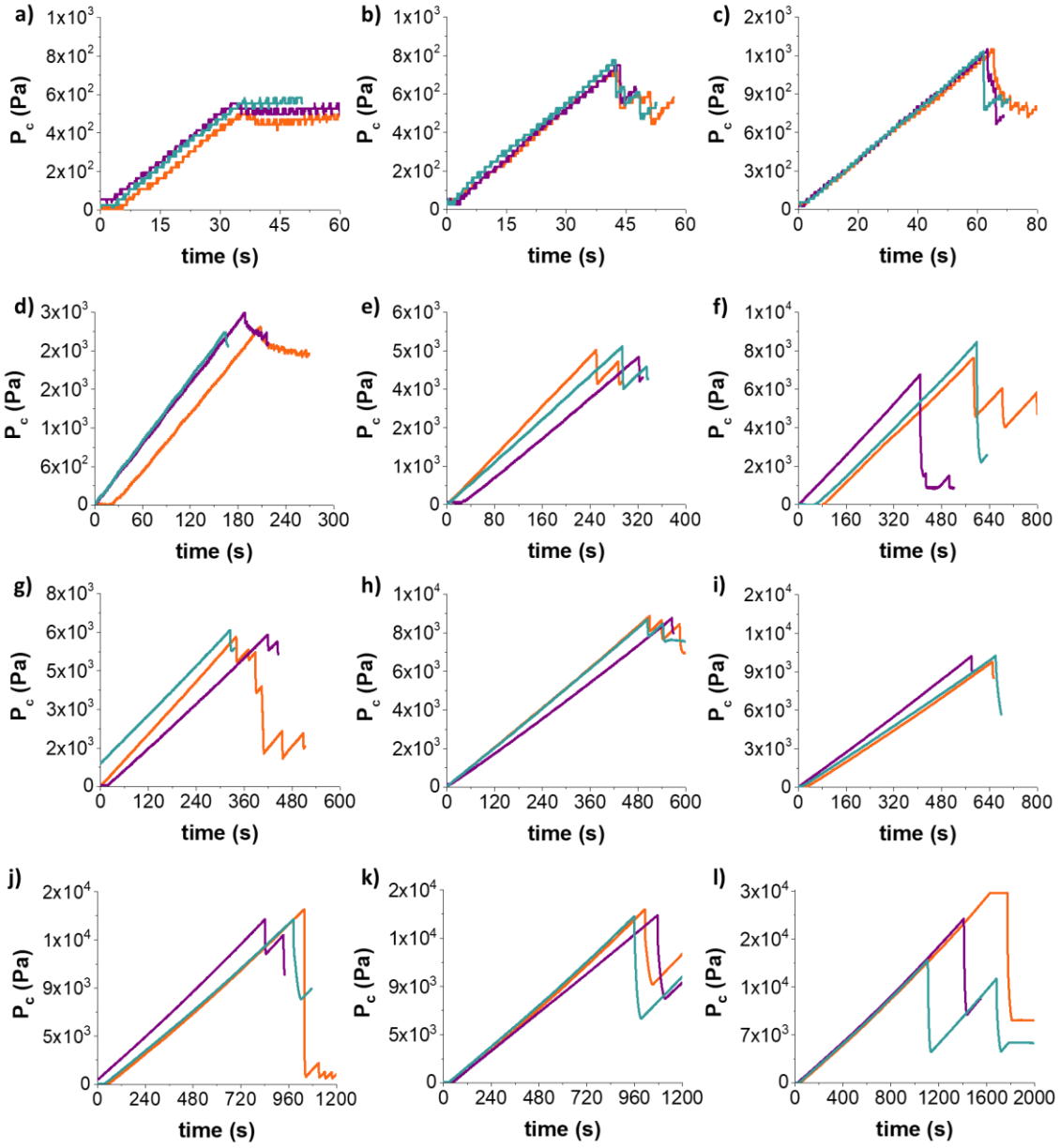

Figure 3.5 Cavitation data for gelatine at (a) 10 mg mL^{-1}; (b) 20 mg mL^{-1}; (c) 30 mg mL^{-1}; (d) 40 mg mL^{-1}; (e) 50 mg mL^{-1}; (f) 60 mg mL^{-1}; (g) 70 mg mL^{-1}; (h) 80 mg mL-1; (i) 90 mg mL-1; (j) 100 mg mL-1; (k) 110 mg mL-1 and (l) 120 mg mL-1. The purple, orange and cyan lines represent three repeated measurements.

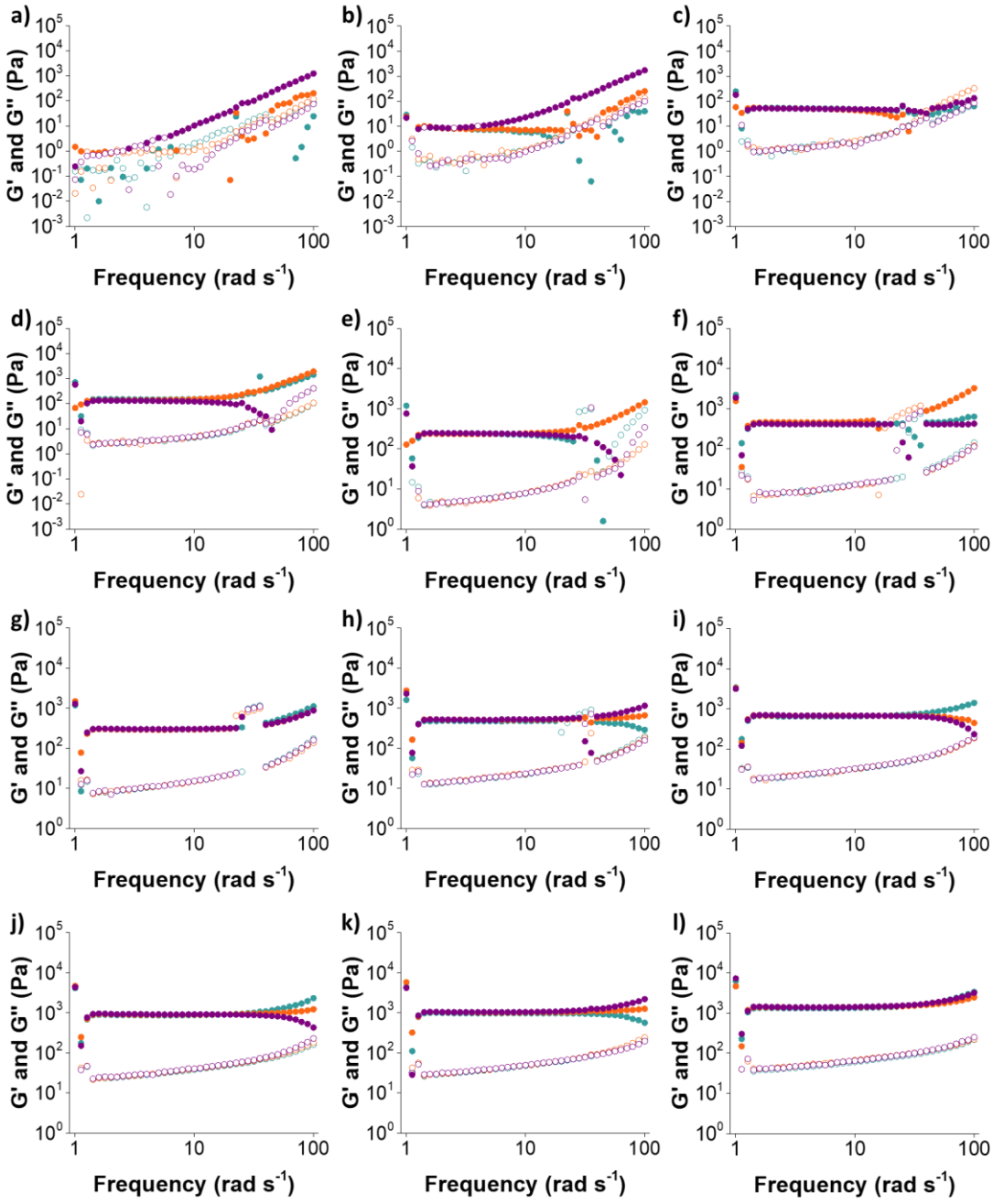

Figure 3.6 Frequency sweeps for gelatine at (a) 10 mg mL^{-1}; (b) 20 mg mL^{-1}; (c) 30 mg mL^{-1}; (d) 40 mg mL^{-1}; (e) 50 mg mL^{-1}; (f) 60 mg mL^{-1}; (g) 70 mg mL^{-1}; (h) 80 mg mL^{-1}; (i) 90 mg mL^{-1}; (j) 100 mg mL^{-1}; (k) 110 mg mL^{-1} and (l) 120 mg mL^{-1}. The purple, orange and cyan lines represent three repeated measurements.

Gelatine gels showed a frequency-independent behaviour and the storage moduli increased with concentration (Figure 3.6). Similarly, the critical pressure increased with concentration (Figure 3.5). Both shear and cavitation modulus

showed a similar trend when compared at different concentrations (Figure 3.7a), where values of both moduli increased with concentration. The cavitation moduli are an order of magnitude greater than shear moduli (Figure 3.7a). There is an excellent correlation between both moduli (Figure 3.7b), with a R^2 of 0.99. The value of the proportionality constant, k_{sc}, is 18.93 ± 0.53.

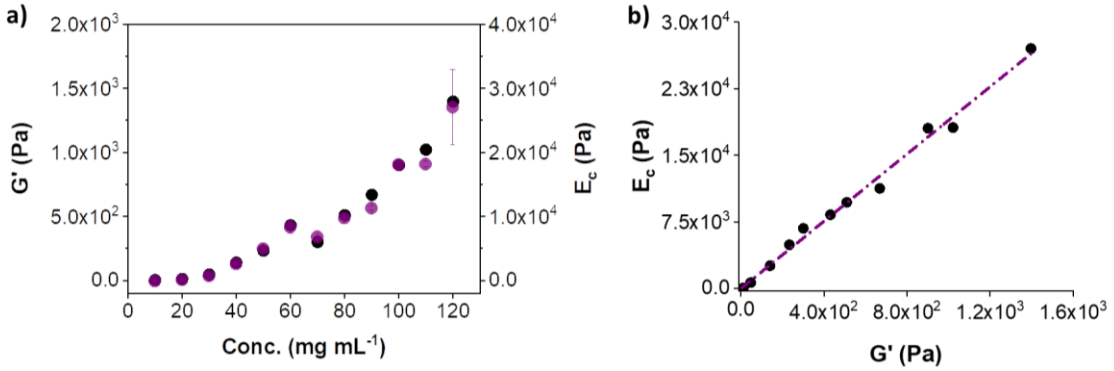

Figure 3.7 (a) Storage shear modui (black data) and cavitation moduli (purple data) as a function of concentration for gelatine gels. (b) Storage shear moduli against cavitation moduli for gelatine gels. The slope provides the value for k_{sc} (R^2=0.99).

3.2.3.II. PVA Gels

Following this, PVA gels were selected in order to both further validate our technique and also to compare to the original work of Zimberlin et al.[17] These gels are formed by the cross-linking of the PVA with borax.[41] The gels evolve with time,[17] so in this experiment a series of samples were prepared and analysed at different times. Both critical pressure and shear rheology modulus were measured as a function of time, t=0 represents the time at which the solution of PVA was first synthesised. PVA gels were frequency independent (Figure 3.8) and reproducible. The critical pressures also showed good reproducibility (Figure 3.9).

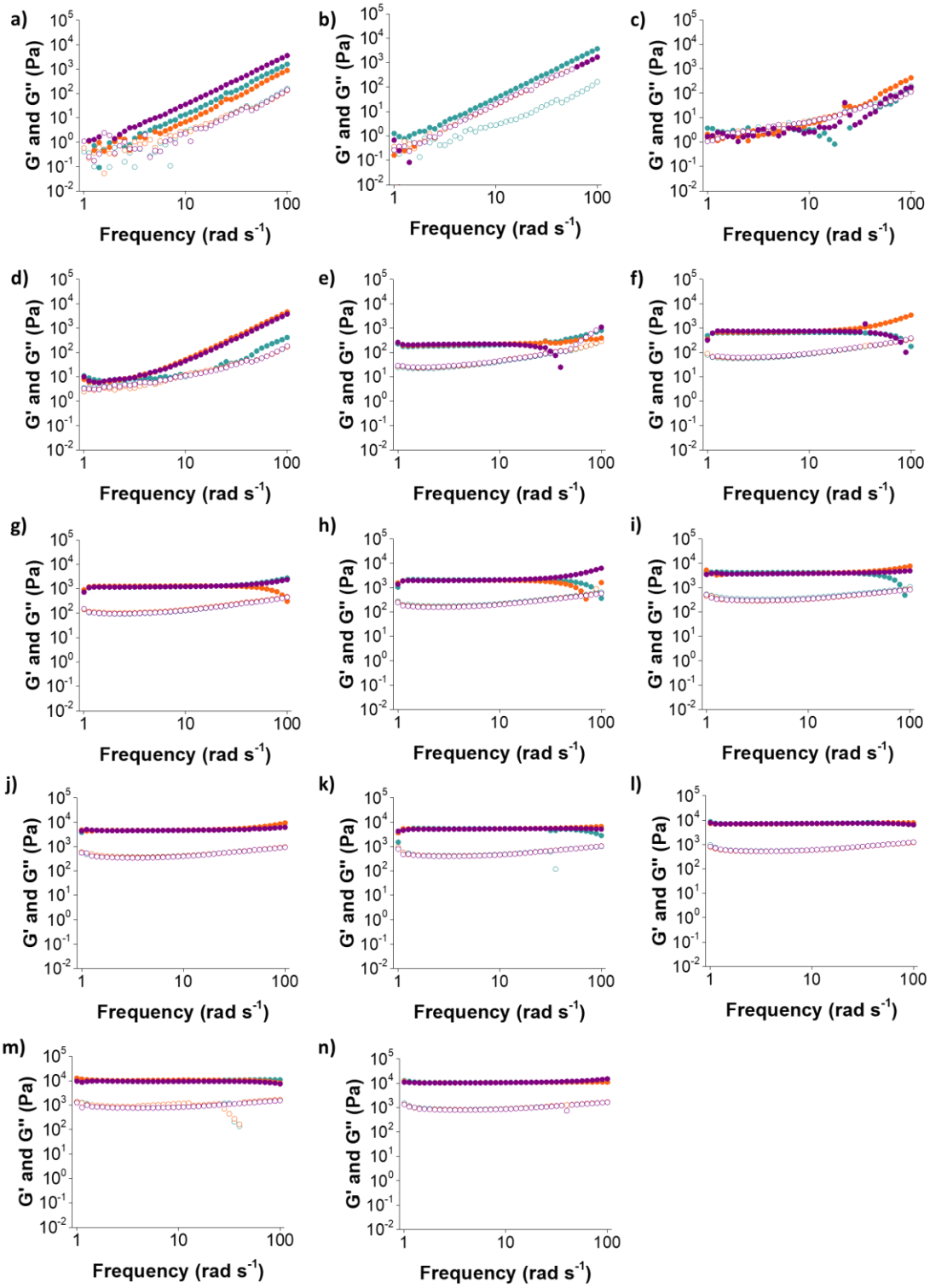

Figure 3.8 Frequency sweeps for PVA gels at (a) day 1; (b) day 2; (c) day 3; (d) day 4; (e) day 5; (f) day 6; (g) day 7; (h) day 8; (i) day 9; (j) day 10; (k) day 12 and (l) day 15 after being synthesised. The purple, orange and cyan lines represent three repeated measurements.

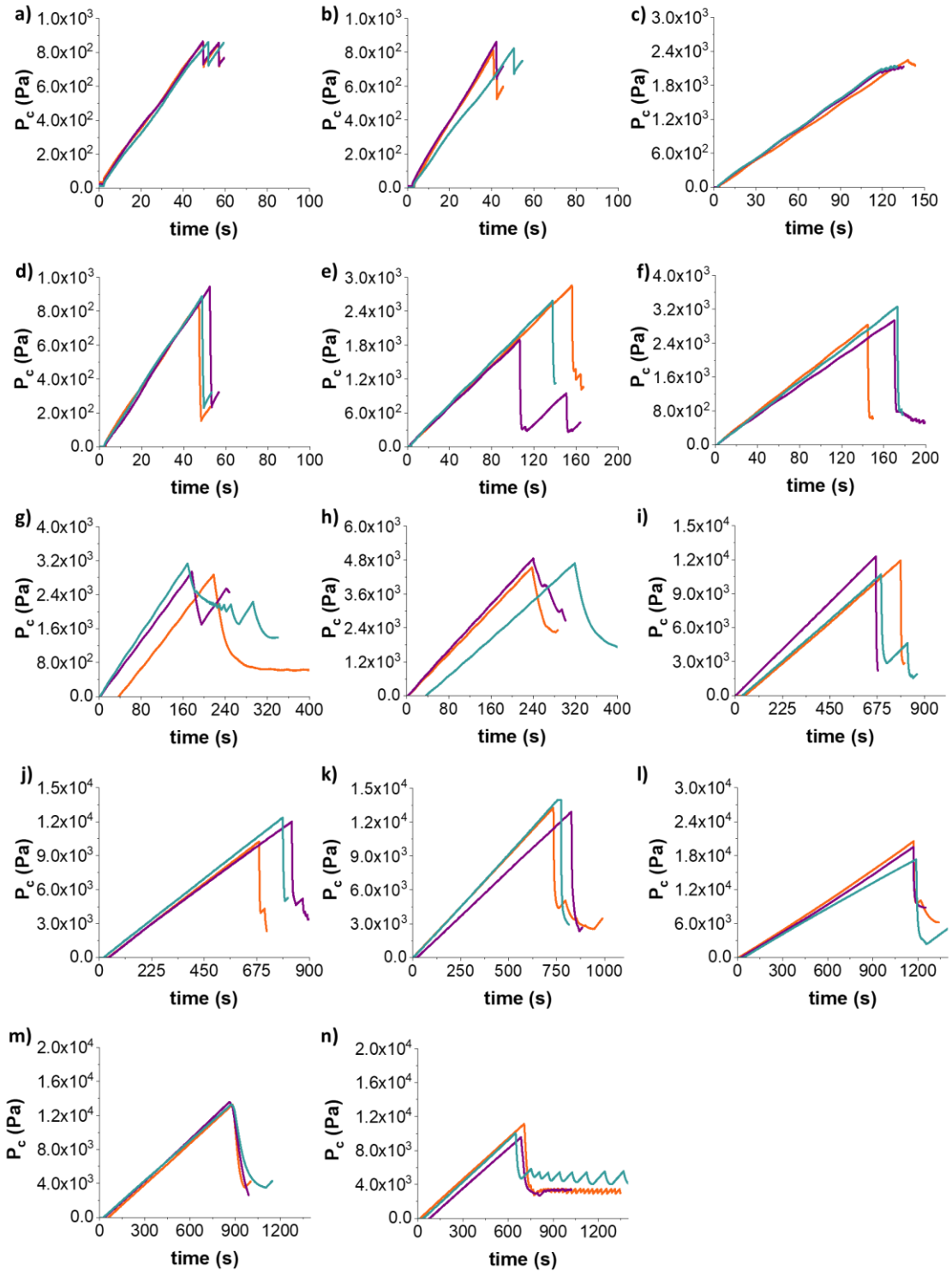

Figure 3.9 Cavitation data for PVA gels at (a) day 1; (b) day 2; (c) day 3; (d) day 4; (e) day 5; (f) day 6; (g) day 7; (h) day 8; (i) day 9; (j) day 10; (k) day 12; (l) day 15; (m) day 18 and (n) day 20 after being synthesised. The purple, orange and cyan lines represent three repeated measurements.

PVA gels are not formed immediately; gelation takes some time. This can be seen from both the cavitation and shear rheology, where it takes around six days before a significant increase in either P_c or G' is recorded (Figure 3.10). This is in agreement with the work of Zimberlin et al.[17] From tan δ (G"/G', Figure 3.10), a gel has not formed until t = 6 days, from which point tan δ remains essentially constant. The pressure values collected before t = 6 days are linked to those of a viscous solution. Over time, physical cross-links occur in the polymer network, and a gradual increase in shear storage moduli is observed using shear rheology (Figure 3.10a). However, that is not the case for data collected with the cavitation rheometer. The critical pressure increases up to t = 15 days broadly in line with the shear rheology data. However, after this time, the local pressure drops (Figure 3.10a). We highlight here that the two techniques probe different length scales; shear rheology measures the elastic moduli of a bulk sample, while cavitation rheology quantifies the elasticity at a local point within the material. As such, we hypothesise that the underlying microstructure of the PVA gels starts to change after a certain time, which will just affect a local point in the material but will not affect the bulk elasticity. The agreement at earlier times shows the validity of the technique, especially when compared with the gelatine data above, whilst these latter data show the power of using both techniques to understand the gels at different length scales.

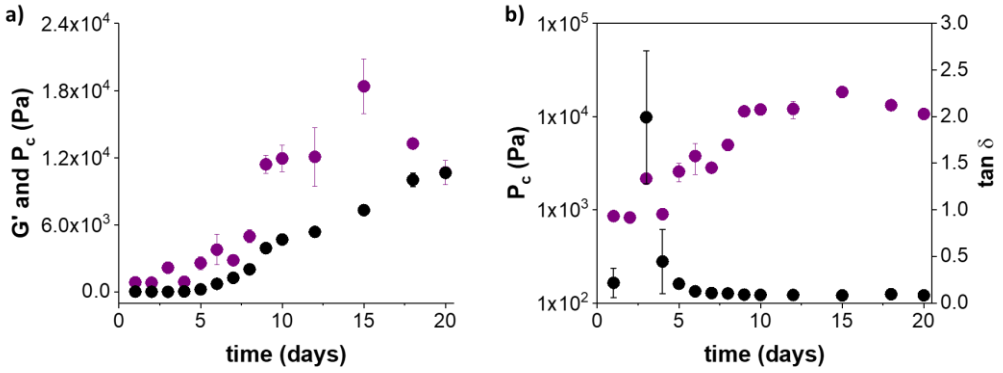

Figure 3.10 (a) Storage shear moduli (black data) and critical pressure (purple data) as a function of time for PVA gels. (b) tan δ (black data) and critical pressure, in logarithmic scale (purple data), as a function of time for PVA gels.

3.2.4. Characterisation of LMWGs

3.2.4.I. Selection of LMWG

Since the reliability of our cavitation rheology approach has been validated, we then moved to our area of interest, low molecular weight gels (LMWGs). We selected two different dipeptide-based gelators **1** and **3** (Figure 1.4 and Figure 3.11). We have previously reported in detail on gels formed from both of these[13, 39, 42] and so they represent good test cases.

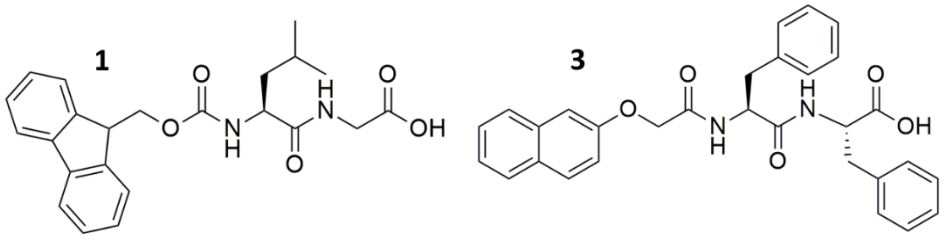

Figure 3.11 Chemical structures of **1** (FmocLG) and **3** (2NapFF).

In both examples, the dipeptide is conjugated to an aromatic component at the N-terminus. These dipeptides are both very effective gelators and can be used to form gels in different ways. [13, 39, 43] In all cases here, a self-supporting gel was formed (Figure 3.12a). Specifically, here two different methods were used to trigger the gelation of the dipeptide-based LMWG. The first method, the solvent trigger, consists of the dissolution of the gelator in a water-miscible solvent such as DMSO, followed by the addition of water.[44] The final pH of these hydrogels was typically around 3.36 and 3.73 for gels formed from **1** and **3** respectively. Gels form quickly by this method, and we have previously shown that this method leads to an underlying microstructure of spherulitic domains of fibres.[13] Examples of spherulitic domains formed in gels of **1** and **3** respectively are shown in Figure 3.12b and Figure 3.12d.

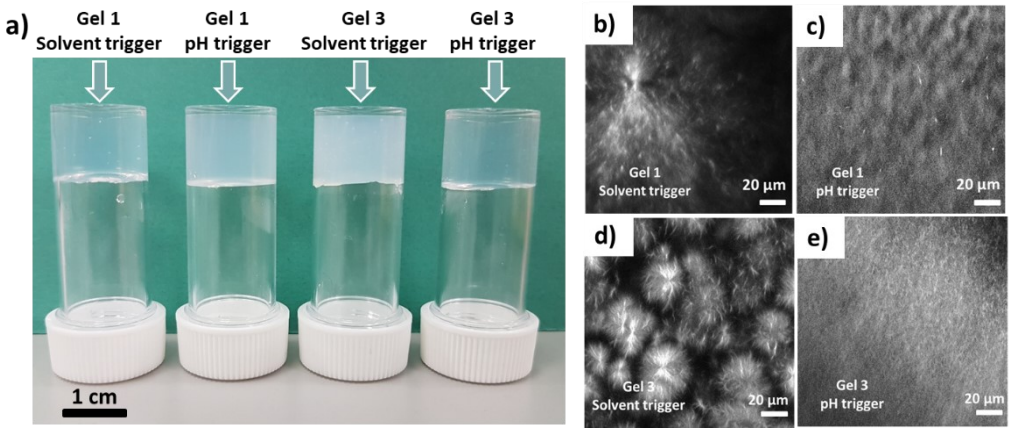

Figure 3.12 (a) Photograph of (left to right) a gel of **1** using DMSO and GdL, and a gel of **3** using DMSO and GdL. All gels at a concentration of 4 mg mL^{-1}. (b) – (e) Confocal images of gels of **1** using a solvent trigger (b) and a pH trigger (c). Confocal images of gels **3** using a solvent trigger (d) and a pH trigger (e).

1 and **3** were selected to use in our cavitation technique because of our understanding of the differences in the underlying microstructure. We would expect that differences in the microstructures would lead to different correlation k_{sc} constant values. Images for gels of **1** and **3** at different concentrations show that no changes are observed in the microstructure for the same trigger (Figure 3.13 and Figure 3.14).

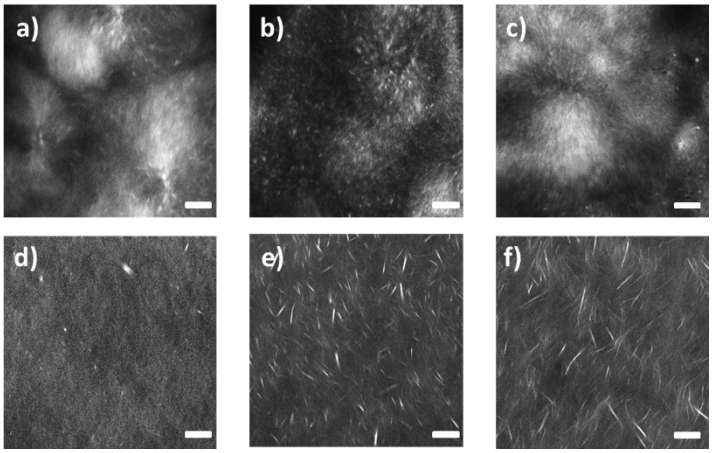

Figure 3.13 Further confocal images for gel **1** prepared at (a) 4 mg mL^{-1}, (b) 8 mg mL^{-1} and (c) 12 mg mL^{-1} using a solvent trigger; (d) 4 mg mL^{-1}, (e) 8 mg mL^{-1} and (f) 10 mg mL^{-1} using the pH trigger. The scale bar represents 20 µm.

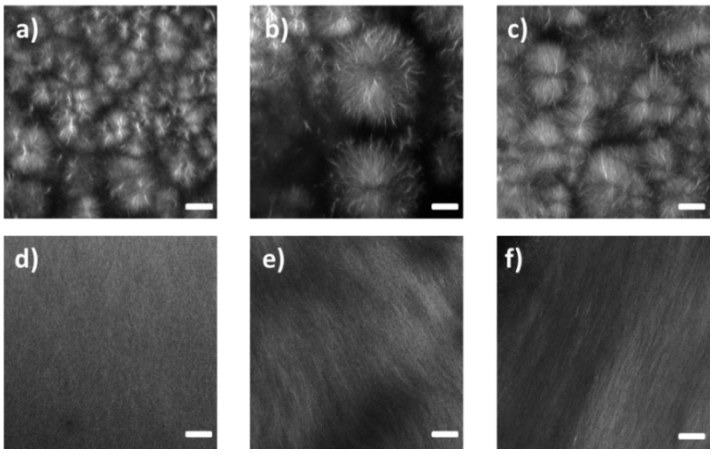

Figure 3.14 Further confocal images for gel **3** prepared at (a) 4 mg mL-1, (b) 8 mg mL-1 and (c) 12 mg mL-1 using a solvent trigger; (d) 4 mg mL-1, (e) 8 mg mL-1 and (f) 10 mg mL-1 using the pH trigger. The scale bar represents 20 μm.

3.2.4.II. Rheological Characterisation of Gels of 1

Gels of **1** were examined at different concentrations. Shear rheology data showed a frequency-independent behaviour when using solvent and pH triggers (Figure 3.15 and Figure 3.16 respectively), with shear modulus increasing with concentration.

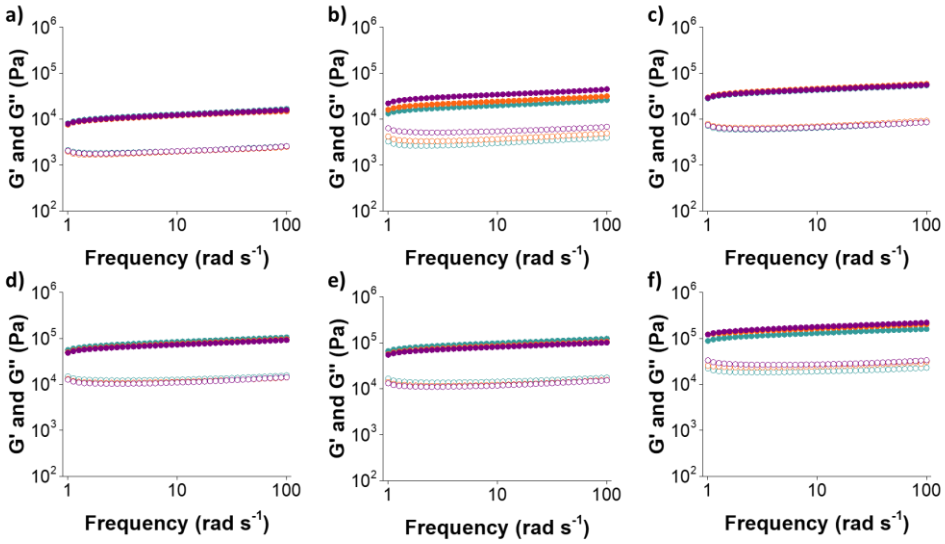

Figure 3.15 Frequency sweeps for gel **1** prepared at a DMSO:water ratio of 1:9. Data are shown for gel **1** at (a) 4 mg mL^{-1}; (b) 6 mg mL^{-1}; (c) 8 mg mL^{-1}; (d) 10 mg mL^{-1}; (e) 12 mg mL^{-1}; (f) 14 mg mL^{-1}. The purple, orange and cyan data represent three repeated measurements.

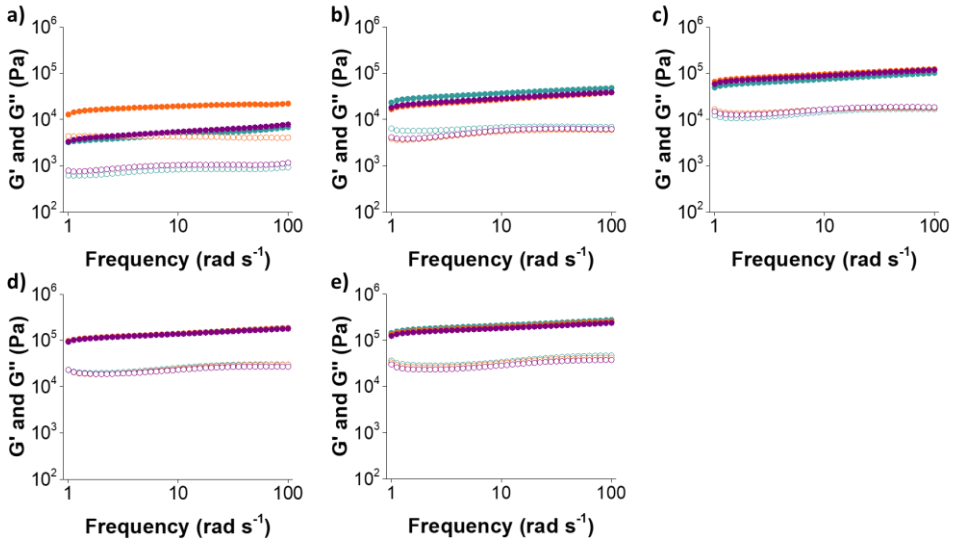

Figure 3.16 Frequency sweeps for gel **1** prepared using GdL. Data are shown for gel **1** at (a) 2 mg mL^{-1}; (b) 4 mg mL^{-1}; (c) 6 mg mL^{-1}; (d) 8 mg mL^{-1}; (e) 10 mg mL^{-1}. The purple, orange and cyan data represent three repeated measurements.

Similarly, cavitation analysis shows excellent reproducible data at all concentrations for gel **1** using both triggers (Figure 3.17 and Figure 3.18).

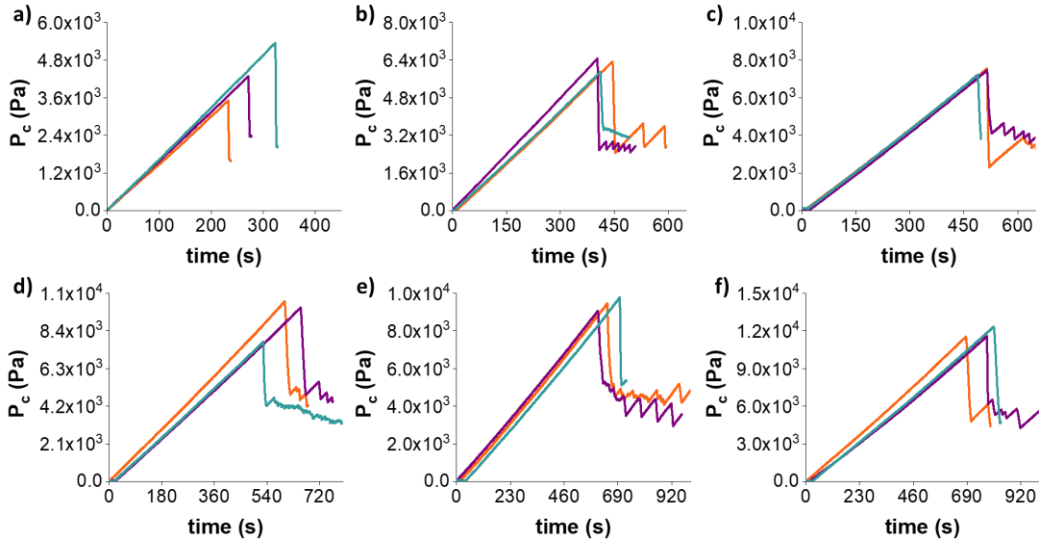

Figure 3.17 Cavitation data for gel **1** prepared at a DMSO:water ratio of 1:9. Data are shown for gel **1** at (a) 4 mg mL^{-1}; (b) 6 mg mL^{-1}; (c) 8 mg mL^{-1}; (d) 10 mg mL^{-1}; (e) 12 mg mL^{-1}; (f) 14 mg mL^{-1}. The purple, orange and cyan lines represent three repeated measurements.

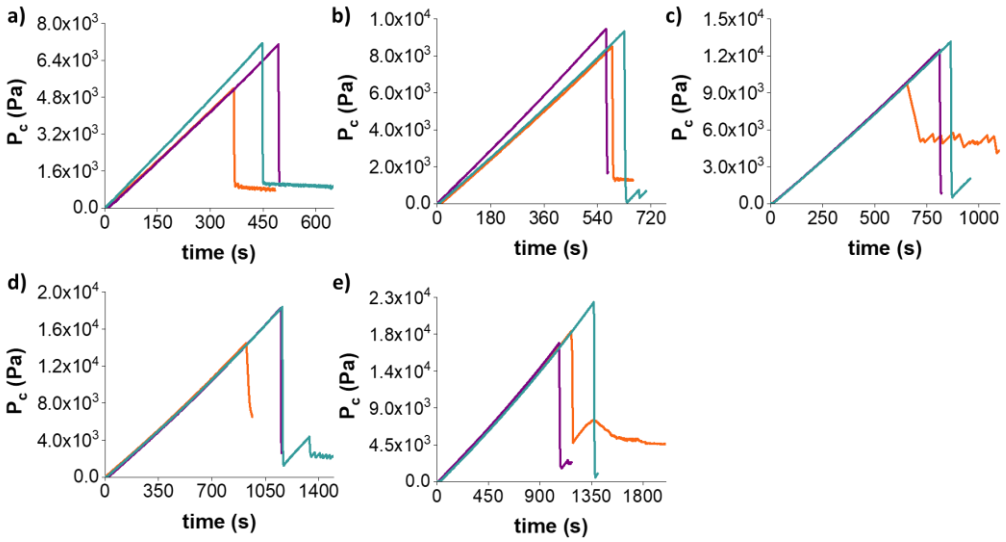

Figure 3.18 Cavitation data for gel **1** prepared using GdL. Data are shown for gel **1** at (a) 2 mg mL^{-1}; (b) 4 mg mL^{-1}; (c) 6 mg mL^{-1}; (d) 8 mg mL^{-1}; (e) 10 mg mL^{-1}. The purple, orange and cyan lines represent three repeated measurements.

3.2.4.III. Rheological Characterisation of Gels of 3

Gels of **3** were analysed in the same way. Storage modulus (Figure 3.19 and Figure 3.20) and critical pressure (Figure 3.21 and Figure 3.22) were examined at different concentrations using the two different triggers.

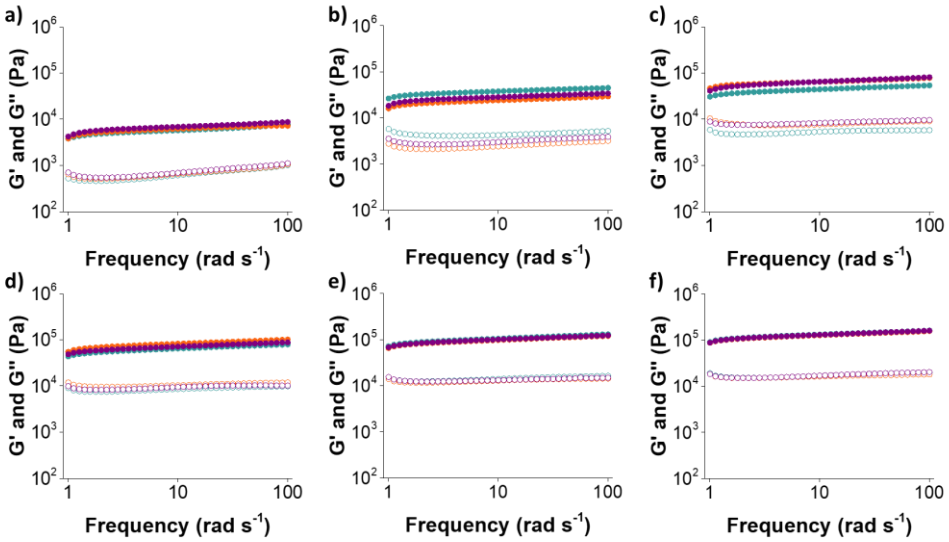

Figure 3.19 Frequency sweeps for gel **3** prepared at a DMSO:water ratio of 2:8. Data are shown for gel **3** at (a) 2 mg mL^{-1}; (b) 4 mg mL^{-1}; (c) 6 mg mL^{-1}; (d) 8 mg mL^{-1}; (e) 10 mg mL^{-1}; (f) 12 mg mL^{-1}. The purple, orange and cyan data represent three repeated measurements.

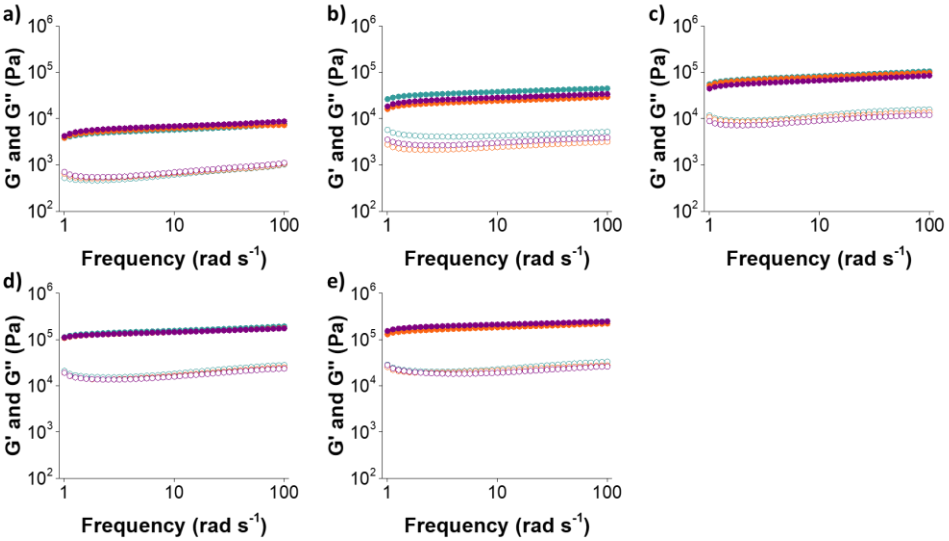

Figure 3.20 Frequency sweeps for gel **3** prepared using GdL. Data are shown for gel **2** at (a) 2 mg mL^{-1}; (b) 4 mg mL^{-1}; (c) 6 mg mL^{-1}; (d) 8 mg mL^{-1}; (e) 10 mg mL^{-1}. The purple, orange and cyan data represent three repeated measurements.

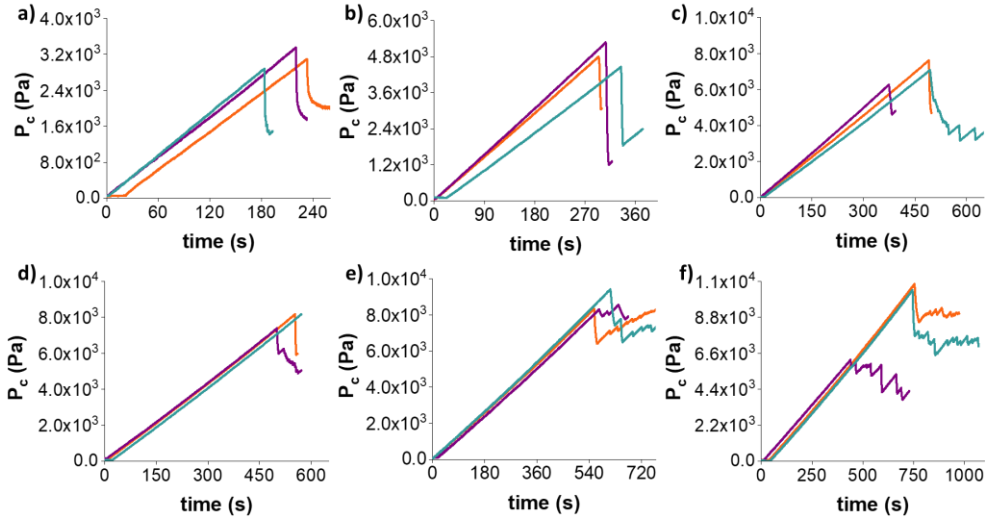

Figure 3.21 Cavitation data for gel **3** prepared at a DMSO:water ratio of 2:8. Data are shown for gel **3** at (a) 2 mg mL^{-1}; (b) 4 mg mL^{-1}; (c) 6 mg mL^{-1}; (d) 8 mg mL^{-1}; (e) 10 mg mL^{-1}; (f) 12 mg mL^{-1}. The purple, orange and cyan data represent three repeated measurements.

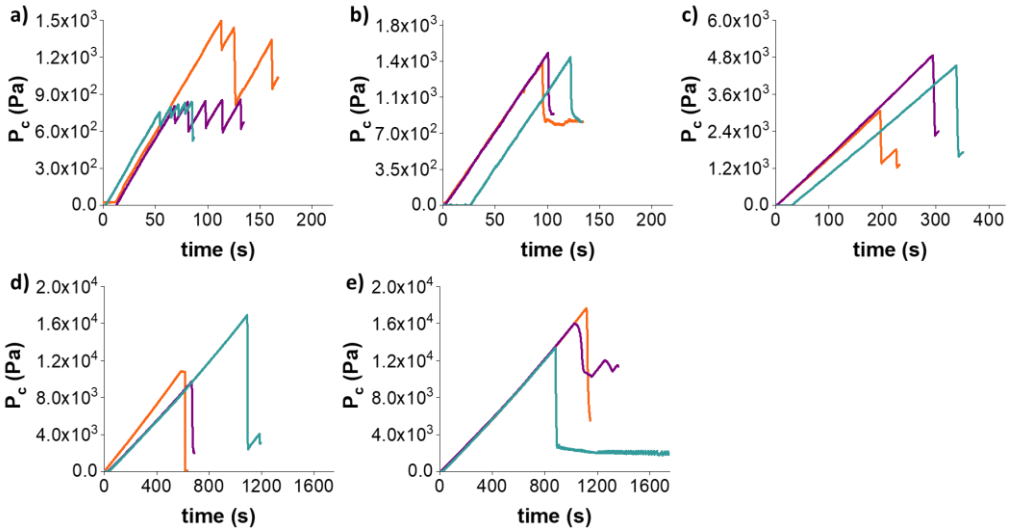

Figure 3.22 Cavitation data for gel **3** prepared using GdL. Data are shown for gel **2** at (a) 2 mg mL^{-1}; (b) 4 mg mL^{-1}; (c) 6 mg mL^{-1}; (d) 8 mg mL^{-1}; (e) 10 mg mL^{-1}. The purple, orange and cyan data represent three repeated measurements.

Both G' and P_c increased with concentration. Storage modulus again showed a frequency-independent response in all cases and the critical pressure values were again reproducible.

3.2.5. Shear Rheology *versus* Cavitation Rheology

Shear and cavitation moduli were evaluated as a function of concentration for gels of **1** and **3** using both triggers (Figure 3.23). For gels formed using **1**, the shear and cavitation moduli show a similar trend with concentration in both cases (Figure 3.23a and Figure 3.23b). Similarly, for gels formed from **3** with both triggers, both moduli show a good correlation (Figure 3.23c and Figure 3.23d).

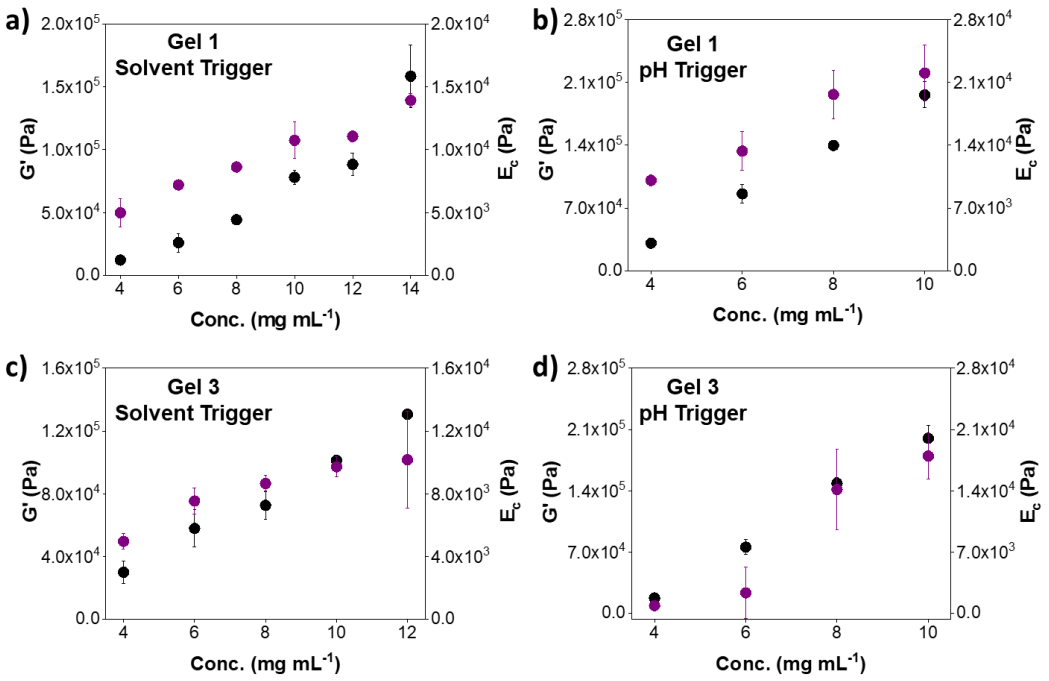

Figure 3.23 Shear moduli (black data) and cavitation moduli (purple data) as a function of concentration for gel **1** using (a) solvent-trigger and (b) pH-trigger and for gel **3** using (c) solvent-trigger and (d) pH-trigger.

3.2.5.I. Relationship Between Shear and Cavitation Rheology, k_{sc}

The relationship between both techniques is accessed by plotting the cavitation moduli against the shear moduli at different concentrations (Figure 3.24). The slope of the linear regression corresponds to the value of the constant k_{sc}, which can be used to interconvert between both moduli. The data show an excellent correlation fitting between both techniques in all cases with R^2 ranging from 0.92 to 0.98.

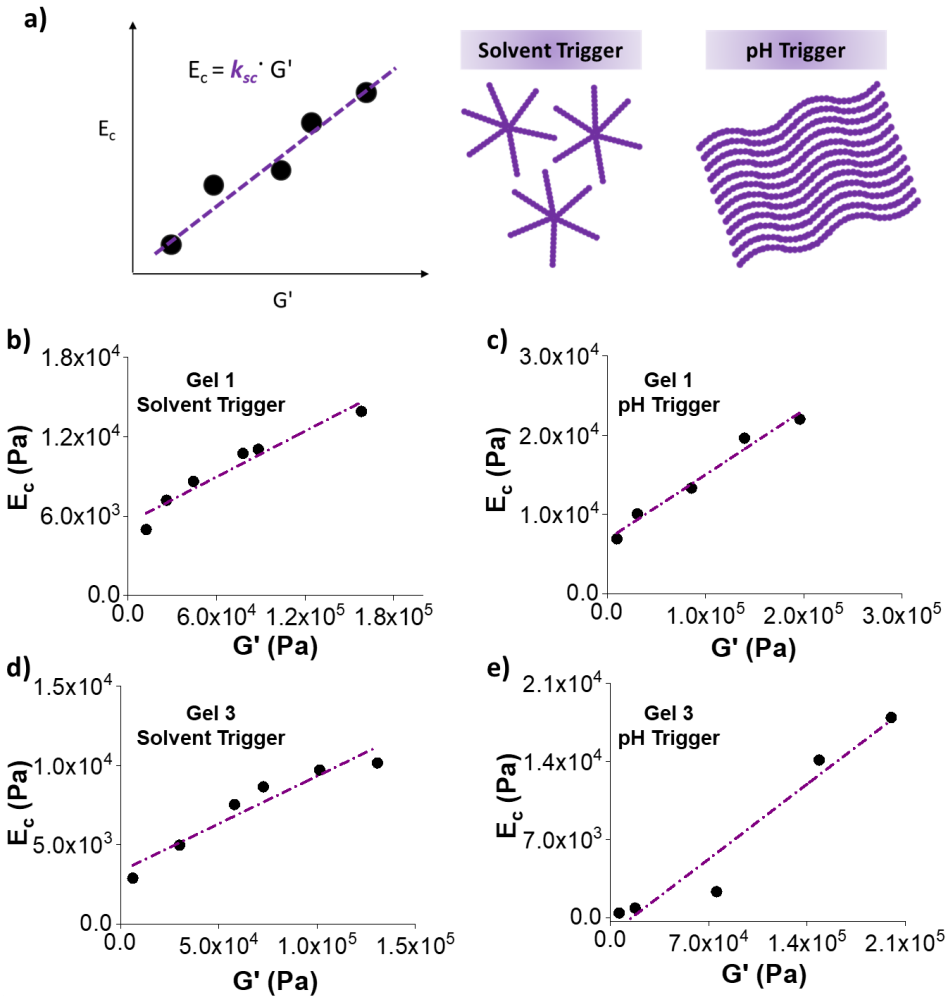

Figure 3.24 (a) Schematic representation of the linear regression between cavitation and shear moduli and the differences in microstructure when using a solvent or pH trigger. Cavitation moduli plotted against shear moduli for gel of **1** using (b) a solvent trigger, (c) a pH trigger; and gel of **3** using (d) a solvent trigger and (e) a pH trigger. Slope of linear regression display the constant k_{sc} values. (R^2= 0.94, 0.98, 0.92 and 0.94, respectively).

For gel **1**, the value of k_{sc} was determined to be 0.06 ± 7.47 E^{-3} when using the solvent-trigger (Figure 3.24b, Table 3.1). A higher k_{sc} of 0.08 ± 7.41 E^{-3} was obtained when using the pH-trigger (Figure 3.24c, Table 3.1). Similar constant values were obtained for gel **3**, with a k_{sc} of 0.06 ± 8.88 E^{-3} and 0.09 ± 13.75 E^{-3} for the solvent-trigger (Figure 3.24d, Table 3.1) and pH-trigger (Figure 3.24e, Table 3.1) respectively. Whilst similar in value, these are statistically different values. We note that the linear regression to the data does not go through the origin. We believe that this a result of there being a minimum gelation concentration below which no gels are formed and therefore it is not meaningful to effectively extrapolate to the value at zero concentration.

If rather than comparing k_{sc}, we compared the inverse function $1/k_{sc}$, it will be easier to pinpoint the effect of the microstructure on the evaluation of k_{sc} since the values are represented in higher scale (Table 3.1). From the resulting values, we believe that the differences in k_{sc} values for gels formed by the two triggers are due to the different underlying microstructures. What is notable here is the similarity in k_{sc} /($1/k_{sc}$) values for gel **1** and **3** when using the same trigger; the constant values collected are remarkably similar in both LWMGs (Table 3.1).

Table 3.1 k_{sc} and $1/k_{sc}$ values for gel **1** and gel **3** using a solvent and pH trigger.

	Gel	k_{sc}	Standard Error k_{sc}, (10^{-3})	$1/k_{sc}$	Standard Error $1/k_{sc}$	R^2
Solvent trigger	**1**	0.06	7.47	17.36	0.36	0.94
	3	0.06	8.88	16.64		0.92
pH trigger	**1**	0.08	7.41	12.25	0.85	0.98
	3	0.09	13.75	10.55		0.94

3.2.5.II. Effect of the Needle Diameter on Cavitation Rheology

Moreover, varying the needle diameter could be used as a mean of measuring the mechanical properties at different scales. Some researchers have also investigated the transition from cavitation to fracture in soft materials by

varying the needle size.[20-22, 25, 32] Differences in the needle size will affect the critical pressure, hence altering the cavitation modulus and consequently k_{sc} values. Here, we examined the effect of changing the needle size to examine gel **3** made using a solvent and a pH trigger. Until now, a 210 µm radius needle was used in our cavitation rheometer. If we use a smaller needle (60 µm in radius), differences in the gradient for cavitation modulus *versus* shear modulus are observed. This affects k_{sc} values for both triggers (Figure 3.25a and b). We highlight that for gel made of **3** using the pH trigger, the data collected using a needle radius of 60 µm do not fit to a power law.

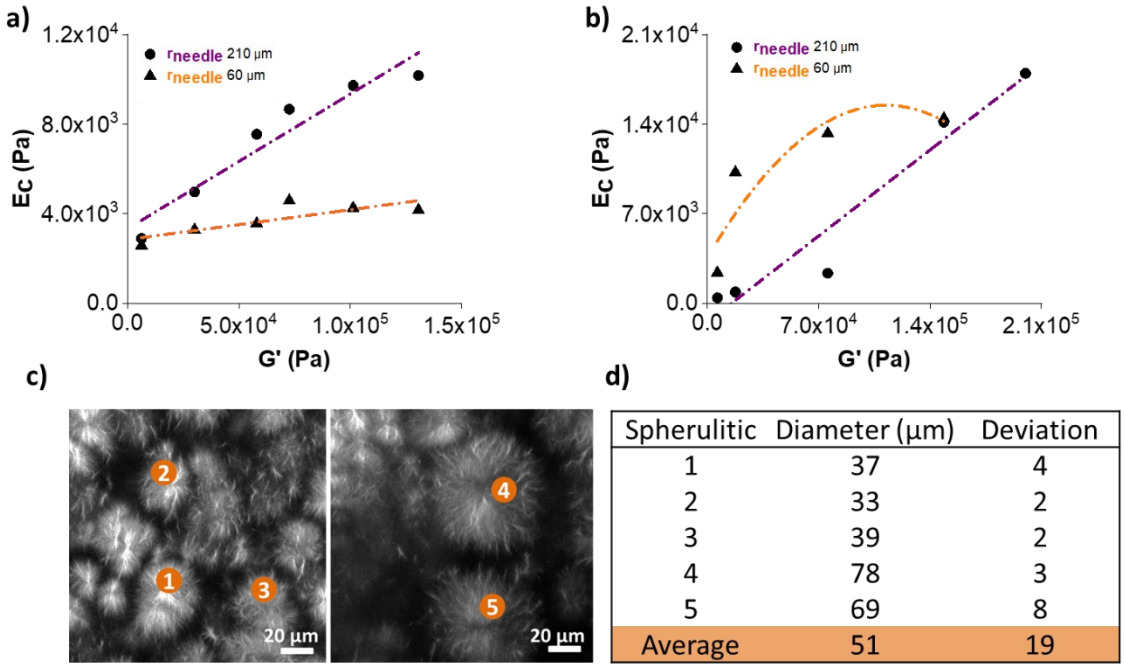

Spherulitic	Diameter (µm)	Deviation
1	37	4
2	33	2
3	39	2
4	78	3
5	69	8
Average	51	19

Figure 3.25 Comparison of the relationship between cavitation and shear moduli for different needle radii for a gel of **3** using (a) a solvent trigger and (b) a pH trigger. (c) Images of gel **3** using a solvent trigger at 4 mg mL^{-1} (left) and 8 mg mL^{-1} (right). (d) Size of the highlighted spherulitic domains in (c). ImageJ software was used to measure the diameters of each structure. The deviation values are the result of three different measurements for each structure.

Interestingly, the size of one of the needle radii is comparable to the size of the spherulitic domains in solvent triggered gels (Figure 3.25c). This indicates microstructure is likely influencing P_c since lower radii are expected to give

higher values of P_c.[20,32,33] However, we show this is not the case for our system, where the smaller needle size gives smaller P_c values. These data further support the sensitivity of cavitation rheology to local elastic response.

3.2.5.III. Comparing k_{sc} Values within the Literature

Thus far, we have shown the reliability of our cavitation technique, which has been tested on gelatine, PVA gels and in different dipeptides using different triggers. In addition, we observed that the microstructure plays an important role when the elastic response of these materials is quantified using the cavitation technique. Therefore, we believe it is important to compare our k_{sc} values with those been reported in the literature (Figure 3.26).

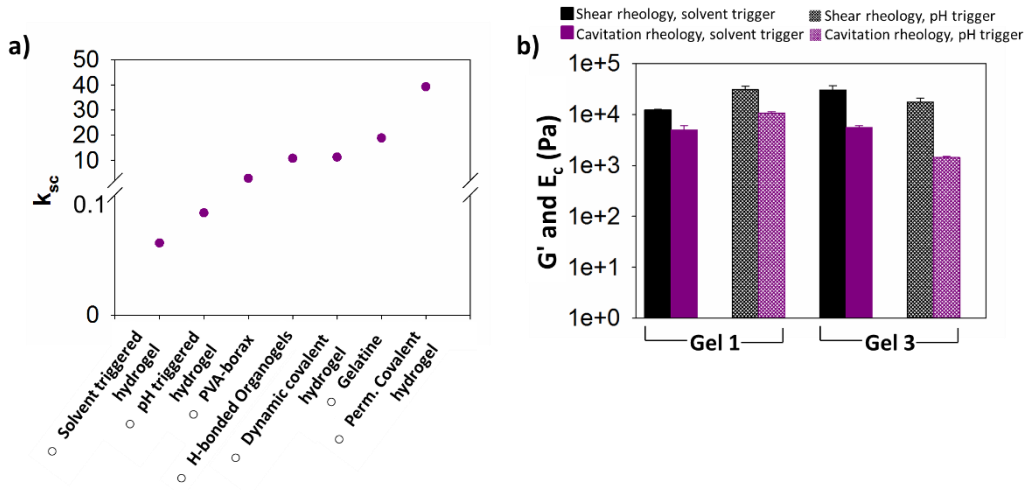

Figure 3.26 (a) Comparison our LMWGs k_{sc} values with values already reported in the literature for different gels.[38] The break in the y-axis ranges from 0.1 to 1. (b) Elasticity values for shear (black data) and cavitation (purple data) moduli at 4 mg mL^{-1} for gel **1** and gel **3** using the solvent-trigger (solid data) and pH-trigger (patterned data).

Surprisingly, our LMWG show the lowest values of k_{sc}, not exceeding 0.1, while the constant values for other gels range from 3 to 40 (Figure 3.26a). We associate these considerable differences in k_{sc} values to the differences in stiffness of the gels. For our LMWG systems, the shear modulus is greater than

the cavitation moduli (Figure 3.26b), in contrast to what is been reported for other gels in the literature.[24, 25]

3.2.6. New Insights into the Cavitation Rheology Technique

As k_{sc} is defined as the gradient between cavitation modulus (y-axis) versus shear modulus (x-axis), the greater the shear modulus, the lower the gradient and so the k_{sc}. We highlight one example to expand on this. Fei et al. reported a 12-HSA gel with a stiffness of around 600 Pa and a critical pressure of around 5200 Pa.[26] For one of our gels, gel **1** using a solvent switch, the stiffness is around 20,000 Pa, whilst the critical pressure is roughly 5700 Pa. If we compare both gels, the critical pressures are very similar; however, the stiffness is much greater for our gel. We believe that there is an influence of the strain at which the gels break. The 12-HSA gel breaks at >10% strain (Figure 3.27b), whilst our gel breaks at 3 % strain (Figure 3.27a).

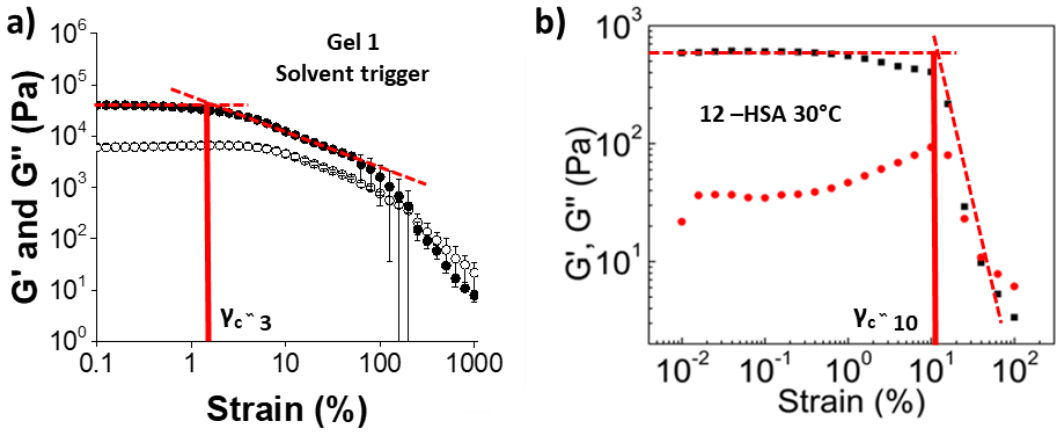

Figure 3.27 Strain sweeps for (a) gel **1** using a solvent trigger and (b) 12-HSA gel. Data and graph (b) is from reference [24]. For gel **1** error bars represent three repeated measurements to ensure reproducibility.

Similarly, for gel **1** using a pH trigger and gel **3** using both triggers, the critical strain is no larger than 5% and the stiffness is in the order of 100 000 Pa, while gelatine and PVA-borax break at higher strains (around 800%) and the stiffness does not exceed 1000 Pa (Figure 3.28). Hence, whilst the absolute G' is higher for our LMWG, this is offset by the low breakage strain. It therefore seems likely

that the value of P_c (and hence k_{sc}) depends on both the absolute modulus as well as the breakage strain.

The cavitation rheology data give a greater insight into the networks that have been formed as compared to bulk rheology where the slight differences in absolute moduli are difficult to interpret. Understanding these differences is important; we have shown that the underlying microstructure links to the ability to 3D print such gels for example.[45]

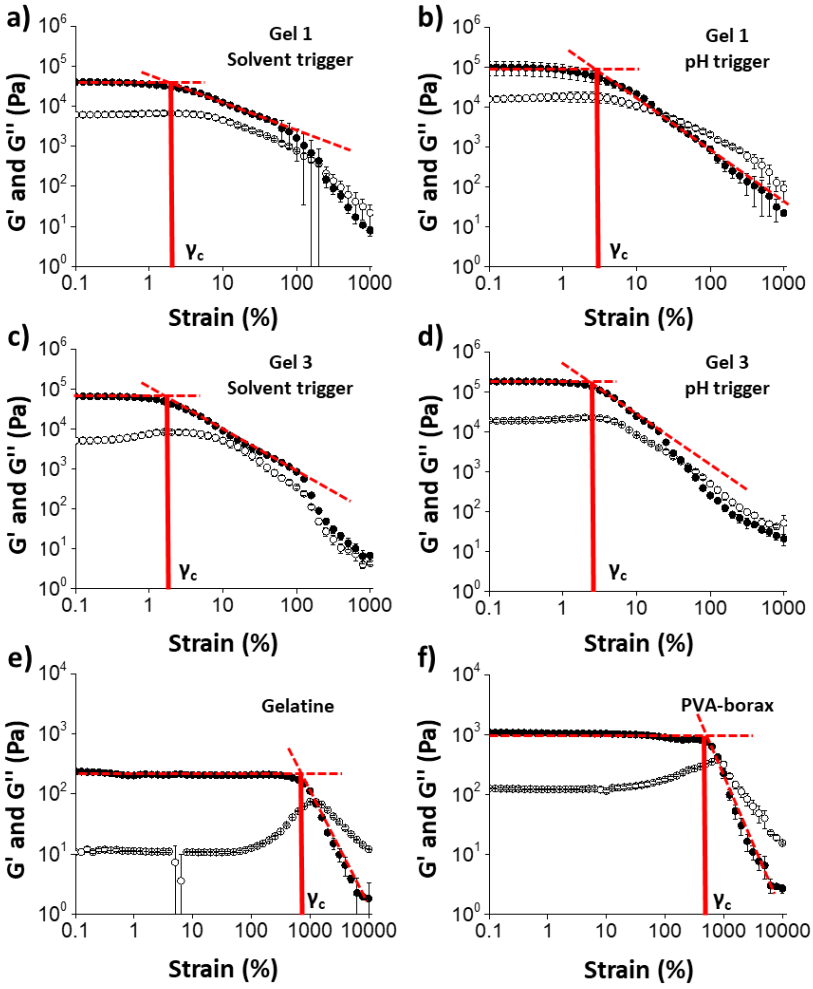

Figure 3.28 Strain sweeps for (a) gel **1** using a solvent trigger, (b) gel **1** using a pH trigger, (c) gel **3** using a solvent trigger, (d) gel **3** using a pH trigger, (e) gelatine and (f) PVA-borax gel. The intersection between the linear-viscoelastic region and the section from where G' and G'' start to deviate from linearity represent the critical strain, γ_c. Gels (a-d) at 6 mg mL^{-1}, gelatine at 60 mg mL^{-1} and PVA-borax gel 5 days after synthesis.

3.3. Conclusions

In summary, we have shown that cavitation rheology can be used to investigate our low molecular weight gel systems at the micrometre scale. We investigated the relationship between the shear moduli and the cavitation moduli for a range of different gels. We demonstrate that the microstructure plays a fundamental role for the examined k_{sc} constant. Depending on the trigger used, different k_{sc} values were assessed, those being the same even when different low molecular weight gelators were studied. The values are statistically different, and correlate with the structures that lead to the gel. We highlight that the values are very different to other gels examined here and elsewhere. This correlates with the significantly lower strains at which our gels break compared to other examples.

Traditional shear rheology measures the bulk properties within the material while cavitation technique is clearly influenced by the mechanical properties at the micrometre length. Cavitation rheology is a powerful technique that can investigate in detail the microstructure of our LMWGs at a different scale that the traditional shear rheology cannot access. It should also be possible to use this technique to measure smaller volumes of gel than traditional rheology, as well as measuring patterned or otherwise inhomogeneous gels.

3.4. Experimental

3.4.1. Materials

All chemicals were purchased from Merck unless otherwise stated.

PVA (poly(vinyl alcohol)) hydrogels. PVA hydrogels were prepared as described before.[46] A 13,000-23,000 M_W and 98 % hydrolysed polymer was heated at 90 °C in a solution containing DMSO:water in a 40:60 ratio and 2% boric acid was added as a cross-linking agent. This solution was heated

overnight and left the solution to cool down at room temperature to form a gel. All samples were made of 10% PVA.

Gelatine. Gelatine hydrogels were made from a beef gelatine powder supplied by Dr. Oetker. Water was added to the gelatine powder and heated at 50 °C for 1 hour. Then solution was left to cool down and form the gel.

LMWG: Dipeptides **1** (FmocLG) and **3** (2NapFF) were synthesised by Dave Adams and Bart Dietrich (University of Glasgow).[43-47]

3.4.2. Samples preparation

Solvent-Triggered Gels. Stock solutions of gelator were prepared at different concentrations by dissolving the weighed gelator in DMSO. Upon complete dissolution of the gelator, distilled water was added to make the sample up to a final volume of 2 mL gel. The volume of DMSO and water used varied depending on the final ϕ_{DMSO} desired. The sample was then left to gel overnight before analysis (~ 18 hours).

pH-Triggered Gels. A stock solution of each gelator was prepared at different concentrations by weighing the required amount of gelator and adding dilute sodium hydroxide solution (1 molar equivalent of a 0.1 M solution) and water and stirring until fully dissolved. The gelator stock solution was added to a pre-weighed amount of glucono-δ-lactone, GdL (3 molar equivalents of GdL for each equivalent of gelator) and gently shaken to dissolve all GdL. The sample was left to stand to allow gelation to occur overnight (~ 18 hours).

3.4.3. Instrument and Procedures

Oscillatory Shear Rheology.

All rheological measurements were performed using Anton Paar Physica MCR 101 and MCR 301 rheometers. A cup and vane system was used to perform frequency sweeps. 2 mL gels were prepared in 7 mL Sterilin vials and left

overnight (~ 18 hours) at room temperature to gel before measurements. Frequency sweeps were performed at 25 °C in a range of frequencies from 1 to 100 rad s^{-1} at a constant strain of 0.5 % to ensure being within the linear viscoelastic (LVER) region. The storage modulus (G') at 10 rad s^{-1} was used to compare with the maximum pressure, P_c, obtained with the cavitation rheology. All measurements were repeated three times to ensure reproducibility.

Cavitation Rheology.

Cavitation experiments were carried out using a lab-built instrument. It includes a syringe pump (World Precision Instruments AL-1000) assembled into a 10 mL Hamilton™ 1000 series Gastight syringe for air pumping. A high precision manometer "CRAB (Cavitation Rheology Analyser Box)" with data logging capability was custom-built to control and record the pressure. A digital manometer was connected into the system via Y-junction and used to calibrate and double check pressure readings from the CRAB. The air rate pumped was 0.4 mL min^{-1} and a needle gauge 22 (inner diameter, 420 µm) and gauge 26s (inner diameter, 120 µm) were used. A conductivity probe controls the needle immersion depth by sending a signal to an 3D printer, which allows to precise positioning the needle below the surface of the sample.

Confocal microscopy.

Confocal images were taken using a Zeiss LSM 710 confocal microscope with a LD EC Epiplan NEUFLUAR 50X (0,55 DIC) objective. All samples were prepared in a Greiner Bio-One CELLviewTM 35 mm plastic cell culture dish with a borosilicate glass bottom. Fluorescence from Nile Blue was excited using a 634 nm He-Ne laser and emission was detected between 650 and 710 nm. Samples were prepared *in-situ*, using the methodology described above. All gels triggered using a solvent switch were stained with a 0.1 wt % Nile Blue solution. The Nile Blue was added to the DMSO-gelator solution to a final Nile Blue concentration of 2 µL mL^{-1}. To stain the pH switched samples, a 0.1 wt% Nile Blue solution was prepared and added to the gelator solution to a final Nile Blue concentration of 2 µL mL^{-1}.

3.5. References

1. P. Terech and R. G. Weiss, *Chem. Rev.*, 1997, **97**, 3133-3160.

2. R. G. Weiss, *J. Am. Chem. Soc.*, 2014, **136**, 7519-7530.

3. N. M. Sangeetha and U. Maitra, *Chem. Soc. Rev.*, 2005, **34**, 821-836.

4. X. Du, J. Zhou, J. Shi and B. Xu, *Chem. Rev.*, 2015, **115**, 13165-13307.

5. A. R. Hirst, B. Escuder, J. F. Miravet and D. K. Smith, *Angew. Chem. Int. Ed.*, 2008, **47**, 8002-8018.

6. E. V. Alakpa, V. Jayawarna, A. Lampel, K. V. Burgess, C. C. West, S. C. J. Bakker, S. Roy, N. Javid, S. Fleming, D. A. Lamprou, J. Yang, A. Miller, A. J. Urquhart, P. W. J. M. Frederix, N. T. Hunt, B. Péault, R. V. Ulijn and M. J. Dalby, *Chem*, 2016, **1**, 298-319.

7. B. O. Okesola and D. K. Smith, *Chem. Soc. Rev*, 2016, **45**, 4226-4251.

8. N. Singh, M. Kumar, J. F. Miravet, R. V. Ulijn and B. Escuder, *Chem. Eur. J.*, 2017, **23**, 981-993.

9. Y. Lan, M. G. Corradini, R. G. Weiss, S. R. Raghavan and M. A. Rogers, *Chem. Soc. Rev.*, 2015, **44**, 6035-6058.

10. J. Raeburn, A. Zamith Cardoso and D. J. Adams, *Chem. Soc. Rev.*, 2013, **42**, 5143-5156.

11. E. R. Draper and D. J. Adams, *Chem*, 2017, **3**, 390-410.

12. I. Ramos Sasselli, P. J. Halling, R. V. Ulijn and T. Tuttle, *ACS Nano*, 2016, **10**, 2661-2668.

13. L. Chen, J. Raeburn, S. Sutton, D. G. Spiller, J. Williams, J. S. Sharp, P. C. Griffiths, R. K. Heenan, S. M. King, A. Paul, S. Furzeland, D. Atkins and D. J. Adams, *Soft Matter*, 2011, **7**, 9721-9727.

14. F. Del Giudice, M. Tassieri, C. Oelschlaeger and A. Q. Shen, *Macromolecules*, 2017, **50**, 2951-2963.

15. V. Breedveld and D. J. Pine, *J. Mater. Sci.*, 2003, **38**, 4461-4470.

16. N. Yang, R. Lv, J. Jia, K. Nishinari and Y. Fang, *Annu. Rev. Food Sci. Technol.*, 2017, **8**, 493-521.

17. J. A. Zimberlin, N. Sanabria-DeLong, G. N. Tew and A. J. Crosby, *Soft Matter*, 2007, **3**, 763-767.

18. J. A. Zimberlin and A. J. Crosby, *J. Polym. Sci., Part B: Polym. Phys.*, 2010, **48**, 1423-1427.

19. J. A. Zimberlin, J. J. McManus and A. J. Crosby, *Soft Matter*, 2010, **6**, 3632-3635.

20. S. Kundu and A. J. Crosby, *Soft Matter*, 2009, **5**, 3963-3968.

21. J. Cui, C. H. Lee, A. Delbos, J. J. McManus and A. J. Crosby, *Soft Matter*, 2011, **7**, 7827-7831.

22. J. Meid, F. Dierkes, J. Cui, R. Messing, A. J. Crosby, A. Schmidt and W. Richtering, *Soft Matter*, 2012, **8**, 4254-4263.

23. M. S. Chin, B. B. Freniere, S. Fakhouri, J. E. Harris, J. F. Lalikos and A. J. Crosby, *Plast. Reconstr. Surg.*, 2013, **131**, 303e-305e.

24. P. Fei, S. J. Wood, Y. Chen and K. A. Cavicchi, *Langmuir*, 2015, **31**, 492-498.

25. S. M. Hashemnejad and S. Kundu, *Soft Matter*, 2015, **11**, 4315-4325.

26. L. E. Jansen, N. P. Birch, J. D. Schiffman, A. J. Crosby and S. R. Peyton, *J. Mech. Behav. Biomed. Mater.*, 2015, **50**, 299-307.

27. K. C. Bentz, S. E. Walley and D. A. Savin, *Soft Matter*, 2016, **12**, 4991-5001.

28. S. B. Hutchens, S. Fakhouri and A. J. Crosby, *Soft Matter*, 2016, **12**, 2557-2566.

29. J. Kang, C. Wang and S. Cai, *Soft Matter*, 2017, **13**, 6372-6376.

30. T. Cohen and A. Molinari, *Int. J. Solids Struct.*, 2015, **69-70**, 544-552.

31. S. Raayai-Ardakani, Z. Chen, D. R. Earl and T. Cohen, *Soft Matter*, 2019, **15**, 381-392.

32. A. Blumlein and J. J. McManus, *J. Mater. Chem. B.*, 2015, **3**, 3429-3435.

33. A. Blumlein, N. Williams and J. J. McManus, *Sci. Rep.*, 2017, **7**, 7346.

34. M. P. Milner and S. B. Hutchens, *Extreme Mech. Lett.*, 2019, **28**, 69-75.

35. C. W. Barney, C. E. Dougan, K. R. McLeod, A. Kazemi-Moridani, Y. Zheng, Z. Ye, S. Tiwari, I. Sacligil, R. A. Riggleman, S. Cai, J.-H. Lee, S. R. Peyton, G. N. Tew and A. J. Crosby, *Proc. Natl. Acad. Sci.*, 2020, **117**, 9157.

36. J. Zimberlin, N. Sanabria-Delong, G. Tew and A. J. Crosby, *Soft Matter,* 2007,**3**, 763-767

37. L. Pavlovsky, M. Ganesan, J. G. Younger and M. J. Solomon, *Appl. Phys. Lett.*, 2014, **105**, 114105-114105.

38. K. C. Bentz, N. Sultan and D. A. Savin, *Soft Matter*, 2018, **14**, 8395-8400.

39. C. Colquhoun, E. R. Draper, R. Schweins, M. Marcello, D. Vadukul, L. C. Serpell and D. J. Adams, *Soft Matter*, 2017, **13**, 1914-1919.

40. A. M. Fuentes-Caparrós, B. Dietrich, L. Thomson, C. Chauveau and D. J. Adams, *Soft Matter*, 2019, **15**, 6340-6347.

41. E. Z. Casassa, A. M. Sarquis and C. H. Van Dyke, *J. Chem. Educ.*, 1986, **63**, 57.

42. D. J. Adams, M. F. Butler, W. J. Frith, M. Kirkland, L. Mullen and P. Sanderson, *Soft Matter*, 2009, **5**, 1856-1862.

43. D. J. Adams, L. M. Mullen, M. Berta, L. Chen and W. J. Frith, *Soft Matter*, 2010, **6**, 1971-1980.

44. A. Mahler, M. Reches, M. Rechter, S. Cohen and E. Gazit, *Adv. Mater.*, 2006, **18**, 1365-1370.

45. M. C. Nolan, A. M. Fuentes Caparrós, B. Dietrich, M. Barrow, E. R. Cross, M. Bleuel, S. M. King and D. J. Adams, *Soft Matter*, 2017, **13**, 8426-8432.

46. A. Samzadeh-Kermani, M. Mirzaee and M. Ghaffari-Moghaddam, *Adv. Biol. Chem.*, 2016, **6**, 1-11.

47. L. Chen, S. Revel, K. Morris, L. C. Serpell and D. J. Adams, *Langmuir*, 2010, **26**, 13466-13471.

CHAPTER 4

Mechanical Characterisation of Multi-layered Hydrogels: A Rheological Study for 3D Printed Systems

This Chapter is adapted in part from the following publication:

"Mechanical characterization of multi-layered hydrogels: A rheological study for 3D printed systems"
Biomacromolecules, **2021**, 22, 4, 1625–1638
A. M. Fuentes-Caparrós, Z. Canales-Galarza, M. Barrow, B. Dietrich, J. Läuger, M. Nemeth, E. R. Draper and D. J. Adams

Z.C.G. was responsible for preliminary work on the rheological characterisation and fabrication of multi-layered hydrogels. A.M.F.C. was responsible of the conceptualisation, methodology and collection of the rheological data. A.M.F.C. also collected the confocal microscopy images, carried out the UV-Vis analysis and the 3D printing experiments. M.B. assisted in optimising the rheometer set-up for the different experiments, the rheology experiments conceptualisation and data analysis. B.D. was responsible of printing different items needed for rheological analysis and the maintenance of the 3D printer. J.L. and M.N. were responsible of evaluating the rheological discussion and gave input in the final draft of the paper. E.R.D. helped with the conceptualisation of the experiments and discussion of the rheological data. D.J.A. supervised the project and assisted in the conceptualisation of the experiments and discussion of the data. D.J.A. also synthesised the gelator molecule. The original draft of the paper was written by A.M.F.C. and D.J.A., with inputs of all authors.

4.1. Introduction

Low molecular weight hydrogels (LMWGs) are formed by the self-assembly of small molecules into long anisotropic structures, mainly fibres, through non-covalent interactions.[1-4] These fibres entangle and/or crosslink, immobilising the solvent and forming a self-supporting 3D network.[3] Such hydrogels are mainly composed of water but still possess properties more reminiscent of a solid and can therefore exhibit both elastic and viscous responses.[5] In fact, the viscoelastic nature of this class of material makes them potentially suitable for multiple biological applications such as tissue engineering, where materials capable of mimicking living tissues are needed.[6] Furthermore, such hydrogels can encapsulate different types of molecules including proteins, growth factors and signalling molecules that will facilitate cell proliferation and differentiation.[7] Another key property is the ease of disrupting the interactions that hold together the molecules, making this class of materials responsive to a wide variety of external stimuli (for example, light, enzymes or heat).[8-10] As such, there is a significant interest in this class of materials, with much of the emphasis being on their applications in biomedical fields, such as controlled drug delivery, self-healing and scaffolding for tissue engineering. [11-13]

Hydrogels can be used as cell-containing scaffolds for tissue engineering by delivering cells into damaged tissues and reconstructing organs in similar shapes. Strategies in the field of tissue engineering and regenerative medicine are committed to 3D scaffolds that mimic the natural extracellular matrix, which supports cell adhesion, migration, differentiation and proliferation.[11] One strategy requires seeding cells onto a 3D scaffold that supports *in vitro* tissue formation, which is then implanted into a patient for tissue repair. Intrinsically, the purpose of tissue engineering is to develop responsive living tissues with properties similar to those of living tissues that are intended to be replaced.

Typically, LMWGs are prepared as uniform systems with homogeneous properties.[14] However, it is possible to make hierarchical hydrogels containing

different layers with specific mechanical properties in order to mimic living-like tissues.[15] Organs, for example, are spatially heterogeneous in terms of composition and, therefore, different cell types coexist within them. Consequently, multi-layered hydrogels with different mechanical properties are of interest as an excellent option for 3D scaffold construction for tissue engineering.[16] In recent years, a great deal of interest has been put into the fabrication of multi-layered scaffold-based hydrogels for tissue engineering and regenerative medicine.[17-19]

Most recently, multiple technologies have been developed for the fabrication of hydrogels consisting of multiple layers including photolithography, microfluidics and three-dimensional (3D) (bio)printing.[16] 3D printing or additive manufacturing is a technology based on the computer-controlled layer-by-layer deposition of material (ink) that can create complex and well-defined three-dimensional objects with almost any shape or geometry.[20] 3D printing technology has revolutionised the biomedical field by providing a tool capable of manufacturing materials with unique control, flexibility, speed and precision.

Extrusion-based 3D printing is useful for scaffold construction and has been used extensively for hydrogel printing over the last decade.[21,22] 3D printers are widely used to print polymer gels for the fabrication of (bio)materials.[23-25] However, due to the poor mechanical properties that LMWGs possess and the relatively small number of gelators with appropriate thixotropic characteristics, make their use underestimate for extrusion-based 3D printing. Nevertheless, interest in the use of 3D printing LMWGs is growing.[26-28] The main considerations for a suitable ink are its printability, structural adhesion and stability after printing. In terms of printability, shear-thinning and thixotropic hydrogels are ideal candidates as they can be easily extruded and they recover their original shape after the stress is released.[29, 30] Nolan et al. have previously reported the printability of some LMWGs using an extrusion-based printer and optimised the printing conditions.[26] Gels formed from spherulitic domains of fibres exhibited better printability compared to gels formed from dense fibrous

networks. The differences in printability relies in the fact that spherulitic domains do not present as much random orientations of fibres compared to a dense fibrous network with flow through a nozzle. Hydrogels made using a solvent trigger, which results in the formation of spherulitic-like domains of fibres, are more suitable for 3D printing than pH-triggered gels, where a more uniform distribution of long fibres is formed that is more affected by the shear stress during extrusion.[26] In general, for supramolecular gels formed via non-covalent interactions, the printability of the gel using an extrusion approach depends not only on the yield point of the gel, but also on how well it recovers after being extruded, i.e. on its thixotropic nature.[31, 32]

From a rheological point of view, control of the mechanical properties of printed hydrogels is crucial for the formation of an appropriate environment for cells growth, ensuring appropriate cellular functions. Many studies have focused on the dynamic modification of the stiffness and elasticity of the hydrogels using different approaches as a means of tuning their physicochemical properties.[33] It is common to find in the literature the suitability of hydrogels for 3D printing by assessing their mechanical properties before printing, with little if any rheological characterisation of the gels after they have been printed. As such, it is presumably assumed that the resulting mechanical properties of the printed materials are not affected by the printing process, which seems unlikely considering the process involved. This lack of measuring post-printing is undoubtedly due to the difficulty in carrying out such measurements. In addition to demonstrating the ability of forming 3D printed materials into complex shapes and structures, it is also necessary to evaluate the effect of the printing process on the mechanical properties of the resulting 3D printed system. Numerous researchers have reported the ability to use 3D printing to fabricate polymer-based gel constructs.[23-25] Where the mechanical properties are assessed for gels after printing, very few studies choose rheology as the main characterization technique. Mondal et al. used sodium-gelatine hydrogels for 3D printing scaffolds. The stiffness of the resulting printed constructs were evaluated using rheology.[34] More often compression tests are used to characterize the mechanical properties of the printed constructs.[35-37]

From the best of our knowledge, the changes in shear moduli of different patterned multi-layered gels using rheology have not been reported in the literature. There have been examples where compression tests have been used to calculate the moduli. Hu and co-workers, for example have tested the mechanical properties of a multi-layered chitosan gel in which each layer possessed different properties using a tensometer. The mechanical properties were evaluated for each layer.[38] Nguyen et al. also examined the compressive modulus of multi-layered constructs of polyethylene glycol (PEG)-based hydrogel which exhibited spatially-varying mechanical properties.[39] They characterised each individual layer by separating each layer within the gel construct. The properties of each layer were measured independently.

In this Chapter, we show that the use of different rheological methods allows the characterisation of not only the mechanical properties of individual layers within a 3D printed gel, but also the contribution of each layer to the resulting multi-layered system. We show not only the importance of evaluating the mechanical properties of the gels after printing, but also how using different protocols for rheological characterisation could interfere on the determined rheological properties.

4.2. Results and Discussion

4.2.1. Multi-layered Gels Preparation

FmocFF (**4**, Figure 1.4 and Figure 4.1a) is one of the most widely used LMWG as it forms gels at physiological pH and is commercially available.[40-42] As a first step towards a comprehensive rheological characterisation of 3D printed LMWGs, multi-layered hydrogels of **4** were prepared *in situ* for mechanical property benchmark comparison. (Figure 4.1b). This was achieved by preparing multiple independent self-supporting layers using a solvent trigger one on top of each other after the lower layer had gelled. For each layer, a known amount of **4** was dissolved in dimethyl sulfoxide (DMSO) and water added such that the final ratio of DMSO:H_2O was 3:7. This drives a phase separation that results in

spherulitic-like domains of fibres being formed that entangle to form a self-supporting gel (Figure 4.1c).[43, 44]

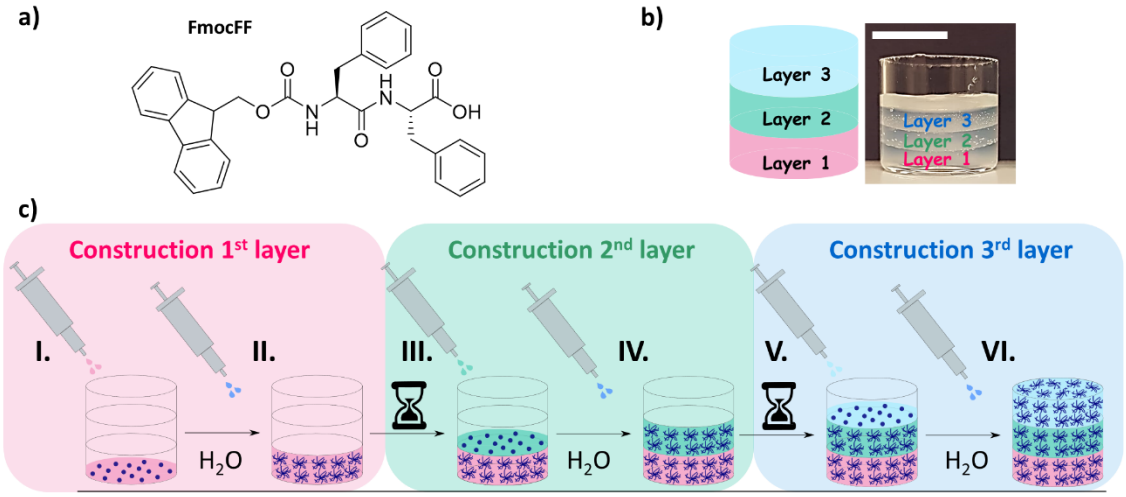

Figure 4.1 (a) Chemical structure of FmocFF, **4**; (b) Schematic and a photograph of a three-layered hydrogel construction respectively. The scale bar represents 1 cm; (c) schematic of the process by which a three-layered hydrogel is formed in situ. To form the first layer (I) **4** dissolved in DMSO is pipetted into the container and (II) water is added to trigger gelation. The same methodology was used to form the second (III)-(IV) and third (V)-(VI) layers.

The different hydrogel layers were prepared with different mechanical properties by varying the concentration of **4**. Specifically, we used two different concentrations of **4**, 5 mg mL^{-1} and 15 mg mL^{-1} for the softer and stiffer gels respectively (Figure 4.2a). Gels made in both concentrations form similar microstructures with spherulitic-like domains of fibres (Figure 4.2b). We also examined the assembly kinetics for both concentrations of the gelator by measuring the changes in turbidity over time at 600 nm (Figure 4.2c). At this wavelength, **4** does not absorb light and therefore changes in absorbance can be ascribed to changes in turbidity. For **4** at a concentration of 5 mg mL^{-1}, there is an initial increase in absorbance as soon as the water is added, corresponding to the nucleation phase, followed by a gradual decrease in turbidity which correspond to the formation of fibres.[43-45] For **4** at a concentration of 15 mg mL^{-1}, a similar trend can be observed for absorbance with the difference that the absorbance is much higher. In both cases, after 10 minutes there are no further changes in absorbance and therefore, we assume the gel network is totally

formed. To ensure gelation was complete, we allowed 30 minutes to pass before preparing the next layer.

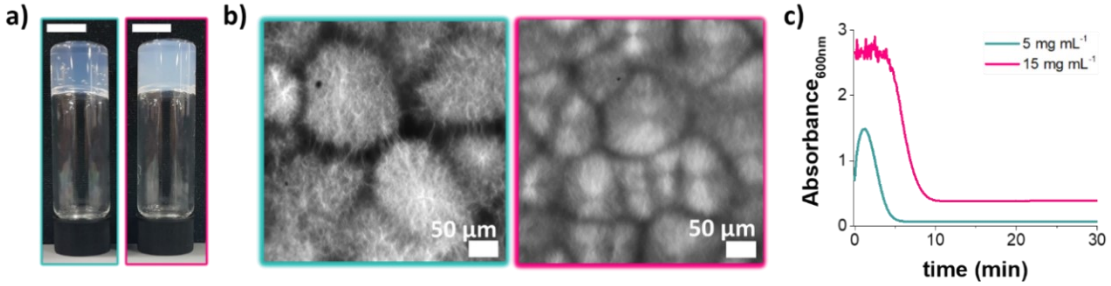

Figure 4.2 (a) Photographs of hydrogels prepared at a concentration of (left) 5 mg mL^{-1} and (right) 15 mg mL^{-1} of **4** using a ratio of DMSO:H_2O of 3:7. The scale bar represents 1 cm and the gel volumes are 2 mL. (b) Confocal images of gels formed at concentrations of **4** of (left) 5 mg mL^{-1} and (right) 15 mg mL^{-1} at a ratio DMSO:H_2O of 3:7. The scale bars represent 50 µm. (c) Changes in absorbance at 600 nm with time after adding water to a solution of either **4** at 5 mg mL^{-1} (cyan) or 15 mg mL^{-1} (pink) in DMSO.

DMSO is broadly accepted below 10% (v/v) for biological purposes.[46] However, since we just intend to prove the applicability of rheological methods to characterise multi-layered hydrogels, we considered DMSO at 30% (v/v) in view of well-defined hydrogels being formed from **4**.

In the following discussion, we initially focus on gels that are 8 mm thick in total. This thickness allows us to effectively demonstrate that we can probe and understand layered gels. We then move to gels of 2 mm total thickness, before finally comparing our data for layered gels to 3D printed systems.

Since we intend to compare the rheological properties of multi-layered systems prepared in situ with those delivered using an extrusion-based 3D printing technique, we designed a specific container in which prepare the gels that would be suitable for both techniques. We used a 3D printed a container (Figure 4.3a) which would allow to directly extrude our gels using 3D printing and also prepare the same multi-layered gels in situ. To probe these gels by rheology, we used two different measuring geometries, vane (Figure 4.3b) and parallel

plate (PP) (Figure 4.3c). The PP geometry is widely used for hydrogel rheological characterisation with sample thickness between 0.5-2mm, while the vane is less common, but effective for rheometry on soft materials that can be prepared in cups which could be susceptible to pre-shear caused by sample loading on to a plate.[47] Both geometries measure bulk flow of material, however their configuration is different in that a parallel plate measures from the top of the bulk sample, whereas the vane penetrates into sample without completely destroying the overall structure. We considered that the two different modes of operation could affect the resulting measured mechanical properties and trends associated with their layering.

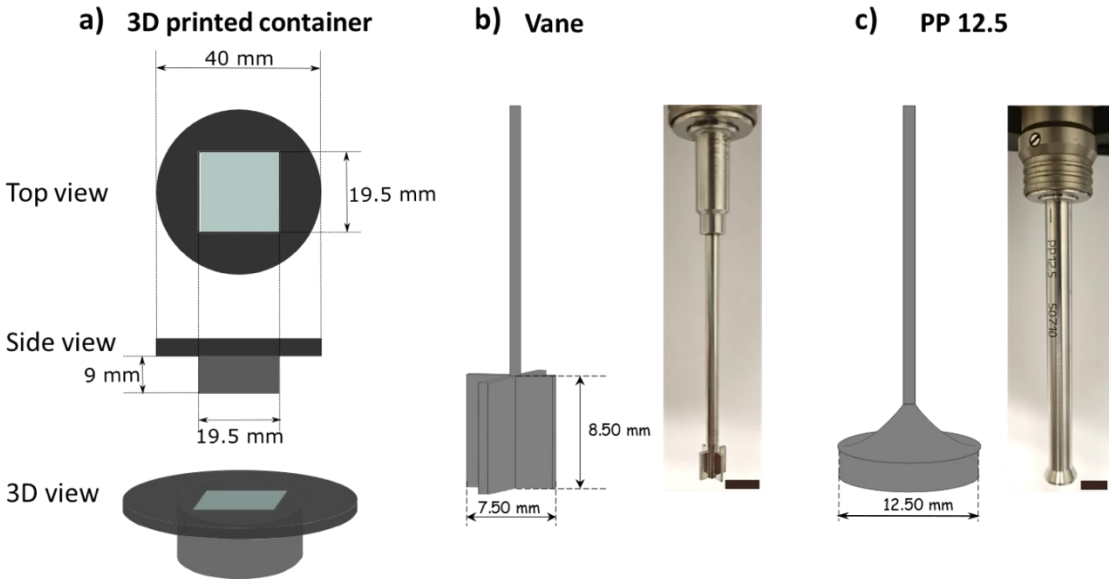

Figure 4.3 (a) Diagram of the 3D printed container. Diagrams and photograph of the different geometries used for rheological measurements and their dimensions; (b) cup and vane geometry, (c) parallel plate PP12.5 geometry. The scale bars represent 10 mm.

4.2.2. Vane Geometry

The vane geometry is advantageous for measuring heterogeneous samples that may slip using the parallel plate.[48] However, some considerations need to be taken in order to get reliable measurements. During measurements, the vane delineates a path along which the stress applied is inversely proportional to the square of the radius (Figure 4.4a-c).[49] Inside the limits defined by the vane

blades radius (R_v), the material moves guided by the blades. However, the stress decays gradually outside these limits (Figure 4.4b). Differences in the radius between R_v and the wall container (R_c) will therefore have an effect on the calculated rheological parameters (Figure 4.4c). Similarly, the position of the vane during measurements can affect the rheological properties being measured (Figure 4.4d). Differences in the vane position will determine the height/thickness of gel touching the vane blades and, therefore, the rheological parameters measured. On top of that, the vane geometry is a relative measuring system that do not have a constant shear rate throughout (like cones and cylinders) and therefore the CSS (controlled shear stress) factor can be manually set by the user to calculate the speed at certain point in the measuring system. The CSS and CSR (controlled shear rate) factors for the vane geometry used are 2700 Pa m^{-1} Nm^{-1} and 1 min s^{-1} respectively. The CSS factor on the geometry assumes that the vane rotor is fully submerged in the sample. Therefore, to calculate correct G' and G" values for rheological measurements we divided both moduli by the percentage of the measuring system (i.e., vane rotor) that was actually submerged in the multi-layered gel systems.

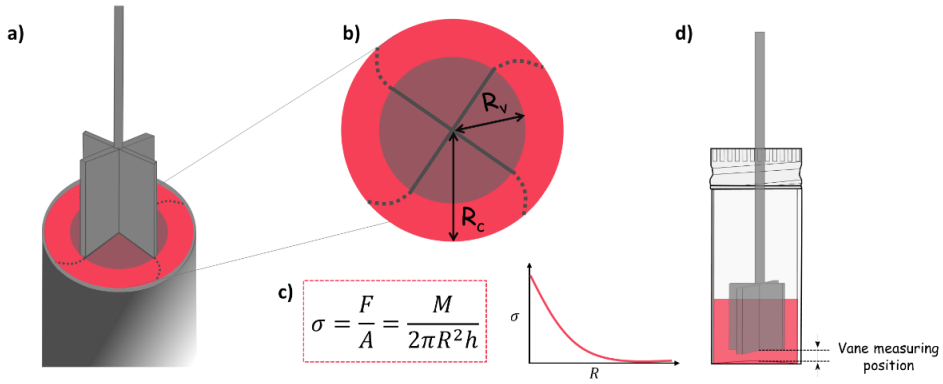

Figure 4.4 (a) Cartoon of a four bladed vane geometry inserted into a hydrogel (red) for measurement. (b) Inset of the shearing profile the material experiences during measurements. Inside the limits defined by the vane blade radius (R_v), the material moves guided by the blades. However, the stress decays gradually outside these limits; i.e., for the material trapped between the vane blades and the wall container. The distance between the centre of the vane and the wall of the container is defined as R_c. (c) (Left) equation that defines the shear stress, where F is the normal force (N), A is the surface (m^2), M is the torque (N m), R (or R_v) is the radius (m) and h is the thickness (m) of the material being examined and (right) profile showing the gradual decay of the shear stress as the radius increases. (d) Cartoon showing the position of the vane within a sample and the gap left between the vane and the bottom part of the container in which the gels are made.

Since the distance between the vane blades and the wall container in which the gel is made will affect the measured rheological properties (Figure 4.4), we optimised a setup that would allow to minimise such distance. We used a hollow metal cylinder of 16.5 mm in diameter (Figure 4.5c), compared to the vane diameter of 7.5 mm, to "cut" the gel for measurements. As such, the amount of gel trapped between the vane blades and the hollow metal cylinder wall is minimum (4.5 mm), thus avoiding artifacts that could affect the stress applied to the bulk gel during measurements. We used the hollow metal cylinder setup for all measurements conducted using vane and PP geometries (Figure 4.5d). Additionally, to ensure the concentric position of the hollow metal cylinder in

the 3D printed container, we used a cover lid (Figure 4.5b) for the container with a hollow in the middle in which the hollow metal cylinder fits perfectly.

Summarising, the procedure used to prepare the multi-layered gels for rheological measurements is as follows; firstly, we prepare the multi-layered gels inside the 3D printed container as explained previously (Figure 4.5e). Then we settle the hollow cover lid on top of the container (Figure 4.5f) followed by the hollow metal cylinder (Figure 4.5g) to chop the gel and some Blu Tack® to make sure it will not move during measurements. Finally, we place it into the corresponding rheometer system and set the corresponding measuring geometry (Figure 4.5d and Figure 4.5h).

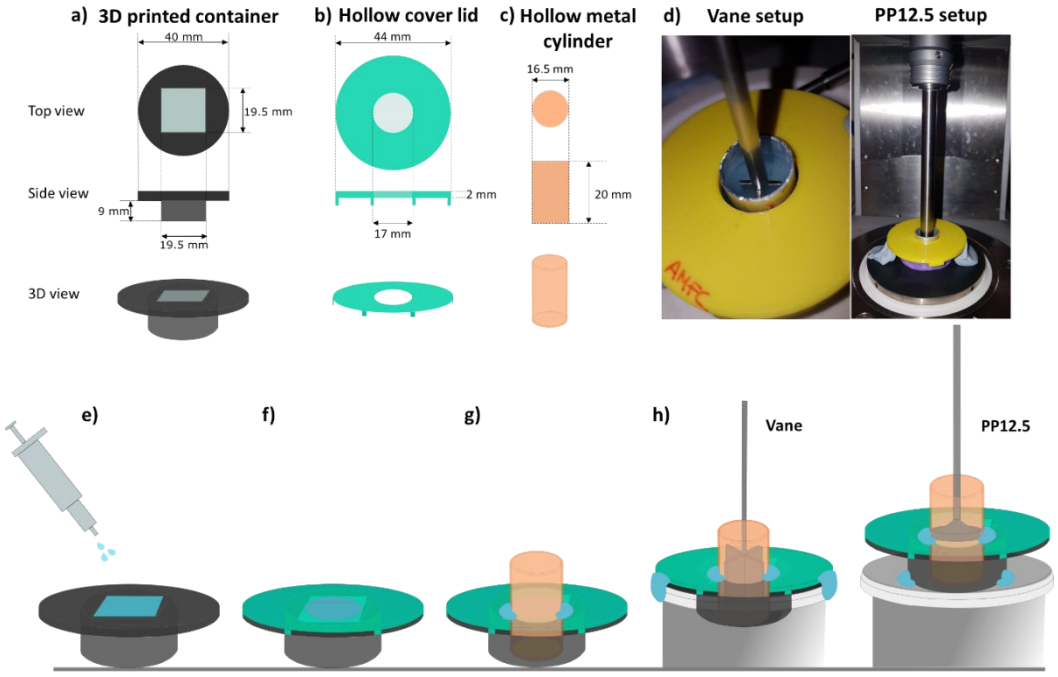

Figure 4.5 Layout of (a) the 3D printed container, (b) the hollow cover lid and (c) the hollow metal cylinder. (d) Photographs of (left) the setup for vane measurements and (right) PP12.5. (e)-(h) Schematic showing the procedure followed to load the samples for rheological measurements; (e) gel is prepared inside the container; (f) then a hollow cover lid is positioned on top of the container and (g) the hollow metal cylinder is inserted in the hollow and fixed in place with some Blu Tack®; (h) then we place it on the corresponding system depending on which geometry we will use and again some Blu Tack® is used to ensure the container will not move during measurements.

4.2.3. Parallel Plate Geometry

Rheological measurements using the parallel plate geometry present some advantages. When a PP geometry is used, the measuring gap can be controlled, which can be advantageous, as gels with different thicknesses can be measured. However, this has implications that need to be considered for measurements.

In a typical experiment, the sample is placed on the rheometer base plate and the PP geometry is lowered to the desired gap. Here, we used a controlled setup which lowers the PP12.5 geometry to a position where the detected normal force is 0.05 N (Figure 4.6a). That is, the PP12.5 will be in the measuring position when it just touches the surface of the gel and compresses it with 0.05 N of force.

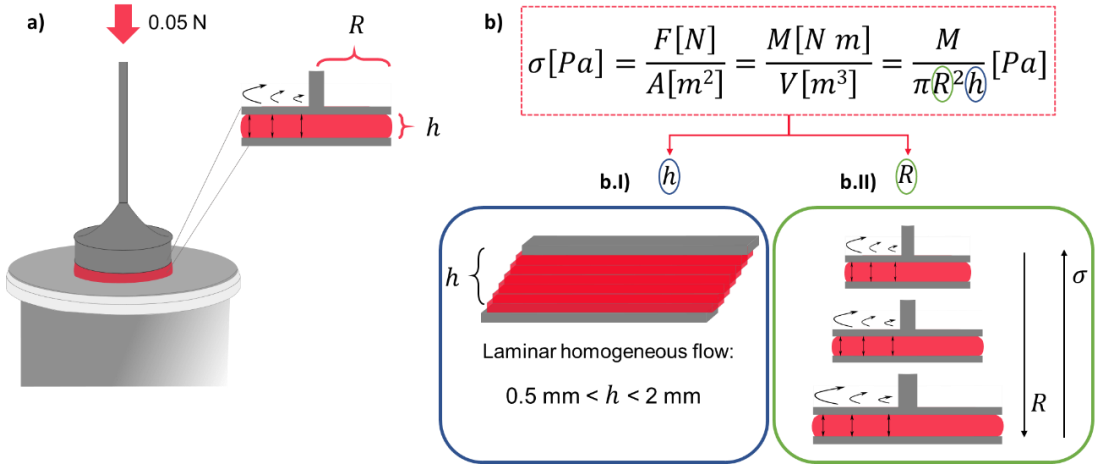

Figure 4.6 (a) Cartoon showing the setup of a typical experiment using a PP geometry, where the sample is placed between the geometry and the base plate. In this case, the PP12.5 geometry is lowered to a gap (h) where the detected normal force is 0.05 N. (b) Equation showing the dependence of shear stress (σ, in Pa) on the radius (R, in m) of the PP and the measuring gap width (h, in m); where F is the shear force (N), A the shear area (m^2), M the torque (N·m) and V is the volume of sample between the two plates (m^3). Schematic representing (b.I) the laminar flow of a material using PP and (b.II) the shear stress dependency on the size of the geometry used.

During measurements, the shear rate is not constant along the geometry, being higher in the outer part of the PP (Figure 4.6a).[48] The shear stress applied also depends upon the size of PP used (Figure 4.6bII) and the thickness of the sample, i.e. the measuring gap (Figure 4.6bI).[50] To ensure homogeneous laminar flow of the material, the sample needs to range between 0.5 mm and 2 mm in thickness.[51] Laminar flow is not guaranteed if the sample height is outside of these limits. Likewise, the shear stress is also influenced by the size of the PP used, being higher for smaller sizes of PP geometries.[51] As for the vane geometry, the CSS (2617.89 Pa m^{-1} Nm^{-1}) and CSR (0.65364 min s^{-1}) factors were also manually set for the PP measuring system.

4.2.4. Rheological Characterisation of 8 mm Multi-layered Gel Systems Prepared *in situ*

Eight different experiments consisting of three-layered gel systems of 8 mm in thickness were carried out (experiments 1-8, Figure 4.7a). Together they represent a gradient in the mechanical properties, which was modulated by changing the concentration of **4** and position of each layer within the gel system. Both, vane and PP geometries were used to characterise experiments 1-8. PP geometry is not suitable for any samples with 8 mm thickness, but we use it to highlight the sensitivity of the vane. For measurements using the vane geometry, different positions of the vane were used. These are positions A, B, and C, which correspond to the vane embedded at 0.5 mm from the bottom of layer 1, layer 2, and layer 3, respectively (Figure 4.7b). For measurements using the PP12.5 measuring system, the PP is placed on the top surface of the gel system (Figure 4.7b).

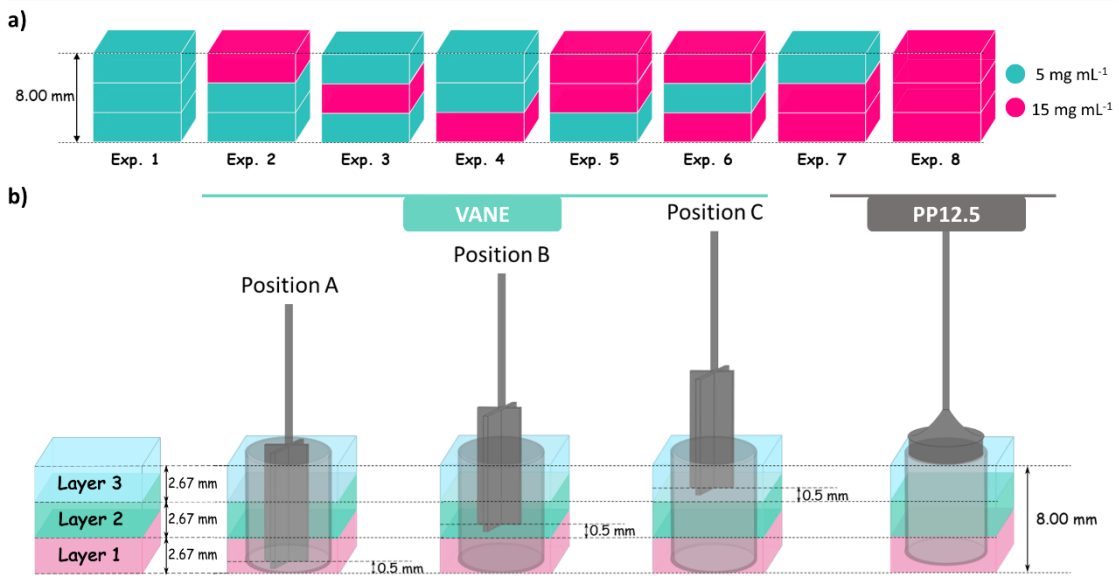

Figure 4.7 (a) Cartoon representing experiments 1-8, where each hydrogel is made of three-layers. All cartoons represent 8 mm gels (2.67 mm each layer) in which the cyan and pink layers represent gels formed from 4 at a concentration of 5 mg mL^{-1} and 15 mg mL^{-1} respectively. (b) Schematic representation of the different rheological protocols being used for the vane and PP12.5 geometries. Layers 1 (bottom), 2 (middle) and 3 (top) are represented in pink, green and blue respectively. The vane geometry in positions A, B and C correspond to the vane embedded at 0.5 mm from the bottom of layers 1, 2 and 3 respectively. The PP12.5 geometry is positioned on the surface of the top layer (blue) at an induced compressional normal force of 0.05N.

For the measurements carried out using the PP, normally the geometry is manually lowered to the desired measuring gap. However, the measured stiffness can be affected by the induced compressional normal force during measurements.[52] For gels formed using **4**, there is a dependence of the compressional force being applied to the gel before measurements on the resulting storage modulus (Figure 4.8a-b). As such, we used a setup where the PP geometry was lowered to a position where the detected normal force was 0.05 N. This force is low enough to detect the gel and stop the measuring system without compressing the gel significantly.

The rheological properties of the hydrogels prepared using **4** were investigated by means of strain sweeps, using strains ranging from 0.01% to 1000% at an angular frequency of 10 rad s^{-1}. The values for storage modulus, G', were determined from the average of G' in the linear viscoelastic region (LVER) for each experiment (Figure 4.8c). The LVER was determined as the region where G' and G" remain constant up to a strain amplitude at which the gel starts breaking (~0.6-0.7%) and both moduli deviate from linearity (highlighted region in Figure 4.8c). To define the critical strain (γ_c), we draw a line tangent to LVER and another line tangent to the non-linear region. The intersection of both lines will assert the value of γ_c (Figure 4.8c).

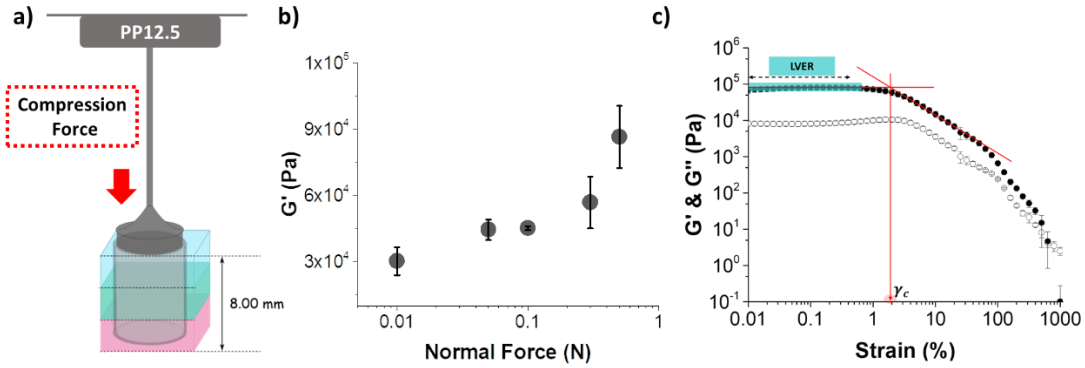

Figure 4.8 (a) Cartoon of the PP12.5 setup. (b) Storage modulus G' versus the normal force applied to the gel before starting measurements using a PP12.5 measuring system on a 2.67 mm height gel of **4** at a concentration of 5 mg mL-1. (c) Example of strain sweep showing the LVER region (highlighted in blue) and the γ_c (marked in red).

Firstly, experiments 1-8 of 8 mm thickness were investigated using the vane geometry at positions A, B, and C (Figure 4.9). The sensitivity of the vane goes beyond the simple fact of being able to measure differences in the mechanical properties at different positions within a gel system. To understand this in detail, we carried out a deep analysis of the results shown in Figure 4.9.

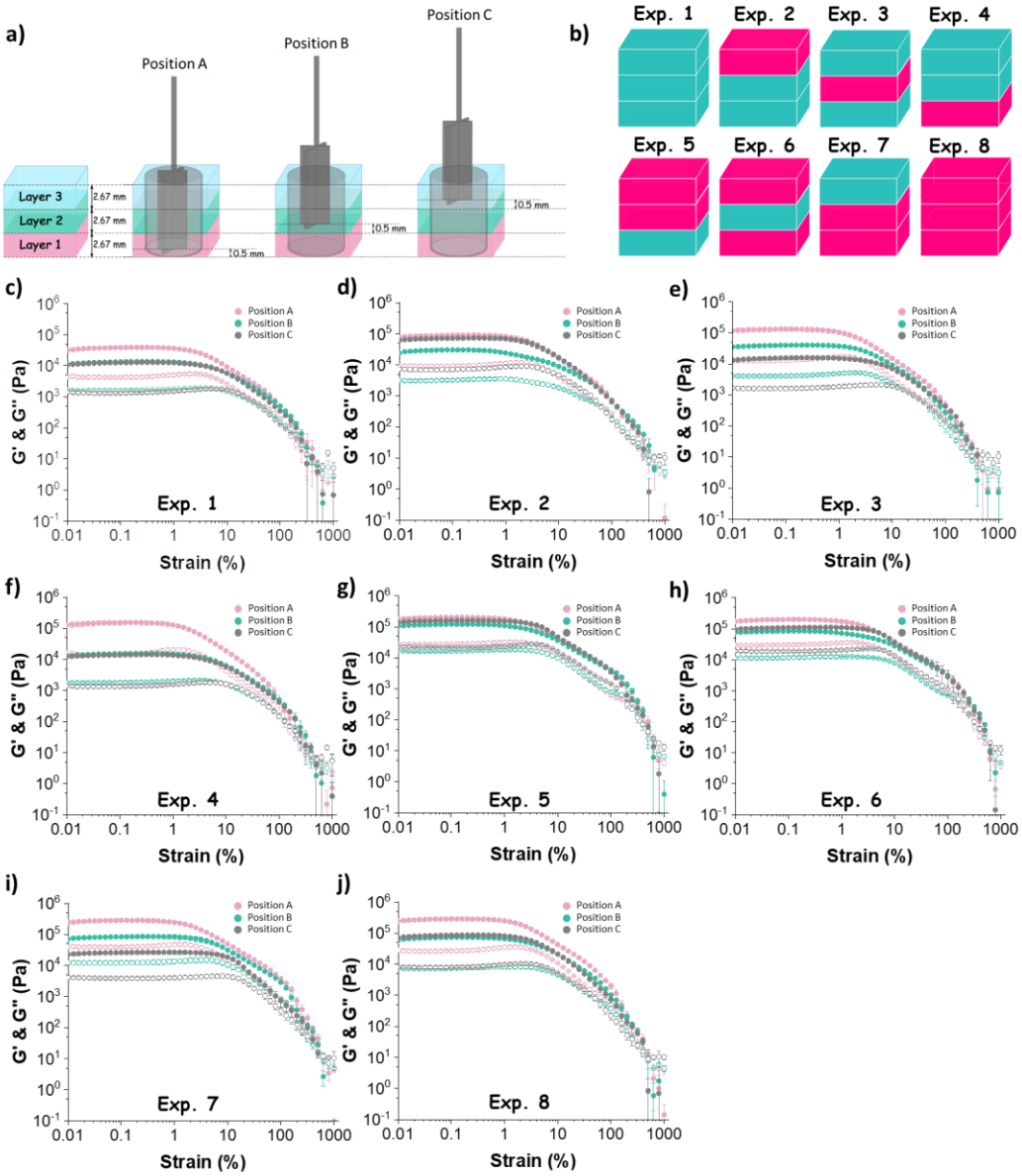

Figure 4.9 Rheological data for 8 mm three-layered gels using the vane geometry. (a) Schematic representing three different positions used for the vane measurements in an 8 mm three-layered gel; position A, B and C correspond to the vane located at 0.5 mm above the bottom surface of layers 1, 2 and 3 respectively. (b) Cartoons showing gel layers in experiments 1-8. Each gel stack is made up of 3 layers, where the cyan and deep pink layers represent 5 mg mL^{-1} and 15 mg mL^{-1} of **4** respectively. (c)-(j) Strain sweeps for experiments 1-8. The three sets of strain sweeps correspond to the vane measuring at position A (pink data), B (green data), and C (grey data). The error bars represent the standard deviation for three measurements. Closed and opened symbols represent G' and G", respectively.

For the rheological measurements using the vane in position A, where the vane is inserted in the bottom layer and touching all of layers 1, 2 and 3, the stiffness increases linearly for experiments 1 to 8 (Figure 4.10c). Such a linear increase in G' is a result of the specific distribution of the different layers within the gel system. Experiment 1 (three layers of 5 mg mL^{-1}) and experiment 8 (three layers of 15 mg mL^{-1}) are the controls, and in between them the layered gels are made of different combinations of the two concentrations of **4**. If we consider experiments 2-4, the difference between them is the distribution of the layers (Figure 4.10a). Each of these is formed from two layers of a concentration of 5 mg mL^{-1} and one layer at a concentration of 15 mg mL^{-1} with the difference being the absolute position of the gel layer at a concentration of 15 mg mL^{-1}. Considering the total concentration is kept constant (two layers of 5 mg mL^{-1} and one of 15 mg mL^{-1}), we can interpret the increase in stiffness in experiments 2-4 as being due to the absolute position of the stiffer layer; there is an increase as the 15 mg mL^{-1} gel layer is closer to the bottom of the container where the vane is embedded. For experiments 5-7 again there is an increase in stiffness from 5 to 7. These gels are now formed from two layers of 15 mg mL^{-1} and one layer of 5 mg mL^{-1}. Again, the stiffness depends on the relative positions of these layers, with the stiffest overall gel being that where both the 15 mg mL^{-1} layers are closer to the bottom (experiment 7). Notably, the stiffness for experiments 5 and 6 is constant. The difference between these is the distribution of the bottom and middle layers (one layer of 5 mg mL^{-1} and one of 15 mg mL^{-1}). This is interesting since it reveals that both the bottom and middle layers contribute significantly to the total stiffness of the gel. But then a question arises; why do the stiffness for experiments 3 and 4 increase rather than staying constant as for experiments 5 and 6? We hypothesise that this has to do with the properties of the top layer, which is made of a concentration of 5 mg mL^{-1} for experiments 3 and 4, and 15 mg mL^{-1} for experiments 5 and 6. The stiffer layer (15 mg mL^{-1}) is likely to dominate the vane measurements. As such, for experiments 3 and 4, the increase in stiffness is due to one 15 mg mL^{-1} layer being close to the bottom of the layered system, while for experiments 5 and 6 there are two layers of concentration 15 mg mL^{-1} that will dominate the stiffness measurements, minimising the contribution of the 5 mg mL^{-1} layer. All

of this shows that the rheological parameters being measured using the vane at position A are likely to be influenced by the properties of the neighbouring layers in which the vane is inserted as well as the properties of each individual layer.

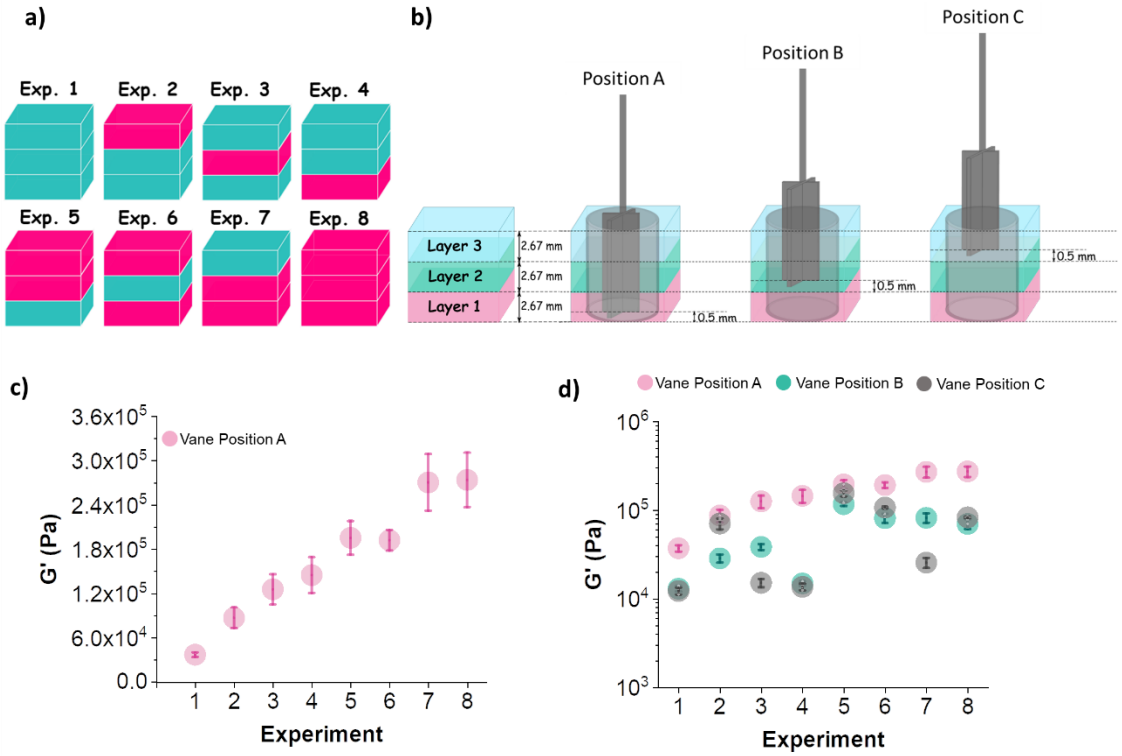

Figure 4.10 (a) Cartoons showing gel layers in experiments 1-8. Each gel stack is made up of 3 layers, where the cyan and deep pink layers represent 5 mg mL^{-1} and 15 mg mL^{-1} of **4** respectively. (b) Schematic representing three different positions used for the vane measurements in an 8 mm three-layered gel; position A, B and C correspond to the vane located at 0.5 mm above the bottom surface of layers 1, 2 and 3 respectively. (c) G' for experiments 1-8 using the vane in position A. (d) G' values for experiments 1-8 in log scale using the vane in position A (pink circles), B (green circles) and C (grey circles).

In the same way, we measured the rheological properties of layered gels 1-8 using the vane in position B (Figure 4.10d, green circles). Here, the vane is inserted into the middle layer (layer 2) so that it is only in contact with layers 2 and 3 (middle and top). In this case, the changes in G' do not follow a linear trend as for the measurements of the vane in position A. There is an initial

linear increase in stiffness between experiments 1, 2 and 3, but then the stiffness drops for experiment 4. For experiments 1 and 2, with the vane in position B, the increase in G' is firstly due to the vane being in contact with two layers of 5 mg mL^{-1} and then one of the layers is swapped with a 15 mg mL^{-1}. The increase in G' between experiments 2 and 3 is due to the stiffer layer being closer to the layer in which the vane is embedded. Then, the G' value drops for experiment 4, in which only two layers of 5 mg mL^{-1} are being measured. The values of G' for experiments 1 and 4 are very similar, coinciding with the fact that in both experiments the two top layers are 5 mg mL^{-1}. These results show the effectiveness of using the different positions of the vane to characterise different layers within a multi-layered system. As another demonstration of the capability of this method, a decrease in stiffness when comparing experiment 5 and 6 is noticeable. The middle and top layers of experiment 5 are both made of gels at a concentration of 15 mg mL^{-1}, whereas for experiment 6 these are at a concentration of 5 mg mL^{-1} and 15 mg mL^{-1}, respectively. The decrease in G' is due to the vane being embedded within the 5 mg mL^{-1} layer in experiment 6, making the stiffness of the system lower compared with experiment 5.

The rheological properties of experiments 1-8 were also assessed using the vane in position C (Figure 4.10d, blue circles), in which it is only embedded in the top layer of the multi-layered hydrogel. In this case, we can see a different trend for G', where the stiffest values are found for experiments 2, 5, 6 and 8, which are the experiments in which the top layer is at a concentration of 15 mg mL^{-1}. If we compare experiments 5 and 6, there is a noticeable decrease in G', which corresponds with the middle layer being swapped from 15 mg mL^{-1} to 5 mg mL^{-1}. As such, when the vane is used in position C, not only the top layer is contributing to the resulting rheological parameters, but also the properties of the layer below.

It is important to highlight that one would expect the modulus of a multi-layered gel prepared at a constant concentration of the gelator (for example experiments 1 and 8) to be the same at different vane positions. Experiments 1 and 8 show very similar G' values for the vane at positions B and C. However,

the G' for experiments 1 and 8 when the vane is in position A are higher. These differences could be explained as an edge effect of having the vane close to the bottom of the container in which the samples are prepared. Therefore, the position of the vane at which you measure the gel properties can affect the resulting G' values, but when comparing the data at different positions this method is sensitive enough to detect differences in the mechanical properties of each individual layer within the multi-layered gel system.

From the discussion above, it is clear that this method is capable to characterise not only individual layers within a multi-layered hydrogel, but also the contribution of the neighbouring layers. This is important for tissue engineering and regenerative medicine applications, as it is recognised that cells "sense" the neighbouring elastic environment, which influences intracellular processes.[53, 54] It could also be used to detect whether neighbouring gels layers, or even surfaces could have an effect on bulk properties of gels.

4.2.4.I. Vane *versus* Parallel Plate for 8 mm Gel Systems

We also used the PP12.5 geometry to characterise layered gels 1-8 (Figure 4.11). It is common to find in the literature rheological properties of hydrogels being measured using a PP measuring system.[45, 52, 55, 56] Both parallel plates and vanes are considered "relative" measuring systems as they do not have a constant shear rate throughout the measuring gap so a point needs to be selected to measure the shear rate. The operational software calculates the shear rate by multiplying the rotational speed by CSR factor owing to a specific point on the geometry. These same factors are applied when pre-setting strain. We show the differences in the measured rheological properties for experiments 1-8 using the vane in position A and the PP12.5 (Figure 4.12). It is important to understand here that as we are using two relative systems, we should not necessarily get the same G' values for vane and plate when measuring the same material, however we can compare the trends of the measuring systems.

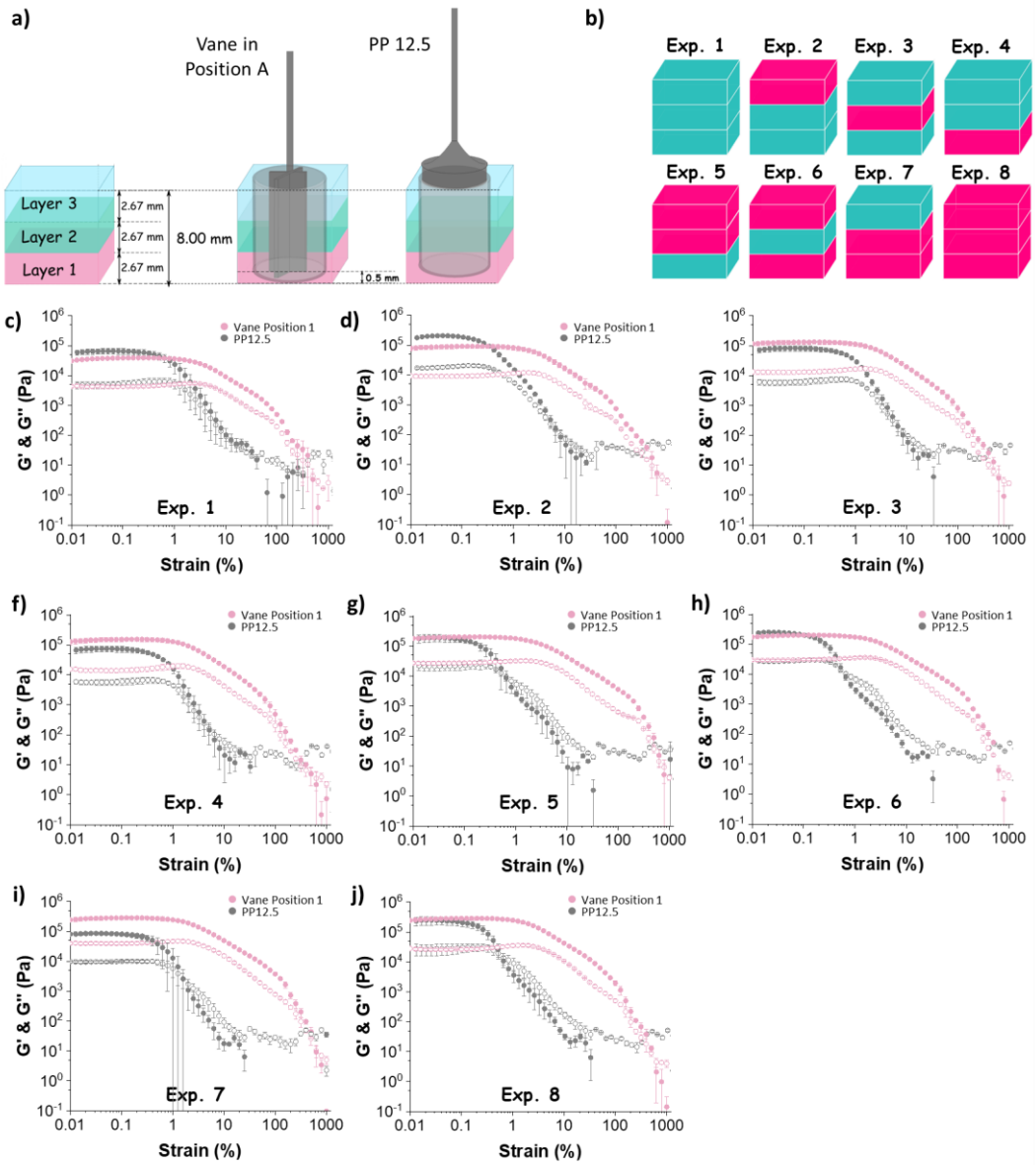

Figure 4.11 Rheological data for 8 mm three-layered gels comparing the measurements with vane and PP12.5 geometries. (a) Schematic showing the setup for the vane and PP12.5 measurements. (b) Cartoons representing experiments 1-8. Each experiment uses a stack of 3 gel layers, where the cyan and deep pink layers represent 5 mg mL^{-1} and 15 mg mL^{-1} of **4** respectively. (c)-(j) Strain sweeps for experiments 1-8. The pink data correspond to the measurements using the vane in position A and the grey data show the strain sweep measured using the PP12.5. The error bars represent the standard deviation for three measurements. Closed and opened symbols represent G' and G", respectively.

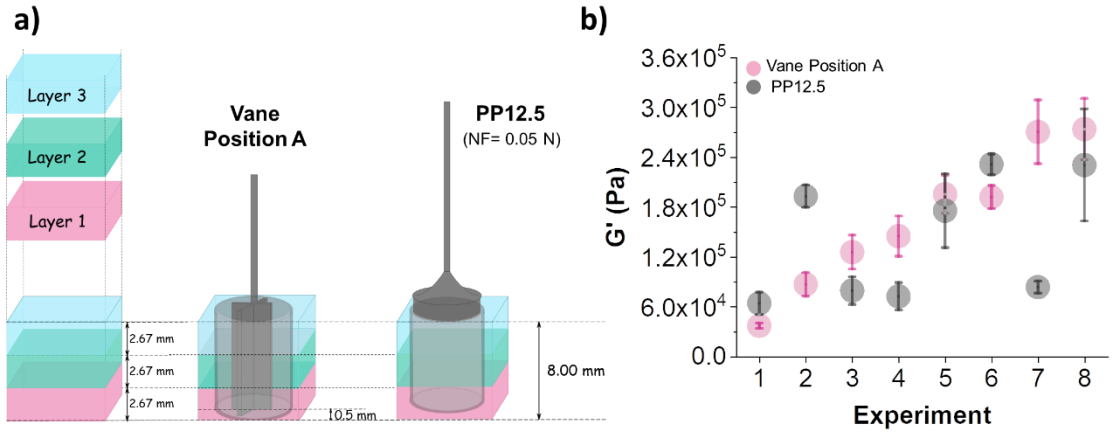

Figure 4.12 (a) Schematic of (left) vane at position A and (right) PP12.5 on top surface of the multi-layered gel. (b) Comparison of G' for experiments 1-8 using both the vane in position A (pink circles) and the PP12.5 (grey circles). The error bars represent the standard deviation of three different measurements.

The trend of the measured G' values for experiments 1-8 differs between the data collected with vane and those collected with the PP12.5 measuring system (Figure 4.12b). As an example, for experiment 2 the stiffness values are very different using both geometries. The measured G' using PP12.5 and the vane are 2 x 10^5 Pa and 8 x 10^4 Pa respectively. For this specific experiment, the top layer is formed at a concentration of 15 mg mL^{-1}, while the bottom and middle layers are formed from gels at a concentration of 5 mg mL^{-1}. For the PP12.5 geometry, the top layer has a greater contribution to the measured properties than the middle and bottom layers. For experiment 7, where the top layer is at a concentration of 5 mg mL^{-1} and the middle and bottom layers are at 15 mg mL^{-1}, we encounter the opposite situation; the highest G' corresponds to the vane geometry measurement. This again shows that the PP12.5 measurements are more likely to be dominated by the top layer, which in this case is the softer layer, and make the G' value be lower compared to the G' measured with the vane, which takes into account the three layers. Furthermore, the measurements carried out using the PP geometry seem to present larger error bars after the critical strain (Figure 4.11 and Figure 4.12b). This could be due to the fact that the PP is much more likely to slip quicker compared to the vane geometry.

4.2.5. Factors Affecting the Mechanical Properties of Gels

From these rheological results, we are able to not only characterise single layers in a multi-layered hydrogel, but also quantify the input that the rest of the layers are making to the system as a whole. To further characterise such systems, we implemented various tests. From Figure 4.10d, we showed the effect of using the vane at different positions within a set of experiments where the distribution of layers is arranged in such a way that the mechanical properties of each gel system can be tuned. For experiments 1 and 8, where the gel is made up of three layers of 5 mg mL^{-1} and 15 mg mL^{-1} respectively, the stiffness of the gel is independent of the vane position (Figure 4.13a,b). However, as mentioned above, the G' values at position A are affected by the vane being close to the bottom of the container in which the gel is prepared and therefore needs to be taken into account. We also considered 8 mm gels made of one layer at a concentration of both 5 mg mL^{-1} and 15 mg mL^{-1} of **4** (experiment 1* and experiment 8* respectively, Figure 4.13a). We evaluated the rheological properties by using the vane at positions A, B and C (Figure 4.13c) and compared with the counterparts three-layered systems (experiments 1 and 8). If the layers were not well integrated and secured together, the interface between the layers could lead to delamination or slip of the gel system and interfere with the rheological properties. We show very similar trends for G' measured with the vane at positions B and C for one-layered and three-layered gels (Figure 4.13c). This implies that there is no delamination or slip between the layers. However, G' values are slightly affected at position A for the multi-layered gel compared to the bulk gel. We attribute these changes in stiffness to the fact that for a bulk gel there is only one gel-air interface, whereas for a three layers gel there are three air-gel interfaces and some mixing between the different layers could lead to effects on the resulting mechanical properties being measured.

Similarly, we also examined the effect of changing the height of the gel being measured, keeping the vane at position A (Figure 4.13d,e). For both concentrations of **4**, we found that G' being measured is independent of the

total thickness of the gel as long as the concentration used to make the gel is constant.

In an attempt to find other factors that would affect the mechanical properties being measured, we considered two-layer gel systems made of a concentration of 5 mg mL^{-1} and 15 mg mL^{-1} layers (experiment 1:8 and 8:1, Figure 4.13f). We compared the G' values of exp. 1:8 with experiment 3 (where a third layer is added) and experiment 8:1 with experiment 4 (where a third layer is also added), see Figure 4.13f. We observed slightly differences in G' values when comparing the two layers gels to the same gel in which a third layer was added (Figure 4.13g). Furthermore, we demonstrated that the mechanical properties of the third layer also affect the mechanical properties being measured (Figure 4.13g). This can be seen when we compare experiment 3 with 5, and experiment 4 with 6, where the difference is the concentration used to make the top layer.

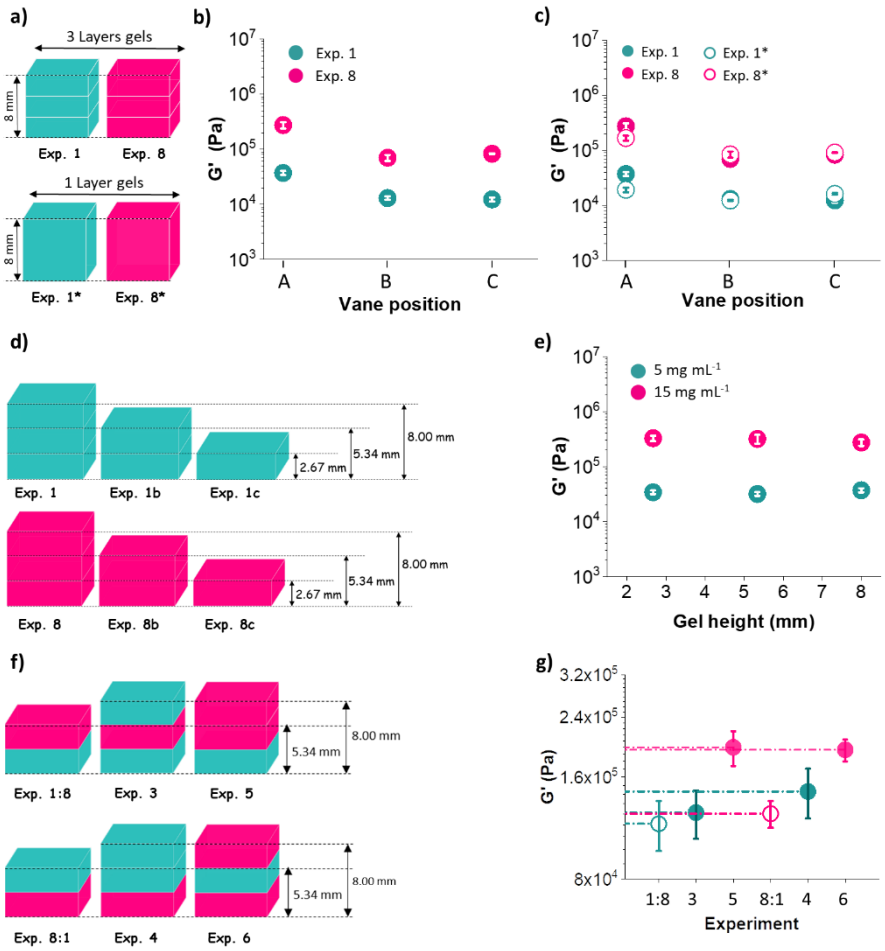

Figure 4.13 (a) Cartoons for experiments 1 and 8 (three-layered gels) and experiments 1* and 8* (mono-layered gels). (b) G' versus the vane at positions A, B and C for experiments 1 (cyan circles) and 8 (pink circles). The linear fits are represented with dotted lines and the trend is very similar for both experiments. (c) G' versus the vane at positions A, B and C for experiments 1 (filled cyan circles), 8 (filled pink circles), 1* (hollow cyan circles) and 8* (hollow pink circles). (d) Schematic representation of gels made of different heights. The cyan and pink layers represent gels formed from **4** at a concentration of 5 mg mL^{-1} and 15 mg mL^{-1}, respectively. (e) Evolution of G' with gel height measured with the vane at position A. The linear fits are represented with dotted lines and are very similar for both concentrations. (f) Schematic representing different experiments made of different heights and distribution of layers. The cyan and pink layers represent gels formed from **4** at a concentration of 5 mg mL^{-1} and 15 mg mL^{-1}, respectively. (g) G' values for the experiments represented in (f) using the vane in position A.

4.2.6. Rheological Characterisation of 2 mm Multi-layered Gel Systems Prepared *in situ*

Up to now, we have shown a broad investigation of the rheological properties of 8 mm thick three-layered gels using the vane and PP geometries. For PP measurements, according to various standard testing methods a gap of between 0.5 mm to 2 mm is recommended for obtaining reproducible data.[57] At gaps larger than this it is difficult to know whether you are conducting a bulk measurement or just the contribution from the top of the material.[57] As such, we decreased the height of layered gels 1-8 from 8 mm to 2 mm (Figure 4.14a). For three-layered 2 mm gels, each layer therefore now represents 0.67 mm of gel. For the vane measurements, we positioned the vane at 0.3 mm from the bottom of the container to ensure the vane was touching at least the 50 % of the bottom layer (Figure 4.14b).

4.2.6.I. 8 mm Gels *versus* 2 mm Gels

Firstly, we examined the trend of G' for experiments 1-8 in both 8 mm and 2 mm gel systems (Figure 4.14c). Individual strain sweeps of experiments 1-8 made of 2 mm in height and measured using the vane and PP geometries can be found in Figure 4.15 Interestingly, for vane measurements there is sometimes a pronounced peak in G" at the end of the linear viscoelastic region. Such a peak is often due to some microstructural rearrangement before the structure begins to yield and sometimes it can indicate a slow crossover into a slip regime. This behaviour is not observed, or at least much weaker, in the 8 mm gel systems (Figure 4.11). Therefore, we propose this is due to heterogeneities at the layer boundaries. In the 2 mm gel systems, the range of layer borders are relatively larger compared to the overall sample thickness. The effect is also more pronounced with layers made of the higher concentration of gelator **4**. As an example, if we compare experiments 1 and 8, there is a more pronounced peak of G" for experiment 8 (Figure 4.15). It seems that with two layers of the higher concentration in connection to each other the G"-peak effect is the highest. On top of that, we highlight the slip effect

observed in the PP measurements for 8 mm and 2 mm systems (Figure 4.11 and Figure 4.15 respectively). The moduli decrease much faster towards increasing strain when using the PP12.5 system compared to the vane measurements.

As for 8 mm gels, the G' values show an increasing trend for 2 mm gels, except for experiments 4 and 6, which deviate from the increasing trend. This could be due to the vane not being entirely embedded in the bottom layer and therefore the greater contribution to the vane measurements relies on the middle and top layers. We examined the data for experiments 1-8 made on 2 mm gels. Initially, an increasing trend for experiments 1, 2 and 3 is observed followed by a drop of the G' value for experiment 4. From these results, one might contemplate the possibility of the vane not being in contact with enough of the bottom layer during measurements. However, if we observe the distributions of each layer for experiments 1 and 4, the only difference is the bottom layer being made of **4** at a concentration of 15 mg mL^{-1} for experiment 4, compared to a layer of 5 mg mL^{-1} of **4** for experiment 1. The values of G' for both experiments 1 and 4 are different, experiment 4 being stiffer. With this we confirm that the bottom layer is contributing to the rheological parameters being measured. Again, there is an increase in the value of G' for experiment 5, this being higher than G' for experiment 3 (this makes sense since the total gel concentration for experiment 5 is higher than for experiment 3), followed by a drop of stiffness for experiment 6, after which there is again an increase in G' for experiments 7 and 8. We show that the bottom layer contributes to the measured G' by observing the stiffness values for experiments 1 and 4. However, the deviation from the increasing trend of G' observed for individual experiments, hints that although the bottom layer contributes to the measurements, the contribution is limited. Therefore, we examined the amount of gel from the bottom layer which is contributing to the measurements using the vane for 8 mm and 2 mm gels. Considering that for 8 mm gels (each layer consists of 2.67 mm of gel) the vane is used at a position of 0.5 mm, only 2.17 mm (~81 %) of layer 1 is contributing to the measurements. Conversely, for 2 mm gels (in which each layer represents 0.67 mm of gel) the vane is

positioned at 0.3 mm from the bottom, this resulting in only 0.37 mm (~55%) of layer 1 committing to the rheological measurements.

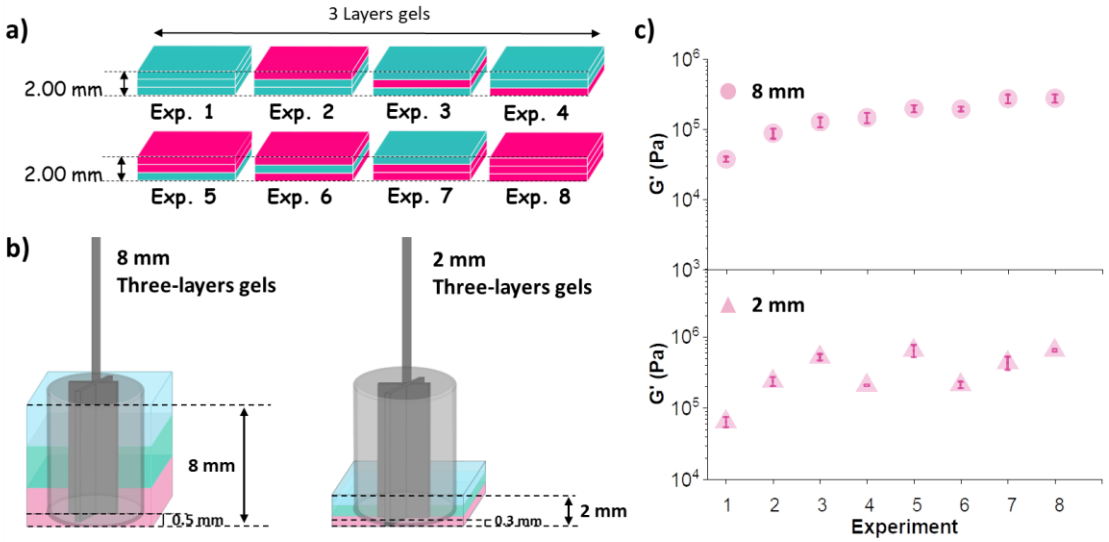

Figure 4.14 (a) Schematic showing experiments 1-8 where the height of the gel is 2 mm. (b) Cartoons showing the setup used for (left) 8 mm gels using the vane at 0.5 mm from the bottom layer and (right) 2 mm gels using the vane at 0.3 mm from the bottom layer. (c) Evolution of G' for experiments 1-8 of 8 mm (pink circles) and 2 mm (pink triangles) gels thickness.

4.2.6.II. Vane *versus* Parallel Plate for 2 mm Gel Systems

Furthermore, we investigated again the effect of using different measuring systems (Figure 4.15). For PP measurements, the same setup was used as for characterising 8 mm gels, where the geometry PP12.5 compresses the gel 0.05 N before starting the experiment. The vane measurements were taken at 0.3 mm from the bottom layer. We can also observe differences in the rheological trends with the vane and PP12.5 (Figure 4.15c-j). When the multi-layered gels display a gradient in concentration and are measured with a PP the values of G' are heavily dominated by the top layer owing to the configuration of the geometry during the measurement.

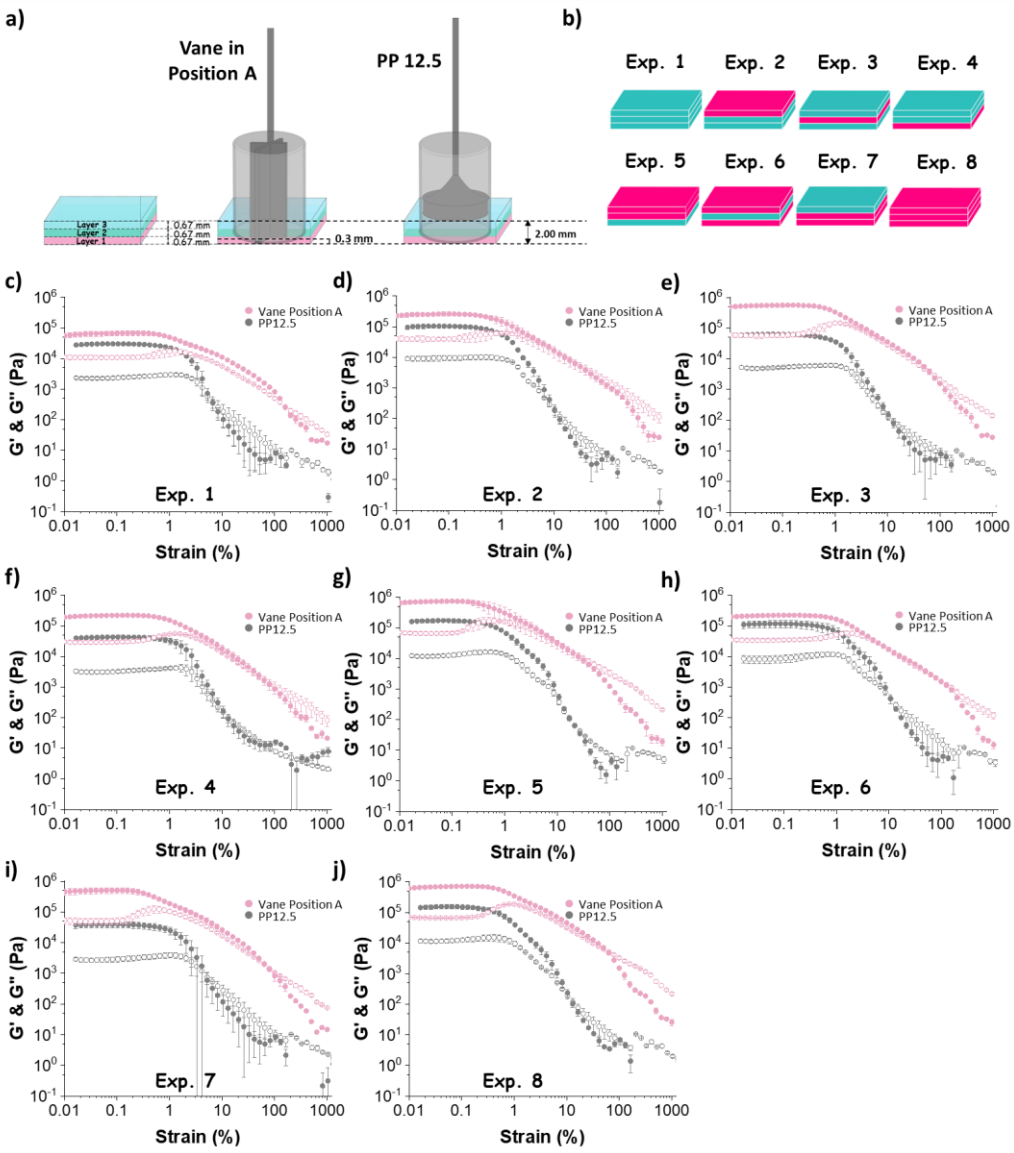

Figure 4.15 Rheological data for 2 mm three-layered gels comparing the measurements with vane and PP12.5 geometries. (a) Schematic showing the setup for the vane and PP12.5 measurements. (b) Cartoons representing experiments 1-8. Each experiment uses a stack of 3 gel layers, where the cyan and deep pink layers represent 5 mg mL^{-1} and 15 mg mL^{-1} of **4** respectively. (c)-(j) Strain sweeps for experiments 1-8. The pink data correspond to the measurements using the vane in position A and the grey data show the strain sweep measured using the PP12.5. The error bars represent the standard deviation for three measurements. Closed and opened symbols represent G' and G", respectively.

An important comparison in Figure 4.16a is between Exp 2 and Exp 7 for PP12.5. Exp 2 has one 15 mg mL^{-1} layer at the top and two layers of 5 mg mL^{-1} below whereas Exp 7 has one layer of 5 mg mL^{-1} on the top and two 15 mg mL^{-1} below. The G' value is higher in Exp 2 than Exp 7 even though the overall concentration in all three layers is actually higher in Exp 7. The vane does in fact record a higher G' in Exp 7 than it does in Exp 2 because it is feeling the contribution of all 3 layers in the measurement. This really highlights the sensitivity of the vane compared to the parallel plate for multi-layered systems, as we are not limited by measuring gap or contribution from the top layer. The thickness of samples that could be measured using a vane are only limited by the size of the vane itself and could be tailored for multi-layers ranging from less than 2 mm up to over 50 mm for example. Finally, comparing the rheological data for 8 mm and 2 mm gels using the PP12.5 (Figure 4.16b), we conclude that the trend of G' for experiments 1-8 is the same no matter the total height of the multi-layered gels, however, there are noticeable differences in the values of stiffness being measured for different gel thicknesses.

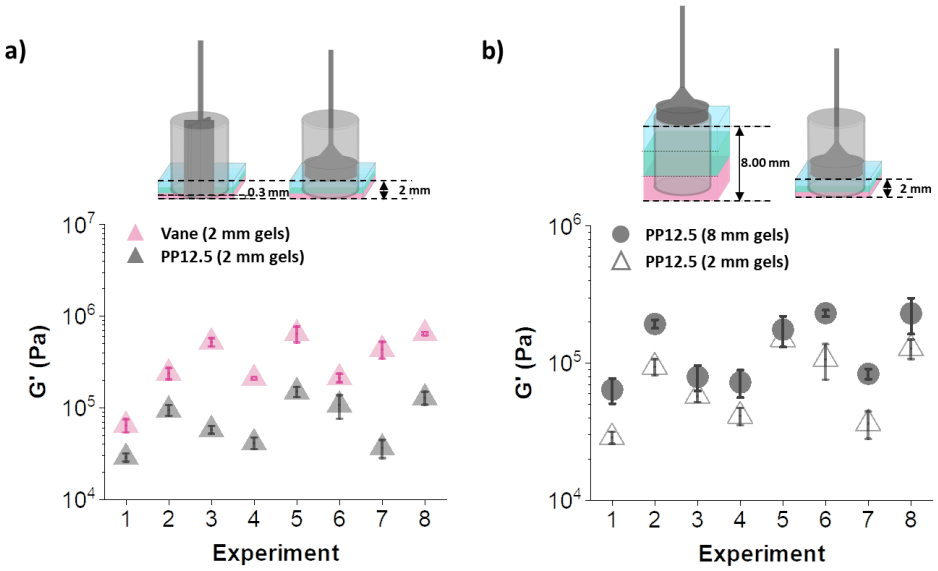

Figure 4.16 (a) (top) Cartoons showing the setup used for 2 mm gels using the vane at 0.3 mm from the bottom layer and the PP12.5 geometry and (bottom) evolution of G' for experiments 1-8 using the vane (pink triangles) and PP12.5 (grey triangles). (b) (top) Cartoons showing the setup used for 8 mm and 2 mm gels using the PP12.5 geometry and (bottom) evolution of G' for experiments 1-8 using the PP12.5 for 8 mm (grey circles) and 2 mm (grey triangles) gels. The error bars represent the standard deviation of three different measurements.

4.2.7. Rheological Characterisation of 3D Printed Gel Systems

Having proved the usability and effectiveness of the different rheological methods to characterise the mechanical properties of multi-layered hydrogels, we move on to characterise 3D printed systems using the vane and cup method we used above.

4.2.7.I. Optimisation of 3D Printing Parameters

We have previously shown the suitability of some LMWGs for 3D printing[26] and, therefore, gels with an underlying microstructure formed of spherulitic domains of fibres such as **4** can be printed effectively. Thus, lines of 50 mm length of **4** at a concentration of 5 mg mL^{-1} and 15 mg mL^{-1} were printed and the printing parameters were optimised using an extrusion-based 3D printer (Figure 4.17).

Firstly, gels of **4** at a concentration of 5 mg mL^{-1} were extruded using a range of different shear rates (Figure 4.17b-c) while varying the extrusion volume from 4 µL mm^{-1} (Figure 4.17b) to 6 µL mm^{-1} (Figure 4.17c).

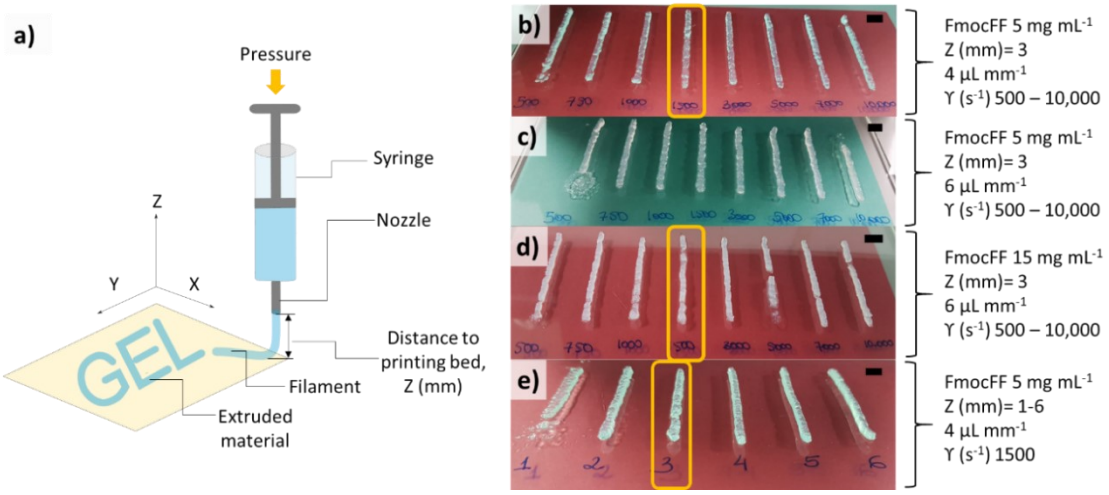

Figure 4.17 Photographs of optimised 3D printed lines of gels of **4** at a concentration of (b), (c) and (e) 5 mg mL^{-1} and (d) 15 mg mL^{-1}. In each photograph, the length of the printed lines is 50 mm. For (b), (c) and (d) the shear rate applied during extrusion is (from left to right) 500, 750, $1{\cdot}10^3$, $1.5{\cdot}10^3$, $3{\cdot}10^3$, $5{\cdot}10^3$, $7{\cdot}10^3$ and $1{\cdot}10^4$ s^{-1} and the distance between the nozzle and the printing bed is 3 mm. For (d) the shear rate applied is 1500 s^{-1} and each printed line was printed using a distance from the nozzle to the printing bed of (left to right) 1, 2, 3, 4, 5, and 6 mm. The total volume of printed gel is 200 µL for (a), (c) and (d), and 300 µL for (b). All gels were prepared in a 3 mL syringe in 3 mL volume before extrusion. The scale bars represent 1 cm in all cases.

Under visual inspection, lines printed at a shear rate of 1500 s^{-1} and a total volume of 200 µL (extrusion volume of 4 µL mm^{-1}) exhibited smoother and more continuous printed lines (Figure 4.17b). The distance between the nozzle and the printing bed, Z, was also evaluated, 3 mm being the optimal height (Figure 4.17e). In the same way, gels of **4** at a concentration of 15 mg mL^{-1} were also evaluated under a range of shear rates for gels using a total volume of 200 µL per line. The same printing parameters used for the gels at a concentration of 5 mg mL^{-1} resulted in homogeneous printed gels at a concentration of 15 mg mL^{-1} (Figure 4.17d).

We have previously shown the effectiveness of printing lines of gels of **4** in multiple layers.[26] Here we also demonstrate that it is possible to print more complex structures made up of multiple layers of gel (Figure 4.18a).

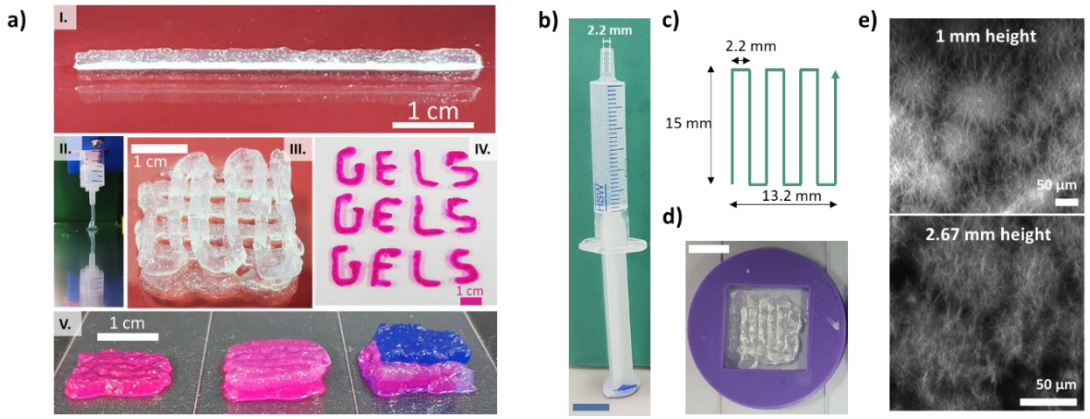

Figure 4.18 (a) Photographs of 3D printed gels of **4** at a concentration of 5 mg mL^{-1}; (a.I.) A 50 mm printed line. (a.II.) Deposition of a gel filament onto the printing bed; (a.III.) Scaffold of three printed layers; (a.IV.) Printed text. (a.V.) (left to right) 1-layer, 2-layer and 3-layer systems using a serpentine pattern and dyed with Rose Bengal (layer 1), no dye (layer 2) and Nile Blue A (layer 3). All scale bars represent 1 cm. (b) Photograph of a 3 mL syringe with concentric slip tip. Inside it, 3 mL of gel at a concentration of 5 mg mL^{-1} was made. (c) Schematic showing the pattern used to 3D print the gels at different layers for rheological characterisation. (d) Photograph of a single layer of **4** at a concentration of 5 mg mL^{-1} gel printed using the serpentine pattern. The scale bar represents 1 cm. (e) Confocal images of gels of **4** at a concentration of 5 mg mL^{-1} and (top) 1 mm in height and (bottom) 2.67 mm in height. Gels were prepared in a container with the same dimensions as the 3D printed container used throughout. The scale bars represent 50 µm in both cases.

4.2.7.II. Rheological Characterisation of Multi-layered Gel Systems Before and After 3D Printing

For such systems, many studies rely on the rheological characterisation of the gels before printing due to the difficulty of doing so for gels post-extrusion. Here we show the effect that extrusion-based 3D printing has on the properties of a hydrogel of **4**. As a preliminary test, a single layer of gel of **4** at a concentration of 5 mg mL^{-1} was extruded from a 3 mL syringe (Figure 4.18b) into a container (Figure 4.18d) in a serpentine pattern (Figure 4.18c) through the nozzle (inner diameter of 2.2 mm). The height of the printed gel was evaluated using the rheometer (more information is given in Section 4.4.3.I), and was found to be 1.86 ± 0.06 mm.

Even if we showed above that differences in the height of the gel do not affect the rheological parameters being measured (Figure 4.13e), and either does the microstructure of the gel being formed (see Figure 4.18e), we prepared a gel of 2 mm height for comparison with the printed gel using a nozzle of 2.2 mm of inner diameter. The rheological data show that the stiffness of the gel is affected by the printing process (Figure 4.19a). The storage modulus, G', for the gel before printing is $8.25 \times 10^4 \pm 7.84 \times 10^3$, whilst the G' for the printed gel is $5.08 \times 10^4 \pm 5.01 \times 10^3$. The differences in stiffness for the gel before and after printing are meaningful, showing that only 62% of the initial G' value is recovered and thus it cannot be assumed that gels are not affected by the printing process.

The microstructure is also affected by the printing process (Figure 4.19b). Before printing, the gel shows the presence of spherulitic domains of fibres. After extrusion, there is still presence of fibres although the microstructure domain has been disturbed, resulting in a microstructure with increased domain size. During extrusion, the spherulitic domains are sheared as they go through the nozzle of the syringe. As a result, the fibres are displaced, thus changing the size of spherulitic domains. It is important to highlight that gels which present a spherulitic microstructure are easy to extrude since we avoid the

effect of random orientations during flow, as it is the case of dense fibrous netwroks.[31] Further, the spherulitic domains underlying the gel microstructure are complex in nature, which could lead to some differences in the printed microstructures when trying to replicate the same printed gel system. However, we show here the reproducibility in terms of storage modulus for the hydrogels containing spherulitic domains of fibres after extrusion, which emphasizes that even heterogeneities in the microstructure leads to reproducible bulk properties of the printed hydrogel.

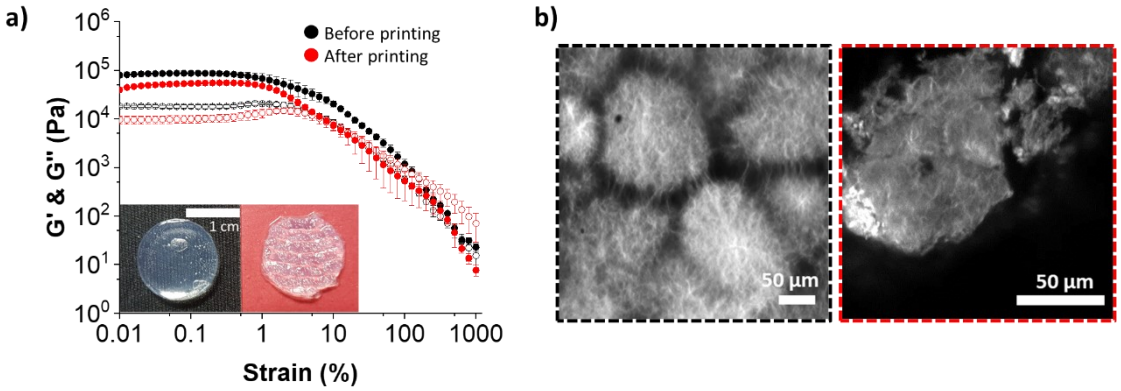

Figure 4.19 (a) Strain sweep for a gel of **4** at a concentration of 5 mg mL^{-1} and 2 mm height before printing (black data) and 1 layer after printing (red data). The rheological measurements were carried out using the vane at a measuring position of 0.5 mm. The error bars represent the standard deviation for three measurements. The insets show photographs of a gel of **4** at concentration of 5 mg mL^{-1} (left) before and (right) after printing. (b) Confocal images for a gel of **4** at a concentration of 5 mg mL^{-1} (left) before and (right) after printing. The scale bars represent 50 µm.

We also examined the recovery of the mechanical properties of gels made of **4** at the two concentrations by applying a high shear rate to disrupt the gels (Figure 4.20a). Recovery tests were performed applying a variable stress at a frequency of 10 rad s^{-1} (within the viscoelastic region). Initially, 0.5% of strain was applied while monitoring G' and G" over 180 seconds. A strain of 300% was then applied for 60 seconds then stopped and immediately a strain of 0.5% was again applied for an additional 180 seconds to monitor recovery. We repeated this cycle three more times for gels made of **4** at concentrations of 5 mg mL^{-1}

and 15 mg mL^{-1} (Figure 4.20a). The gels recover up to 47.5% and 29.5% of their original value of G' after the first high shear deformation for concentrations of 5 mg mL^{-1} and 15 mg mL^{-1} respectively. However, the gels start to breakdown significantly in the successive cycles for both concentrations of **4**. Therefore, the gel of **4** at a concentration of 5 mg mL^{-1} was allowed a longer recovery time (Figure 4.20b). After 12 hours of recovery, the gel recovers up to 76% of the original G' value.

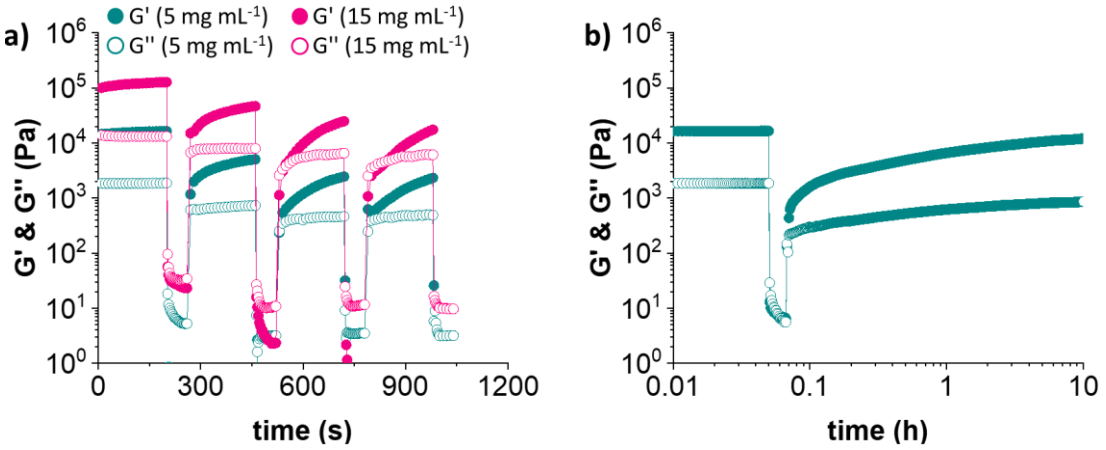

Figure 4.20 (a) Recovery test of gels of **4** at concentrations of 5 mg mL^{-1} (cyan data) and 15 mg mL^{-1} (pink data). Initially, 0.5% of strain was applied while monitoring G' and G" over 180 seconds. A strain of 300% was then applied for 60 seconds then stopped (~300 s) and immediately a strain of 0.5% was again applied for an additional 180 seconds to monitor recovery. This cycle of low-high strain was repeated three times. (b) Long recovery test for gel of **4** at 5 mg mL^{-1} also using 0.5% strain for 180 seconds, then a high strain of 300% during 60 seconds and then left to recover for 10 hours. Closed and opened symbols represent G' and G", respectively.

We then moved on to inspect more complex systems: two layers and three layers gels of **4** at a concentration of 5 mg mL^{-1} were investigated (Figure 4.21a). Again, the differences in stiffness for gels before and after printing are notable, the printed gels being less stiff compared with the gels before extrusion. Gels of 1, 2, and 3 layers recover up to 62%, 65% and 84% of their initial G' values respectively (Figure 4.21a). Additionally, we were able to evaluate the mechanical properties of the gels in experiments 1-8 after printing

(Figure 4.21b). Gels 1-8 before printing were prepared in situ in the 3D printed container as mentioned earlier in this Chapter. Each gel is made of three layers, each layer 2.67 mm high. The three-layered systems are thus made up of 8 mm of gel. To measure gels 1-8 after printing, each layer was extruded in a serpentine pattern into the 3D printed containers with the appropriate concentration of **4** (Figure 4.18c and d). The vane in position A was used to evaluate the rheological properties of the gels before and after printing.

Once again, we show the effect of the printing process on the mechanical properties of the printed three-layered gels. As for gels prepared in situ, there is also an increasing trend of G' for experiments 1-8 after they are extruded. There is an initial sharp linear increase in stiffness for experiments 1-4, then the G' starts to level off for experiments 4-7 with a gradual increase in stiffness and then again a sharp increase for experiment 8 (Figure 4.21). This shows that we are capable of characterising the same experiments 1-8 before and after 3D printing with a high degree of control and that we are able to identify the differences in terms of mechanical properties.

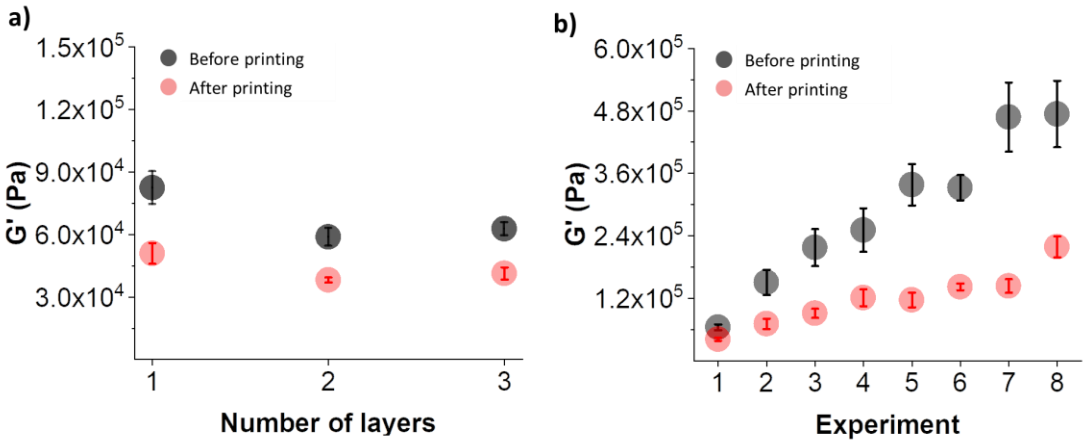

Figure 4.21 (a) G' against the number of layers of gels made of **4** at a concentration of 5 mg mL-1 before (black data) and after (red data) printing. (b) Evolution of G' for experiments 1-8 (black data) before and (red data) after printing. For all printed systems a shear rate of 1500 s^{-1} and extrusion volume of 4 µL mm^{-1} were used.

4.3. Conclusions

We have developed a rheological method to characterise the mechanical properties of multi-layered hydrogels prepared in situ and post printing with a high degree of control. We prepared three-layered hydrogels with tuneable mechanical properties in each layer by varying the concentration of the gelator **4** layer by layer. From rheological results, we show that not only a high degree of control of the mechanical properties of the individual layers within the multi-layered constructs can be achieved, but also that the contribution of each layer to the resulting combined properties being measured can be assessed. We also emphasise the differences of using different measuring systems for rheological measurements, as it highly impacts on the resulting properties being measured, again highlighting the need to measure gel properties as close to the intended use as possible for accurate representation of the investigated systems.

The mechanical properties of the gels before and after 3D printing have also been examined. We show that the properties of printed gels made of **4** are highly influenced by the extrusion process. This is important for biological applications, where an appropriate environment for cells growth is crucial to ensure appropriate cellular functions. We present this study as a guide for assessing the mechanical properties of 3D printed gels and we hope it will aid in the characterisation of new biomaterials made with cutting-edge technologies such as 3D printing.

4.4. Experimental

4.4.1. Materials

4 was prepared as described previously by Dave Adams (University of Glasgow).[58] Deionised water was used throughout. All other chemicals were purchased from Merck Life Sciences and used as received.

4.4.2. Experimental details

4.4.2.I. Construction of multi-layered hydrogels

Preparation of a single layer hydrogel.

To prepare a gel using the solvent trigger approach, **4** is firstly dissolved in a suitable water-miscible organic solvent and then deionised water is added in one aliquot, which will lower the solubility of the molecule, thus forcing the self-assembly into 1D structures. Here, we used DMSO as the solvent, such as the final ratio of DMSO:H_2O was 3:7. Typically, in order to prepare 1 mL gel of **4** at a concentration of 5 mg mL^{-1}, 5 mg of **4** are dissolved in 300 μL of DMSO and pipetted into the container in which the gel is going to be formed, followed by the addition of 700 μL of H_2O in one aliquot using a pipette. In the same way, to form 1 mL gel at a concentration of 15 mg mL^{-1} of **4**, 15 mg of the gelator are dissolved in 300 μL of DMSO followed by the addition of 700 μL of H_2O in one aliquot using a pipette. The sample is then left overnight at room temperature without being disturbed, to allow gelation to occur. The sample is sealed with parafilm to avoid evaporation.

Preparation of multi-layered hydrogels.

Multi-layered hydrogels were prepared in situ. Multiple independent self-supporting layers of gels were formed one on top of each other using a solvent trigger. Specifically, we prepared three-layers hydrogels in situ. Three-layers hydrogels of multiple thicknesses were prepared as follows. Firstly, a known amount of **4** dissolved in DMSO is pipetted into the container (Figure 4.22b), followed by the addition of deionised water in one aliquot. Once the water is added, there is a phase separation where nucleation centres are formed, followed by the growth of fibres, that expand and form a spherulitic multi-domain fibre network (Figure 4.22c). Absorbance measurements at 600 nm were conducted for both concentrations of 5 mg mL^{-1} and 15 mg mL^{-1} of **4** to shed light on the assembly kinetics (Figure 4.22a). For **4** at a concentration of 5 mg mL^{-1}, there is an initial increase in absorbance as soon as the water is added, corresponding to the nucleation phase, followed by a gradual decrease in

turbidity (Figure 4.22a, cyan data). This change in turbidity is related to the formation of fibres underpinning the gel phase and a plateau is reached after 7 minutes. For **4** at a concentration of 15 mg mL^{-1}, the same trend is observed where the system is initially highly scattering and then the turbidity decreases gradually, corresponding to the formation of fibres, until a plateau is reached after 10 minutes (Figure 4.22a, pink data). The difference between the two concentrations is the final turbidity (higher turbidity for the more concentrated system) as well as the time needed for the assembly process to be completed, being 7 minutes and 10 minutes for concentrations of 5 mg mL^{-1} and 15 mg mL^{-1} of **4** respectively. Out of an abundance of caution, we waited 30 minutes before preparing the next layer. After this time, the same procedure was repeated, i.e., a known amount of **4** dissolved in DMSO was pipetted carefully on top of the first layer (Figure 4.22d). This step is quite arduous since we need to make sure that the DMSO solution containing the gelator is well distributed along the surface of the previous layer but also avoid interfering with that layer. To do this, we distribute drops of the solution containing **4** in DMSO on to different points of the previous layer being careful to not put a lot of pressure when pipetting, to avoid breaking the base layer. Once there is solution covering all the surface of the previous gel layer, we pipette the water in one aliquot but again applying mild pressure (Figure 4.22e). Prior to the addition of water, if the solution containing **4** in DMSO is not well distributed along the surface, it is probable that the gel will not fill the dimensions of the container in which it is being made. Since the gel takes a few minutes to form, immediately after the water is added we can help the gel cover the whole are by using a tiny pipette tip to drag the "sol-to-gel" system to the walls of the container and wait 30 minutes before starting to prepare the next layer. After this time, we prepared the third layer following the same methodology. **4** in solution was added to the top of the second layer carefully (Figure 4.22f), followed by the addition of water (Figure 4.22g). As a result, three self-supporting independent layers of gels are formed (Figure 4.22h). In all cases, we always made sure the DMSO solution containing **4** was uniformly distributed along all gel surface, thus ensuring homogeneous gelation when water was added. Parafilm was used to prevent evaporation or drying.

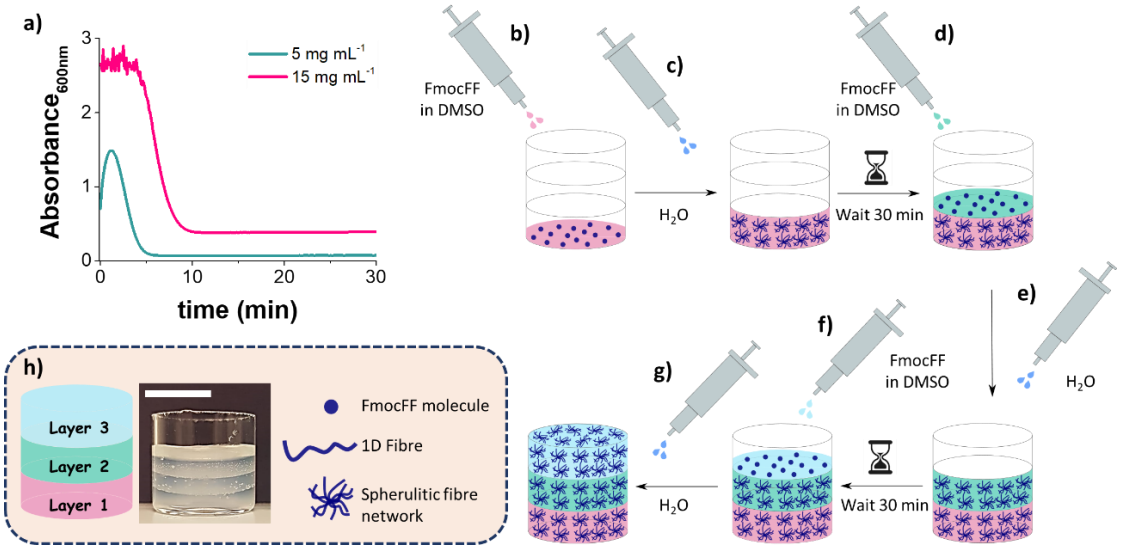

Figure 4.22 (a) Changes in absorbance at 600 nm with time after adding water to a solution of either **4** at 5 mg mL^{-1} (cyan) or 15 mg mL^{-1} (pink) in DMSO. (b-g) Schematic representation of the process by which a three-layers hydrogel is formed in situ using a layer-by-layer self-assembly method. To form the first layer (b) **4** dissolved in DMSO is pipetted into the container and (c) water is added to trigger gelation. Before starting to prepare the next layer, we wait 30 minutes to ensure the gel is completely formed. The same methodology was used to form the second (d)-(e) and third (f)-(g) layers. (h) From left to right, cartoon showing the resulting three-layered gel, a photograph of a three-layered hydrogel made of **4** at 5 mg mL^{-1} using 30% DMSO, where each layer is 2.67 mm thick (the scale bar represents 1 cm) and cartoons describing the differences between a molecule of **4**, fibre and a spherulitic 3D network.

4.4.3. Instruments and Procedures

4.4.3.I. Oscillatory Shear Rheology

Rheological measurements were performed using a MCR 301 rheometer (Anton Paar) and Rheoplus/32 v3.40 software. Different geometries were used, including a four-bladed vane in cup geometry (Figure 4.23a) and a parallel plate, PP 12.5 (Figure 4.23b). As we intend to compare the rheological properties of multi-layered systems prepared in situ with those delivered using

an extrusion-based 3D printing technique, we designed and 3D printed a container suitable for both techniques (Figure 4.23c).

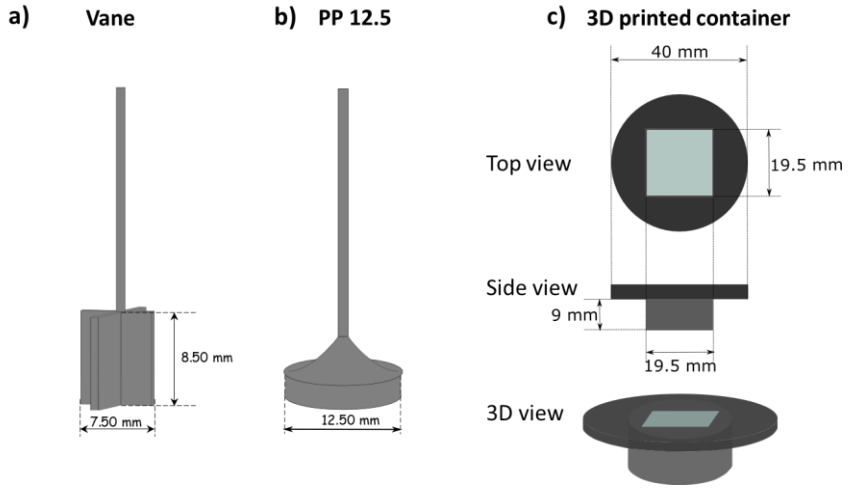

Figure 4.23 Diagrams of the different geometries used for rheological measurements and their dimensions; (a) cup and vane geometry, (b) parallel plate PP12.5 geometry and (c) 3D printed container.

- **Preliminary tests**

Before collecting the data for the different multi-layered systems, we carried out some trial tests using different setups for rheological measurements. In our group, we normally prepare 2 mL gels in 7 mL Sterilin vials (Figure 4.24a) for rheological measurements. Since we intend to compare the mechanical properties of gels before and after 3D printing, Sterilin vials were not suitable to extrude the gels inside. As such, we optimised a 3D printed container in which we could directly extrude gels using 3D printing and also prepare the same gel systems in situ. To compare the effect of using different containers to make gels for rheological measurements, we prepared a gel of **4** at a concentration of 5 mg mL^{-1} and 30% DMSO of 8 mm in height in two different containers. This is, one in the Sterilin vial and a second one in the 3D printed container. Furthermore, we also quantified the effect of using different gel gaps between the vane blades and the wall container in which the gel is made on the rheological properties. For this purpose, we prepared a

third gel in the 3D printed container and we used the metal hollow cylinder (Figure 4.24b) with the same inner diameter as the Sterilin vial to "chop" the gel prepared inside the 3D printed container. This means that the gap between the vane blades and the wall container will be the same using a Sterilin vial or the 3D printed container with the hollow cylinder (Figure 4.24c).

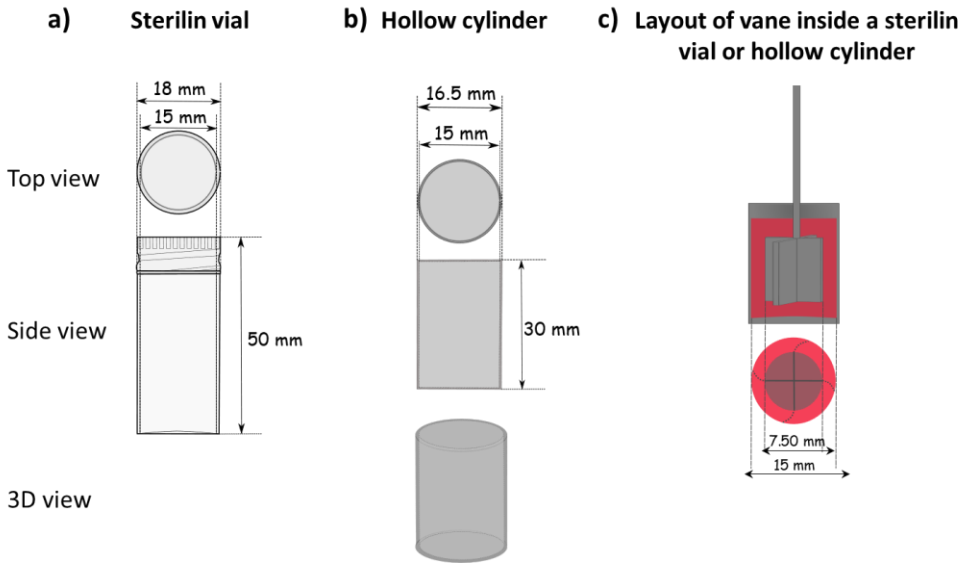

Figure 4.24 Diagrams of (a) Sterilin vial, (b) hollow metal cylinder and (c) setup using the vane inside a Sterilin vial or hollow metal cyinder.

A series of experiment were then carried out (experiments I-V, Figure 4.25). 2 mL gels inside a Sterilin vial corresponds to a height of 8 mm. As such, 8 mm gels were prepared in the printed containers for comparison. We studied the effect of measuring the mechanical properties using different setups (Figure 4.25):

I. A Sterilin vial containing a gel of 8 mm in height (or 2 mL).
II. The 3D printed container with 8 mm gel and using the vane for measurements.
III. The 3D printed container with 8 mm gel chopped with the hollow cylinder and using the vane for measurements.
IV. The 3D printed container with 8 mm gel and using the PP12.5 for measurements.

V. The 3D printed container with 8 mm gel chopped with the hollow cylinder and using the PP12.5 for measurements.

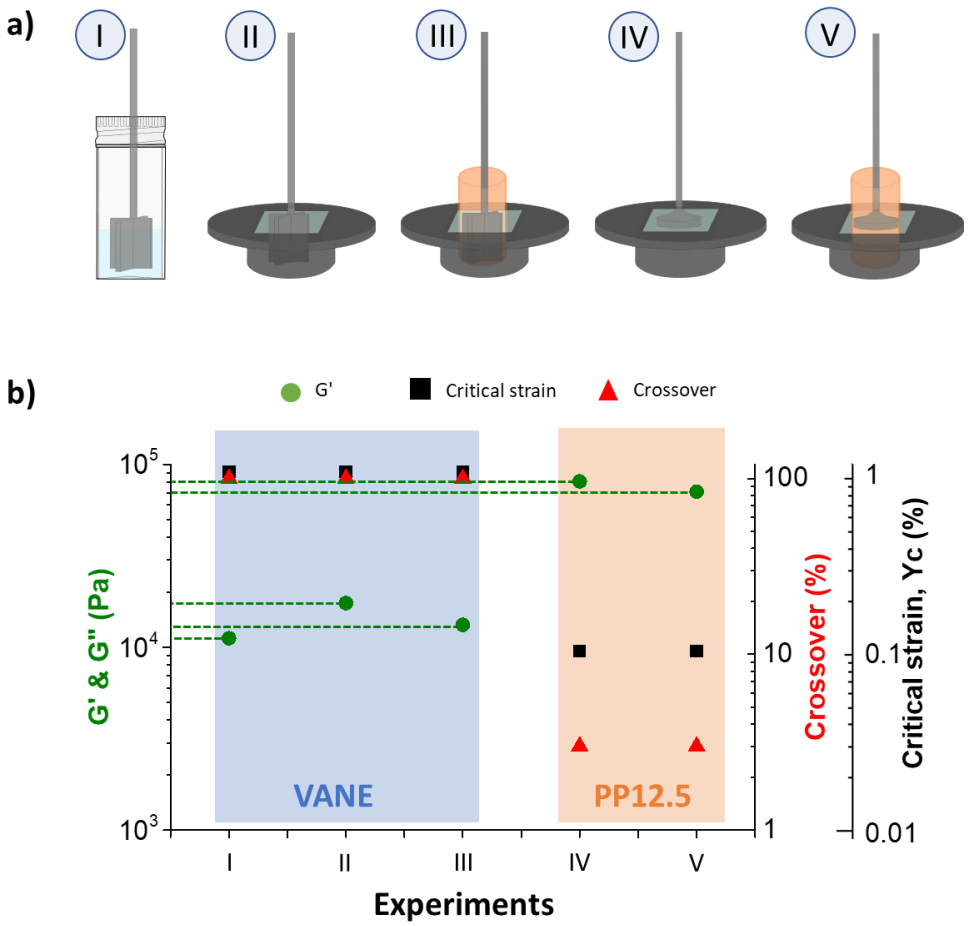

Figure 4.25 (a) Cartoons showing the different setups: (I) Sterilin vial and vane geometry; (II) 3D printed container and vane geometry; (III) 3D printed container with the hollow cylinder and vane geometry; (IV) 3D printed container and PP12.5 geometry and (V) 3D printed container with the hollow cylinder and PP12.5 geometry. (b) Graph showing the rheological data for experiments I-V. Green circles, black squares and red triangles represent G', the critical strain and the crossover respectively.

From Figure 4.25b we observe different G' values depending on the setup used. The stiffness highly depends on the geometry used for measurements. Specifically, the G' values measured using the geometry PP12.5 are much higher than those using the vane geometry. Besides, for the same geometry, different stiffnesses arise depending on the container in which the gel has been made.

Comparing experiments II and III, for example, we can observe noticeable differences on the measured G' values. The difference between these two experiments is the distance between the vane blades and the wall container. Similarly, for experiments IV and V, we also observe differences in the measured stiffness depending on the distance between the PP12.5 geometry edge and the wall container. On top of that, for experiments I and III, where the distance between the vane blades and the wall container is the same, the values of G' are very similar. These results suggest that it is important to control the distance between the measuring system edge and the wall of the container during rheological measurements. Critical strain and crossover are likely not to be affected by the container dimensions in which the gels are made.

- **Strain sweeps.**

The strain sweeps were carried out from 0.01 % to 1000 % strain at a frequency of 10 rad s^{-1}. The linear viscoelastic region (LVER) was determined as the region where G' and G" remain constant up to a strain amplitude at which the gel starts to deviate from linearity. The values of G' used throughout were taken as the average of the G' values in the LVER. To define the critical strain (γ_c), we draw a line tangent to LVER and another line tangent to the non-linear region. The intersection of both lines will assert the value of γ_c (see Figure 4.26).

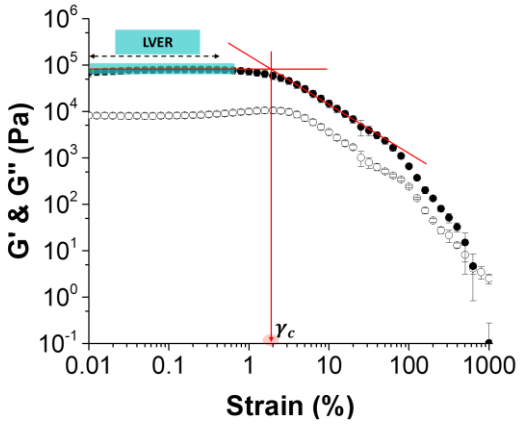

Figure 4.26 Example of strain sweep showing the LVER (highlighted in blue) and the γ_c (marked in red).

- **Vane geometry.**

The vane geometry used for rheological measurements is the ST10-4V-8.8/97.5-SN18190 model (Anton Paar). The vane geometry has four blades and a flat surface that sticks out into the sample and that pushes the material as the blades move while the torque is measured as a function of the rotation angle and rate (Figure 4.23a).[49] The vane geometry is advantageous for measuring heterogeneous samples that may slip using the parallel plate.[48]

For the present paper, multi-layered gels were prepared in 3D printed containers in situ and using an extrusion-based 3D printing technique. Three-layer gels of various thicknesses were prepared, building up 8 mm and 2 mm total height gels. Furthermore, the three-layered gel was made of varying mechanical properties that could be modulated by simply changing the concentration of **4**.

8 mm multi-layered hydrogels

For 8 mm three-layered gels, each layer is 2.67 mm thick (Figure 4.27a). For these gel systems we developed different setups for the vane measurements; we varied the position of the vane in such a way that the distance between the bottom surface of each layer and the bottom part of the vane was kept constant. As a result, three different positions were used for measurements using the vane geometry; position A corresponds to the vane located at 0.5 mm above the bottom surface of layer 1, position B corresponds to the vane at 0.5 mm above the bottom surface of layer 2 and position C corresponds to the vane positioned at 0.5 mm above the bottom surface of layer 3 (Figure 4.27b).

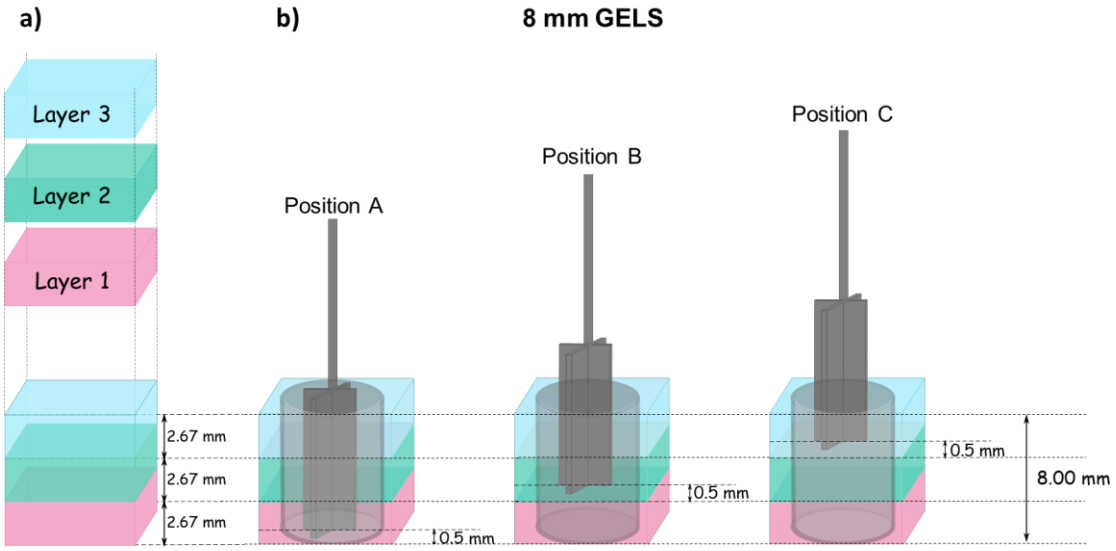

Figure 4.27 Schematic representation of 8 mm three-layered gels made in situ. (a) Illustration of a three-layered system in which each layer is made of 2.67 mm of gel, building up an 8 mm gel stack. (b) Schematic showing three different positions for the vane measurements; positions A, B and C correspond to the vane located at 0.5 mm above the bottom surface of layers 1, 2, and 3, respectively.

2 mm multi-layered hydrogels

For 2 mm three-layered gels, each layer is 0.67 mm thick (Figure 4.28). In this case, the vane geometry was only used at one position; this is at 0.3 mm from the bottom surface of layer 1. Due to the thinness of each layer (0.67 mm), a gap of 0.3 mm was used in order to guarantee that the vane was embedded and in contact with at least 50% of layer 1, which would not be possible if a gap of 0.5 mm were used.

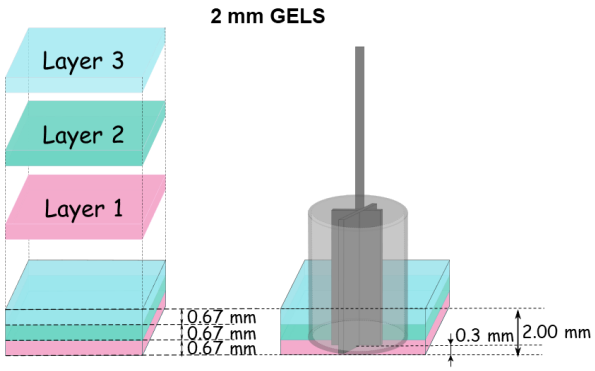

Figure 4.28 Schematic representation of 2 mm three-layered gels made in situ in which each layer is made of 0.67 mm of gel, building up a 2 mm gel stack. Also shown is the position of the vane 0.3 mm above the bottom surface of layer 1 for measurements.

- **Optimisation of vane measurements.**

In order to get reliable data, it is important to control the position of the vane for each measurement, since every sample was prepared in a different 3D printed container. As such, we first evaluated what the 0 mm position would be for the vane in each container. In order to do so, we loaded each individual 3D printed container in the rheometer plate (Figure 4.29-I, II, III) equipped with the vane and lowered the vane until a normal force of 0.5 – 0.6 N was detected by the vane (Figure 4.29-IV). That position was identified as the 0 mm position, which corresponds to the vane touching the bottom surface of the container. We did this for every single container, since despite having been printed with the same design, the PLA plastic used to print them is firstly melted and then cooled down to room temperature during printing which causes slight differences in the dimensions between different 3D printed containers. Acetone vapour was also used to seal pores and smooth the container surface before first use. Once we optimised the setup for each individual 3D printed container, they were used independently for different samples and vane positions.

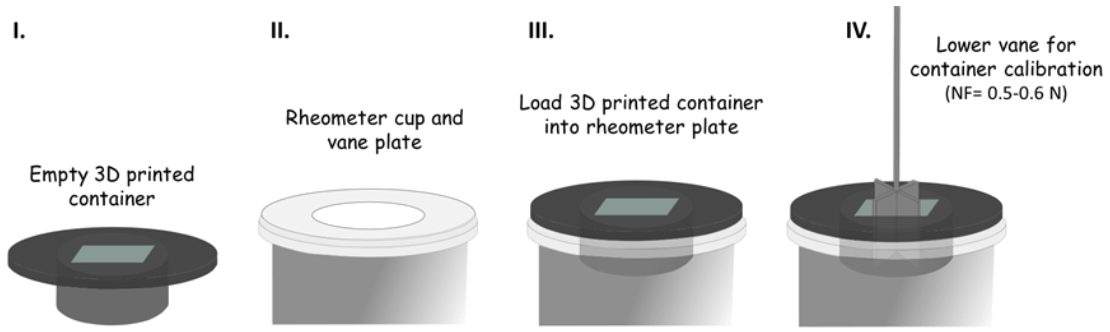

Figure 4.29 Schematic representing the process for calibrating every container that will be used to hold the multi-layered gels. (I), (II) and (III) loading of the 3D printed container into the rheometer plate and (IV) lowering of the vane until a normal force of 0.5-0.6 N is detected. This is set as the 0 mm position.

- **PP12.5 geometry.**

The PP12.5 geometry used for rheological measurements is the PP12.5-SN50710 model (Anton Paar), Figure 4.23b. When a PP geometry is used, the measuring gap can be controlled, which can be advantageous, as gels with different thicknesses can be measured.

Multi-layered gels were prepared in the 3D printed containers in situ and using the extrusion-based 3D printing technique. The same experiments measured using the vane geometry were also analysed with PP12.5. Three-layer gels of various thicknesses were prepared, building up 8 mm and 2 mm gel stacks.

For both 8 mm and 2 mm three-layered gels, the PP12.5 geometry is positioned on the top surface of the gel using the controlled setup where the PP stops when it detects a normal force of 0.05 N (Figure 4.30a-b).

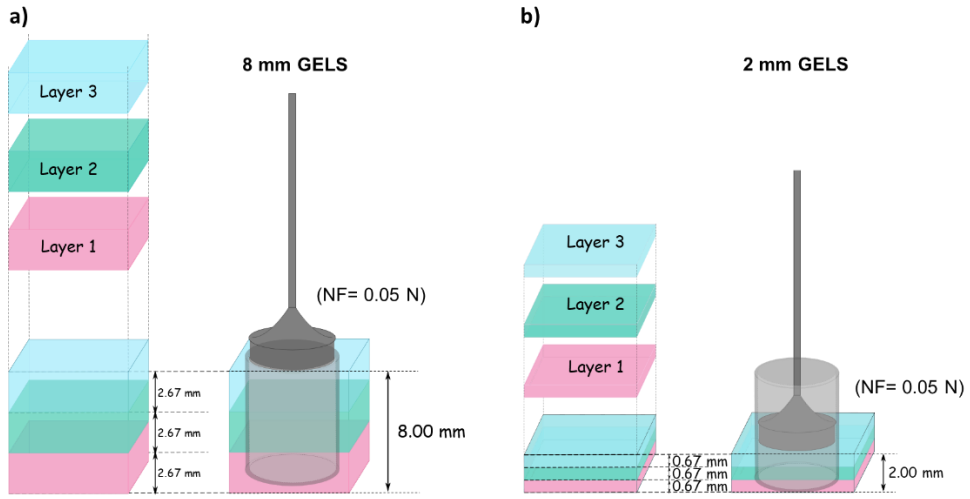

Figure 4.30 Schematic representation of (a) a three-layered system in which each layer is made of 2.67 mm of gel, building up an 8 mm stack and (b) a three-layered system in which each layer is made of 0.67 mm of gel, building up a 2 mm stack. In both cases a PP12.5 geometry is used for measurements. The PP12.5 is lowered using a controlled system that stops when the geometry detects a normal force of 0.05 N on the surface of the gel.

Before starting the measurements in a parallel system, setting the zero gap is necessary for the PP geometry. The zero gap is used as a reference for all gap settings. Likewise, setting the zero gap properly is fundamental since the rheometer will calculate the rheological parameter according to the zero-gap position. As an example, the shear strain γ is defined as $\gamma = \varphi/h$, where φ corresponds to the deflection (in m) and h correlates the height/thickness/gap (in m) of the gel being measured. By definition, the strain depends upon the height of the gel being measured and hence it is important to appropriately set the zero gap. Normally, the zero gap is set on the base plate and then the sample is placed on top of it. However, in the present project the gels were made inside the 3D printed containers. This would not allow to set the zero gap on the empty container before measurements since the gels were already prepared inside. Instead, we set zero gap on the base plate and we stuck the 3D printed container with the gel on top of it for measurements. Subsequently, the resulting strain values are based on the "measured gap" rather than the "real gap" (Figure 4.31a). As a consequence, we needed to apply a correction

factor to rectify the values of strain. As an example, for a measured gap of 8 mm, a 100% strain would equal to a deflection within the material of 8 mm. If instead of 8 mm, the real gap/height of the gel is 1 mm, the measured deflection of 8 mm would correspond to a strain of 800%. In order to amend this, we applied a correction factor to the strain values measured. We firstly converted the deflection values from degrees to length units taking into account the perimeter of the circular PP12.5 geometry. Next, with the deflection values converted to distance, we worked out the real strain by dividing it by the height of gel (Figure 4.31b). The graph in Figure 4.31c, shows the differences in the strain profile before (black circles) and after (red circles) correcting the values of strain.

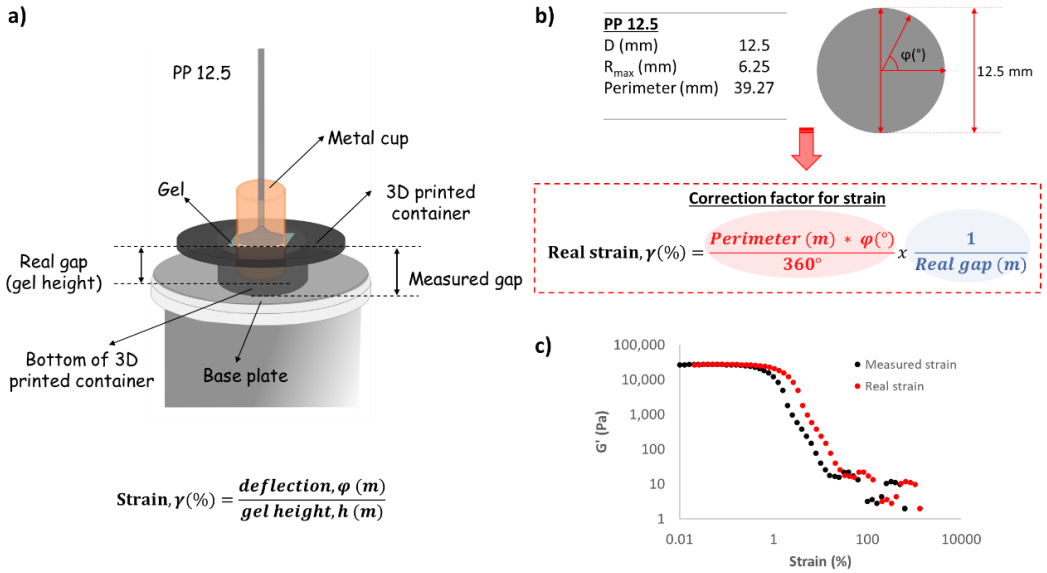

Figure 4.31 (a) Schematic representation of the setup used for rheological measurements using PP12.5 geometry on a gel made inside a 3D printed holder. The PP12.5 is on the top surface of the gel; the difference between this eight and the bottom of the container is the real gap. (b) Correction factor applied to the measured strain values for a PP12.5 geometry. This factor takes into account the change in units of deflection from degrees to meters (highlighted in red) and also the height of the gel (highlighted in blue). (c) Graph representing one example of strain sweep comparing the rheological profile being measured by the rheometer (black data) and the modified profile taking into account the correction factor for strain values (red data).

- **Real gap/height of the gel made inside 3D printed container.**

The height of the gels was determined by subtraction of the measured gap with the gel made inside the container and the gap for the empty container (measuring the thickness of the container bottom). Both measurements were made using the controlled setup (0.05 N) for the PP12.5 geometry.

- **Methodology for preparing gels for rheological measurements using vane and PP12.5 measuring systems.**

The procedure used to prepare the multi-layered gels for rheological measurements is as follows. Firstly, we prepare the gel inside the 3D printed container (Figure 4.32a,e). Then place the cover lid with a hollow on top of the container (Figure 4.32b,f) followed by the metal hollow cylinder (Figure 4.32c,g) to chop the gel into a repeatable shape and size and some Blu Tack® to make sure it will not move during measurements. Finally place the assembly into the rheometer and set the appropriate measuring geometry (Figure 4.32d,h).

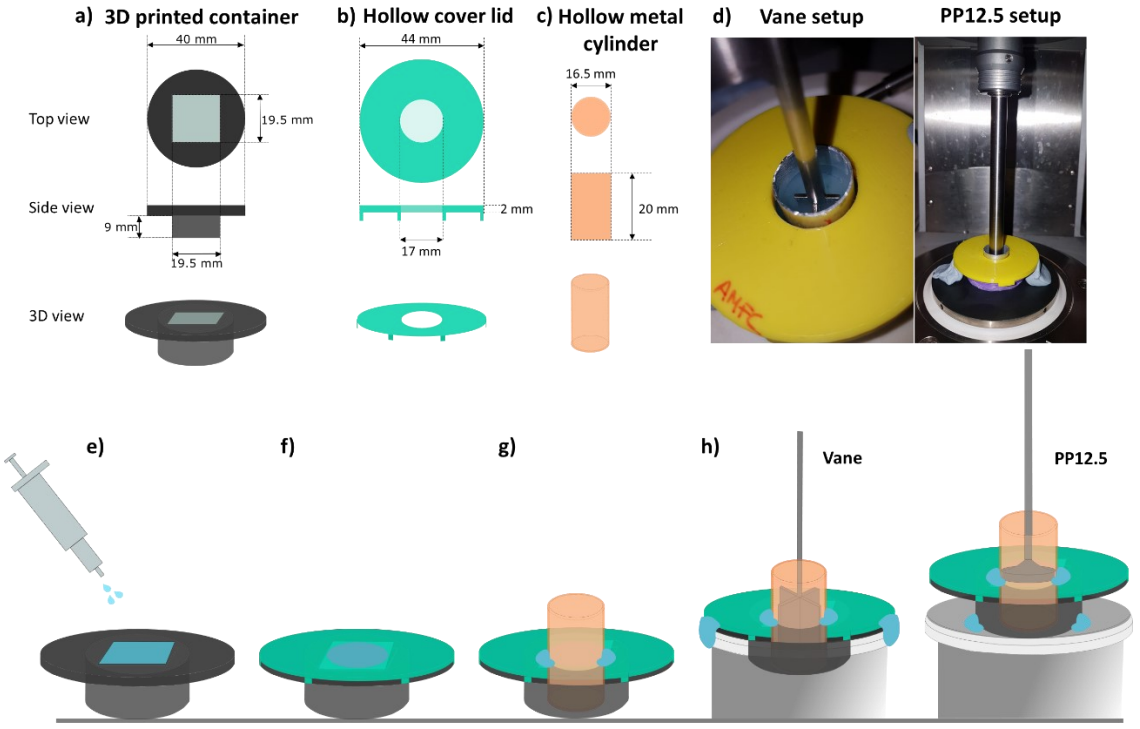

Figure 4.32 Dimensions of (a) the 3D printed container, (b) the cover lid and (c) the metal hollow cylinder. (d) Photographs of (left) the setup for vane measurements and (right) PP12.5. (e)-(h) Schematic showing the procedure followed to load the samples for rheological measurements; (e) Gel is prepared inside the container; (f) then a cover lid with a hole is positioned on top of the container and (g) the metal hollow cylinder is inserted in the hole and fixed in place with some Blu Tack®; (h) the entire assembly is then placed on the corresponding system depending on which geometry will be used and some Blu Tack® is used to ensure the container will not move during measurements.

4.4.3.II. Confocal microscopy.

Confocal images were taken using a Zeiss LSM 710 confocal microscope with a LD EC Epiplan NEUFLUAR 50X (0,55 DIC) objective. Samples before printing were prepared inside the 3 mL syringe with the tip cut. Once the gel was made, the plunger was used to expel the gel and a layer was cut off using a scalpel. For the gels after printing, they were pre-made as described for the samples before printing, and then they were extruded using the optimised parameters onto a glass slide. Fluorescence from Nile Blue was excited using a 634 nm He-Ne laser

and emission was detected between 650 and 710 nm. All gels triggered using a solvent switch were stained with a 0.1 wt % Nile Blue A solution in water. The Nile Blue was added to the DMSO-gelator solution to a final Nile Blue concentration of 2 μL mL^{-1} of gel.

4.4.3.III. UV-Vis absorption spectroscopy.

Absorbance spectra for gels made of **4** were collected over time (30 min) at 600 nm on an Agilent Cary 60 UV–Vis spectrophotometer (Agilent Technology, California, United States) using Cary WinUV, kinetic Application v5.0.0.999 software. All samples were prepared in a 1 mm path length quartz cuvette. Firstly, water was added into the cuvette and then a DMSO solution containing the gelator was added, such that the final ratio of DMSO:water was 3:7. After DMSO was added, the mixture was mixed quickly with the help a needle. The total volume of gel examined was 300 μL for both concentrations of 5 mg mL^{-1} and 15 mg mL^{-1} of **4** at 25 °C.

4.4.3.IV. 3D Printing.

The extrusion-based 3D printer used is a RepRap Ormerod 2 version 528.4 with some modifications. We have discussed it in detail in our previous publication.[26]

For the experiments, gels were prepared in a 3 mL volume in a 3 mL syringe by firstly adding **4** dissolved in DMSO and then the water to trigger gelation. Before printing, some parameters need to be optimised in order to achieve high-quality 3D printed lines, among which we highlight the volume of the gel extruded, the speed of extrusion, the printer movement speed, and the printing height. For the different printing scenarios, each parameter was optimised to a rate of extrusion of 4 μL mm^{-1} and a shear rate of 1500 s^{-1}. The shear rate refers to the rate at which the gel is extruded through the nozzle of the syringe and was calculated for a Newtonian fluid following the equation: $\dot{\Upsilon} = \frac{4\,V}{\pi\,t\,r^3}$, in which V is the volume of gel extruded, r is the inner radius of the nozzle and t is the time of extrusion. As an example, to print a 50 mm gel line at a shear rate of

1500 s^{-1} and rate of extrusion of 4 µL mm^{-1}, 200 µL of gel were extruded in 0.13 seconds. The diameter of the nozzle used for extrusion was 2.2 mm. We highlight that we considered the Newtonian fluid shear rate equation to express different printing shear rates conditions, even though we know it is not fully representative. However, for the different experiments carried out in this Chapter we just wanted to optimise a "shear rate" value at which the printed gel was uniform (even if it is does not represent the true value). Before printing, the gels were prepared in a 3 mL volume in a 3 mL syringe following the same procedure as described in Section 1: Preparation of a single layer hydrogel. Then we used the 3D printer to extrude our gels using the optimised parameters and they were left to settle for 5 minutes before being transferred into the rheometer for measurements.

4.5. References

1. N. M. Sangeetha and U. Maitra, *Chem. Soc. Rev.*, 2005, **34**, 821-836.

2. R. G. Weiss, *J. Am. Chem. Soc.*, 2014, **136**, 7519-7530.

3. P. Terech and R. G. Weiss, *Chem.l Rev.*, 1997, **97**, 3133-3160.

4. X. Du, J. Zhou, J. Shi and B. Xu, *Chem.l Rev.*, 2015, **115**, 13165-13307.

5. M. de Loos, B. L. Feringa and J. H. van Esch, *Eur. J. Org. Chem.*, 2005, **2005**, 3615-3631.

6. M. P. Nikolova and M. S. Chavali, *Bioact. Mater.*, 2019, **4**, 271-292.

7. H. K. Lau and K. L. Kiick, *Biomacromolecules*, 2015, **16**, 28-42.

8. E. R. Draper, E. G. B. Eden, T. O. McDonald and D. J. Adams, *Nat. Chem.*, 2015, **7**, 848-852.

9. Y. Huang, Z. Qiu, Y. Xu, J. Shi, H. Lin and Y. Zhang, *Organic & Biomol. Chem.*, 2011, **9**, 2149-2155.

10. C. d. l. H. Alarcón, S. Pennadam and C. Alexander, *Chem. Soc. Rev.*, 2005, **34**, 276-285.

11. H. Geckil, F. Xu, X. Zhang, S. Moon and U. Demirci, *Nanomedicine (Lond)*, 2010, **5**, 469-484.

12. S. Gupta, M. Singh, A. R. M, P. S. Yavvari, A. Srivastava and A. Bajaj, *RSC Advances*, 2016, **6**, 19751-19757.

13. S. Uman, A. Dhand and J. A. Burdick, *J. Appl. Polym. Sci.*, 2020, **137**, 48668.

14. D. J. Adams, M. F. Butler, W. J. Frith, M. Kirkland, L. Mullen and P. Sanderson, *Soft Matter*, 2009, **5**, 1856-1862.

15. G. Liu, Z. Ding, Q. Yuan, H. Xie and Z. Gu, *Front. Chem.*, 2018, **6**.

16. F. Yanagawa, S. Sugiura and T. Kanamori, *Regen. Ther.*, 2016, **3**, 45-57.

17. P. Wang, Y. li and M. Jiang, *Colloids Surf. B.*, 2018, **171**, 85-93.

18. M. P. Cuchiara, A. C. B. Allen, T. M. Chen, J. S. Miller and J. L. West, *Biomaterials*, 2010, **31**, 5491-5497.

19. T. Xu, W. Zhao, J.-M. Zhu, M. Z. Albanna, J. J. Yoo and A. Atala, *Biomaterials*, 2013, **34**, 130-139.

20. Y. He, F. Yang, H. Zhao, Q. Gao, B. Xia and J. Fu, *Sci. Rep.*, 2016, **6**, 29977.

21. L. Ning and X. Chen, *Biotechnol. J.*, 2017, **12**, 1600671.

22. S. Kyle, Z. M. Jessop, A. Al-Sabah and I. S. Whitaker, *Adv. Healthc. Mater.*, 2017, **6**, 1700264.

23. D. J. Richards, Y. Tan, J. Jia, H. Yao and Y. Mei, *Isr. J. Chem.*, 2013, **53**, 805-814.

24. Y. Yan, X. Wang, Y. Pan, H. Liu, J. Cheng, Z. Xiong, F. Lin, R. Wu, R. Zhang and Q. Lu, *Biomaterials*, 2005, **26**, 5864-5871.

25. C. X. F. Lam, X. M. Mo, S. H. Teoh and D. W. Hutmacher, *Mater. Sci. Eng. C*, 2002, **20**, 49-56.

26. M. C. Nolan, A. M. Fuentes Caparrós, B. Dietrich, M. Barrow, E. R. Cross, M. Bleuel, S. M. King and D. J. Adams, *Soft Matter*, 2017, **13**, 8426-8432.

27. Q. Qin, F. Yang, X. Zhang, T. Shi, Y. Shao, H. Sun, C. Chen, J. Hao and Z. Guo, *Int. J. Refract. Hard. Met.*, 2019, **84**, 105014.

28. H. Yang, S. Zhang, K. Liu and Y. Fang, *RSC Advances*, 2016, **6**, 109969-109977.

29. Z. Gong, Y. Yang, Q. Ren, X. Chen and Z. Shao, *Soft Matter*, 2012, **8**, 2875-2883.

30. Y. Liu, S. Ling, S. Wang, X. Chen and Z. Shao, *Biomater. Sci.*, 2014, **2**, 1338-1342.

31. C. Yan, A. Altunbas, T. Yucel, R. P. Nagarkar, J. P. Schneider and D. J. Pochan, *Soft Matter*, 2010, **6**, 5143-5156.

32. P. R. A. Chivers and D. K. Smith, *Nat. Rev. Mater.*, 2019, **4**, 463-478.

33. N. Johari, L. Moroni and A. Samadikuchaksaraei, *Eur. Polym. J.*, 2020, **134**, 109842.

34. A. Mondal, A. Gebeyehu, M. Miranda, D. Bahadur, N. Patel, S. Ramakrishnan, A. K. Rishi and M. Singh, *Sci. Rep.*, 2019, **9**, 19914.

35. M. D. N. I. Shiblee, K. Ahmed, A. Khosla, M. Kawakami and H. Furukawa, *Soft Matter*, 2018, **14**, 7809-7817.

36. J. Wei, J. Wang, S. Su, S. Wang, J. Qiu, Z. Zhang, G. Christopher, F. Ning and W. Cong, *RSC Advances*, 2015, **5**, 81324-81329.

37. Y. Jiang, J. Zhou, C. Feng, H. Shi, G. Zhao and Y. Bian, *J. Mat. Sci.*, 2020, **55**, 15709-15725.

38. J. Nie, W. Lu, J. Ma, L. Yang, Z. Wang, A. Qin and Q. Hu, *Sci. Rep.*, 2015, **5**, 7635.

39. L. H. Nguyen, A. K. Kudva, N. S. Saxena and K. Roy, *Biomaterials*, 2011, **32**, 6946-6952.

40. V. Jayawarna, M. Ali, T. A. Jowitt, A. F. Miller, A. Saiani, J. E. Gough and R. V. Ulijn, *Adv. Mater.*, 2006, **18**, 611-614.

41. A. Mahler, M. Reches, M. Rechter, S. Cohen and E. Gazit, *Adv. Mater.*, 2006, **18**, 1365-1370.

42. C. Diaferia, G. Morelli and A. Accardo, *J. Mater. Chem. B.*, 2019, **7**, 5142-5155.

43. J. Raeburn, G. Pont, L. Chen, Y. Cesbron, R. Lévy and D. J. Adams, *Soft Matter*, 2012, **8**, 1168-1174.

44. N. A. Dudukovic and C. F. Zukoski, *Langmuir*, 2014, **30**, 4493-4500.

45. R. Orbach, L. Adler-Abramovich, S. Zigerson, I. Mironi-Harpaz, D. Seliktar and E. Gazit, *Biomacromolecules*, 2009, **10**, 2646-2651.

46. M. Verheijen, M. Lienhard, Y. Schrooders, O. Clayton, R. Nudischer, S. Boerno, B. Timmermann, N. Selevsek, R. Schlapbach, H. Gmuender, S. Gotta, J. Geraedts, R. Herwig, J. Kleinjans and F. Caiment, *Sci. Rep.*, 2019, **9**, 4641.

47. J. Stokes and J. Telford, *J. Non-Newton. Fluid*, 2004, **124**, 137-146.

48. H. A. Barnes, *A handbook of elementary rheology*, University of Wales Institute of Non-Newtonian Fluid Mechanics, Wales (UK), 1st edn., 2000.

49. C. E. Owens, A. J. Hart and G. H. McKinley, *J. Rheol.*, 2020, **64**, 643-662.

50. A. Perazzo, J. K. Nunes, S. Guido and H. A. Stone, *Proc. Nat. Acad. Sci.*, 2017, **114**, E8557-E8564.

51. C. W. Macosko, *Rheology : principles, measurements, and applications*, VCH, New York, NY, 1994.

52. G. Ciccone, O. Dobre, G. M. Gibson, J. M. Rey, C. Gonzalez–Garcia, M. Vassalli, M. Salmeron–Sanchez and M. Tassieri, *Adv. Healthc. Mater.*, 2020, **9**, 2000517.

53. P. Roca-Cusachs, V. Conte and X. Trepat, *Nat. Cell Biol.*, 2017, **19**, 742-751.

54. J. Z. Kechagia, J. Ivaska and P. Roca-Cusachs, *Nat. Rev. Mol. Cell Biol.*, 2019, **20**, 457-473.

55. Enateri V. Alakpa, V. Jayawarna, A. Lampel, Karl V. Burgess, Christopher C. West, Sanne C. J. Bakker, S. Roy, N. Javid, S. Fleming, Dimitris A. Lamprou, J. Yang, A. Miller, Andrew J. Urquhart, Pim W. J. M. Frederix, Neil T. Hunt, B. Péault, Rein V. Ulijn and Matthew J. Dalby, *Chem*, 2016, **1**, 298-319.

56. E. Y. Du, F. Ziaee, L. Wang, R. E. Nordon and P. Thordarson, *Polym. J.*, 2020, **52**, 947-957.

57. T. G. Mezger, *The Rheology Handbook*, Vincentz Network, Hanover, Germany, 4th edn., 2014.

58. D. J. Adams, L. M. Mullen, M. Berta, L. Chen and W. J. Frith, *Soft Matter*, 2010, **6**, 1971-1980.

CHAPTER 5

Conclusions

5.1. Conclusions

Low molecular weight gels are a fascinating and effective class of material. Due to their intrinsic reversibility, dynamism and broad range of mechanical properties, LMWGs are suitable for various potential applications that span from material sciences to biomedical sciences. As such, understanding the mechanical properties is key in determining whether these materials are potentially applicable for unique on-demand applications. Within this thesis, we demonstrated the tuneability of the properties of a multicomponent gel system as well as established a new method to link the microstructure and bulk properties of a series of dipeptide hydrogels. Furthermore, we developed new rheological methods to characterise the mechanical properties of multi-layered 3D printed hydrogels.

Firstly, predicting the properties of a gel formed from a particular low molecular weight gelator remains an empirical science. Hence, a more pragmatic approach is to find robust LMWG and develop methods for controlling, modulating and modifying the properties of the gels that can be formed. In Chapter 2, we have demonstrated that using an annealing approach on a multicomponent gel system allow us to control and tune the mechanical properties of the resulting gel. Not only we were able to tune the mechanical properties of the multicomponent system, we were also able to selectively anneal just one component within the mixed system. This gives the gel completely different mechanical properties than if both components were annealed together. This is the first example where an annealing approach has been examined on a multicomponent gel system, which is significantly more complex compared to the already reported single component systems. Multicomponent systems provide added opportunities to prepare gels with different mechanical properties that cannot be achieved using only one component gel system. In the future, this approach could be used in different gel systems and so open up new opportunities to control gel properties on demand to provide tuneable and triggerable materials.

Since the understanding and tuneability of LMWGs mechanical properties are of growing interest, it is therefore important to understand and determine the gel properties over different length scales. This could allow great insight for example in mixed gels, where the number of scenarios become increasingly complex. However, characterising a gel system across multiple length scales can sometimes be an issue. In Chapter 3, we have established a new method to link the microstructure and bulk properties of a series of dipeptide hydrogels. We used a solvent and pH triggers to form gels from a series of dipeptides, which resulted in differences on the gel microstructure depending on the trigger used. Traditional oscillatory rheology (or bulk rheology) and cavitation rheology were used to measure the elastic modulus of the bulk gels and in a local point (at the micrometre scale) respectively. We studied the relationship between the two rheology techniques through a constant K_{sc}. Interestingly, we found a correlation between the constant K_{sc} and the underlying microstructure of the gels. In conclusion, we proved that cavitation rheology can be used to characterise in detail the gels microstructure at a different scale compared to bulk rheology and suggests potential to characterise patterned or inhomogeneous gels at the micrometre scale.

3D (bio)printing holds incredible potential in the biomedical field for example, where hydrogels are used as cell containing scaffolds. One of the main issues is the difficulty to characterise the gels after printing. In Chapter 4, we developed a series of rheological methods to characterise 3D printed multi-layered hydrogels. Oscillatory rheology was used as the main characterisation technique. Firstly, we combined multiple rheological protocols to characterise a series of multi-layered hydrogels by using a vane geometry embedded at different positions within the gel. We used this method to characterise a series of multi-layered gels prepared in situ for benchmark comparison, and then we expanded this method to characterise the same multi-layered gels prepared using 3D printing. We demonstrated that it is possible to characterise the properties of each individual layer within a 3D printed gel system but also, we were capable to quantify the contribution of each layer to the resulting bulk gel mechanical properties. We also studied the effect of using different

measuring systems for rheological analysis, as it highly impacts on the resulting properties being measured. Lastly, we studied the effect of the 3D printing process on the resulting gel mechanical properties. Interestingly, we were capable to quantify the differences on the mechanical properties of the printed gels with those prepared before printing. The stiffness of the printed gels is influenced by the shear stress at which they are exposed during extrusion. In conclusion, we developed a method to characterise multi-layered hydrogels which provides fundamental principles to characterise 3D printed biomaterials. We hope this study will open up new opportunities to characterise new biomaterials on demand.

In conclusion, we have used rheology to tune and characterise the mechanical properties of low molecular weight gels at different length scales. These materials have been used in a wide range of biomedical applications including drug delivery, tissue engineering, cell culture and cancer research. Some of the described methods are novel and the results show that we have a high degree of control on the characterisation of (3D printed) hydrogel systems. For example, we were able to characterise the properties of gel systems after 3D printing with the potential to be used in the biomedical sciences. Due to the difficulty to characterise gel properties after printing, others rely on the assumption that there is no change in properties from a pre-printed gel. Here we have demonstrated an effective method to characterise such class of materials after printing with potential to be used as cells containing scaffolds.